PHYSICAL, OPERATIONAL AND ECONOMIC RESILIENCE OF COASTAL ENERGY NETWORKS

Thesis submitted in accordance with the requirements of the University of Liverpool for the degree of Doctor in Philosophy

by

Thomas Prime

School of Environmental Science

Department of Geography and Planning

July 2016

DECLARATION

This thesis is the result of my own work and includes nothing which is the outcome of work done in collaboration except where specifically indicated in the text. It has not been previously submitted, in part or whole, to any university of institution for any degree, diploma, or other qualification.
In accordance with The University of Liverpool guidelines, this thesis does not exceed 100,000 words.

Signed:_____

Date:_____

Thomas Prime, MSci.

Contributions by authors to manuscripts:

Chapter 2: Prime T, Brown JM, Plater AJ (2015) Physical and Economic Impacts of Sea-Level Rise and Low Probability Flooding Events on Coastal Communities. PLoS ONE 10(2): e0117030. doi:10.1371/journal.pone.0117030

T. Prime: principal investigator and author, data processing, analysis and plot creation

J.M. Brown: manuscript development, and advice on figure plot creation

A.J. Plater: manuscript development, and advice on figure plot creation

Chapter 3: Prime, Thomas; Morrissey, Karyn.; Plater, Andrew J. (submitted) FLORA: Flood Defence Real Option Analysis Methodology for Energy Infrastructure

T. Prime: principal investigator and author, data processing, analysis and plot creation

K. Morrissey: manuscript development, and advice on figure plot creation

A.J. Plater: manuscript development, and advice on figure plot creation

Chapter 4: Prime, Thomas; Brown, Jennifer M.; Plater, Andrew J. 2016 Flood inundation uncertainty: the case of a 0.5% annual probability flood event. Environmental Science & Policy, 59. 1-9. 10.1016/j.envsci.2016.01.018

T. Prime: principal investigator and author, data processing, analysis and plot creation

J.M. Brown: manuscript development, and advice on figure plot creation

A.J. Plater: manuscript development, and advice on figure plot creation

ABSTRACT

PHYSICAL, OPERATIONAL AND ECONOMIC RESILIENCE OF COASTAL ENERGY NETWORKS

THOMAS PRIME

This body of research contributes to the planning of future coastal adaptation. The various studies that make up this thesis have been undertaken at different locations around the coast of the UK ranging from a regional study covering the Northwest UK to smaller site locations at Fleetwood, Dungeness, Bradwell and Sizewell. The research focuses on establishing an exploratory numerical model that simulates a range of plausible extreme events made up of a combination of different flood sources: storm surge, sea-level rise, high river flow and wave overtopping. In addition to examining the areal and depth extents of flooding, the physical impacts are converted into an economic cost to support cost:benefit analysis resource allocation for climate change adaption to extreme events. The simulations showed that the flood sources do not combine in a linear way and that relying on one source of flooding to estimate the impact of an extreme event can under-estimate the economic impact of said event by up to 7.7 times, and the physical extent by up 3 times.

This also highlights the non-linearity in increasing flood inundation extent and resulting economic cost. Different ways of disseminating the inundation information have been explored, particularly for local stakeholders such as residents to see the impact of the extreme event. Moving on from flood water depths, further research has assessed the economic impact of potential future sea-level rise on coastal energy infrastructure. For this body of work the infrastructure considered is electricity distribution substations. These

substations are assessed in a Real Options economic framework to determine when it is beneficial to invest in flood defences to protect that infrastructure. The research found a tipping point in 2030 in the number of energy distribution assets in NW England where the damage cost due to extreme events increased the benefit that would result from building demountable flood defences that can be deployed around the electricity substation during an extreme event enabling the substation to be resilient to that event. Here, investment achieves sufficient potential averted damage cost to make it cost-effective to invest in defences. This Real Options methodology is able to assess options for intervention across a large region at local spatial scales, supporting optimal allocation of when and where investment resources should be deployed or deferred to ensure the energy infrastructure remains protected against future climate change.

Quantifying the uncertainty in flood risk assessments where different combinations of water level and significant wave height have the same annual joint probability of 0.5% is a further contribution of this research. It was found that combinations with the highest extreme water levels generated the largest flood extent for a gravel barrier coast. Therefore, increasing extreme water levels consequent upon future sea-level rise and climate change drive an increasing risk of extensive floodplain inundation. Extreme event combinations that comprise a large significant wave height will have a correspondingly lower extreme water elevation to maintain the 0.5% annual probability. This lower extreme water elevation means that the larger waves will break further offshore, reducing the impact of these waves. This will reduce the impact of the event leading to reduced wave run-up and lower overtopping rates. The use of the longest peak period associated with the relevant significant

wave height, consistent with swell waves is important as re-simulating events with wind wave conditions rather than swell, resulted in no flood inundation.

This research has shown that ensuring a coastline is resilient to a given annual joint probability extreme event needs to consider that many different combinations of wave height and extreme water level equally apply and give a wide range in overwashing rates and inundation extents. It also highlights that managers need to focus on extreme water levels combining with swell waves, as these lead to the greatest flood inundation. Using this method will allow the testing the range of extreme events that meet the criteria and give coastal managers and stakeholders more confidence that the defences are resilient to the standard of protection specified.

Research has also examined the morphological resilience of saltmarsh and barrier beach coastlines. In the case of saltmarshes, numerical modelling examined how the ability to reduce wave run-up changes as it erodes. Two critical saltmarsh widths were discovered, one at 810 m and the other at 270 m. The wider width is a threshold where the linearly increasing wave run-up with decreasing saltmarsh width changes to a constant wave run-up value despite a further decrease in width. The narrower critical width denotes another threshold where the constant wave run-up value changes to a linearly increasing one, but at a rate three times faster than before the before first threshold width. The research shows that a saltmarsh is able to maintain the resilience it provides before the first threshold until the narrower threshold width is reached. As well as width, the height of the saltmarsh edge is also important, with heights below 2 m having much less resilience or greater wave run-up values.

The findings from the study showed that maintaining a saltmarsh wider than 270 m and height greater than 2 m above the beach will have the greatest impact on wave attenuation. For barrier beaches there is a very clear linear relationship between the slope of the gravel barrier and the wave run-up experienced. This relationship emphasizes that the slope of the barrier is the dominant factor in controlling wave run-up. Increasing the height of the barrier and narrowing the barrier did not impact on the wave run-up in either a negative or positive way. Across the whole studied section of coastline, it was found that wider barrier beaches decrease the wave run-up experienced during an extreme event by around 0.2 m, thus increasing the resilience of the coastline. A key assumption and limitation in this study is that it was assumed that the barrier beach was fixed in place during the extreme event and would not deform. This was to allow comparison between the different scenarios of height and width change.

A threshold at 125 m width was found where wave run-up was reduced by 0.8 m compared with widths narrower than 125 m. Above a barrier height of 5 m it was found that there was no control on the wave run-up, where a linear relationship was present below this height. A critical height at 4.3 m was found where barrier heights below this were no longer resilient to the extreme event being simulated. The main finding was that barrier slope variable is the best indicator in assessing the resilience of a gravel barrier located at the top of a beach. In summary, this thesis demonstrates the value of exploratory modelling within an economic framework for assessing future options for climate change adaptation at the coast, and for providing decision makers with illustrative tools for enabling appropriate and timely resource allocation.

ACKNOWLEDGEMENTS

I would like to thank all my supervisors for the help, advice and feedback that they have provided during the course of this work. I would particularly like to thank Dr Jenny Brown, Prof Andy Plater and Dr Karyn Morrissey for all their help and contributions towards my paper publications and manuscript development.

This research was funded by the Engineering and Physical Science Research Council (EPSRC) as part of the Adaptation and Resilience of Coastal Energy Supply (ARCoES) research project (EPSRC EP/I035390/1). ARCoES is also part of the ARCC Adaptation and Resilience in the Context of Change Knowledge Network. Acknowledgement must also be made to the National Oceanography Centre (NOC) for the provision of research facilities and resources throughout this project.

Thanks are also due to the many friends and colleagues (too many to name) across all the institutions and departments I have come into contact with during my time here. I have enjoyed spending time and socialising with you all and hope to spend more time and work with you in the future.

Finally, my greatest acknowledgment has to go to my wife Kelly for all the support and encouragement she has provided me during this undertaking and also to my son Austin who has done his best to hinder my work in the last 10 months! Only joking, thank you both for being there for me and I look forward to your support in my future work. I dedicate this achievement to you both.

Table of Contents

List of Figures

List of Tables

1 Rationale

The Earth's climate is changing. Global temperatures are increasing and in the future increased mean sea levels will become apparent. Sea level has the potential to increase by up to 1.8 m relative to present-day levels, although this magnitude has a 95% chance of not occurring by 2100 (Jevrejeva et al., 2014). Increased storminess, significant wave height and tidal range are also possible, although the magnitude and likelihood of these is much less certain (Lowe et al., 2009). The combination of these potential changes means that coastal communities and associated critical infrastructure will be under more pressure from extreme events in the future (Stevens et al., 2015).

Critical infrastructure provides essential services to keep modern society going, examples being railways and other transport links, communication lines and finally, electricity generation, transmission and distribution. While there are many risks to critical infrastructure, such as increased temperatures, droughts etc. (Energy Network Association, 2009), the body of work presented in this thesis focuses on the impact of coastal flooding, both at the present day and using projections of future mean sea level. Critical infrastructure and communities on the coast and in floodplains are protected by defences, these are designed to be resilient to a defined standard. A common defence standard is to be able to withstand a 1 in 200 year extreme event (Wyse, 2015). Increased mean sea level will give the apparent effect of extreme events occurring more often, thus reducing the resilience capacity of infrastructure (Wadey et al., 2014). Resilience can be defined as the capacity to recover quickly from difficulties - for this body of research the difficulties are considered to be coastal flooding that occurs during an extreme event.

Relatively small increases in mean sea level can have a large impact on the probability of occurrence. A rise in the mean sea level of 0.28 m in Blackpool, UK would reduce the probability of a 1 in 250 year event to 1 in 50 years (A. McMillan et al., 2011). If no adaptation measures are taken, consequential impacts on society will follow (Stevens et al., 2015). For example, an increased likelihood of floodplain inundation will lead to inundated homes, regional electricity blackouts and damage to railways, which are commonly routed along the coast and through floodplains. Investment in improving or building new defences needs to be made to ensure resilience capacity is maintained or increased. However, knowing exactly which defences need building/improving and when this is best done is dependent on the sea-level rise (SLR) realised.

The uncertainty surrounding SLR is large, particularly over a long time horizon (Jevrejeva et al., 2012). Current projections estimate a range of 1.35 m between the 5th and 95th percentile of global SLR in 2100 (Jevrejeva et al., 2014). Building for a 95th percentile rise of 1.8 m would most likely waste resources as the defences are likely to end up being over-engineered for the climate that is realised over the defences' lifetime. Equally, building for a 5th percentile rise of 0.45 m is highly likely to result in defences that are not sufficiently resilient as they will not be built high enough to withstand the changing climate that is likely to be realised over the life of the defences. Both of these outcomes can be classed as sub-optimal, too much or too little investment will have resulted in wasted resources - either in over-spending on defences or in damage and clean-up costs for extreme events that overwhelm the weaker defences (Woodward et al., 2011).

Critical infrastructure in the floodplain depending on the SLR realised has the potential to benefit from flood defence investment. If the defences remain resilient then the saved damage costs that would have arisen during an extreme event if the defences were not present are considered to be a benefit. If this benefit is greater than the cost of building and maintaining the defences then it has a cost:benefit ratio (CBR) greater than zero and it is therefore beneficial to invest in flood defences. The number of infrastructure assets that would have a CBR greater than zero will vary depending on the amount of SLR that is attained in the future. The large uncertainty in SLR projections makes it difficult to determine which assets will benefit positively from building flood defences. One method that takes the uncertainty in to account is to value the option of investing or deferring flood defence investment (Black and Scholes, 1973; Cox et al., 1979). This process highlights the asset that would benefit from investment now and those that would benefit from deferring the investment. This deferral allows better projections of SLR to be made in the future, which will then help to inform the decision to invest or defer in the future.

So far extreme water levels have been assumed to be the only factor that contributes to coastal flooding during an extreme event, but other factors also effect the resilience of critical infrastructure. The occurrence of extreme waves during an extreme water level event can significantly increase the impact of the event. Being resilient to wave action as well as extreme water levels is very important for infrastructure directly on the coast. Determining the annual likelihood of occurrence for an extreme flooding event on the coast requires thinking about more than just the probability of a given still water height occurring (Hames and Reeve, 2007). The wave conditions that occur at the point of this still water level are also important as they can enable water to overwash defences at a lower threshold than the still

water level alone through a variety of processes such as wave set-up, run-up and overtopping. For coastal critical infrastructure, knowing the probability as a combination of water level and wave height occurring would be beneficial in ensuring defences are resilient to a given annual probability of occurrence (Hawkes et al., 2002). Unfortunately, there are many combinations of wave height and water level that have the same probability of occurrence, i.e. high water levels with low wave heights have the same probability of high wave heights at lower water levels (P.J. Hawkes and Svensson, 2006). These will have different contributions to any flood inundation that may arise. Engineering defences to withstand a given probability of occurrence is more complicated than if just considering still water levels alone.

The size and shape or morphology of coastal defences has an impact on the wave run-up and therefore the resilience of these defences to extreme events. Changing the height and width of these defences could show the impact that these changes would have on the coastline's resilience to a given extreme event. Saltmarshes can provide resilience to the coast during extreme events, where waves are attenuated when passing over the saltmarsh surface (Möller et al., 2014a). They also have a linear relationship where the response of the saltmarsh to wave action remains linear with increasing wave energy. It was found the extreme events do not contribute to the erosion of saltmarshes but it is the impact of moderate storm events that is the dominate factor (Leonardi et al., 2016). The width of saltmarshes contributes to the resilience of the coast, determining how resilient different saltmarsh widths are to extreme events will show how the resilience of the coastline will change as the marsh erodes.

For regions that include a fluvial floodplain as well as a coastline, waves, storm surges and high river flows can all potentially contribute to an extreme flood event. Coastal communities could be subjected to larger inundation extents and damage cost from extreme events in the future due to a changing climate, particularly if the different flood sources combine together (Le et al., 2007). The different inundation extents from different combinations of wave, river and surge flood sources, and resulting costs in clean-up and repair of the different areas of a coastal community require clear understanding.

The research questions investigated in this thesis are

1. What is the effect of combining different coastal flood sources while also being under a plausible future climate scenario on a coastal community?
2. Given the large uncertainty surrounding climate change, when and where is there a net benefit in investing in flood defences that protect energy infrastructure?
3. Can we quantify the uncertainty surrounding the flood risk that could result from a given probability of an extreme event?
4. How much resilience does a saltmarsh contribute to a coastline and how does it diminish as the marsh erodes? What are the key factors in controlling the resilience of the marsh?
5. What are the major morphological factors that help to control a gravel barrier's contribution to the resilience of the coastline?

Chapter 1 examines the question, what is the impact of combining different flooding sources and climate change pressures? It details a flood mapping method that has been used to assess the flood costs and hazard for a coastal community from a combination of storm surge, river

flow, waves and sea-level rise. Results in the form of the economic cost of extreme events, along with "traffic light" vulnerability ratings showing flood depths in the form of brick layers, enables local stakeholders to see the impact of extreme events on their houses or local areas. When is it cost effective to invest in flood defences given the uncertainty surrounding climate change? Chapter 2 answers this question by extending the economic analysis from Chapter 1 to cover sea-level rise up to 2100 and applying it specifically to energy infrastructure. By expanding the analysis to cover future sea-level rise projections, the decision to invest in energy infrastructure flood defences or defer the investment can be made at regional scales but with an assessment performed at a local spatial scale.

Some of the many other uncertainties in assessing flood risk and vulnerability are explored in chapters 3, 4 and 5. How large is the uncertainty in flood risk surrounding an extreme event? Different combinations of two flood risk sources, such as extreme water level and significant wave height can have the same annual probability of occurrence. Chapter 3 shows how much uncertainty is present in inundation extent and flood hazard across a range of extreme event combinations that have the same annual probability. What impact will the erosion of soft defences such as saltmarshes have on the resilience of a coastline? Chapter 4 investigates the impact of eroding saltmarshes on the resilience of coastal sea defences. The change in wave run-up based on decreasing saltmarsh width and height is explored within this chapter.

Following on from the erosion of a saltmarsh impacting resilience, the fifth and final research chapter examines how the resilience of a gravel barrier beach to extreme events is affected by morphological changes. This chapter identifies the dominant factors in determining how

resilient a gravel barrier defence is to a given extreme event. Finally, the five research chapters are drawn together with some conclusions and implications of the research in chapter 7. Details of the models used in the research and data availability are provided in the appendices.

2 Physical and Economic Impacts of Sea-Level Rise and Low Probability Flooding Events on Coastal Communities

2.1 Abstract:

Conventionally flood mapping typically includes only a static water level (e.g. peak of a storm tide) in coastal flood inundation events. Additional factors become increasingly important when increased water-level thresholds are met during the combination of a storm tide and increased mean sea level. This research incorporates factors such as wave overtopping and river flow in a range of flood inundation scenarios of future sea-level projections for a UK case study of Fleetwood, northwest England. With increasing mean sea level, it is shown that wave overtopping and river forcing have an important bearing on the cost of coastal flood events. The method presented converts inundation maps into monetary cost. This research demonstrates that under scenarios of joint extreme surge-wave-river events the cost of flooding can be increased by up to a factor of 8 compared with an increase in extent of up to a factor of 3 relative to "surge alone" event. This is due to different areas being exposed to different flood hazards and areas with common hazard where flood waters combine non-linearly. This shows that relying simply on flood extent and volume can under-predict the actual economic impact felt by a coastal community. Additionally, the scenario inundation depths have been presented as "brick course" maps, which represent a new way of

interpreting flood maps. This is primarily aimed at stakeholders to increase levels of engagement within the coastal community.

2.2 Introduction:

2.2.1 The significance of coastal flooding and storm surges

It is estimated that 46 million people were affected by flooding globally in 1990 (Hoozemans et al., 1993), this number is set to increase due to increasing mean sea levels. If 1m of sea-level rise (SLR) occurs by 2100 with no other change e.g. resilience measures, it is estimated that this number would rise to 60 million people (Nicholls et al., 1999).

Examples of the devastating impacts of coastal flood events include the impacts of Hurricane Katrina, which caused 1570 deaths in Louisiana and caused $40-50 billion dollars of monetary losses (Kates et al., 2006). It is predicted that it will take up to 8-11 years to reconstruct the urban infrastructure and environment (Kates et al., 2006). More recently Hurricane Sandy produced a catastrophic storm surge which among other areas hit a section of the US coastline stretching from New Jersey to Rhode Island which contributed to a damage cost in excess of $50 billion dollars and 72 direct fatalities (Galarneau et al., 2013). Storm surges in the Bay of Bengal have caused widespread flooding and loss of life, for example the Bhola Cyclone in 1970.

The UK is also susceptible to coastal flooding. A classic historical example is the North Sea storm surge that occurred in 1953 with a surge greater than 2.3 m in the North Sea, causing devastation in the UK and continental Europe. It resulted in the loss of over 1800 lives in the

Netherlands (Gerritsen, 2005) and 300 deaths in east and southeast England (Baxter, 2005). This proved something of a 'tipping point' in coastal planning, in response to this event sea walls were repaired and raised to increase the resilience of the country to coastal flooding. The Delta Plan in the Netherlands was established and led to construction of barriers across several of its estuaries over the next decades (Wolf and Flather, 2005). In 1953 many people were not aware of their vulnerability to storm surge flooding and received no warning, meaning that they were unprepared for the floodwater. Lack of communications inhibited the warning of other areas that flooding was imminent and prevented the request of external assistance (Jonkman and Kelman, 2005). Since 1953 there have been other notable extreme storm surge events, such as November 1977 with a 1.2 m surge at Fleetwood, December 1981 with a surge greater than 2 m in the Bristol Channel and over 0.5 m in parts of the Irish Sea. Other notable events include January 2005 where surges between 0.5 m and 1.5 m occurred all the way from Holyhead to Dover and December 2013 with a surge of over 1 m in the Irish Sea and over 2 m in the North Sea (SurgeWatch, 2016). These events have had a lesser impact due to the building of coastal defences (Steers et al., 1979). From this point on we use the term "storm tide" to consider the combined tidal and surge water level, the total high water level posing as the potential flood risk and hence threat to life and infrastructure.

In the UK it is estimated that there are approximately six million UK properties (one in six of all properties) currently exposed to some degree of flood risk, with 600,000 properties in areas of significant risk (DEFRA, 2012). The UK floods in 2007 were estimated to have cost businesses £740 million; this is on average around £100,000 per affected business, with some taking 27 weeks to return to normal. Through appropriate risk management it is possible to become more resilient to these flooding events and gain economic benefit. It has

been estimated for Europe that every £1 spent on adaptation and resilience measures represents 4 times its value in potential damage avoided (HM Government, 2013). The government has planned to spend £2.42 billion on flood and coastal erosion risk management between April 2011 to March 2015 (DEFRA, 2012). From the 4 to 1 ratio mentioned above, this should provide £9.68 billion in benefits to the UK economy. However the impact of flooding is still felt; over the period 23/12/2013 to 28/02/2014 flooding has so far resulted in 18,700 insurance claims at a cost of £451 million (ABI, 2014).

2.2.2 Impacts of Increased Mean Sea Level

Assuming no adaptation to increasing coastal flood risk, the expected annual damage (EAD) in England and Wales due to coastal flooding is predicted to increase (Hall et al., 2006). Present-day EAD to residential and non-residential properties is of the order of £1.3 billion for the UK as a whole (DEFRA, 2012). For residential properties alone the expected annual damage from tidal and river flooding in England and Wales is projected to increase from £640 million currently to over £1.1 billion by the 2020's under a Medium UK Climate Projections 2009 (UKCP09) emissions scenario (HM Government, 2013). There are a range of SLR projections that are available for coastal flood risk assessment. The Intergovernmental Panel on Climate Change (IPCC) have recently updated their global projections of SLR which range from 28 to 98 cm by 2100 (Stocker et al., 2013). Focusing on the UK, planning and environmental management practitioners refer to the UKCP09 projections (Lowe et al., 2009). Under the medium emissions scenario these have a range of 0.21 m to 0.68 m in London by 2095, which is based on earlier IPCC sea-level rise projections, with their maximum plausible scenario H++ being 1.9 m (Lowe et al., 2009). Beyond 2100

there is less published data, however Jevrejeva et al. (2012) have projected values up to 2500AD, with values ranging from 0.13 m to 11.51 m depending on confidence level and projected climate scenario (Jevrejeva et al., 2012).

Projections of future SLR values are very uncertain, with continued concern that large increases in the 21st century are possible and cannot be ruled out (Nicholls et al., 2011). One of the biggest sources of uncertainty is the response of the large ice sheets on Antarctica and Greenland. For a temperature rise of 4 °C or more by 2100 a SLR between 0.5 m and 2 m is estimated (Nicholls et al., 2011). The probability of SLR occurring that is at the higher end of these projections is low but unquantifiable. However, a SLR of this magnitude would have a huge impact on the globe with up to 2.4% of the global population being displaced (Nicholls et al., 2011). SLR needs to be monitored closely to detect any accelerations in the rate of rise, and climate-induced processes need to be better understood (Nicholls et al., 2011).

The impact of coastal storms is increasing due to SLR increasing the frequency of extreme water levels which will increase the occurrence and impact of storm surges (McInnes et al., 2003) and waves (Lowe et al., 2001). Even a small increase of mean sea-level (MSL) can change the return period of an extreme water level. e.g. a SLR of 0.28 m will turn a 1 in 250 year extreme water level to a 1 in 50 year extreme water level in the area of study for this paper (A. McMillan et al., 2011).

This is also true of other environmental events; the increase of MSL alters not only the extreme wave heights but also the frequency of occurrence of extreme wave conditions (Chini et al., 2010). In addition to SLR there are many variables that affect coastal flooding; these range from a changing climate (i.e. possible increases in the occurrence and strength

of storms) to coastal defence degradation. (Buijs et al., 2007; Lowe et al., 2009). Future increases in storminess are assumed to not be a significant factor (Lowe et al., 2009). In addition to surge and SLR other factors are sometimes considered within coastal flood risk analysis. The most common is wave overtopping where the discharge of water over sea defences is modelled and fed into the flood inundation model. Much less common, is river flow, where a high river flow is taking place at the same time as a storm surge with a resulting increase in flood inundation. In modelling studies these processes require multiple models to be coupled together (Gallien et al., 2014). If either of these events occurs over the same period as a storm tide then they can significantly affect the flood extent and depths of inundation. The combination of river and surge inundation is known to be non-linear (Maskell et al., 2013).

SLR is again important for other flood factors as the elevated water level enables other processes to breach coastal sea defences. With increased mean sea-level (MSL), a threshold will be reached when wave overtopping will become a significant hazard due to the increased frequency of extreme sea level events. (Chini and Stansby, 2012). This is also true of river flows as higher MSL means that rivers are more likely to break their banks along tidal reaches and flood estuarine communities. Knowing these tipping points for sea level is important for long-term adaptive coastal management as it identifies possible future state changes within a system and when a change in planning strategy may be required.

2.2.3 Coastal Inundation Modelling

There are many different types of flood inundation model, one dimensional (1D), two dimensional (2D), coupled 1 and 2 dimensional (1D/2D) and finally 3 dimensional (3D) models. 1D models are widely used to model fluvial hydraulics using 1D finite difference solutions of the Saint-Venant equations (Bates and De Roo, 2000). 1D models are unable to resolve complex floodplain flow fields and require post-processing to produce realistic flood extents. 2D models can achieve this and allow the complex interaction of channel and floodplain flow fields to be simulated. Such modelling is now more feasible through improvements in computational resources and affordability. This is important when trying to model urban flooding, meaning that recent urban flood modelling efforts have been focussed on coupling a 1D model with a 2D model. This is where a 1D river channel model is complemented by a 2D model of the floodplain. Examples of this type of model are LISFLOOD-FP, Delft-FLS, SOBEK1D2D, MIKE FLOOD, ISIS and TUFLOW (Gilles and Moore, 2010). However, 2D models are unable to model structural elements that may produce super-critical flows (Gilles and Moore, 2010). Finally the last type of model is a 3D model, an example of this is Delft3D which is a coupled 2D/3D model that can be used for investigating hydrodynamics, sediment transport, morphology and water quality (Gilles and Moore, 2010).

Some of the above models are able to simulate tidal forcing, and wave overtopping is also considered for many coastal flood modelling approaches. This is important as wave overtopping can have a big impact on flood extent as events that do not overtop flood defences in 2D simulations could still experience flooding due to wave overtopping (Smith

et al., 2011). In addition to tidal forcing and wave overtopping high river flows could also be considered, although it is currently not commonplace to consider this flood source for coastal flooding studies. This paper develops an accessible methodology that couples a 2D storage cell flood inundation model with a 1D shallow water Boussinesq wave model which allows the effect of wave overtopping sea defences to be added to a storm tide flood simulation.

Other forms of flooding or defence failure could also be considered, these include still water overflow and sea defence breaches. Neither of these are covered by this method, as still water overflow would require higher extreme sea levels beyond the scope of this paper. Breach inundation modelling could be undertaken for the area but it would require knowledge of the age and condition of the defences as this will be strongly correlated with likely defence failures. These are areas of future work as breaches in defences can be incorporated into the flood model and timed to occur at a defined point during the simulation.

2.2.4 Addition of River and Wave forcing

Being able to combine a storm tide and river flow with wave overtopping allows a more complete picture of the risk and hazard a coastal community faces. For example, the impacts are under-estimated using a 2D raster model in isolation. However, the inundation model used here (LISFLOOD-FP (Bates et al., 2010)) is flexible enough to allow the incorporation of rivers and wave overtopping. A river flow hydrograph can be assigned to a section of the model boundary falling across a river mouth to simulate the river inflow, while wave

overtopping flow rates for chosen extreme wave heights and period at varying water elevations can be set as inflows at the top of the sea defences to simulate wave overtopping within the model domain.

This study aims to identify the importance of wave overtopping and river flow, when calculated as monetary costs, in coastal flood scenarios with increased MSL.

2.2.5 Inundation Scenarios

Figure 2.1 shows the data inputs required for each of the proposed inundation scenarios. Section 3 details the data availability and how it is used in the scenarios. Some data are directly used within the process, e.g. the extreme water level data, river hydrograph etc., and some required derivation via pre-processing or model simulation, for example wave overtopping rates and the SLR parameter used.

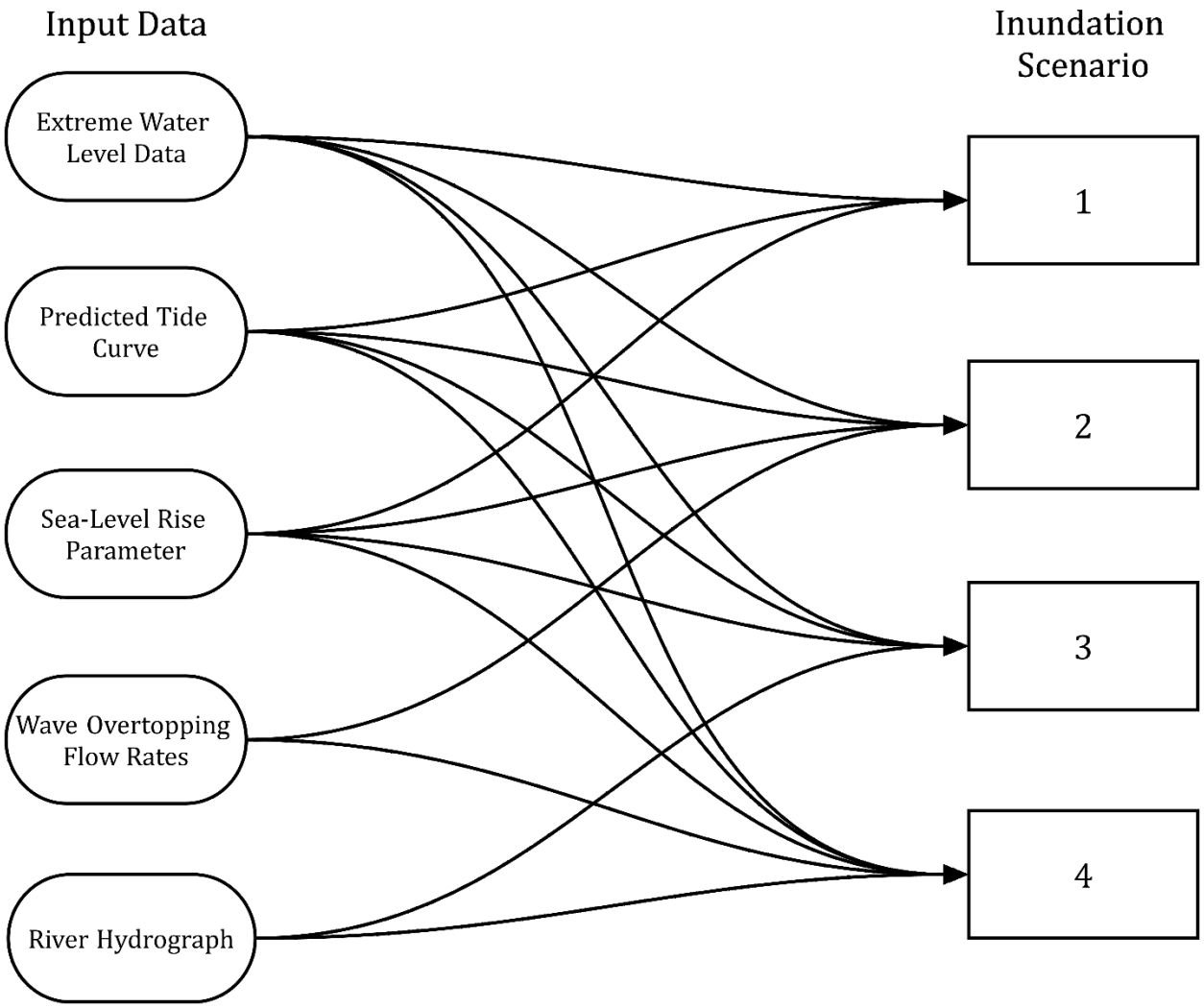

Figure 2.1: Flow chart showing the input data used for each of the four scenarios

2.3 Site Selection

The site that has been selected to trial this methodology is the Fleetwood coastline in Lancashire, northwest England, UK. Its location in relation to the rest of the UK is shown in Figure 2.2. This figure also shows the location of the tide gauge at Heysham used for tidal prediction to generate the time-varying water elevation boundary curves. Fleetwood was selected as a study site as historically it is extremely susceptible to flooding, with coastal

flooding occurring in 1927 with 6 deaths and again in 1977 when 1,800 properties were flooded, leading to the current concrete sea walls being constructed (Green, Carl, 2014). Both the 1927 and 1977 flooding was caused by storm surges. During the 9th to 12th November 1977; as recorded at Heysham, the surges were 1.8 m high and occurred one to two hours earlier than the peak of a high spring tide (Zong and Tooley, 2003). The vulnerability of Fleetwood to these historical extreme events has been alleviated by the current sea defences built in 1977. However, with increasing mean sea-level the impact of storm surges is increasing. There is interest from stakeholders in the area such as the local council in the resilience of the current defences and if adaptation to climate change will be required.

Figure 2.2: Map of the UK showing where Fleetwood and the tide gauge at Heysham are located (Edina Digimap, 2013)

Recently in the UK there have been a cluster of events that have caused major damage and disruption (Wadey et al., 2014). During a storm surge that occurred on 5th December 2013 there was a minimal amount of flooding at this location, this was due to spray being blown over the sea defences by the high winds. The concrete walls built after the 1977 flood successfully prevented any wave overtopping. At Heysham the surge height was 2.15 m, which is a larger surge than in 1977, showing that the current resilience of Fleetwood is significantly greater than it was before the flooding in November 1977. Examining the Environment Agency dataset that provides 16 different return periods at 2 km intervals along the UK coastline the closet matching return period for the total water level experienced at the case study site during the December 2013 extreme event was 1 in 75 years with an confidence interval of 0.2 m (A. McMillan et al., 2011). The Blackpool wave rider buoy data (CEFAS Wavenet, 2014) for the same period demonstrates that the wave height and period were found to have a return period in of a 100 years, if the 140-year UKCP09 model wave data is used as the basis for return period analysis (Leake et al., 2009). The highest recorded water elevation that occurred at Heysham during the 5th December surge was 6.15 m above Ordnance Datum (AOD). The scenarios with increased mean sea levels that are explored in this paper are at a higher value than this with an increase of approximately 0.85 m. This takes into account a longer return period (1 in 250 rather than 1 in 75) and a potential SLR parameter (0.65 m).

The model domain (Fig 2.3) is 9 km by 8.3 km and is centered on the areas of Fleetwood and Thornton-Cleveleys, with parts of Anchorsholme to the south. This is an area of low-lying land vulnerable to wave and river flooding, with extensive sea defences that have recently been refurbished. The model domain also contains the River Wyre. The protection provided

by the sea defence ranges from a 1 in 500 year extreme water level (EWL) down to a 1 in 20 year EWL (Environment Agency, 2013). The area to the west of the Wyre is predominantly urban residential housing, with some industrial sites close to the river. To the east of the Wyre the area is predominantly rural, with arable land being prominent, along with some urban areas close to the coast in the north. The area is of interest to coastal managers to determine the resilience of the area to future sea-level projections.

While Fleetwood has sea defences to protect it, as demonstrated by the minimal flooding caused by the surge on 5th December 2013, it is vulnerable to SLR. Small amounts of SLR will significantly reduce the return period of the water level during storms and surges that pose a flood risk (A. McMillan et al., 2011). A 1 in 250 year EWL was selected as it relates to the return periods used in shoreline management plans and coastal defence management. After a review of the coastal defence data provided by the Environment Agency (EA), on average most sea defences protecting Fleetwood are designed to cope with a 1 in 200 year EWL.

Table 2.1: Details of sea defences for Fleetwood coastline

Section	Crest Height (metres)	Defence Details along section
1	11	• Concrete and cobble aprons with recurve wall
2	8.3-7.8	• Concrete apron area with re curved wall • Mass concrete wall with promenade
3	7.7-10	• Seawall with stepped revetment • Mass concrete wall with rear splash wall • Concrete and masonry aprons
4	7.7	• Seawall
5	6.9-8.1	• Aprons with wall and promenade to rear • Concrete aprons with small wall and promenade • Beach ridge with promenade • Concrete slab revetment • Concrete and masonry walls
6	7-7.6	• Embankment and splash wall • Embankment and channel flood wall

For the purposes of this study, the sea defences at Fleetwood have been divided into 6 sections (Figure 2.3); these sections were identified using a coastal defence database (Environment Agency, 2013). A significant change in defence crest height defines where a new defence section begins and ends, details of these are listed in Table 2.1.

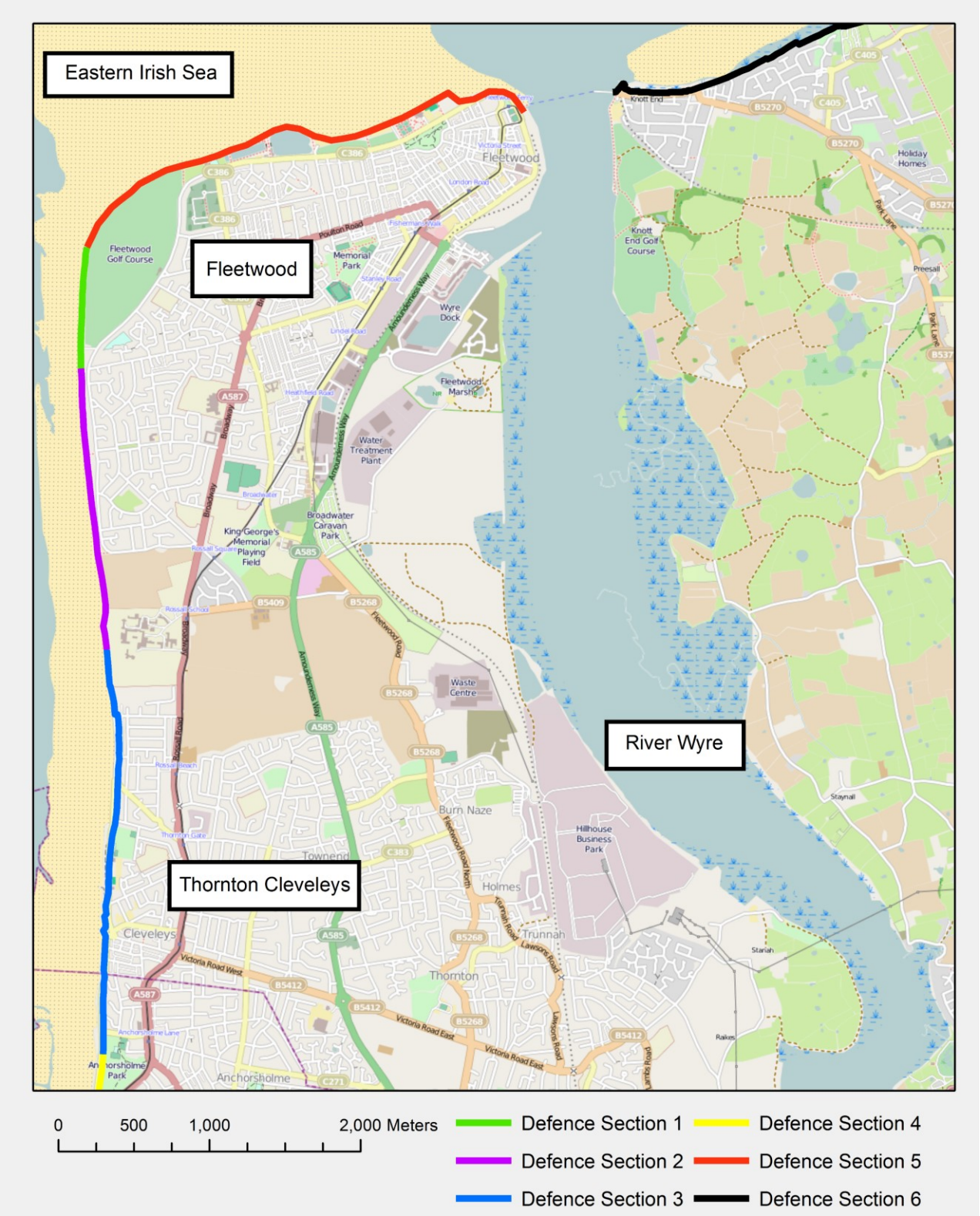

Figure 2.3: Detailed view of the study area, each of the defence sections detailed in Table 1 are shown in varying colours.

2.4 Methods

Figure 2.4 shows a simple flow chart that details the steps taken from taking the input data, and getting the economic cost of the scenario at the end. Figure 2.1 shows which input data is required for each scenario, essentially the tide, surge and SLR inputs remain the same for each scenario, and the only changing factors are the wave overtopping and river flow inputs. Section 1 goes through each of the input data shown in this flow chart (Figure 2.1). Sections 2 to 3 detail the additional steps shown in Figure 2.4. Finally sections 4 and 5, which are not described by the flow charts, provide additional methodology by explaining the sensitivity analysis that was performed, as well as additional model parameters required by the inundation model.

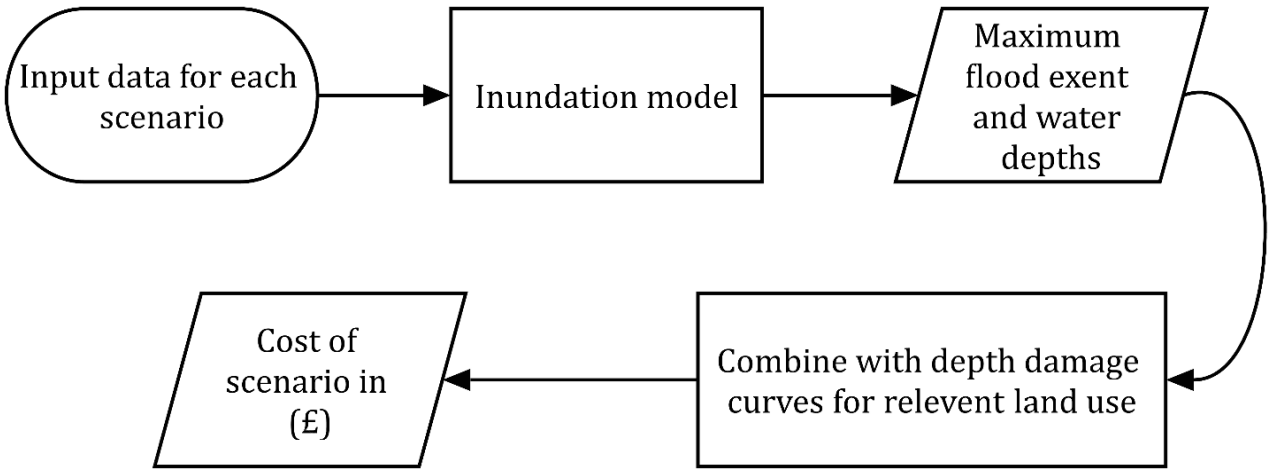

Figure 2.4: Flow chart showing the process followed to derive the cost of each scenario

2.4.1 1 Input data

2.4.1.1 Extreme water level data and predicted tide curve

The EA has provided a geospatial file that has extreme water heights at 16 different return periods every 2 km along the UK coastline (A. McMillan et al., 2011). The 1 in 250 year exceedance values were used in this instance. Every data point that was within the model domain was used to define the extreme water level elevation at the model boundary closest to each data point.

To turn these extreme water level elevations into a time varying surge component, the EA have also provided representative surge curves for various tide gauges around the UK (A. McMillan et al., 2011). The closest one to Fleetwood is Heysham which is approximately 17 km north along the coast. The surge curve varies from 0 to 1 with 1 being the peak of the surge and 0 being no surge, for a simulation time of 100 hrs (red curve Figure 2.5).

The final piece of data required is a predicted tidal curve; this was generated using a piece of software called POLTIPS3 which is available from the national tide sea level facility. The period selected was the 30/09/2015 when a highest astronomical tide is predicted. 15-minute interval data for several days either side of this date were generated and overlaid on to the surge curve, lining up the tide and surge peaks (purple curve Figure 2.5).

The difference between the maximum predicted tidal high water (30th September 2015, Figure 2.5) and the selected extreme water level to be simulated is then calculated. This value is then multiplied by the 0 to 1 values of the surge curve to create the surge elevation over the possible 100 hr storm period, the peak surge occurring at the predicted tidal high water.

The resulting surge elevation is then added to the predicted tidal curve giving a storm tide curve that peaks at the extreme water level selected (green curve Figure 2.5).

Finally, the SLR parameter (calculated in section 1.2) is added to all values to produce the desired target time-varying water elevation. This process was performed on each of the EA data points within the model domain and the resulting time-varying water elevation curve was applied to the relevant sections of the offshore model boundary (blue curve Figure 2.5).

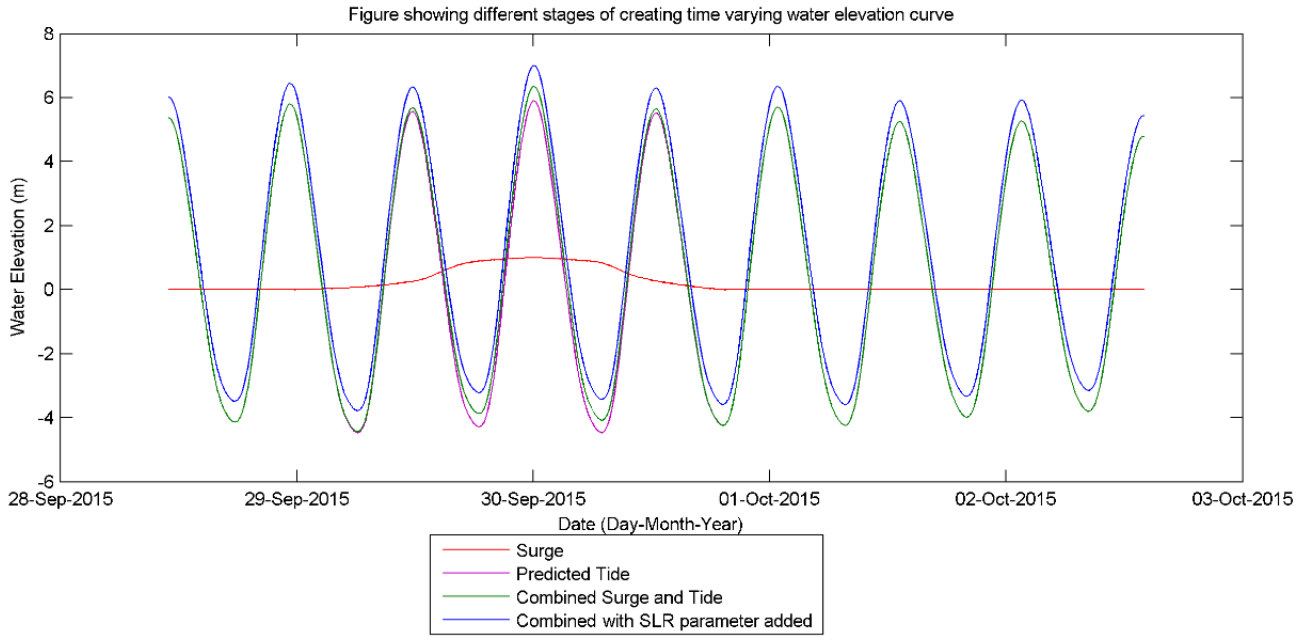

Figure 2.5: Graph showing the different stages in generating the time varying water elevation

2.4.1.2 Sea-level rise parameter

To simulate the worst case scenario, a SLR parameter has to be selected, one that will just stop slightly short of overflowing current sea defences in still water flood simulations. This will show the biggest impact that wave overtopping and high river flows could potentially

have. To identify this parameter level a simple inundation model simulation was run that has a time-varying water level at the boundary, this started at 0 m OD and was then increased by incremental steps of 0.25 m until the still water level overflowed the defences. The water level before this point was selected as the target water elevation that the potential future storm tide would need to achieve. Figure 2.6 shows this schematically, the SLR parameter is the difference between this target water elevation and the current 1 in 250 year extreme water level elevation. This SLR value of 0.65 m has been identified as the tipping point for significantly increased flood risk for the present-day defences in this region. Selecting the SLR parameter in this way makes it an arbitrary figure, one that is not linked to any probabilistic SLR projections. However, the value is within the UKCP09 relative sea-level rise projections by 2100 (Lowe et al., 2009). From closer inspection this value is just below the 0.68 m that makes up the upper range value from 1990 to 2095 for London (being a relative sea-level rise projection this value also takes into account vertical land movement). The parameter selected is also well under the 1.9 m plausible maximum of the H++ scenario provided by UKCP09 for 2100 (Lowe et al., 2009).

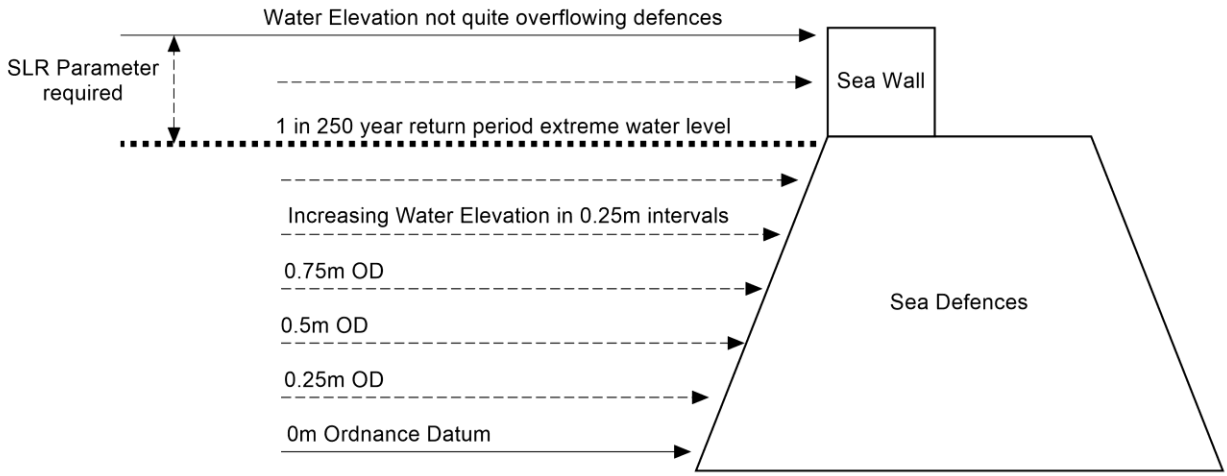

Figure 2.6: Diagram showing how the SLR parameter was selected

2.4.1.3 Wave overtopping flow rates

The Shallow Water Boussinesq Model (SWAB) is a semi-implicit shallow water Boussinesq model that has been developed to account for random wave breaking, impact and overtopping of sea walls (McCabe et al., 2013). This model has been tested against field data for overtopping at Blackpool and Anchorsholme, approximately 11 km south of Fleetwood. It has also been compared with 1:15 scale wave flume tests. Overall the overtopping output from this model has been found to agree well with field and flume measurements (McCabe et al., 2013).

Here, the freely available online SWAB interface has been used to derive overtopping rates for various wave height return periods. This was achieved by extracting the full wave height and period data from UKCP09 datasets for the closest relevant location. Return period analysis was then performed on the wave height and peak periods to calculate the wave height and period exceedance values for 10, 100 and 1000 years. The method used to derive

overtopping rates with SWAB is detailed in Figure 2.7, this flow chart shows the steps made to calculate overtopping rates at 0.1m intervals for the relevant sections of sea defences. The defences have been split into sections (Figure 2.3) and a 1D transect was extracted from the EA airborne laser altimetry (LiDAR) (Environment Agency Geomatics, 2014) which comprises the sea bed, sea defences and the land behind. This transect lies along the most common wave direction for the defence location identified using the UKCP09 data (Lowe et al., 2009). This transect provides the bed profile for the 1D SWAB model, which provides details of the bathymetry fronting the sea defences, the height and shape of the defences and the topography of the floodplain behind. To calculate overtopping, the model starts from a low water elevation value - one that does not cause any overtopping. The model is then run with a selected wave height and period, in this case the 1 in 100 year exceedance value. The model simulates a wave spectrum using the wave height and period inputs. This process is repeated with increased still water heights at 0.1 m intervals at the SWAB model boundary until the water overflows the sea defences. The overtopping rates calculated from the volume overtopped can then have a relationship to water level that allows the time-varying still water height at the boundary of the model to be associated with an overtopping rate. For this study the range of water levels simulated started at 6 mOD and continued to 8 mOD with a 100 year return period significant wave height of 4.3 m.

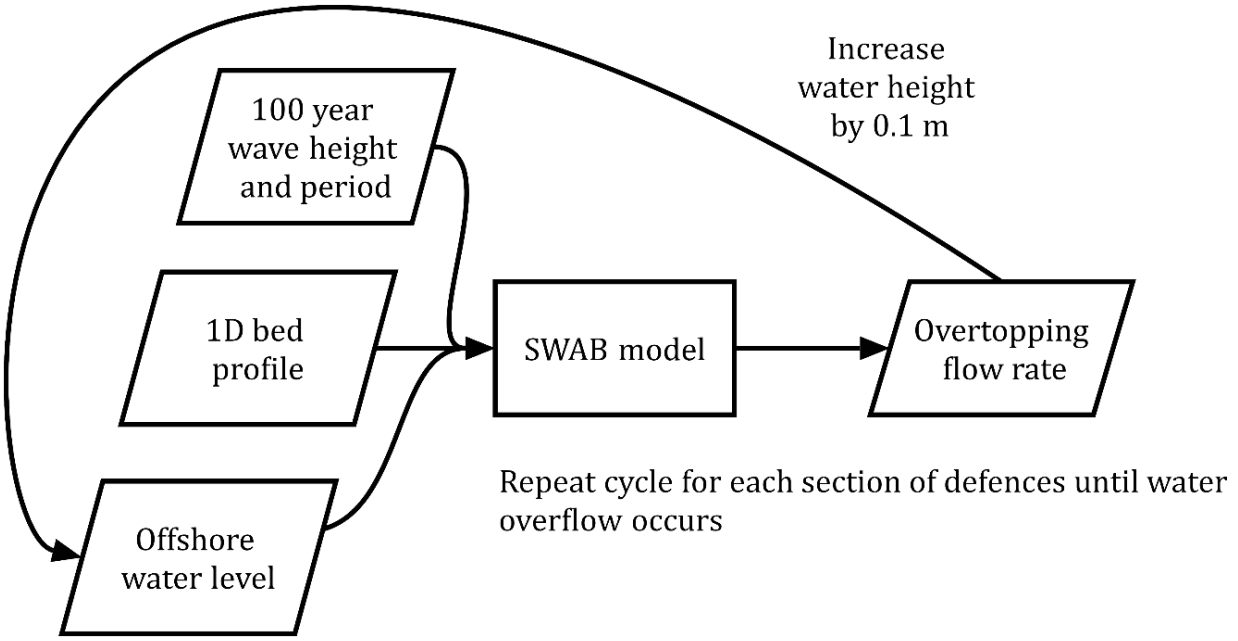

Figure 2.7: Flow chart showing the process of generating overtopping flow rates

This overtopping rate is added into the model domain as a point source of water at any relevant cells, in this case at 5 m intervals (every grid cell) along the top of the seawall defences, to provide the time-varying overtopping during a (in this case 1 in 100 year) event. Repeating this for all of the defence sections it was found that with a sea-level rise parameter of 0.65 m and a storm tide return period of 1 in 250 years only two sets of the defences overflow (Sections 5 and 6 highlighted in Figure 2.3). Figure 2.8 shows the output flow rates for the SWAB model for both section 5 and 6, of the northern defences during the 1 in 250 year storm tide.

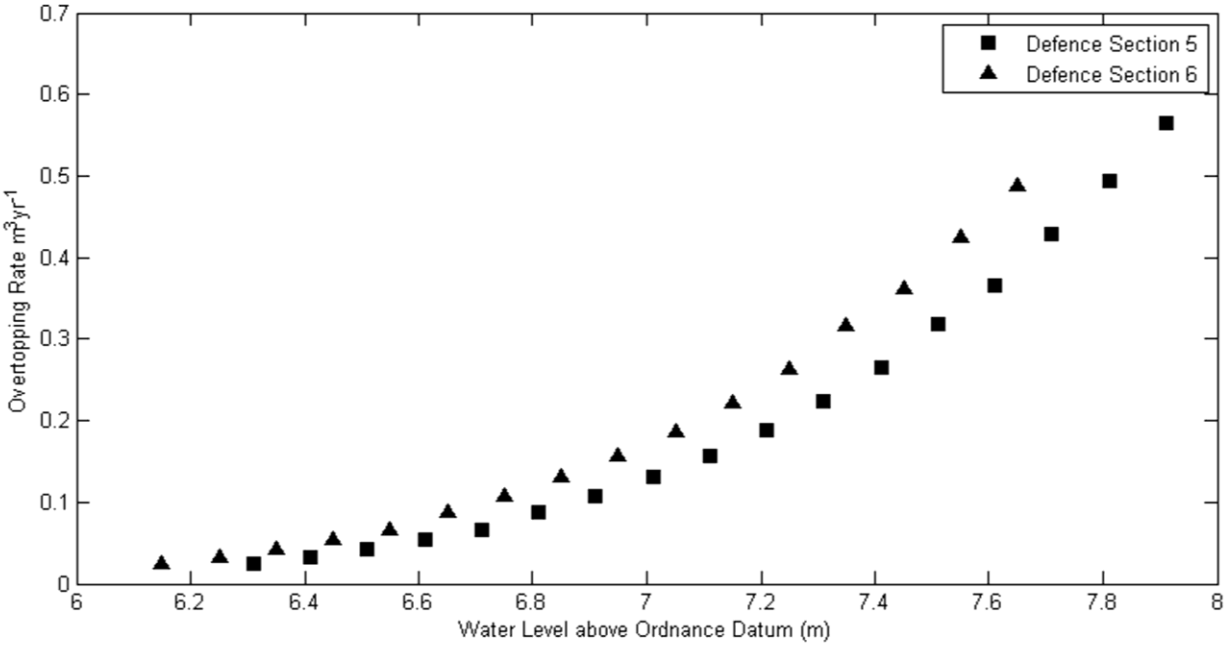

Figure 2.8: Overtopping rates derived by the SWAB model for Defence sections 5 (squares) and section 6 (triangles) during the water elevations of the 250 year storm tide

2.4.1.4 River flow hydrograph

The EA provided a hydrograph that consisted of a suitable high flow river event with a peak flow rate of 150m^3s^{-1}. The gauging station that generated the hydrograph was located on the River Wyre at St. Michaels (Environment Agency Northwest Office, 2013). The high flow event was located in the gauging station's dataset by looking up suitable high flow events within the peaks over threshold (POT) file (Environment Agency, 2009a). Once identified, the EA provided the flow rate at 15 minute intervals matching the input time step of the storm tide allowing the hydrograph to be directly used within the flood simulations. The hydrograph, now representing a high river flow event was aligned within the simulation and timed to peak at the same time as the extreme water level and waves.

The river was simulated by defining the section of the model boundary where the river enters the domain as a time varying water inflow that is forced by the hydrograph time varying flow data (Figure 2.9). The EA also provided the river flow dataset at 15-minute intervals for the period 1976 to 2014. The flow peaks were extracted and a Weibull distribution was fitted which allowed the extrapolation of exceedance values to be calculated. The peak flow of the hydrograph represented a 1 in 50 year extreme river flow rate. Other return periods flow rates could be simulated by scaling the hydrograph to suit the relevant flow rate, in the same manner as the surge curve methodology proposed by the EA. It must be noted that the hydrograph is an example of an observed extreme event and not a statistical representation of all event curves.

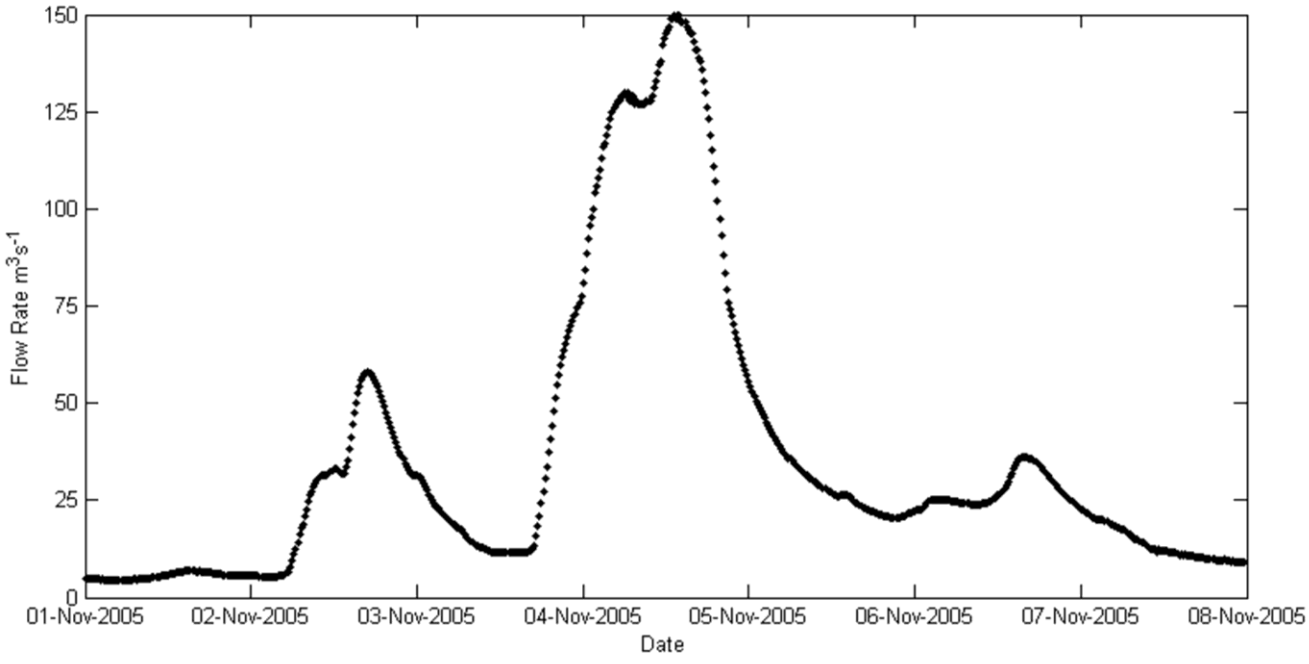

Figure 2.9: Example of a 1 in 50 year Hydrograph for the River Wyre, courtesy of the Environment Agency (Environment Agency Northwest Office, 2013)

2.4.2 Inundation Model

The freely available flood inundation model used here is LISFLOOD-FP (Bates et al., 2010). LISFLOOD-FP is a 2D finite difference inundation model based upon the storage cell approach. This model was first formulated by Bates and De Roo (2000) (Bates and De Roo, 2000) in order to provide a computationally efficient model capable of running on high-resolution LiDAR model domains. It alternatively allows an ensemble of model runs at lower resolution to allow probabilistic determination of variables (e.g. sea-level rise). LISFLOOD-FP has been continually developed since its inception, improving computational runtime and accuracy through inclusion of more realistic features (Bates et al., 2010).

LISFLOOD-FP has been used successfully in coastal applications, such as an assessment of the risk of future flooding in the Severn Estuary (Quinn et al., 2013). By using a probability distribution that is constructed to cover a range of future SLR scenarios by 2100 it was possible to assess the future flood risk to this area, also incorporating the low probability high impact scenarios. Including these low probability scenarios has a significant effect on the flood risk hazard for this study: it was found to increase by 29.7% (Quinn et al., 2013). LISFLOOD-FP has also been used as an inundation model in the Solent, UK (Wadey et al., 2012). The methodology integrated a number of existing approaches for modelling floodplain inundations, including both over topping and defence breaching. The study also noted that the development of practical methods for the application of wave overtopping to the boundaries of coastal inundation models is an important area of future research (Wadey et al., 2012). LISFLOOD-FP has also been used in the Thames estuary for a different approach that simulates extreme sea-level scenarios that could potentially occur if the collapse of the

Western Antarctic Ice Sheet (WAIS) occurs (Dawson et al., 2005). This study combined extreme SLR values that could result from this event with a 1 in 1000 year storm surge. It was found that a new Thames barrier would provide resilience to unexpectedly high SLR because of the large flood storage capacity the barrier would provide (Dawson et al., 2005).

LISFLOOD-FP's ability to explore coastal flooding has been tested on multiple occasions. On one of the occasions the model was tested against a major flooding event that occurred in 1981 (Smith et al., 2011). The goodness of fit between observed and predicted inundation extent is quantified by comparing the sets of image pixels observed to be inundated and predicted to be inundated. Where the pixels overlap and are both inundated this value is equal to 1, if one of the sets of pixels is different to the other then this value is equal to 0 (Bates et al., 2005). Pixel assessment across the whole domain allows the percentage of cells that coincide with each other to be measured giving a goodness of fit score (Bates et al., 2005). In the above case the model scored a goodness of fit for the flood extent of 0.85 (85%), which given the uncertainty in deriving the observed extent is believed to be a good fit (Smith et al., 2011).

The key requirements for LISFLOOD-FP to ensure a good model simulation are an accurate (digital terrain model) DTM, boundary forcing (combination of tidal curve, surge curve and a sea-level rise parameter see section 2.1.1 for more details) and an estimation of the floodplain friction parameters. The DTM data were provided by the EA Geomatics department and consist of a LiDAR survey (Environment Agency Geomatics, 2014). The data have a 1 m horizontal resolution and 0.05 m to 0.15 m vertical accuracy (Environment Agency Geomatics, 2014). To reduce computational cost, the LiDAR data were re-sampled to

5 m horizontal resolution, this reduced the computation time to reasonable levels while maintaining enough detail to resolve urban features such as buildings and roads adequately. Re-sampling did affect the sea defences by smoothing the crest heights. These were digitised back into the raster DTM using a dataset provided by the EA (Environment Agency, 2013). The defence shape file provided the crest heights which were extracted, converted into a raster and mosaicked into the DTM raster file, other topographical features that needed to be removed (such as bridges, which act as artificial dams) or added in (for example lock gates) were digitised into the raster using a similar process. The final grid used within the model was 5 m horizontally with an accuracy of 0.15 m vertically.

2.4.3 Combining with Depth Damage Curves

To place an economic value on the simulated scenario inundation maps, the model cells in each simulation with depths greater than 0.05 m are combined with salt water depth damage curves (Penning-Rowsell et al., 2014). Water depths less than 0.05 m are not considered to be damaging as they are below the vertical accuracy of the LiDAR used for the model domain. Salt water causes more damage than fresh and this is reflected in the depth damage curves. Using these curves the total cost (£M) for each scenario flood event can be calculated. Depth damage curves also vary depending on the land use of the cell inundated, e.g. arable, domestic housing, commercial etc. (see Tables 2.2 and 2.3) and the type of flood water and flood duration. Flood duration is difficult to quantify in these simulations as culverts and drainage measures are not resolved correctly by the 5 m grid. However, the depth damage curves can be selected for different flood durations. With the storm surge lasting for only 44 hours with a significant portion of it occurring during low tide, the short flood duration

curves were used. Arable land-use was classified using the land cover 2007 dataset (OS, 2007). The different cost per hectare categories in Table 2.3 was based on (Penning-Rowsell et al., 2014). Urban, Sea bed, River channel and Salt marsh areas were classified using an Ordnance Survey topography layer (Ordnance Survey, 2013). This layer is a highly detailed view of the landscape which resolves individual buildings, roads and arable areas.

Table 2.2: Salt Water Depth Damage data for Housing, Road and Industrial flood inundation cells based on (Penning-Rowsell et al., 2014)

Housing Damage Curve		Road Curve		Industrial Curve	
depth(m)	cost per flood cell inundated (£)	depth(m)	cost per flood cell inundated (£)	depth(m)	cost per flood cell inundated (£)
0	£0	0	£0.00	0	£0.00
0.05	£3,317	0.25	£9.00	0.25	£1,475.00
0.1	£5,334	0.5	£12.00	0.5	£2,375.00
0.2	£9,109	0.75	£15.00	0.75	£3,075.00
0.3	£11,120	1	£19.00	1	£3,825.00
0.6	£13,525	1.25	£23.00	1.25	£4,425.00
0.9	£14,676	1.5	£29.00	1.5	£5,075.00
1.2	£16,084	1.75	£36.00	1.75	£5,750.00
1.5	£17,383	2	£49.00	2	£6,675.00
1.8	£18,869	2.25	£79.00	2.25	£7,300.00
2.1	£20,134	2.5	£92.00	2.5	£7,875.00
2.4	£21,325	2.75	£98.00	2.75	£8,325.00
2.7	£24,093	3	£110.00	3	£8,825.00
3	£25,308	-	-	-	-

Table 2.3: Inundation cost data for arable flood inundation cells based on (Penning-Rowsell et al., 2014)

Arable Costs	Cost per Hectare per Inundation Event (£)
Arable and Horticulture	1,150.00
Improved Grassland	180.00
Rough Grassland	50.00
Neutral Grassland	100.00

2.4.4 Surge Curve Sensitivity Analysis

Sensitivity analysis on the coincidence of the tidal high water and peak in surge elevation is strongly recommended by the methodology published by the EA (A. McMillan et al., 2011). The procedure followed was to run the flood simulation with the surge curve and tidal high water coinciding, then re-run with the peak surge elevation firstly occurring 2 hours before high tide, and secondly with the peak surge elevation occurring 2 hours after high tide. Comparing the flood extents, volumes and standard deviation of flood depths will show the sensitivity to the relative timing of the two peaks. Table 2.4 shows the output from these three simulations. With an offset of 4 hours (2 hours either side of high tide) the flood extent was found to not change by an area larger than 1000 m^2, the volume varied by a maximum of 30,000 m^3, due to an average depth increase of 0.01 m and the standard deviation by less than 0.01 m. From these results it has been assumed that the simulations are insensitive to surge and tide peak timing. This however only applies to this surge and tidal combination for this domain.

Table 2.4: Inundation statistics for different tide and surge offset simulations

Model Run	Area of Land Inundated (Mm^2)	Volume of Flood Water (Mm^3)	Average Depth (m)	Standard Deviation of Depth
Storm Tide Only Scenario	4.26	4.61	1.08	0.96
Surge peak 2hrs before tide	4.26	4.63	1.09	0.96
Surge peak 2hrs after tide	4.26	4.64	1.09	0.96

2.4.5 Manning's Friction Parameter *n*

The inundation model requires a friction parameter also known as a Manning value *n*, this can be a global value so every cell in the model domain has the same value or varied on a cell by cell basis. For these simulations a cell by cell varied approach was used. This was achieved by using the Ordnance Survey topography layer detailed in section 2.3 (Ordnance Survey, 2013). It was used to produce a grid (Figure 2.10) that had variable friction values depending on the land use. The values shown in figure 2.10 were taken from Purvis et al, 2008 and Burke and Stolzenbach, 1983. Figure 2.10 shows the friction values used for each land-use type.

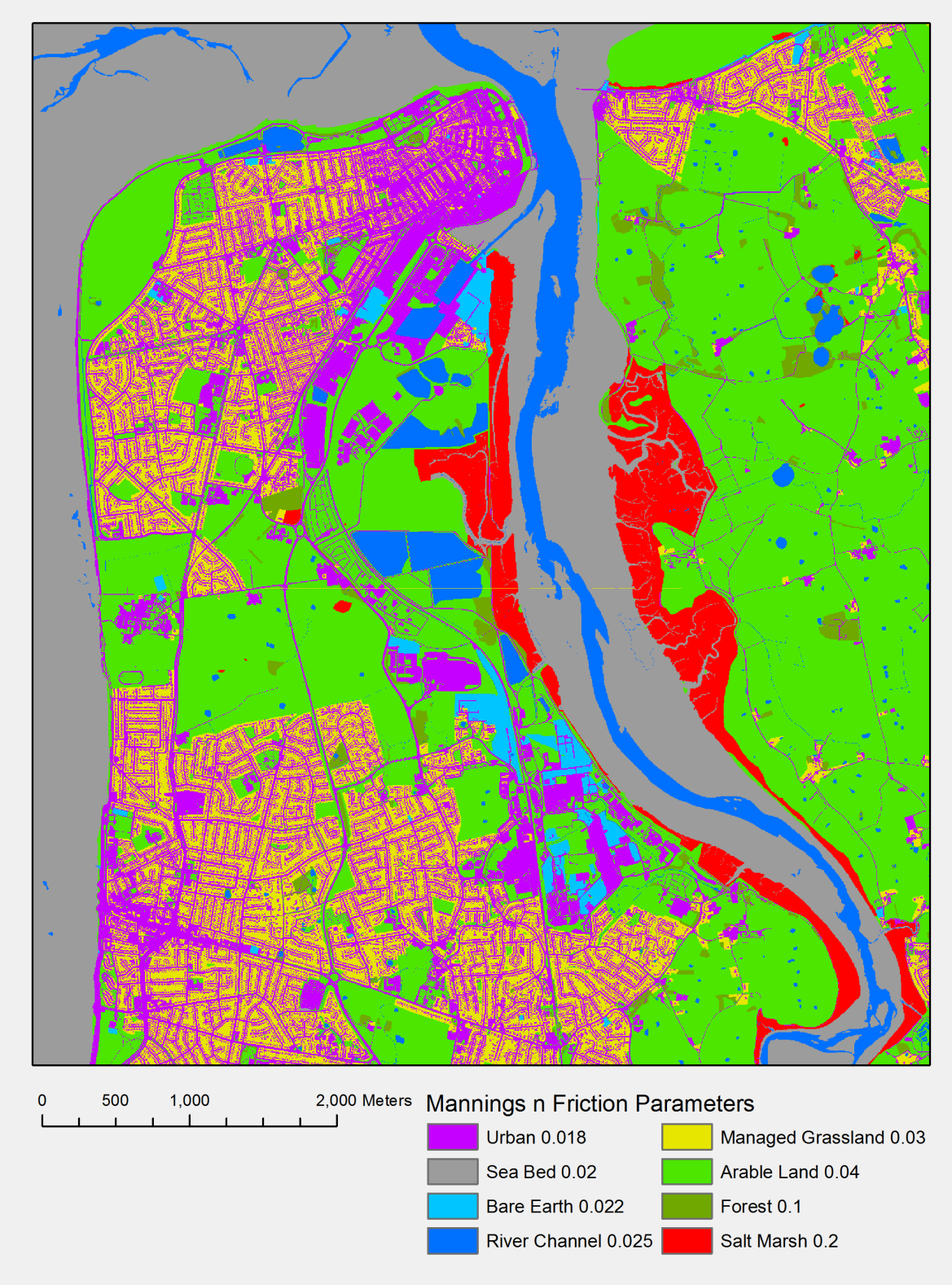

Figure 2.10: Mannings Friction n values for the model domain, the edge of the figure corresponds to the model boundary. (Burke and Stolzenbach, 1983; Purvis et al., 2008)

2.5 Results

The outputs from each simulation detailed in Figure 1 have been displayed over Ordnance Survey topography layer data. The flood extent only shows water depths above 0.05 m as this is below the vertical accuracy of the LiDAR data and a 0.05 m flood depth adds little to the overall cost. Figure 2.11 shows the flood at its maximum extent during the four simulations. All calculated areas, volumes, cost etc. apply to the peak of the storm tide event. Each of the flood sources has had a probability of occurrence calculated for it but the probability of occurrence for each different combination has not been calculated due to the number of variables.

The simulation that comprised a storm tide and SLR, flooded 4.26 Mm^2 of the land area, with a volume of 4.6 Mm^3 of flood water. When the high flow river event was added, this increased to 9.68 Mm^2 in area and 12.2 Mm^3 of water. Removing the river flow and adding 1 in 100 year wave overtopping to the northern defences (the only defences that will overtop in this scenario), covers 8.33 Mm^2 of the land with a volume of 6.99 Mm^3 (Table 2.5). Figure 2.11 shows these inundation projections varying spatially with the high flow river events increasing the inundation extent and depth on the arable east side of the river when compared with wave overtopping. The wave event causes a greater inundation of the urban areas on the west side of the river but with shallower depths on the east side over farm land when compared with the river event. Combining the two events, gives 12.75 Mm^2 of inundation (Table 2.5) of the defined land area with a total volume of 14.04 Mm^3.

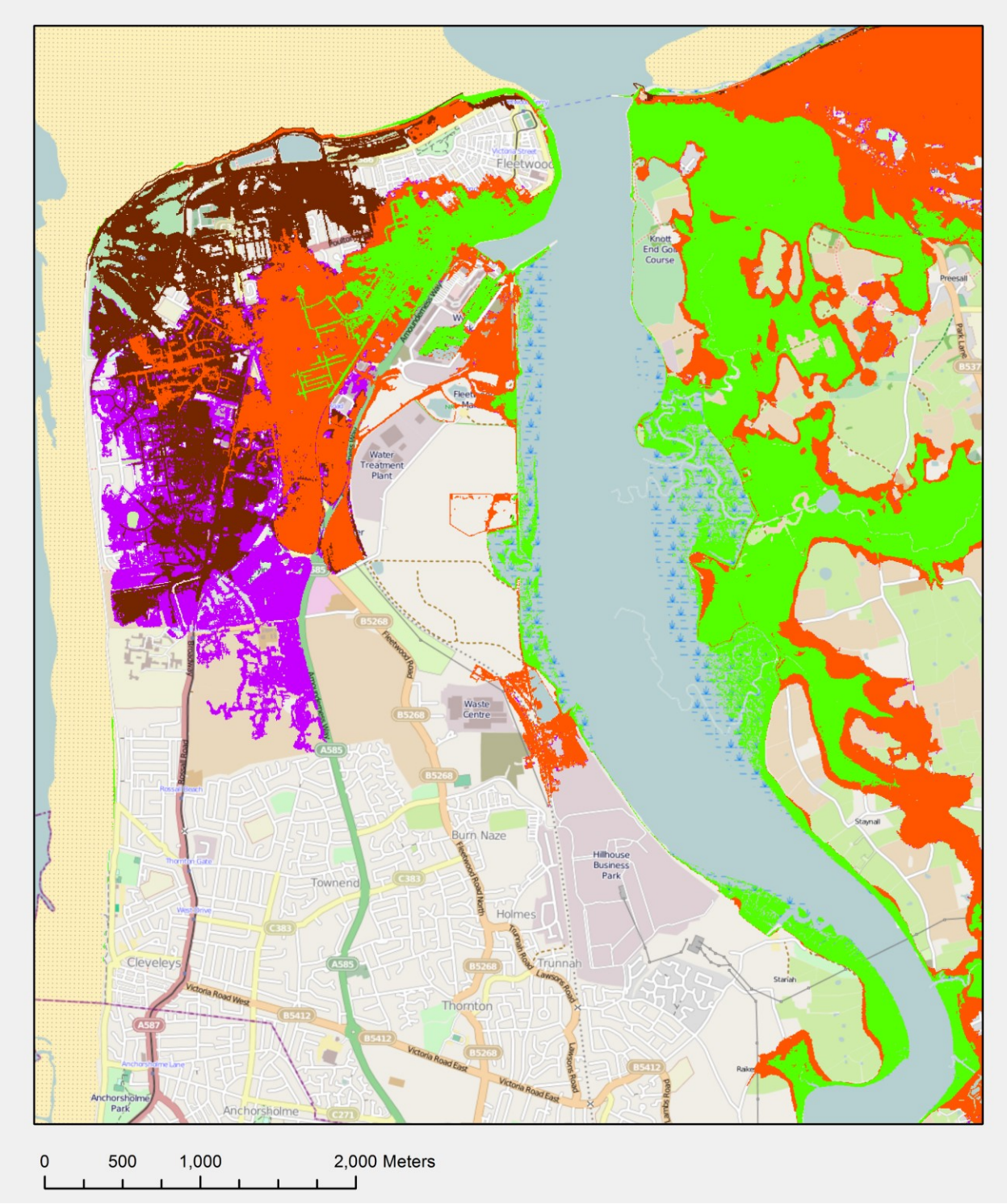

Figure 2.11: Fleetwood Flood Scenarios. Each colour shows the flood extent above 2.25 mOD as a result of a 1 in 250 year storm tide with 0.65 m SLR in isolation (green), with the addition of river flow (orange), wave overtopping (brown) and both waves and river (purple) (Ordnance Survey, 2013)

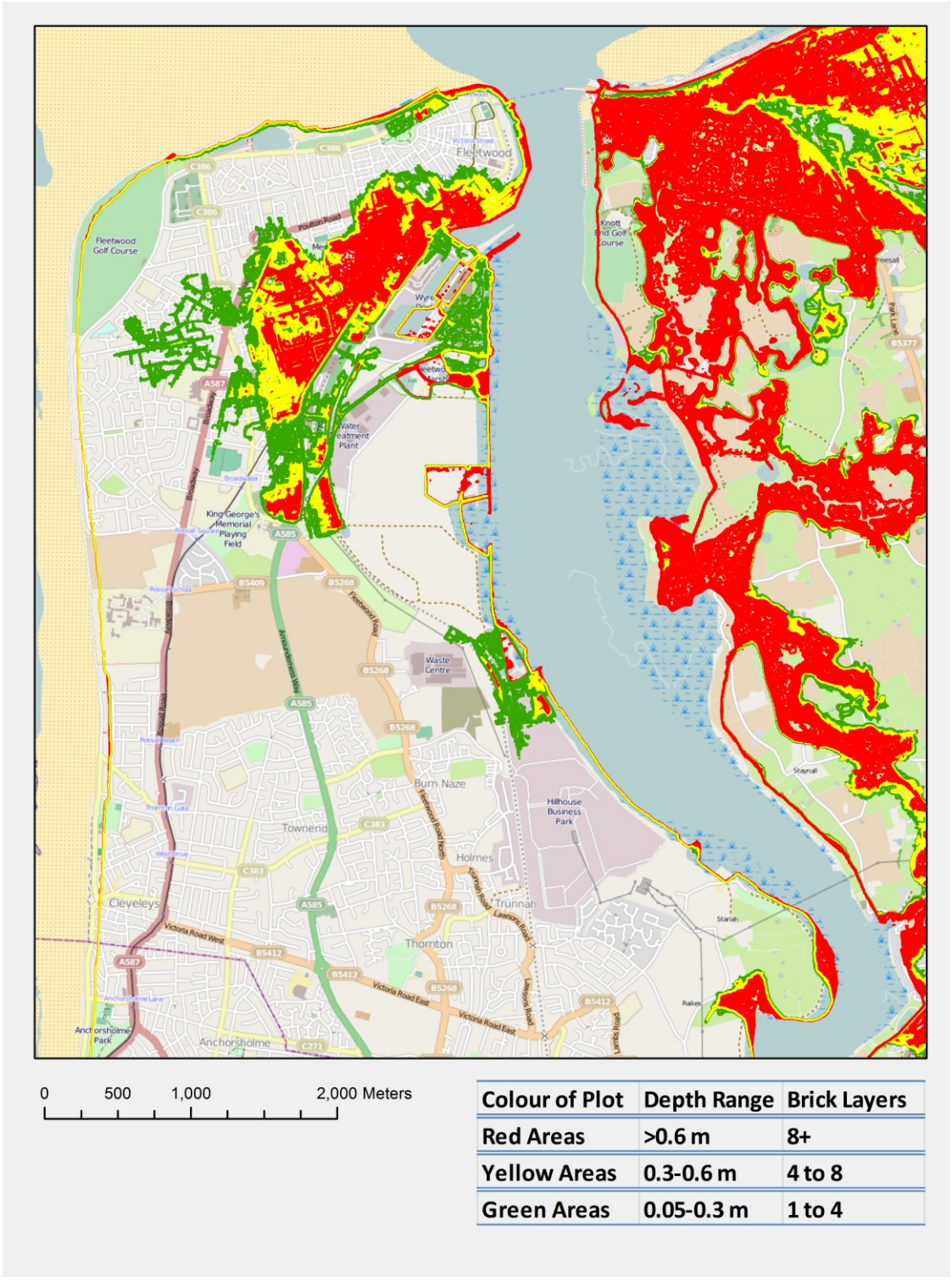

Colour of Plot	Depth Range	Brick Layers
Red Areas	>0.6 m	8+
Yellow Areas	0.3-0.6 m	4 to 8
Green Areas	0.05-0.3 m	1 to 4

Figure 2.12: Example Brick Course Map for the river scenario, 1 in 250 year storm tide, 0.65 m SLR, green areas have flood depths of up to 4 brick courses, yellow areas have flood depths of 4 to 8 brick courses and flood depths of greater than 8 brick courses are in red. (Ordnance Survey, 2013)

Table 2.5: Output statistics for different projected inundation scenarios for a 1 in 250 year storm tide with 0.65m of SLR and additional flood factors

Additional Factor	Area of Land Inundated (Mm^2)	Volume of Flood Water (Mm^3)	Average Depth (m)	Standard Deviation of Depth	Total Cost(£M)
None	4.26	4.6	1.08	0.96	48.87
River forcing	9.68	12.2	1.26	1.01	247.32
Wave overtopping	8.33	6.99	0.84	0.82	224.61
Wave and River	12.75	14.04	1.10	0.97	377.11

The inundated cells have been combined with depth damage curves from section 2.5 for their relevant land-use classification; these are 4 types of arable land (Table 2.3), residential buildings, roads, and industrial buildings. Table 2.6 shows that adding a high river flow event to a storm tide and SLR scenario has an impact of £198.4M increase in cost. Similarly adding wave overtopping creates a cost increase of £175.7M. Combining both forcing together generates an increase of £328.2M.

Table 2.6: Projected costs for each projected inundation scenarios for a 1 in 250 year storm tide with 0.65 m of SLR and additional flood factors

Additional Factors	Arable Land Cost (£M)	Residential Housing Cost (£M)	Road Cost (£M)	Industrial Cost (£M)	Total Costs (£M)
None	0.16	47.68	0.23	0.81	48.88
River forcing	0.26	241.19	0.80	5.07	247.32
Wave overtopping	0.19	218.47	0.62	5.33	224.61
Wave and River	0.28	367.27	1.11	8.44	377.11

Table 2.7 shows the factor increases in area, volume and cost relative to the storm tide with SLR only scenario. Table 2.7 shows that adding a high river flow event to a storm tide and SLR scenario has a factor 2.3 increase in extent but a factor of 5.0 increase in economic cost. Similarly adding wave overtopping has a factor 2.0 increase in extent but a factor 4.6 increase in cost. Combining both forcings together has a factor of 3.0 increase in extent with a 7.7

increase in cost. This indicates that the addition of wave or river forcings causes non-linear increases in cost and extent. Table 2.5 has shown that the factor increase in area and volume is not linear when the two additional forcings are combined together; the same also applies to cost (Table 2.6). It is also clear that using flood extent area as a measure of a flood's impact on a community significantly underestimates the economic impact of the flood. It is shown that the cost increases much more rapidly than the extent/volume of the flood water with more flood sources. It can be seen (Table 2.7) that when using flood extent or area as an indication of impact and not a full spatial depth damage curve cost analysis, under-estimates the economic cost by a factor of 2.2 for the high river flow scenario, a factor of 2.4 for the wave overtopping, and a factor of 2.6 for the combined scenario.

Table 2.7: Comparison of changes in extent and volume and cost for a 1 in 250 year storm tide with 0.65 m of SLR and additional flood factors in comparison to the storm tide with SLR alone.

Additional factors	Factor increase in Area	Factor increase in Volume	Factor increase in cost
River flow	2.27	2.65	5.06
Wave overtopping	1.95	1.50	4.60
Combined	2.99	3.05	7.71

Table 2.8 shows the mean depth with associated standard deviation, the average depth column in Table 2.8 varies from 0.84 m (wave overtopping) to 1.26 m (river forcing). The wave and river scenario has an average water depth of 1.1 m. This is due to the wave scenario having a larger area of relatively low depths which can be quantified by the difference in area compared with the difference in volume for the two scenarios. The river scenario has an increase in inundation volume of 74.5%, compared with only an increase of 16.2% in inundation area. This means that the river is causing more damage (due to deeper depths)

in a smaller urban area while the waves cause less damage (due to shallower depths) but over a bigger urban area.

Table 2.8: Number of building cells inundated with average depth

Additional factors	Number of Building Cells inundated	Mean Depth (m)	Standard Deviation of Depth
River forcing	20238	0.67	0.49
Wave overtopping	22461	0.42	0.34
Combined	32885	0.60	0.46

Waves, while having a lower total economic impact, are likely to have a bigger impact on the community as more buildings are inundated. In the river scenario 20238 grid cells categorised as a residential building (approx. 6746 homes) have been inundated at an average depth of 0.67 m, (Table 2.5) whereas the wave scenario has 22461 building grid cells (approx. 7487 homes) are inundated at an average depth of 0.42 m (Table 2.5). Combining the river and wave scenarios results in 32885 building grid cells (approximately 10,961 houses) being inundated at a mean depth of 0.60 m (Table 2.5).

Figures 2.12 and 2.13 consist of mitigation maps presented as brick course layer maps for both the wave overtopping and river forcing scenario. Brick courses have been defined as a single horizontal layer of bricks in a building which allows a practical way of seeing the impact of the flooding. A brick course has been based on the thickness of a standard brick (0.065 m) and one pointing layer (0.01 m) giving a total height of 0.075 m (Figure 2.14) (Pietruszczak and Niu, 1992). To create these brick course maps, the flood depths have been converted into a contour plot contoured at 0.075 m intervals which have been coloured as follows, green contours showing areas with water depths up 4 brick courses, yellow contours

showing areas with water depths between 4 and 8 brick courses and red contours showing areas with water depths greater than 8 brick courses.

Across all scenarios the worst affected region within Fleetwood is a small area that experiences greater water depths; it is highlighted red area on the west side of the river in both figures 2.12 and 2.13. This area would be a significant hazard during the projected flood events with depths of up to 2.25 m realised. Outside of Fleetwood, the community on the east side of the river that is built along the coastline also experiences significant water depths, especially during the wave overtopping scenario, where the whole area is highlighted red. The red areas on the east side of the river are predominantly salt marshes and arable land which is not significantly affected by short duration flood events. Any areas not covered with a solid colour did not experience any flooding. Water present within the saltmarsh, river and shoreline, i.e. anywhere that normally has water during spring tides has been removed to improve identification of flooded areas for figures 2.11, 2.12 and 2.13.

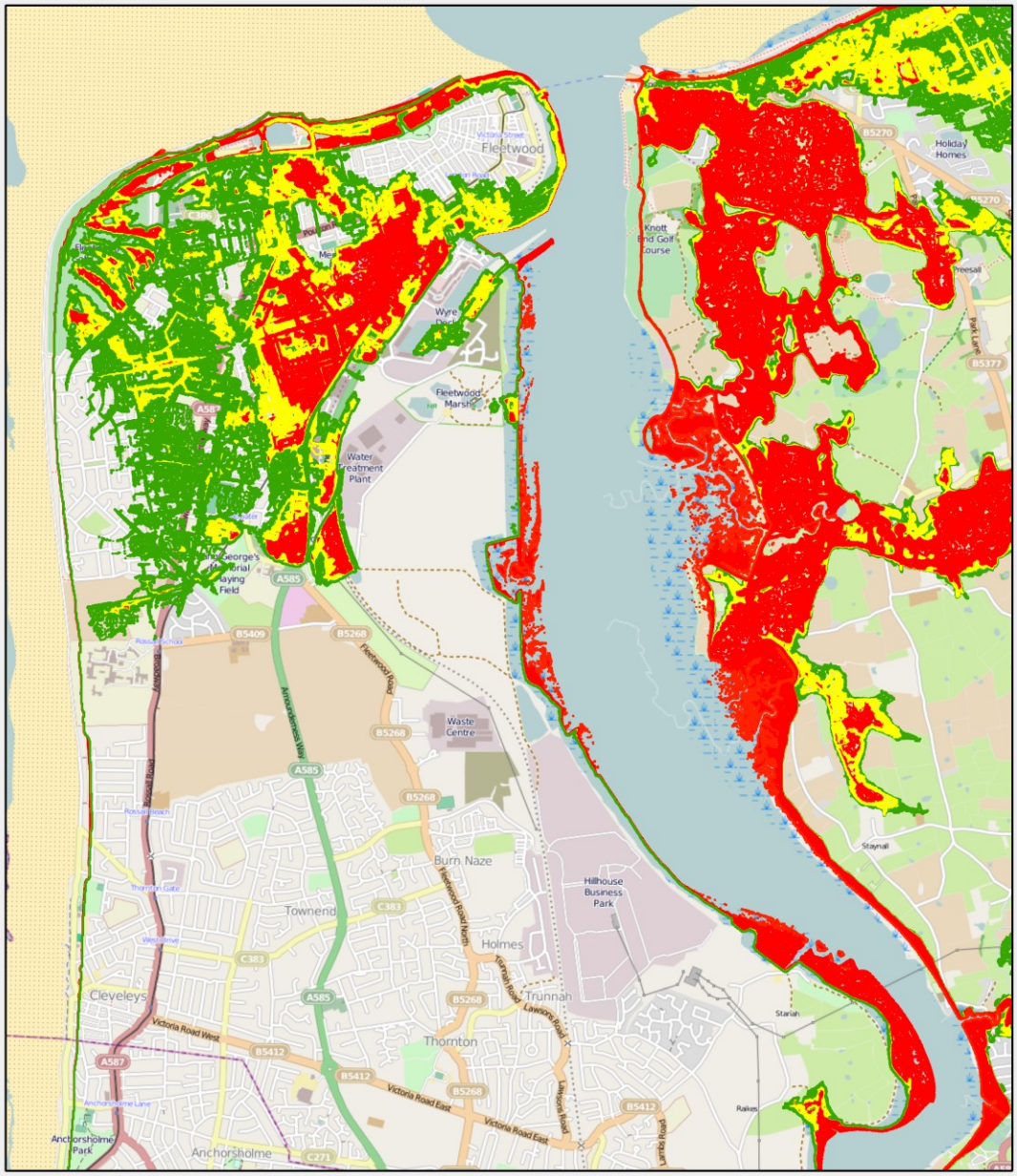

Colour of Plot	Depth Range	Brick Layers
Red Areas	>0.6 m	8+
Yellow Areas	0.3-0.6 m	4 to 8
Green Areas	0.05-0.3 m	1 to 4

Figure 2.13: Example Brick Course Map for the wave overtopping scenario, 1 in 250 year storm tide, 0.65 m SLR, green areas have flood depths of up to 4 brick courses, yellow areas have flood depths of 4 to 8 brick courses and flood depths of greater than 8 brick courses are in red. (Ordnance Survey, 2013)

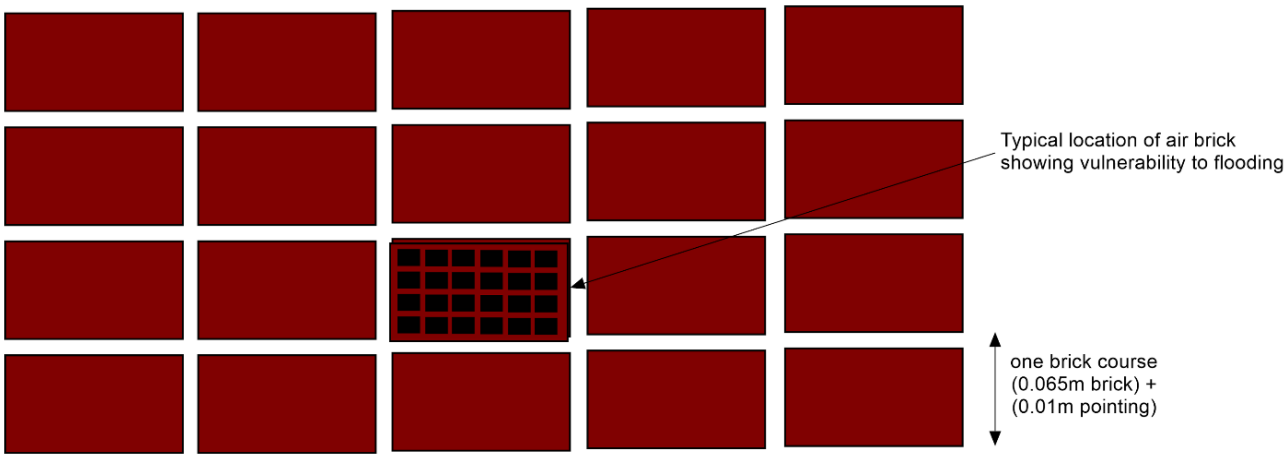

Figure 2.14: Brick course schematic

2.6 Discussion

The scenario flood projections cannot be taken as a prediction of a future event; they are an extreme joint scenario of events with projected SLR. The SLR values used are at the lower probability end of the UKCP09 projections (Lowe et al., 2009), but nevertheless they are still potential outcomes in future climate. Especially if events like the WAIS collapse occur as high levels of SLR are projected as a response to these events.

The recent flooding event in Fleetwood on the 5th December 2013 caused a limited amount of flooding. After discussing the event with the local authority, it was found that water had discharged over the sea defences in the form of windblown spay from waves breaking on the sea defences (Figure 2.15). This is something that currently cannot be added to the inundation model, but if a method could be found to simulate the spray being blown over the defences, then it could be added to the model in a similar manner as the wave overtopping

simulations. This additional capability would be very useful when modelling storm surges like the one that occurred on the 5th of December 2013.

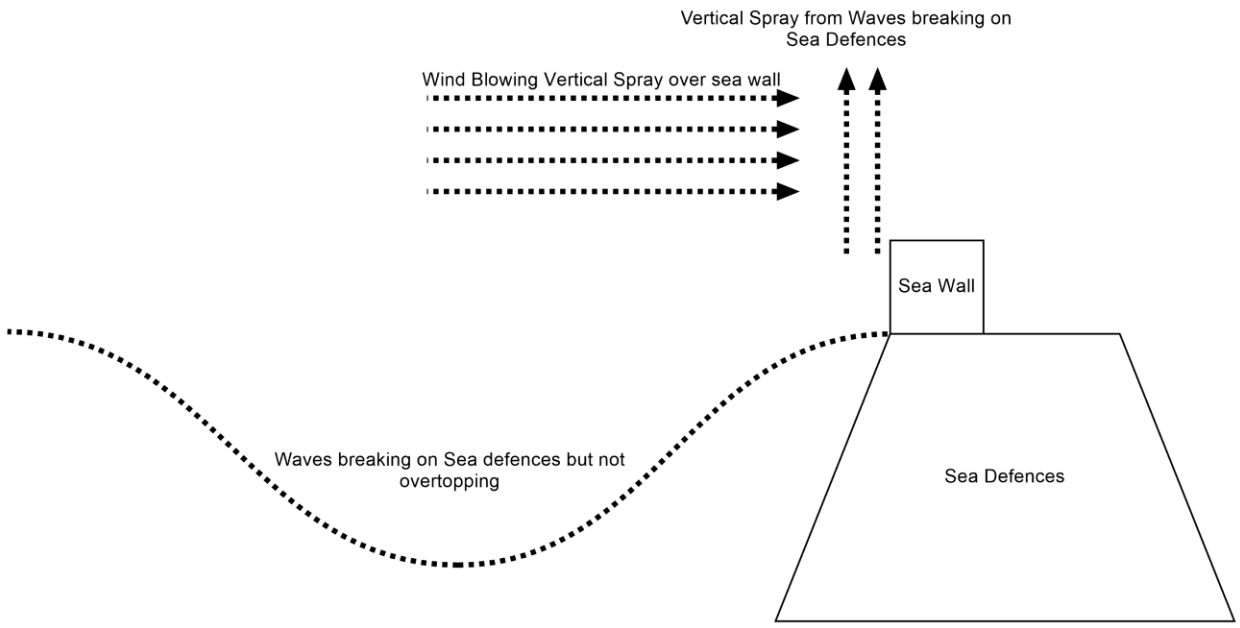

Figure 2.15: Schematic showing wind-blown spray occurring at Fleetwood, during the storm surge on the 5th December 2013

Another factor to acknowledge is that because these events are low probability and represent long-term SLR, any long-term morphological changes that occur during this time period, such as change in the beach profiles and the feedback on tides and wave conditions, will not be accounted for in the methodology. The current shoreline management plan has a "hold the line" policy in this area so it is likely that new defences will be commissioned locally in the future which should be more resilient than the current ones (Halcrow Group Ltd, 2010). Also it should be noted that the inundation model does not account for any changes in the beach profile that may occur in the future, which could affect the flooding in each scenario.

As per section 4, sensitivity analysis was performed on the storm tide flood extent over the Fleetwood domain in response to the timing of tidal high water relative to the surge curve peak. It was found that moving the surge peak 2 hours before and 2 hours after the tide peak slightly increased the average depths of inundation (Table 2.4). The differences in this instance were small (0.01 m), hence it has been assumed that the simulations are insensitive to the relative timing of the surge and tide. However, the analysis is still important as in other cases, with different storm tide, SLR, river and wave forcings, the difference could be significant.

This research shows that adding a high river flow event to a storm tide and SLR scenario increases the flood extent by a factor of 2.3, but increases the cost by a factor of 5. Similarly adding wave overtopping increases the flood extent by a factor of 2.0 but the cost by a factor of 4.6. Combining both forcings together increases the extent by a factor of 3.0 with a 7.7 factor increase in cost. Comparing the changes in extent and volume with the cost indicates that flood risk analysis must consider the economic costs for land usage.

There is significant overlap between the scenarios in Figure 2.11 and it is clear that impacts from either event do not combine in a linear way when simulated together. It is also clear from the breakdown of costs (Table 2.6) that the biggest factor in the make-up of total flooding costs is the cost of residential housing; this is because residential houses have significant costs in clean up and repair (Penning-Rowsell et al., 2014).

To try and mitigate flooding clean up and repair costs to houses the brick course maps (Figures 2.12 and 2.13) can be utilised. They are maps showing green, yellow and red areas that have been flooded. The green and yellow areas are flood water depths under 8 brick

courses, this flood water depth is a significant threshold as houses can be made resilient up to these flood depths. However, for flood depths over 8 brick courses, shown in the red areas of the brick course maps (Figures 2.12 and 2.13), the flood water is likely to cause structural damage if it is unable to enter a property.

As mentioned in the previous paragraph, under 0.6 m water elevation (or 8 brick courses), houses can be made resilient to flooding (Bowker, 2007) flood mitigation measures can be added so the building is able to withstand these flood depths (Bowker et al., 2007). These measures can take the form of periscope air bricks, having the front door elevated requiring steps or a ramp for access and/or a properly fitted cover for the doors of the house which is superior to using sandbags, etc. Recent research carried out by CIRIA (Construction Industry Research and Information Association), the Department for Communities and Local Government (DCLG) and the Environment Agency recommend that for new builds the use of resistance measures should be limited to flood depths of up to 0.6 m. This is because the structural integrity of a standard building may be compromised if the water exceeds this level and puts a high hydraulic load on the property due to flood resilience measures. (Bowker et al., 2007). The possibility of stressing masonry that could induce cracks and leaks is greatly increased above this level (Bowker, 2007). At depths at 0.9 m or greater there is also the risk from large floating debris such as tree trunks and vehicles (Bowker, 2007). Accredited temporary resistance products which cover apertures in buildings have design protection depths of up to 0.9 m and it should be noted that the depth of which structural integrity of buildings is comprised by flood waters is still an active area of research (Bowker, 2007).

From the brick course map in Figure 2.13, it can be seen that it is possible to lessen the impact of the wave scenario in this case study, as the majority of homes at risk will experience less than the flooding threshold for flood resilience measures to be effective. Making the houses resilient from the river scenario (Figure 2.12) will be more costly as it will require river defences and increased river flood storage capacity to keep the flood waters away from the houses or at least mitigate the depth of the flooding to under the threshold for effective flood mitigation measures.

Risk in £yr^{-1} to the coastal communities is notably missing from the results. This is due to the difficulty in calculating the probability of these scenarios occurring. It is plausible for these scenarios to occur at some point in the future, but they are very unlikely to occur in any given year. While the probabilities of each of the events that make up the scenario have been calculated, it is difficult to combine them together into one. This is because the events are not completely independent of each other requiring multivariate analysis to be performed. This is beyond the scope of this paper.

The duration of the flood on a grid cell by grid cell basis is difficult to determine. Although the inundation model is capable of simulating infiltration and drainage, the domain is not sufficiently high enough in detail to resolve all the drainage channels that would be present on the sub-5 m scale. Also, the model would not be able to take into account any pumping work that could be carried out or the drainage provided by any sluice gates. The result from this is that duration times for the drying sections of the simulation are over estimated and cannot be relied on. However, during an extreme flood event the water levels in the drainage

system and groundwater are likely to be high so the maximum flood extent is considered robust, but the drain down and duration of the flooding would not.

This could be improved by running the simulations at a higher resolution but comes at the cost of significantly increased computation time. Being able to define flood water duration for each grid cell in addition to this research would be useful as it would show how long flood waters stay in grid cells, giving coastal managers more information to allow better emergency response planning.

The inundation model also has the ability to output velocities from the simulations, these can be combined with flood depths to generate a flood hazard rating (Wade and Wallingford, 2008). This can be used as part of emergency planning as it will show areas that have a significant hazard to life, values less than 0.75 are considered low hazard, values between 0.75 and 1.25 are moderate hazard, 1.25 and 2.0 are significant hazard and values greater than 2.0 are considered extreme hazard. Even emergency services should not go into areas with a hazard rating of 2 or above (Wade and Wallingford, 2008). Being able to assign these ratings spatially, identifying the highest risk areas would be a significant benefit to coastal communities and coastal managers. Providing information on impacts in areas of high flood risk would allow coastal authorities to warn people living in high risk areas and try to reduce the risk by deploying resilience measures to reduce flood depth heights and velocities.

Being able to calculate the risk in £yr^{-1} for the various scenarios, would be useful in cost-benefit assessments to calculate the most efficient investment options. Examples of these options include:

- Increasing sea defence crest height
- Investing in flood defence mitigation measures at individual house level
- Increasing river flood storage capacity
- Increasing sea defence width to allow height to be increased if needed.

As well as calculating the most efficient investment options, future work could also include deciding the best time to deploy these options and where, for example, which sections of defence to increase in height rather than all of them or which houses would benefit most from resilience measures and when depending on the current level and rate of SLR.

The implications of this work is that areas could be more susceptible to flooding than previous flood inundation models demonstrate as the combination of waves and rivers significantly increases the impact of flood events. This has implications for any community that is located in an area that can be affected by large waves and high river flows.

2.7 Conclusions

We have demonstrated a method to combine accessible physical models to incorporate multiple flood forcing to simulate inundation in coastal flood risk regions where terrain data is available. Using Fleetwood as a case study, a technique to convert the simulated inundation depths into maps of economic impact is demonstrated. Such a conversion is not only applicable to coastal communities but could also be applied to regions at risk of fluvial and/or pluvial flooding. Mapping the economic costs in this way helps to inform flood risk management, providing information to investigate the cost benefit analysis of adaptation

plans to build more resilient communities to future flood risk. The brick course maps have demonstrated a new representation of flood maps that can be easily disseminated to stakeholders and improve engagement.

This study has identified that relying on still water flood simulations can under estimate the economic impact of a plausible future flood event by up to a factor of 7.7. With the addition of other potential flood forcings (in this case wave overtopping and high river flow events), measured parameters are significantly increased creating a much larger impact than if a still water level only scenario was used.

Additionally, using increases in physical parameters to measure the increase in flood impact of an event can lead to under-estimation. In the scenario with additional wave and river forcing, the economic impact increases by a factor of 7.7 over the storm tide only event, where the flood extent only increases by a factor of 2.99.

It has also been shown that the impact from one or the other additional forcings is not linear when combined together. This is illustrated by wave overtopping causing an economic factor increase of 4.6 against the storm tide and SLR only scenario, the high flow river event causing an increase of 5.1 respectively. When these forcings are combined, the factor increase is 7.7 which is less than the sum of the two separate economic impacts of 9.7.

Finally, it has been found in the case of Fleetwood that the main fraction of economic cost is due to residential housing. Mitigation measures that combat the impacts to residential housing should therefore be made a priority in any resilience planning or investment decisions.

In a wider context this paper shows that when performing flood risk assessments of coastal floodplains, it is important to consider additional flood sources, such as wave overtopping in areas with significant wave action, and river flows in areas susceptible to river floods, or in the case of Fleetwood both of these factors. A suitable place to perform this methodology is along the North Wales coastline encompassing the towns of Prestatyn, Rhyl and Towyn and the River Clwyd. For flooding from river flow and storm tide coincidence, the Humber and Thames estuaries are good candidates for this analysis, in which case wave overtopping would be less of a concern due to the lower wave heights experienced in these estuaries.

2.8 Acknowledgements:

The authors wish to acknowledge the following people who have all helped with producing this research article: Paul Bates, University of Bristol for providing the LISFLOOD-FP code to use in the flood simulations; Jeff Neal, University of Bristol for his help in troubleshooting and setting up LISFLOOD-FP; Maurice McCabe, Manchester University for providing access to the online version of the SWAB model and also providing technical assistance; Sveta Jevrejeva, National Oceanography Centre for providing SLR projections and advice; Marissa Lo, for calculating wave height and period exceedance values as used in the SWAB model runs; Samar Tantush for her work on the river flow data and contributions to the river return period analysis. We would also like to take the opportunity to acknowledge Carl Green and Graham Lymbery for their help and advice in selecting Fleetwood as the case study.

3 FLORA: Flood Defence Investment Real Option Analysis Methodology for Energy Infrastructure

3.1 Abstract

The coastal impacts of climate change, including flooding and erosion due to storms and sea-level rise, and the possible adaptation responses have been studied using very different approaches; from very detailed site-specific, process-based investigations and interventions to global macroeconomic assessments of coastal zone vulnerability. This paper presents FLORA, a Flood Defence Real Option Analysis methodology that values potential investment decisions made in the building and maintaining of flood defences around electricity infrastructure at local spatial scales for a large region. Real Option Analysis embraces uncertainty in future climate conditions and flexibility in the management of investment projects to produce a more optimal outcome than with traditional discount cash flow analysis alone. FLORA uses high-level analysis from flood inundation models to assess the cost of flooding for energy infrastructure at the present-day up to the highest plausible sea-level rise for the UK in 2100 known as the H++ scenario, which projects a sea-level rise of 1.9 m. These costs feed into a real option valuation model able to identify which energy infrastructure will benefit from investment, and when. This northwest UK study identifies two infrastructure sites that, today, would benefit from flood defence investment over discount cash flow analysis, increasing to an additional 14 in 2050. FLORA also identifies 46

sites that would benefit from deferring flood defence investment now, reducing to 35 sites in 2050. This method of project valuation can be applied to any feature within the floodplain, e.g. infrastructure or residential housing, making it an adaptable and useful tool in identifying vulnerable features that require investment to ensure they stay resilient to extreme flood events in the future. FLORA is the result of an inter-disciplinary collaboration between hydrodynamic modelling, flood risk assessment and economics. The outputs of FLORA are ideal to be fed into a decision-support tool, allowing stakeholders to interrogate and disseminate information about the spatial locations they are interested in.

3.2 Introduction

The impacts of marine flooding in densely populated and infrastructure-rich coastal cities have received a lot of attention in the climate change impact literature (Bosello and De Cian, 2014). Hurricane Katrina killed more than 900 people from flooding alone on the US Gulf coast in 2005. In Europe, Storm Xynthia killed more than 50 people in 2010 through flooding on the French Atlantic coast. Most recently the super typhoon Haiyan in the Philippines generated storm surges up to 7 m in height and causing widespread damage and considerable fatalities (Lapidez et al., 2015). Coastal areas are characterized by high concentrations of human settlements: population density is on average three times the global mean (McGranahan et al., 2007; Small and Nicholls, 2003) and large numbers of people and assets are already exposed to coastal flooding (Bosello and De Cian, 2014). Exposure to flooding is expected to increase with growing coastal populations and the economic relevance of coastal cities (Nicholls, 2004; Nicholls and de la Vega-Leinert, 2008).

Accordingly, the impact of climate change, particularly sea-level rise (SLR) in coastal areas and cities is a major concern (Handmer et al., 2012; Stevens et al., 2015).

Due to its prevalent location in coastal areas, climate change, sea-level rise and extreme events represent significant challenges to the global energy infrastructure and supply (Reichl et al., 2013). The UK Energy Networks Association (ENA) identifies the biggest pressure to be from coastal flooding - if an electrical substation is flooded. Costs in clean up and repair can be high and ongoing costs in disruption and loss of supply have the potential to add to this significantly (Energy Network Association, 2009). Research has found that electricity generation infrastructure is vulnerable to severe weather and water shortages (Bartos and Chester, 2015; van Vliet et al., 2012); and transmission and distribution infrastructure is likely to be stressed by rising demand and increasing temperatures (Bartos and Chester, 2015; Government Accountability Office, 2014; van Vliet et al., 2012). In addition it is also likely that the impacts may be amplified due to energy system interdependencies, and the compounding effect of multiple climate impacts (Government Accountability Office, 2014).

Increased temperatures contribute to future risk to infrastructure resilience by derating power lines and transformers while also increasing vegetation interference on power lines. An increased likelihood of droughts and heatwaves mean soils are more likely to dry out, creating earthing problems with associated potential ground movement. However, it is currently accepted that the relative impact of these risks will be minor (Figure 3.1) (Cradden and Harrison, 2013; Energy Network Association, 2009, 2007).

A temperate, maritime nation, the UK is susceptible to coastal flooding (Prime et al., 2015). The storm surges in the winter of 2013/2014 caused a large amount of damage in the UK, particularly to infrastructure located on or near the coast. The events of 2013/2014 were clustered together (Wadey et al., 2014) resulting in the stormiest period in 143 years (Matthews et al., 2014). Being resilient to extreme events like storm surges means that there would be little or no damage to repair which could be considerable after a cluster of extreme events impacting on the coast. Under rising mean sea levels that are expected up to and beyond 2100, the damage from coastal flooding is expected to increase so adaptation must be made to combat rising damage cost. The UK has three times as many coastal facilities than any other European country (Brown et al., 2013). The infrastructure or assets that supply electricity to consumers can be split up into three different types of asset:

- Generation assets
- Transmission assets
- Distribution assets

Generation consists of assets that generate electricity, such as coal, oil and gas power stations, but also include nuclear and renewable sources such as wind and solar. Transmission takes the high voltage electricity generated by generators and transmits it nationally and internationally to regions for distribution to consumers. Distribution is where the high voltage electricity is stepped down to more useable voltage for local consumption - this is also where renewable energy generators tend to feed in. This study focuses on the larger distribution infrastructure at risk, the primary and grid substations. Secondary substations are not considered as they are located in the area that they supply and if they are

flooded then the area that they supply is usually also flooded, so the resilience of the area is more important than the impact of the substation being flooded. Other assets in the electricity networks such as pylons, towers, cables etc. are not believed to be typically impacted by or vulnerable to coastal flooding, unless such flooding is long-term and maintenance assess is thus prevented. Investment in maintaining and improving the resilience to coastal flooding is therefore important, particularly when the potential impacts of climate change and sea-level rise are considered. This research does not take into consideration the residual life of the substations as this information was unavailable. This would be a key factor for managers when deciding on future investment and would be beneficial to include in future work.

Combating the impacts of a changing climate will require a multidisciplinary approach, consisting of combining a global assessment of climate change expressed as regional projections of relative sea-level rise in conjunction with a flood inundation model assessing the flood risk at the regional scale, with a financial methodology assessing the relative costs of strategic intervention and flooding damage, clean-up and repair. This approach also provides detail on optimal times for investing in building resilience to the impact of climate change.

3.2.1 Energy Infrastructure, Risks and Investment

All markets require strategic investments in an environment of uncertainty. Typically, the response to this uncertainty is by making corrections on project implementation, investing in stages, and/or deferring projects (Pringles et al., 2015). These decisions to invest or

disinvest depend on the development of events and traditional modelling procedures such as cost-benefit analysis (CBA). The UK ENA produced matrix (Figure 3.1) highlights the different risks that are projected to impact on energy infrastructure by 2100 rated by relative impact and relative likelihood. The greatest impacting and highest likelihood risk to resilience is coastal flooding (R12).

One of the main causes of coastal flooding is from storm surges, which occur when high winds and low atmospheric pressure during a storm raise the level of the tide at the coast. If this occurs in conjunction with a high tide, particularly a spring tide then water levels above the predicted tide can occur resulting in an extreme water level (EWL). This can lead to flooding, resulting in infrastructure damage and failure. It is important that this infrastructure is able to withstand and be resilient to extreme events that could occur now and also in the future. As the infrastructure's resilience; will decrease due to increasing mean sea-levels (Haigh et al., 2010; Menéndez and Woodworth, 2010; Wahl et al., 2011). If future SLR can be known with any degree of certainty, then cost-effective investments in defences to maintain and improve the resilience to coastal flooding could be made. Future SLR has a large degree of uncertainty, which increases the longer the time horizon is for the projection of SLR being made (Jevrejeva et al., 2014). This uncertainty makes the decision to invest in flood defences difficult as building defences based on the most likely estimate of SLR could result in defences that are not adequate for the extreme flood events that are realised in the future; equally building defences to cope with the highest level of SLR projected is highly likely to waste resources due to the low probability of this SLR being attained.

When traditional investment frameworks are applied to infrastructure investments, they readily lead to suboptimal irreversible decisions being made. Under- or over-estimation of the future SLR could lead to investments not being made in substation sites that would benefit from flood defences and investments being undertaken at sites that are unnecessary. The most widely used traditional investment procedure is known as Discounted Cash Flow (DCF) where the future cash flows of a project are compared with the benefits of the project. This technique allows the summation of the economic performance of the project into a single metric known as Net Present Value (NPV). DCF has limitations in its methodology where any flexibility in investment decisions is not accounted for (Majd and Pindyck, 1987; Phung, 1980).

In investment environments where there is uncertainty, such as the future climate, management flexibility can provide economic value and methods that recognize and value this flexibility has been developed in the past. Real option analysis (ROA) has proved to be a powerful approach for addressing this valuation flexibility. ROA has been adapted from financial option analysis, which values stocks and shares to value physical assets. ROA assesses the implied value of flexibility that is embedded in many investment projects. In contrast to DCF valuation that considers management as a passive player, real options assume that management is an active player able to take advantage of new information. This flexibility that results from the acknowledgement that investment plans are modified or deferred in response to the arrival of new information such as updated SLR projections. While the new information can never fully complete the picture it can help to reduce the uncertainty in investment. ROA has been applied to energy generation projects that consider different types of options and uncertainties - these include, flexible investment in nuclear

power plants in Japan, hydroelectric plants in Brazil and renewable energy projects in the UK (Abadie and Chamorro, 2014; Caminha-Noronha et al., 2006; Kiriyama and Suzuki, 2004). Using ROA for other areas of the energy industry such as transmission and distribution networks is much more limited, particularly for investments in increasing the resilience of infrastructure.

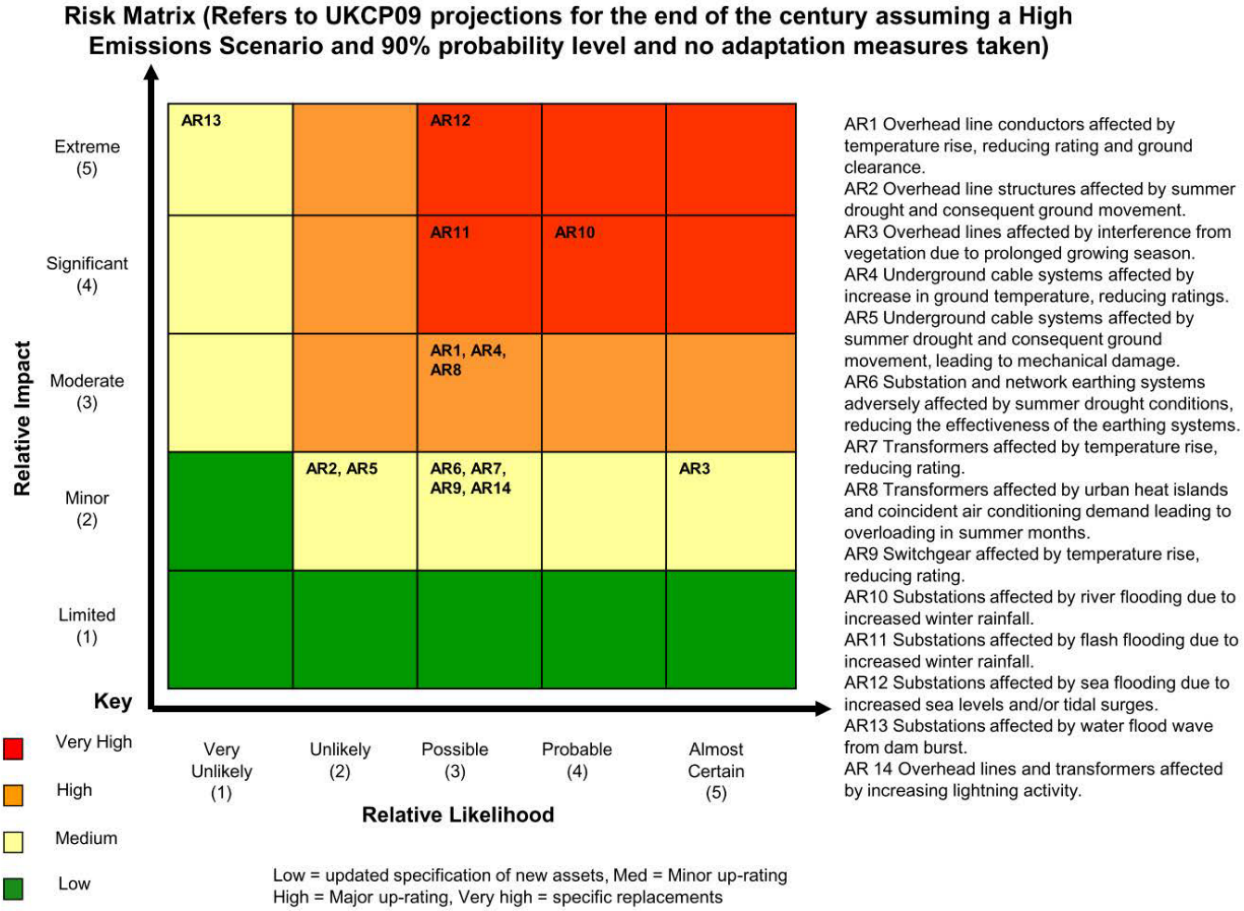

Figure 3.1: Risk matrix showing biggest projected risks to energy infrastructure up to 2100. This assumes that no adaptation measures are taken and that the high emissions scenario of United Kingdom Climate Projections 2009 (UKCP09) at the 90% probability level is the climate scenario that is realised (Energy Network Association, 2009)**.**

3.2.2 Study Site

The site selected for this study is part of the northwest UK coastline running from Southport in the south to Morecambe in the north, incorporating Blackpool and Fleetwood. This case study provides an example of the regional flood hazard to infrastructure to demonstrate how the FLORA methodology could be applied to other regions. Its location is shown within the wider context of the UK (Figure 3.2) and as a close up of the whole area (Figure 3.3). The Environment Agency's (EA) flood risk map presented in Figure 3.4, indicates large parts of this region are in an area of medium to high flood risk.

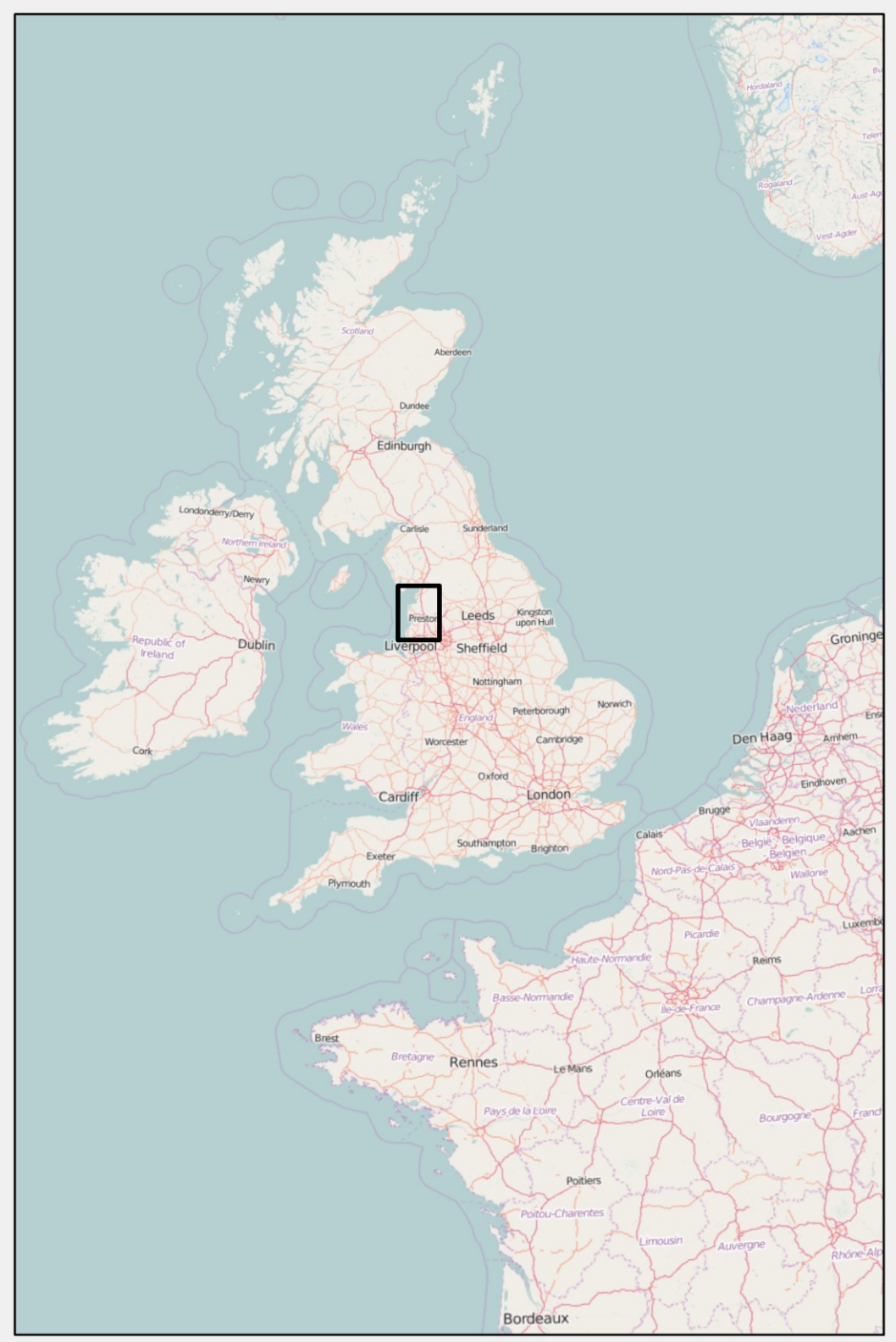

Figure 3.2: Map showing location of study area within the United Kingdom.

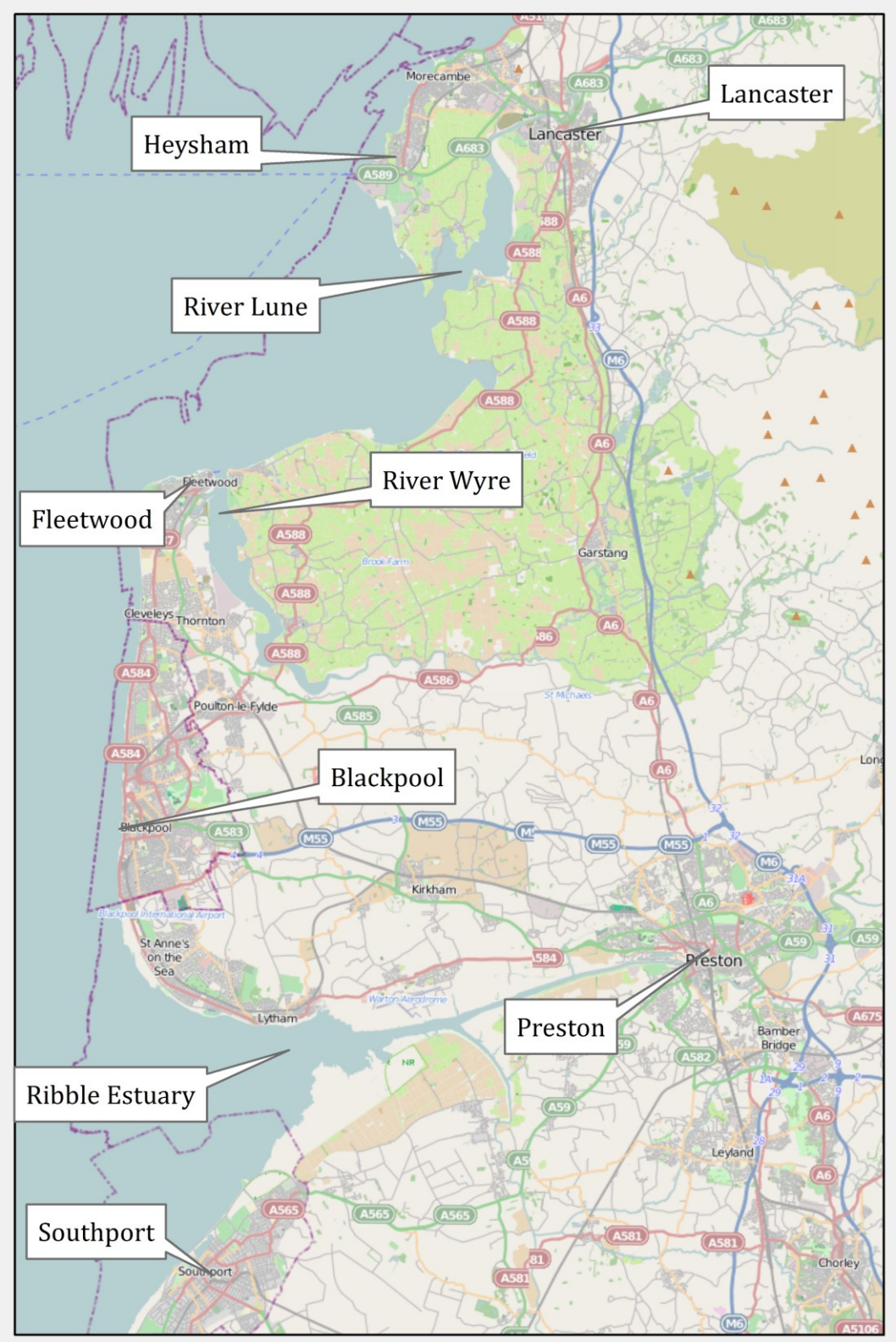

Figure 3.3: Map showing close up of study area with place names

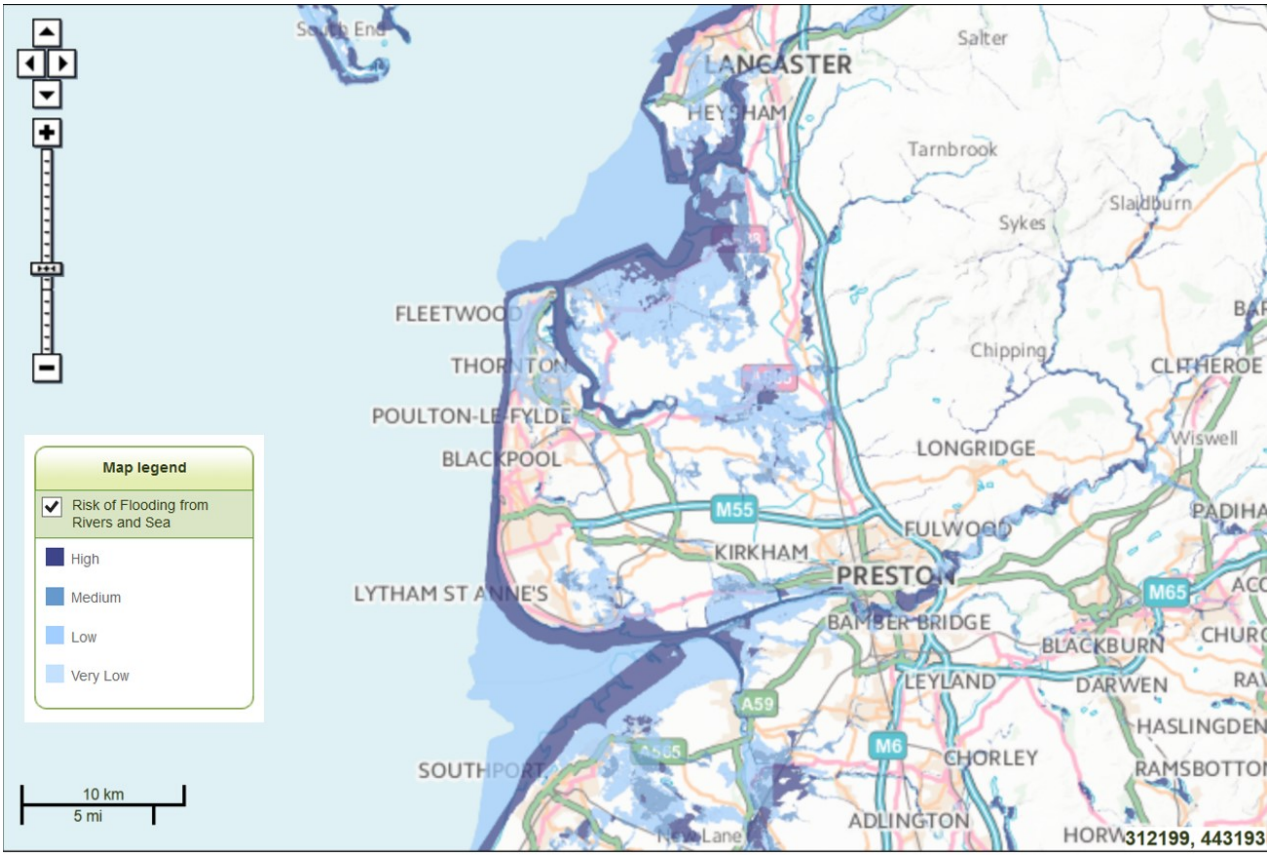

Figure 3.4: showing the extent of the Environment Agency Flood Risk for the study area (Environment Agency, 2016).

Electricity Northwest, the study region's electricity distribution company, provided a database detailing all of their assets and this amounts to over 3000 different assets. Distribution infrastructure has three types of substation, grid, primary and secondary. Grid and primary feed into large areas and consequentially have a large impact on the region if flooded. Grid and primary substations were defined to be any asset on list with a perimeter larger than 30 m. Once this filter had been applied it left 388 assets to assess (Figure 3.5).

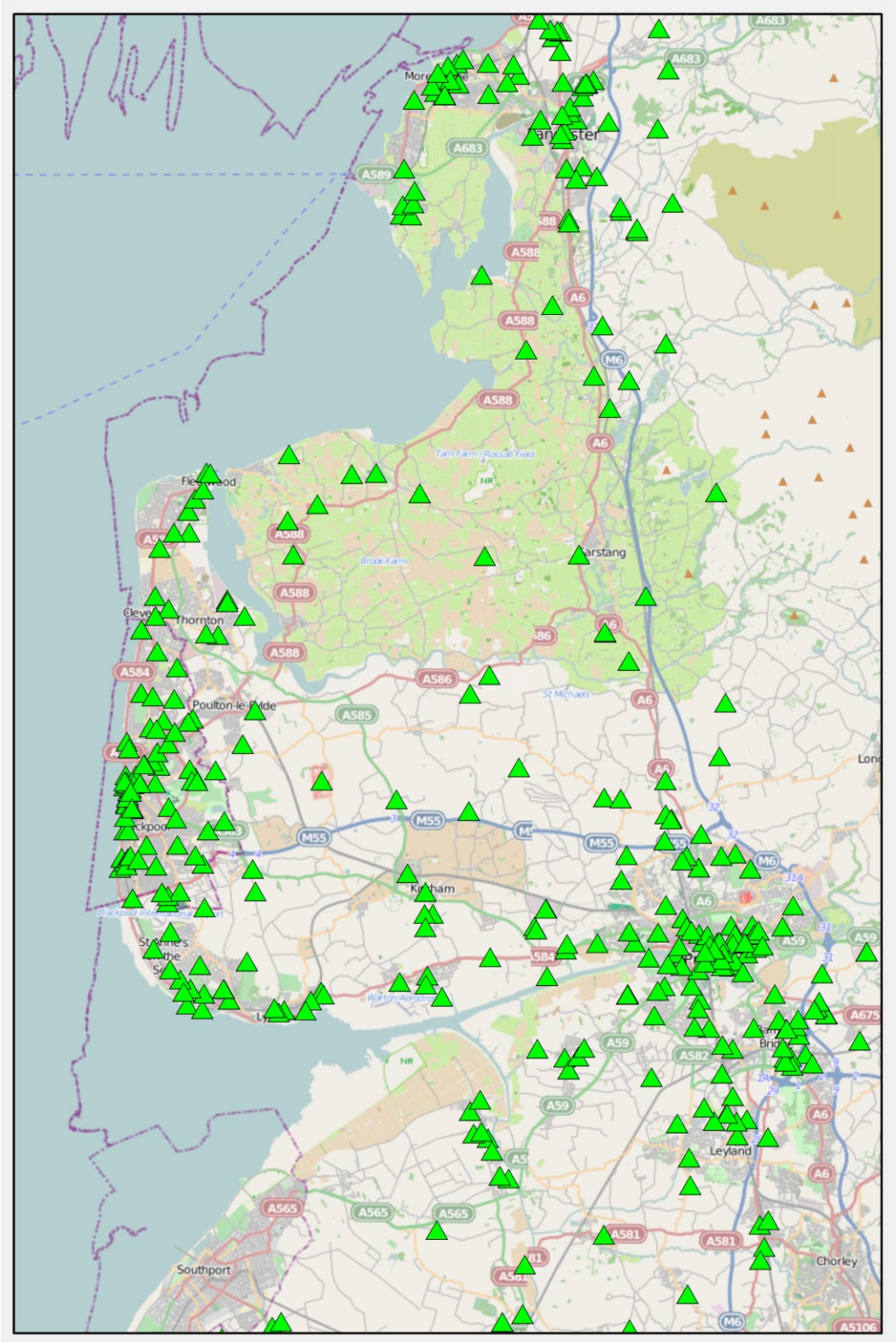

Figure 3.5: Green triangles denote the location of the 388 substations in the study area with a perimeter greater than 30 m.

Figure 3.5 shows the geographical locations of the assets. From Figure 3.5 it is clear that most of the substation assets are located in areas of risk, i.e. close to the coast, rivers etc. Comparing the asset locations with the flood risk map from the EA indicated that some assets are in a flood risk area already and this number will only increase up to 2100. For this study the present-day sea defences will be incorporated in the flood inundation simulations, and assumes that these defences will not be upgraded over the time period of this study.

3.3 Methodology

The methodology presented in this paper, FLORA (FLOod defence Real option Analysis) involves multiple steps to produce an annual cost due to flooding (Figure 3.6). This cost can be viewed as a revenue stream of damage avoided if flood defence investment takes place. The revenue stream will continue for the whole of the defence lifetime and will likely increase over time due to higher costs of flooding with increased mean sea-level. The costs of building and operating the defences can be offset from this revenue stream, giving a net present value for flood defence investment decisions. This means that a SLR projection value is required for every year of the defence life span starting from the potential investment point. In this study the defence life span is 50 years so investment decisions can only be assessed 50 years before the end of the SLR projection, which in this case is 2100. However, longer SLR projection datasets and defences with a shorter life span can be used to increase the investment decision time horizon.

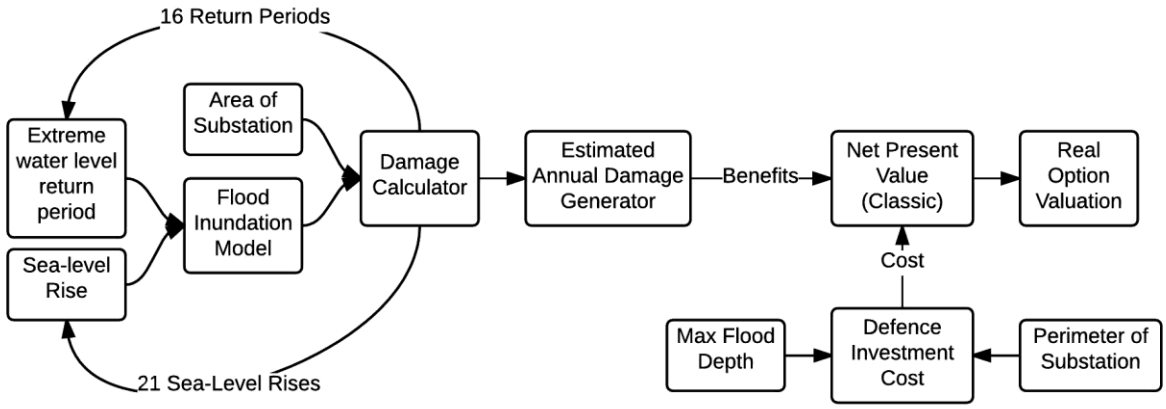

Figure 3.6: Schematic showing the process used to calculate benefits/revenue and costs for input in real option valuation analysis.

3.3.1 Real option analysis

Real option analysis is an extension of financial option theory (Black and Scholes, 1973; Cox et al., 1979). The main feature of financial option theory is that financial assets are valued under uncertainty. While financial options are written as an explicit contract, real options need to be recognized and specified. A financial option is an option that when purchased grants its owner the right but not the obligation to buy/sell a financial asset after a specified period of time. This is comparable to a company that makes strategic investments having the right but not obligation to take advantage in investing in the future. Real options are embedded in plans, projects or investments. An example of this is the ability to postpone or defer an investment to await the arrival of key information. Real options can also be used to value real assets under uncertainty (Farrell, 2012; Kjærland, 2007).

To derive a real option valuation three methods may be used. These include (i) stochastic differential equations, (ii) dynamic programming and (iii) simulation models. Under specific

conditions an option can be valued using a stochastic partial differential equation (PDE). The solution of the PDE provides the value of the option as a direct function of the inputs. The Black-Scholes equation (Black and Scholes, 1973) is considered the seminal work on option valuation theory. Dynamic programming is an approach based on splitting the whole problem into two basic constituents, the immediate decision and a function that summarizes the consequences of all future subsequent decisions starting from the immediate decision. An example of this approach is the binomial lattice (Cox et al., 1979). Finally, the approach used in this study is simulation models where thousands of likely paths of underlying asset evolution are generated by Monte Carlo sampling (Boyle, 1977). For each path the optimal investment strategy is determined and the option return is calculated. The option value is estimated as the average of the option returns for all paths, which will identify which substations would benefit from flood protection and when between the present-day and the end of the investment decision time horizon. The next sections will highlight each of the stages outlined in Figure 3.7 and produce a real option analysis covering all the substations in the study area.

3.3.2 Flood Inundation Simulations

To assess the impact of coastal flooding a flood inundation model was used. LISFLOOD-FP was first formulated by (Bates and De Roo, 2000) in order to provide a computationally efficient two dimensional hydrodynamic flood inundation model. LISFLOOD-FP is a freely available 2D finite difference model based on a storage cell approach. It has been continually developed since its inception, improving computational runtime and accuracy and has been used successfully in coastal flooding applications, including flood assessment within the

study area. LISFLOOD-FP has also been tested on multiple occasions, and was found to have a good fit between the predicted and observed flood inundation extent making it suitable for this study (Smith et al., 2011).

The method used to simulate coastal flooding follows the same methodology as (Prime et al., 2015); where extreme water levels with as determined frequency of occurrence are combined with a synthetic storm surge curve and a predicted high tide to create a storm tide of a specific return period. A SLR parameter can also be added to simulate the storm tide in the future based on SLR projections. Storm frequency data were provided by the Environment Agency (EA) and consist of 16 extreme water level return periods every 2 km along the UK coastline and synthetic surge curves at the major tide gauge locations around the UK (A. McMillan et al., 2011). In Prime et al. (2015) this process was only completed for one extreme water level return period and one sea-level rise projection. However, for this study the process was completed for all 16 return periods provided, from 1 in 1 year up to 1 in 10,000 years. It was also completed for 21 projections of sea-level rise (SLR) 0 to 2 m in 0.1 m intervals. This range of SLR is based on the maximum plausible SLR by 2100 as part of the H++ scenario within UKCP09. A flood simulation is required for each of the combinations of return period and SLR values, which results in 336 different simulations. The simulations given in Prime et al. (2015) took around 36 hours to run across 15 processor cores. The study region is also much larger than in Prime et al. (2015) so in light of this, it was necessary to increase the computational efficiency. To do this the horizontal resolution of the flood model was increased to 50 m from 5 m. The flood inundation model output consists of a grid matching the horizontal resolution of the model domain. It contains the floodwater depth values at the maximum extent of the inundation. A substation site location will correspond

to one of these 50 m grid cells, any flood water depth within this grid cell is assumed to result in the same depth at the substation site. Figure 3.7 shows an example flood inundation output from a simulation for the study area.

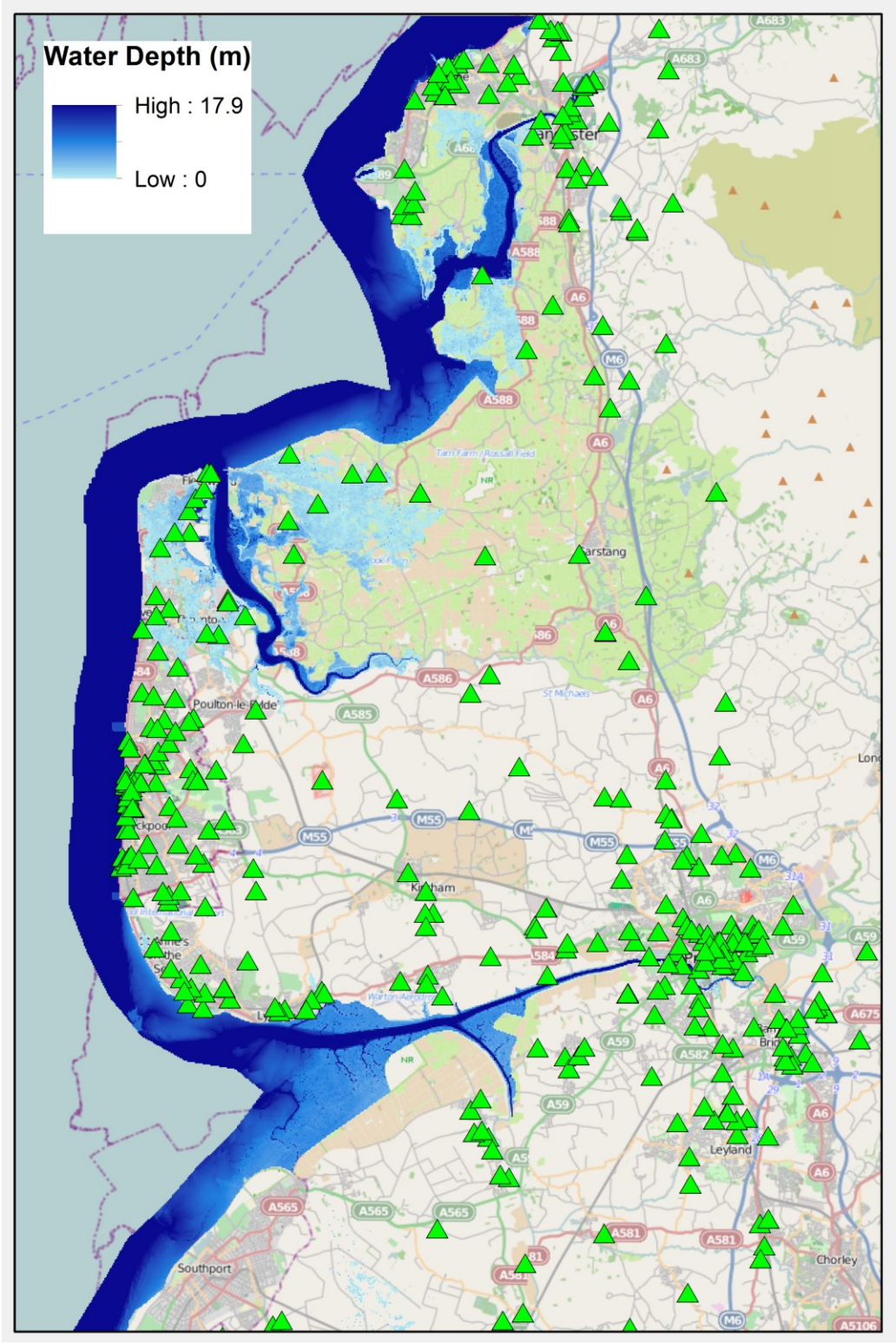

Figure 3.7: Example inundation output for study area, scenario shown is a 1 in 200 year 0.5% annual probability event with 0.5m of SLR realised. Green triangles highlight assets being assessed.

3.3.3 Calculating Economic Damages

To determine the impact of a flood inundation scenario a monetary cost needs to be derived. This is achieved using a depth damage curve (Penning-Rowsell et al., 2014). A depth damage curve shows the relationship between floodwater depth and the relative clean up and repair costs. Beyond the scope of this study, other costs can be added to the curve, that also take into account disruption and compensation paid to consumers also the cost of not transmitting electricity when the substation is damaged. This curve was provided by the Flood and Coastal Erosion Handbook 2014 (Penning-Rowsell et al., 2014). This publication details many different depth damage curves for different infrastructures, different types of residential housing and also different types of arable land. It also provides curves for different forms of flooding, from the type of water (salt water or fresh) to the length of duration (short or long). Short duration is classified as a few days, typical of a storm surge. Whereas long is classified as being over several days, typical timescales of river flooding. For this work the short duration salt water curve for substations was used (Figure 3.8) this also shows the curves used as part of the sensitivity analysis where each monetary value on the short duration salt water curve was increased by 30% and decreased by 30%. The resulting curves will also be used within the analysis to see how sensitive the results are to the monetary damage costs.

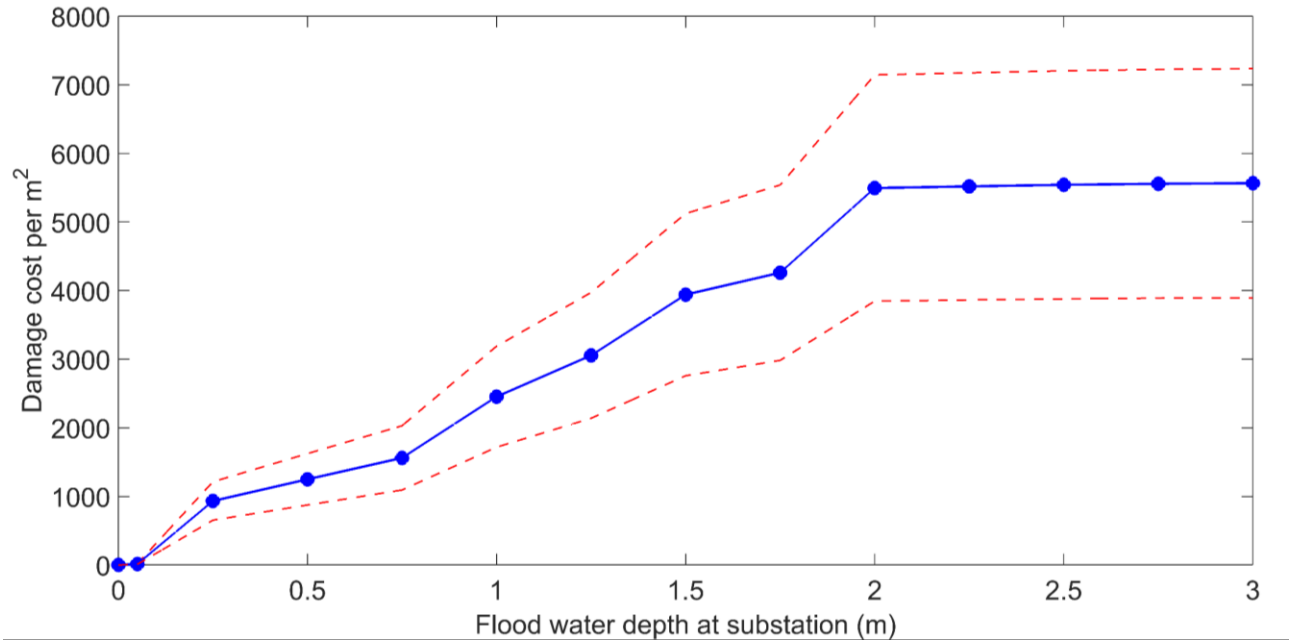

Figure 3.8: Depth damage curve for salt water short duration flooding. Black circles show the cost in flooding in £ per m² for different flood water depths. The dashed lines show the plus and negative 30% values used in the sensitivity analysis (Penning-Rowsell et al., 2014)

For each substation and for each simulation the cost of flooding can be calculated using this curve. Following the methodology used in Engineering Technical Report 138 provided by the Energy Networks Association all substations sites should have a freeboard of 300 mm from flooding so this amount was added to each flood water depth (Energy Network Association, 2009).

3.3.4 Estimated Annual Damage/Vulnerability

Once the cost for each combination of return period and sea-level rise has been calculated at every grid cell that corresponds to a substation site, the estimated annual damage (EAD) at each site can be derived. EAD is the annualized cost of the damage due to flooding for all the return period flood events. Figure 3.9 shows the process in deriving Estimated Annual

Damage (EAD) from the flood water depth value at each substation site location for each of the 336 flood inundation simulations.

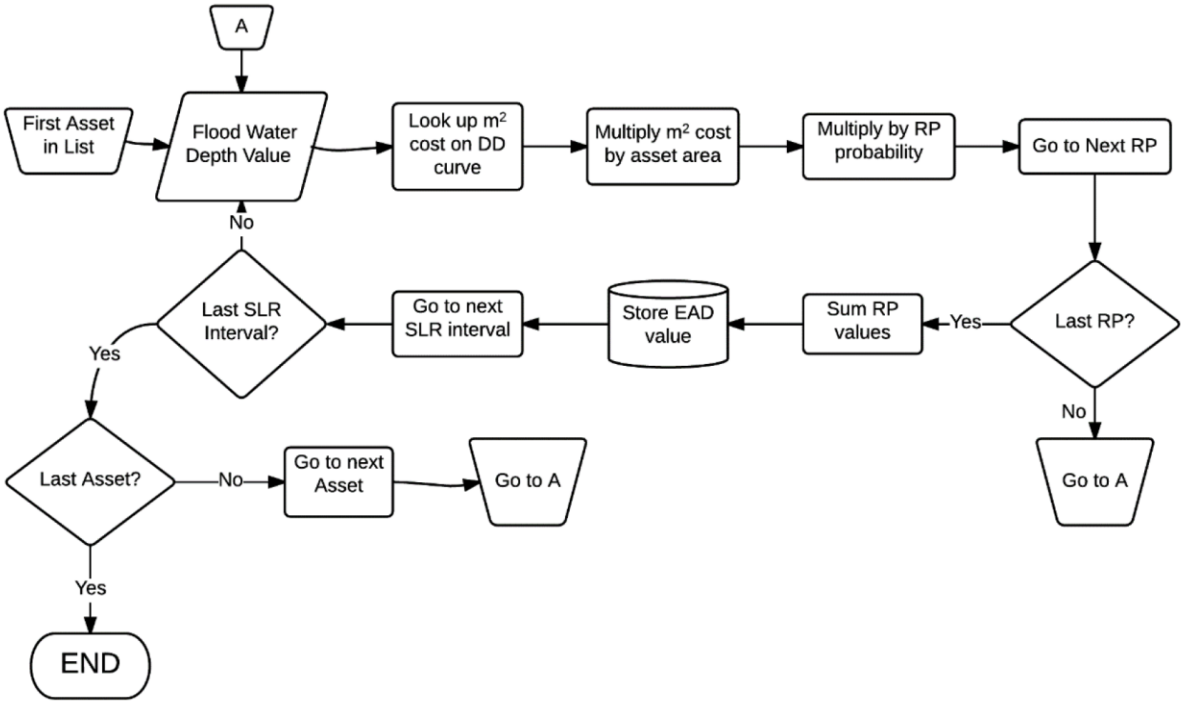

Figure 3.9: Flow chart showing the process in calculating EAD for each grid cell containing an infrastructure asset.

EAD is calculated by multiplying the monetary impact of each of the return period events for each asset by its probability of occurrence. For example, a 1 in 200 year return period has a probability of 0.005 or 0.5%. These values are then summed for each of the 16 return periods at each SLR projection. The output from this is 21 values of estimated annual damage (EAD) ranging from 0 m of SLR (present-day) to 2 m of SLR (H++ scenario). This process is repeated for each of the 388 grid cell that correspond to a substation asset shown in Figure 3.6. An example of one of these EAD versus SLR relationships for substation number 67 is shown below in Figure 3.10.

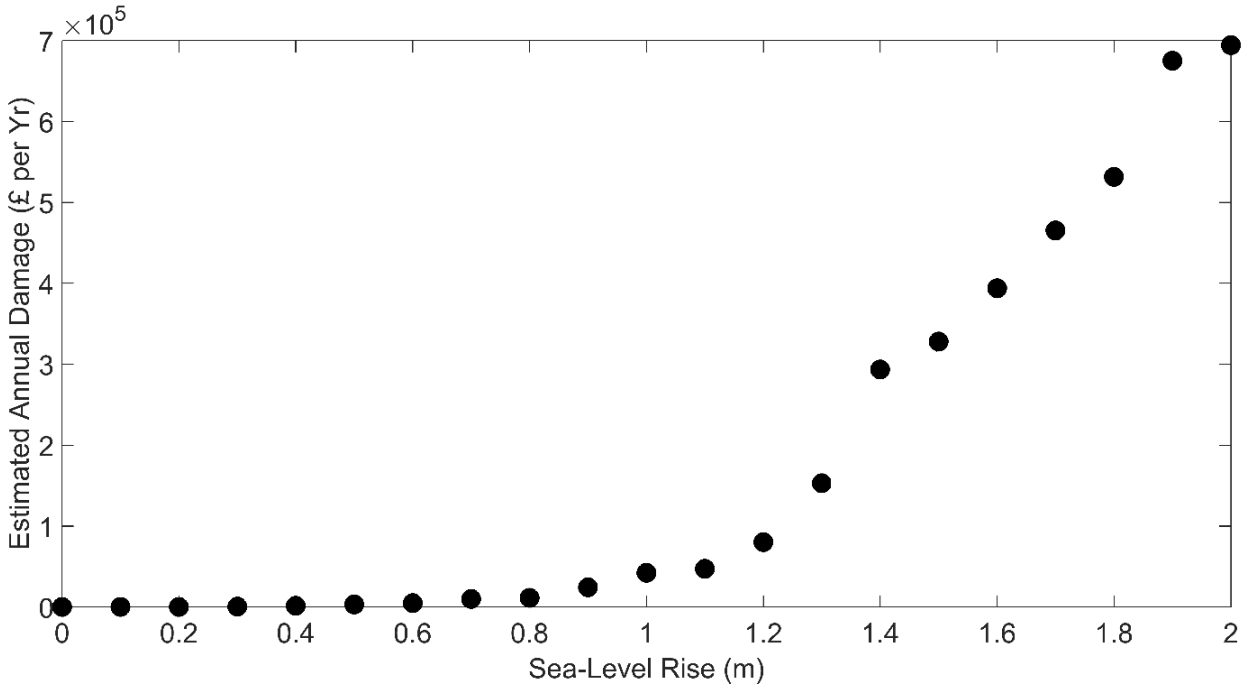

Figure 3.10: Changes in EAD for substation number 67 in study area. Black dots show the increase in EAD in relation to the increase in mean sea-level.

Figure 3.10 shows the EAD at each SLR interval for a substation and it can be seen that there is a threshold or tipping point in EAD where it significantly increases relative to SLR between 1.3 m and 1.4 m for substation 67. Once the SLR to EAD relationship for each asset is calculated the EAD of the asset as a result of coastal flooding can be projected into the future using any given SLR projections.

3.3.5 Sea-Level Rise projections

The sea-level rise projections used in this study are from the UKCP09 (Lowe et al., 2009) high emission scenario regional relative sea-level rise projections for the study area. The majority of large UK key infrastructure providers use UKCP09 within their climate adaptation reports (Duffield and Macgregor, 2012; National Grid, 2010) therefore using this

dataset for this study will be acceptable to most investment managers within these industries.

The data is provided in the form of a 5th, 50th and 95th percentile SLR value for every year up from 2010 to 2100. Global sea-level rise projections could also be used, but consideration needs to made due to the fact that sea-level rise varies spatially around the world so the global values may not be appropriate. As the projections are relative, they also take into account glacial isostatic adjustment (GIA) where the land is still adjusting to the removal of the weight of ice sheets present during the last glacial maximum. This land movement can be positive (uplift) or negative (subsidence) and varies spatially around the world.

As the 5th and 95th percentile SLR projections are equidistant from the 50th percentile, a suitable distribution to fit to these projections would be a normal or Gaussian. Figure 3.11 shows an example this normal or Gaussian distribution for the year 2100.

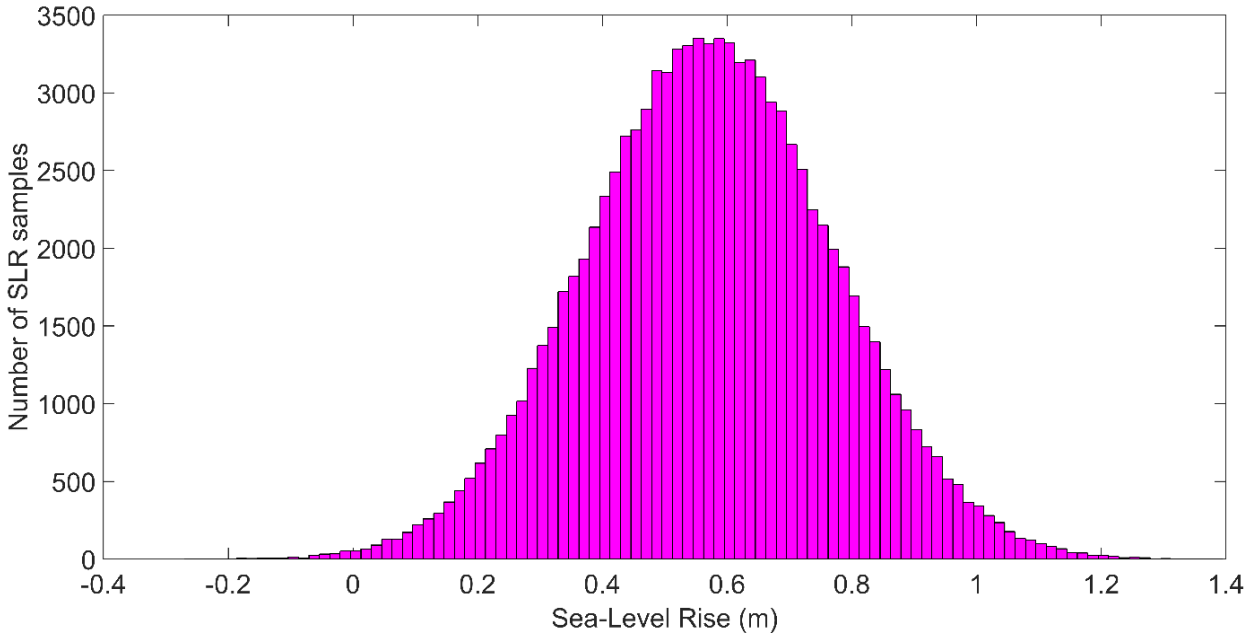

Figure 3.11: Sea-level rise distribution for the year 2100 based on a normal probability distribution.

Using a Monte Carlo analysis, each of the 91 distributions from 2010 to 2100 were sampled a 100,000 times to provide 100,000 possible SLR "pathways" up to 2100. These can then be converted into EAD "pathways" using the SLR vs EAD relationship calculated from the damage costs derived from the flood depths for each substation. These pathways are used to generate revenue streams that flood defences would provide if they were invested in for each asset. Given that the SLR projections start in 2010 this has been considered the present day for all the following economic analysis. A new set of climate projections are in process of being created and should be available in 2018. This would enable the updating of the economic analysis with more up to date SLR projections.

As well as using a normal probability distribution, other distributions could potentially be used. Being able to capture the lower probability but higher impact events would help to potentially identify which assets are vulnerable to these lower probability sea-level rise

projections. As can be seen from Figure 3.12, the 95th percentile SLR value is approx. 1 m. However, the H++ scenario that is part of UKCP09 has a value of 1.9 m, which (while there is no probability attached to this value) recent research projects a 95th percentile value of 1.8 m for global sea-level rise in 2100 (Jevrejeva et al., 2014).

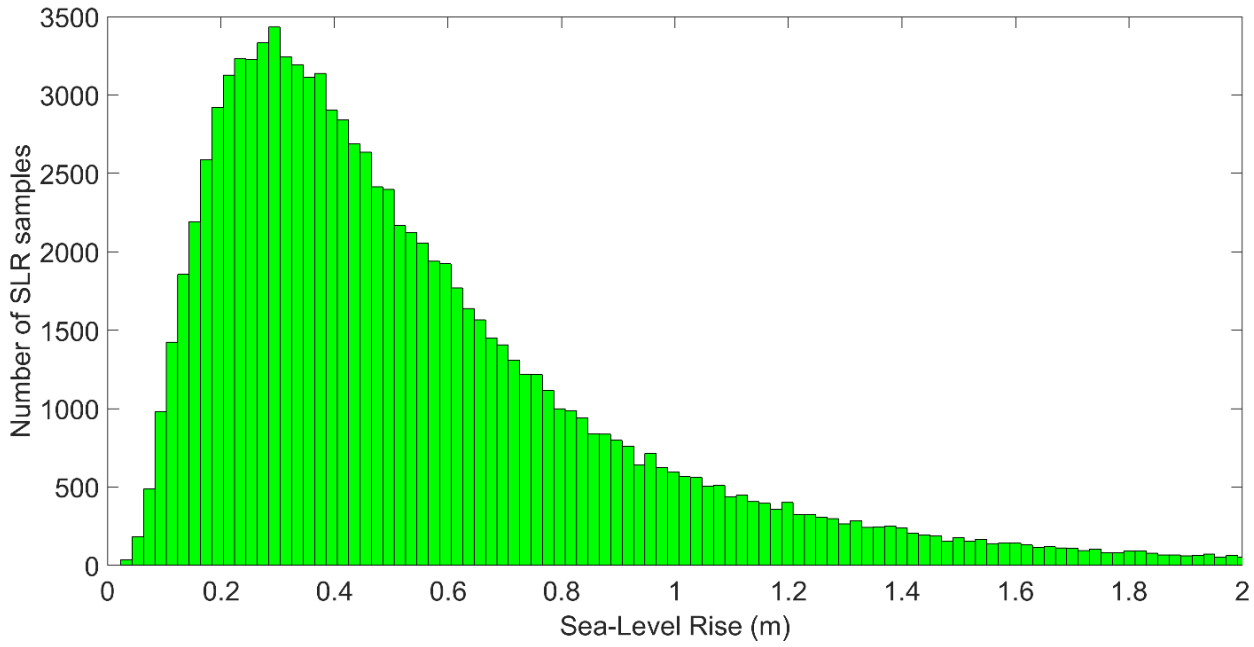

Figure 3.12: Sea-level rise distribution for the year 2100 based on a log-normal probability distribution.

While this is a global SLR projection, the UK experiences SLR values that are comparable to global projections. A log-normal probability distribution is able to capture this as a tail in the probability distribution. Figure 3.12 shows a log-normal distribution based on the same UKCP09 SLR projections for 2100. Using this distribution will result in small samples of sea-level rise that are implausible when compared with current UKCP09 projections. Therefore, a limit of 1.9 m was placed on the distribution matching the current plausible maximum for 2100. For longer time horizons, i.e. beyond 2100 or future SLR projections may result in this

limit being revised upwards. Comparing the results using both sets of probability distributions will show what effect the lower probability high values of SLR have on the vulnerability of energy assets up to 2100.

3.3.6 Discount Rate

Using annual SLR projections up to 2100 to allow the estimation of EAD revenue also requires that EAD to be discounted to the present day. This allows comparison with the defence costs and any defences costs that occur in the future, such as operation costs over the defence life span or deferred building of defences. To do this a discount rate is used, for this study the UK Government Treasury Green Book for infrastructure projects was used to provide the percentage term. This term varies depending on the number of years that have passed, for example the first 30 years is set at 3.5%. This discount rate is applied to all future revenue from the flood defences or EAD and also to the capital costs and costs of operating and building the defences.

3.3.7 Defence Investment Cost

The defence investment cost was calculated by using the perimeter of the asset as the length of defence needed, and multiplying that cost by the £ per m for the type of defences. The £ per m varies depending on the maximum modelled flood water depth at the asset site. This study calculated the cost of demountable barriers but other options can be considered such as permanent defences, temporary barriers and flood proofing the substation buildings. The cost of operating and erecting the defences was also added to the investment cost.

Equation 1 shows the method in calculating the defence investment cost of each asset.

$$DIC = (P \times M + EAO) \quad (1)$$

where:

- DIC = Defence Investment Cost
- P = perimeter length of asset
- M = £ per metre to build defences (dependent on max flood water depth)
- EAO = Estimated Annual Operational Cost (see equation 3)

Calculating the cost per metre to erect the defence and multiplying that by the perimeter of the asset produced the operational costs. This value for each asset is then multiplied by the probability of occurrence for each return period and summed, giving an Estimated Annual Operating cost (EAO). Equation 2 shows this in more detail.

$$EAO = \sum_{t=1}^{n} P \times N \times RP \quad (2)$$

where

- EAO = Estimated Annual Operational Cost
- P = length of perimeter of asset
- N = £ per metre to erect defences
- RP = probability of each Return Period expressed in decimal
- n = number of RP values

This methodology can be applied to other defence types allowing a comparison to be made between defence options.

3.3.8 Net Present Value (classic):

To calculate classic NPV the cash flows in and out of the project need to be discounted and compared. For flood defences the revenue or cash flow in is the EAD accrued for each year over the defence life span based on annual SLR projections. The NPV calculation uses the 50th or most likely annual SLR projection. The cash flow out is the initial cost of building defences and the annual operational costs. All cash flows are discounted to the current time interval and compared. If the costs exceed the revenue generated then building defences is not cost effective, but if the revenue is greater than costs then the investment is cost effective. Basing the revenue on the most likely SLR projection does not take into account the uncertainty in SLR projections and under-estimates the impact of crossing the threshold in EAD where large changes in EAD are present for small changes of SLR (Figure 3.11). If these thresholds occur at lower probability SLR values, then the $NPV_{classic}$ will be suboptimal for a given asset.

$$NPV_{classic} = (PV_{ci} - CapEX - OpEX) \quad (3)$$

$$PV_{ci} = \sum_{t=1}^{L} \frac{EAD}{(1+r)^t} \quad (4)$$

$$CapEX = \frac{DIC}{(1+r)^1} \quad (5)$$

$$OpEX = \sum_{t=1}^{L} \frac{EAO}{(1+r)^t} \quad (6)$$

where PV_{ci} is the discounted revenue over the defence life based on annual 50th percentile SLR projections, CapEX is the cost of building the defences in year 1 and OpEX is the operational cost of the defences over its lifespan. r is the discount rate, L is the lifespan of the defences, DIC is the defence investment cost and EAO is the estimated annual operational cost.

3.3.9 Real Option Valuation

Using simulation modelling this study values the Real Option (RO) to defer or invest; these are decided with the following decision rules and option valuation adapted from Pringle et al 2015:

Table 3.1: The different conditions that need to be met to enable the option to invest, or defer flood defence investment to be exercised.

Option	Condition 1	Condition 2	Condition 3
Defer Investment	$NPV_{max} > 0$	$NPV_{flexible} < 0$	$NPV_{classic} < 0$
Invest Now	$NPV_{max} > 0$	$NPV_{flexible} > 0$	$NPV_{classic} <$ or > 0

- Option to defer: Provides the right to postpone the investment for a set period of time, rejecting the revenue for this deferred period and await the arrival of new and better information the reduces the SLR uncertainty
- Option to Invest: The conditions are favorable at the current time to invest in flood defences

where NPV_{max} is defined as the difference between the discounted maximum revenue that can be generated for each asset based on the mean of the maximum SLR value for 2100 and the discounted capital and operational costs of investing in defences.

$NPV_{classic}$ defined in section 3.2.8 uses the 50th percentile annual SLR projections up to 2100 to produce the revenue which is discounted and compared with the discounted capital and operation costs.

$NPV_{flexible}$ is the flexible NPV value that consists of the $NPV_{classic}$ with the addition of the option value.

$$NPV_{flexible} = NPV_{classic} + Real\ Option\ Value \quad (7)$$

The real option value (ROV) is the mean value of all the Option Returns (OR) calculated from the Monte Carlo EAD pathways. The real option value across all the sampled EAD pathways is calculated as follows:

$$ROV = mean[(Revenue\ Expected\ to\ Earn - Costs) - (Revenue\ Deferred - Costs)] \quad (8)$$

$$ROV = mean\left[\left(PV_{fi} - CapEX - OpEX\right) - \left(PV_{mi} - CapEX - OpEX\right)\right] \quad (9)$$

$$PV_{fi} = \sum_{t=D+1}^{D+L} \frac{EAD}{(1+r)^t} \quad (10)$$

$$PV_{mi} = \sum_{t=1}^{D} EAD(1+r)^t \quad (11)$$

$$CapEX = \frac{DIC}{(1+r)^D} \quad (12)$$

$$OpEX = \sum_{t=1}^{L} \frac{EAO}{(1+r)^t} \quad (13)$$

where PV_{fi} is the discounted revenue over the defence life span if it is executed after the deferral interval, PV_{mi} is the discounted deferred revenue over the deferral interval, CapEX

is the construction costs after the deferral interval and OpEX is the operational costs over the defence life after the deferral interval. Further, r is the discount rate, DIC is the defence investment cost, EAO is the estimated annual operational cost, D is the deferral interval and L is the defence life span. This process is repeated at each time interval to show the changes in options to invest or defer at set intervals based on regional SLR projections.

3.4 Results

For each of the 388 substations, a classic NPV based on DCF methodology has been calculated for every time interval up to 2050 (Table 3.2). Any substation that has a positive value would go ahead with flood defence investment. However, this approach does not value any flexibility in the management process. Additionally, the flexible NPV has been calculated using the Real Option Valuation (ROV) methodology with the number of substations taking options to invest or defer calculated for each time interval up to 2050. The option to invest or defer investment in flood defences has been considered using the decision rules in Table 3.1.

Table 3.2: Numbers of substations that would be invested in based on DCF NPV and Real Option Valuation (ROV) methodology.

Scenario	Option	2010	2020	2030	2040	2050
$\mathbf{NPV_{classic}}$	Invest	4	4	6	6	7
$\mathbf{NPV_{flexible}}$	Invest	6	7	10	15	21
$\mathbf{NPV_{flexible}}$	Defer	46	45	43	38	35

Comparing the results of the DCF and ROV methodology shows that using ROA, investment in flood defences would go ahead for 2 additional substations in 2010, 3 in 2020, 4 in 2030, 9 in 2040 and finally 14 in 2050. Table 3.2 shows that a small number of substations (6)

generate enough revenue from EAD at the present day to cover the cost of building and operating flood defences in 2010. This rises to 21 by 2050 with the biggest increase of 6 being seen between 2040 and 2050. In 2010 46 substations exercise the option to defer investment which by 2050, has reduced to 35 as more substations exercise the option to invest rather than defer.

Table 3.3: The year when a substation would exercise the option to invest in flood defences based on the decision rules in Table 1. Any substation that does not take the investment option has been removed.

Substation Number	Year Invest Option Taken
24	2030
25	2040
26	2050
30	2010
40	2020
58	2010
59	2050
67	2040
104	2040
105	2010
106	2040
107	2010
108	2010
222	2010
350	2030
351	2050
352	2050
355	2040
356	2050
357	2030
384	2050

Table 3.3 presents the year a specific substation would exercise its option to invest based on the decision rules of Table 3.1. The invest option would be exercised when the $NPV_{flexible}$ value or $NPV_{classic}$ is greater than zero. There are 6 substations that would invest in flood

defences in the present day, whereas the majority of additional substations that exercise the option to invest by 2050 do not do so until 2040/2050. This is likely due to a threshold being reached in SLR where the increase in revenue from EAD at this point in time justifies the investment in building and maintaining flood defences at the relevant substations. 2050 is the furthest this methodology can assess based on the operational life of defences being assessed and the length of the regional SLR projection dataset, to extend the time horizon a longer SLR dataset would be required or defences with a shorter life span.

Using model simulation ROA also allows the percentage chance of the $NPV_{flexible}$ being positive (and therefore exercising the option to invest) to be calculated. The ROV is based on the mean option value calculated across the 100,000 SLR pathways. Instead of using the mean option value, the percentage chance of the option value ever making the $NPV_{flexible}$ positive can be calculated instead. By calculating the percentage chance, it is possible to identify assets that would be invested in if a low probability high impact SLR pathway are realised. Table 3.4 below shows the percentage likelihood for flood defence investments for all assets up to 2050 (to simplify the table, any asset that remains at zero percent in 2050 has been removed).

Table 3.4: Percentage chance of a substation asset receiving flood defence investment.

Substation Number	2010	2020	2030	2040	2050
24	0.00	0.04	93.22	100.00	100.00
25	0.00	0.02	2.37	53.88	100.00
26	0.00	0.00	0.13	3.83	48.77
27	0.00	0.00	0.01	0.17	3.92
30	100.00	100.00	100.00	100.00	100.00
40	0.00	92.80	100.00	100.00	100.00
43	0.00	0.00	0.00	0.00	0.44
58	100.00	100.00	100.00	100.00	100.00
59	0.00	0.00	0.00	0.14	93.66
67	0.00	0.00	3.26	99.42	100.00
70	0.00	0.00	0.00	0.01	20.37
100	0.00	0.00	0.00	0.00	0.09
101	0.00	0.00	0.00	0.01	15.04
104	0.00	0.00	0.20	47.45	100.00
105	100.00	100.00	100.00	100.00	100.00
106	0.00	0.00	15.08	99.71	100.00
107	100.00	100.00	100.00	100.00	100.00
108	100.00	100.00	100.00	100.00	100.00
222	70.47	100.00	100.00	100.00	100.00
350	0.00	27.29	100.00	100.00	100.00
351	0.00	0.00	0.01	1.73	93.38
352	0.00	0.00	0.02	3.05	97.81
354	0.00	0.00	0.01	0.29	7.81
355	0.00	0.06	10.49	82.83	100.00
356	0.00	0.00	0.04	8.34	99.97
357	0.00	0.68	100.00	100.00	100.00
384	0.00	0.00	0.03	15.04	99.78

Table 3.4 shows a larger number of substations that could potentially exercise the option to invest. In this case there are 27 assets that have some percentage chance of the revenue from EAD to exceed the cost of building and operating the defences. The additional 7 substations are the ones with percentage chances less than 50%, of these one has a chance of 48.77% in 2050 it may be worth considering this substation for investment. The other substations have percentage chances ranging from 0.1 to 20% indicating they are only likely to be considered

for investment under unlikely high end SLR projections or over a longer time period that the current regional SLR projections do not cover.

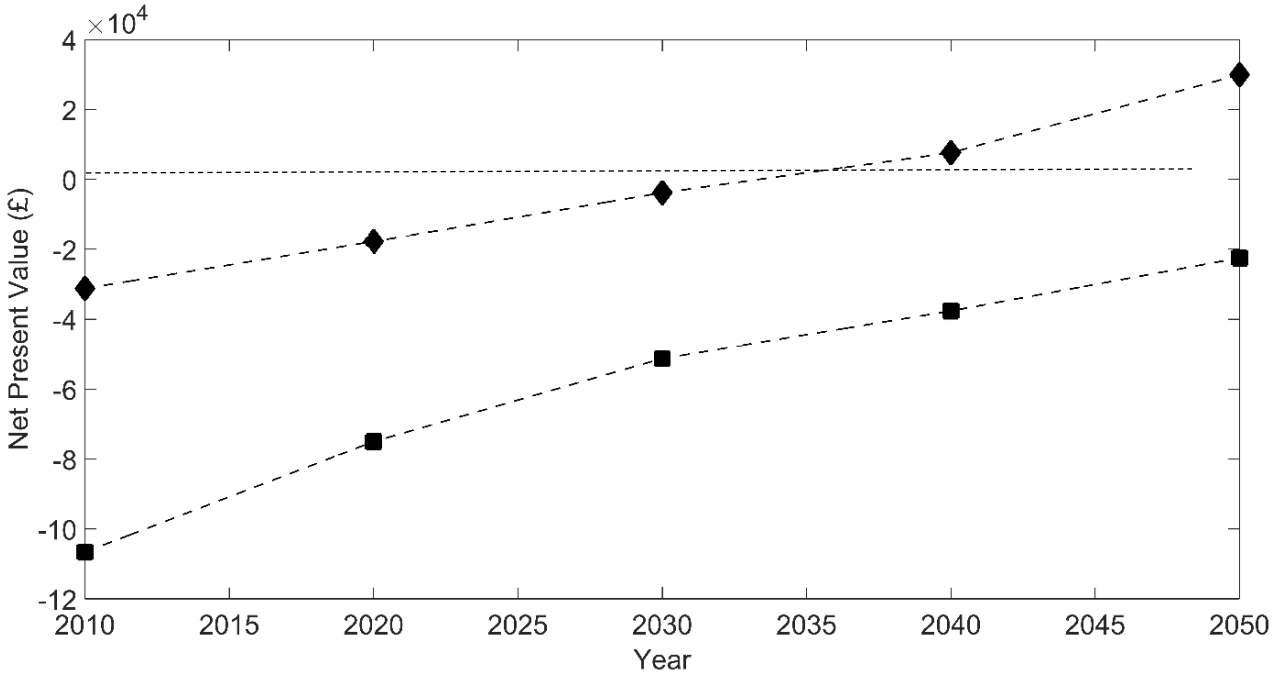

Figure 3.13: NPVclassic values (black squares) and NPVflexible values (black diamonds) at ten year intervals up to 2050 for substation 67. The horizontal dashed line is at zero where the NPV becomes positive and investment would take place.

Figure 3.13 shows the $NPV_{classic}$ and $NPV_{flexible}$ values for substation 67, in which the $NPV_{classic}$ increases up to 2050 but remains negative so investment would not proceed at any point before 2050. The $NPV_{flexible}$ values do become positive in 2040, where the option to invest would be exercised. The ROV analysis has found extra value in the management flexibility, which while negative in 2010 to 2030 is still greater value than the corresponding $NPV_{classic}$ value.

Figure 3.14 below shows the results of the sensitivity analysis that has been performed by varying two key parameters to see their impact on the outcome of the ROV method. The

depth damage curve has been increased and decreased by 30% (Figure 3.8) along with the discount rate provided by the UK Treasury. Finally, changing the probability distributions of SLR used from a normal to a log-normal has also been investigated.

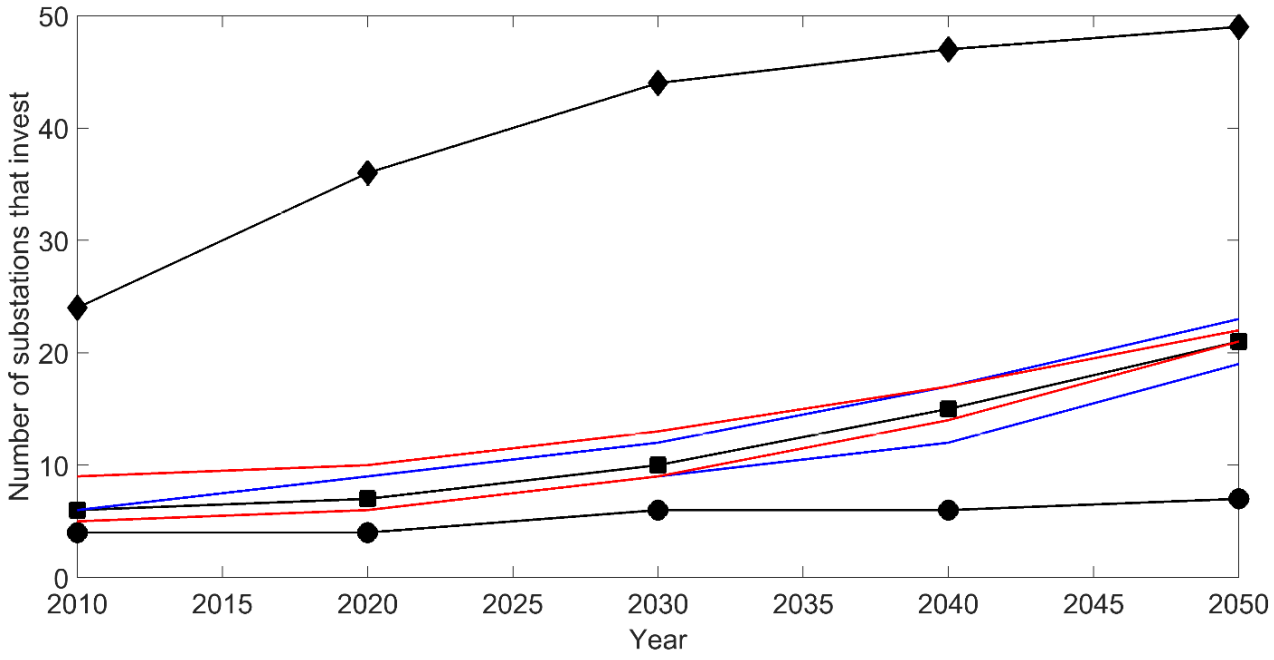

Figure 3.14: Number of substations undertaking flood defence investments up to 2050. For DCF methodology (circles) and ROV methodology (squares). The effect in varying the depth damage curve (blue lines), discount rate (red lines) and log-normal probability distribution (diamonds) is also shown.

Figure 3.14 shows that varying the depth damage curve or discount rate by +/-30% does not have a large effect on the outcome of the analysis, the trend and values are largely the same and always provide more investment opportunities than DCF methodology. Assuming SLR projections have a log-normal distribution has a large effect with increases of 18 in 2010 to a maximum of 34 in 2030 reducing to 18 again in 2050. The reason for large increase is due to the higher levels of SLR that are more likely to occur over the defense's life-span giving increased revenues of EAD making taking the option to invest in defence investment more likely.

The ROV methodology specifies using the mean option value from the 100,000 SLR pathways, but sensitivity analysis was also performed to see what the impact of using a different percentile from the mean would have on the results (Table 3.5).

Table 3.5: Number of substations taking the option to invest, for different percentiles of Option Value based on the SLR pathways

Option Value Percentile Used	2010	2020	2030	2040	2050
25th	5	7	11	14	20
50th (Mean)	6	7	11	15	22
75th	6	7	11	15	22

Table 3.5 shows that there is little sensitivity to the percentile of option value used with a small reduction in substations taking the investment option for the 25th percentile, a reduction of one in 2010, 1 in 2040 and 2 in 2050.

Overall sensitivity analysis has shown that the only variable that significantly affects the results is the use of a log-normal probability distribution of SLR that makes sampling a higher value for future SLR more likely, making more substations more likely to exercise the option to invest due to the resulting higher EAD revenues over the defence lifetime.

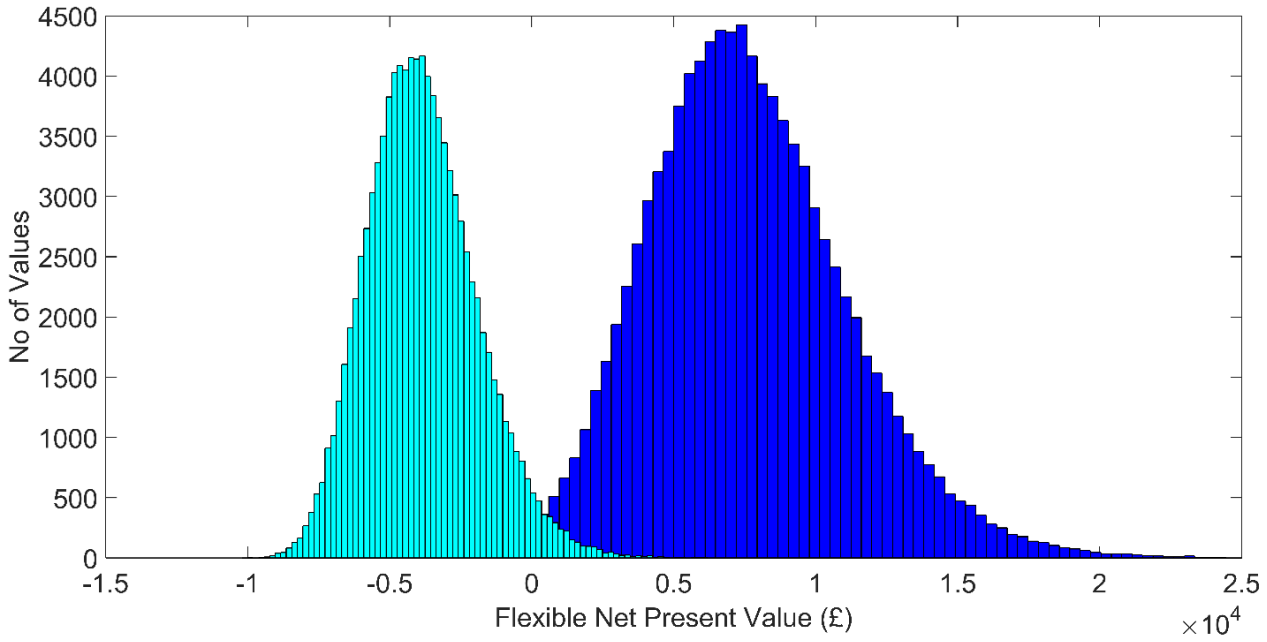

Figure 3.15: Flexible net present value distribution for substation 67 in 2030 (light blue bars) and 2040 (dark blue bars).

Figure 3.15 shows the distribution of $NPV_{flexible}$ across all 100,000 pathways. In 2030 for substation 67 only the upper bars of the histogram are over zero meaning only under low probability high future SLR pathways would the decision to invest be taken here. By 2040 this has changed where the majority of the distribution is over zero with only a minority of the lower probability low level SLR resulting in the decision to invest not being taken. For the analysis, the mean value of the distribution at each time interval has been used.

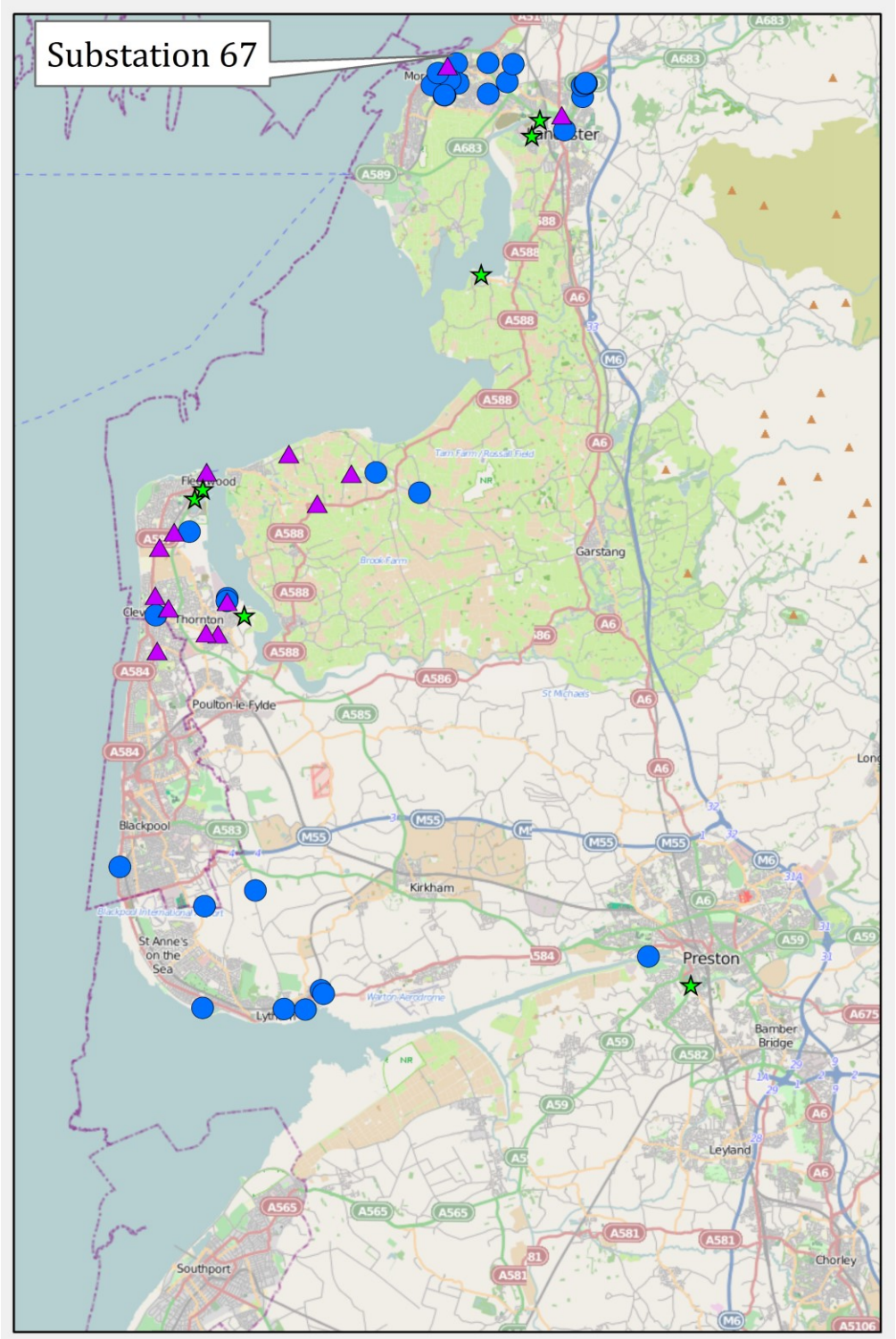

Figure 3.16: Map showing locations of substations in 2050 that would invest in flood defences under DCF methodology (green stars). Substations that have been identified in addition to these that would exercise the option to invest (purple triangles) and the option to defer investment (blue circles) have also been identified.

Figure 3.16 shows the locations of the substations in 2050 that would be invested in based on DCF methodology (black triangles) it also shows the substations that exercise the option to invest (black stars) and also the option to defer investment (black circles). Comparing with Figure 3.5 it can be seen that these substations are very spatially variable with small areas of the map having large numbers of both invest or defer options present. Invest options are predominantly concentrated in the Fleetwood area with a few substations on the banks of the Lune river near Heysham also exercising the invest option. Defer options are also present in these locations, particularly concentrated around the north of Heysham showing that these assets may potentially in the future exercise the option to invest. Finally, some defer options are also present on the north side of the Ribble estuary and river indicating that this is an area that may be at risk beyond 2050. Investments based on DCF methodology are concentrated in Fleetwood close to the River Wyre and also in Heysham close to the River Lune.

3.5 Discussion

The previous section provided results from the FLORA methodology, we will now discuss in more depth. We have found that relying on DCF methods to decide whether to invest in flood defences will end up with suboptimal decisions being made where some projects that would benefit from defences will be missed. This is due to the DCF methodology not taking the uncertainty of future conditions into account as well as the flexibility of management decisions to respond to them.

Sensitivity analysis was undertaken by varying the three key parameters. These include, the depth damage curve that changes a flood water depth into a monetary value. The discount factor that discounts future values to present day ones and the probability distribution used to sample SLR values for a given year. It was found there is some sensitivity to all parameters. Changing the depth damage curve +/- 30% caused a maximum change in the number of invest options of +/- 2 substations. Changing the discount factor by +/-30% also showed some sensitivity with a maximum change of +/- 3 substations. The most significant sensitivity in the results is the assumed probability distribution for SLR values. Changing from a normal to a log-normal distribution that captures the low probability high-end values of projected future SLR shows a maximum increase of 34 substations in 2030. A recent global SLR projection study put the 95th percentile probability of SLR at 1.8 m in 2100 (Jevrejeva et al., 2014), which is a closer match to the log-normal distribution used within this study, showing that using log-normal probability distributions may be more suitable than a normal probability distribution. The latest regional relative SLR projections have been used as a sectoral standard reference, but these were produced in 2009 and are not up to current knowledge regarding SLR.

The trends in both $NPV_{classic}$ and $NPV_{flexible}$ are one of increasing value up to 2050. Most substations that are under assessment within the study always stay negative. This is due to the low EAD revenue if flooding is minor or zero EAD revenue if the substation never floods, regardless of the SLR considered. The benefits brought in building demountable flood defences never exceed their cost of construction and operation. Some substations at the present day have positive $NPV_{classic}$ values. Figure 3.16 shows that a lot of these are located close to major rivers, and care must be taken with these locations due to the low horizontal

resolution of the flood model (50 m) which may cause the flood water depths to be over-estimated. This can be resolved by using an input dataset with higher spatial resolution. At the time of running the inundation model it was too computationally expensive but recently a newer version of the flood model has been released which reduces the computation cost potentially allowing higher resolution domains to be simulated. A good compromise between 5 m and 50 m is likely to be a 10 m horizontal resolution which will provide much more detail than the 50 m grid while having a large reduction in the computational cost when compared with the 5 m grid.

Figure 3.15 shows the distribution of option value for substation 67 in 2030 and 2040, the mean value of the distribution is what is used in the calculation of $NPV_{flexible}$. To see if the outcome is sensitive to the percentile used the 25^{th} and 75^{th} percentiles of option value were considered alongside the 50^{th} in calculating the $NPV_{flexible}$ value. It was found that using the 25^{th} percentile value resulted in the option to invest being exercised in one less substation in 2010, one less in 2040 and two less in 2050, whereas the 75^{th} percentile had the same results as the mean. The results show little sensitivity to the percentile used, so only the 50^{th} percentile needs to be considered within the ROA analysis.

However, considering the full distribution of $NPV_{flexible}$ values can be beneficial as it can highlight additional substations that will require investment if a low probability SLR projection is realised. It also highlights substations that can just miss the option to invest, such as substation 26 where a percentage chance of 48.77% of the pathways result in investment in 2050 meaning that it would exercise an option to defer. If it was over 50%, so more pathways result in investment than defer then it would reach the threshold required

for it to be invested in, warranting a closer analysis. Likewise, other percentage changes on the order of 1% where only 1 in every 100 pathways result in the option to invest being taken show that taking the option to defer is the right one based on the SLR projections used.

As expected, from inspection of the data, the substations at risk overlap to some degree with the Environment Agency's flood risk map (Figure 3.4) but as this map only covers present-day flood risk for a single extreme event it is unable to highlight which assets would have the investment decision to invest in flood defences made or deferred particular with the increasing uncertainty of SLR over time.

FLORA has shown it is able to integrate physical risk from marine flooding with economic considerations of resilience within a flexible ROA methodology that only an interdisciplinary model would be able to provide. FLORA enables timely and cost-effective investment in building flood defences that allow energy infrastructure to remain resilient to extreme events in the face of a changing climate.

3.6 Conclusions

This work has focused on the economic impacts of future sea-level rise on coastal energy infrastructure. Although a UK case study is presented the approach could be applied to energy infrastructure in other coastal regions. Investment is required to maintain the standard of flood protection to important electricity distribution and transmission infrastructure in the face of climate change, or potentially improve it. To date, the impacts of sea-level rise and coastal flooding - and the possible adaptation responses - have been studied using very different approaches, such as very detailed site-specific engineering

studies and global macroeconomic assessments of coastal zone vulnerability. This paper offers a Real Option Analysis framework, FLORA, to value the investment potential of flood defences around electricity infrastructure at local spatial scales for a large region. The results have shown that tipping points in the EAD curves result in thresholds being present, most notably in 2030 where the number substations exercising the option to invest more than doubles by 2050. FLORA has been found to be insensitive to the underlying cost curve that converts flood water depth into cost and also the discount rate used to discount future revenues to the present-day. It is however very sensitive to the probability distribution used to sample annual SLR projections for each SLR pathway to 2100. A log-normal distribution appears to fit global SLR projections well, but for the regional SLR projections a normal SLR projection maybe more appropriate due to the 25th and 75th percentile values being an equidistant from the mean.

As demonstrated, FLORA gives an indication of where and when these investment resources should be deployed. Knowing which assets are vulnerable and require investment now and which are likely to be vulnerable and require investment in the future ensures an optimum allocation of available resources. Thus, the authors believe that both the methods and results presented in this paper will help to inform management policy on deciding where it is cost effective to invest in flood defences and where it is cost-effective to defer investment. It allows a more flexible policy procedure than the policy informed from discount cash flow methods alone.

FLORA can also be fed into a decision-support tool, such as the one described by Knight et al. (2015) which would allow stakeholders to access data for areas of interest, FLORA would

provide flood water depths for each of the extreme events under different SLR scenarios. EAD and defence costs for each substation site would also be available, along with information about which investment option is taken and when. FLORA effectively demonstrates the essential need to combine physical environment and economic modelling to provide effective decision-support for climate change adaptation and optimized investment for building infrastructure resilience.

3.7 Acknowledgements

We would like to acknowledge the ESPRC-funded ARCC “Adaptation and Resilience of Coastal Energy Supply” (ARCoES) project (EPSRC EP/I035390/1) We would also like to acknowledge Electricity Northwest for providing the substation data.

4 Flood inundation uncertainty: the case of a 0.5% probability flood event

4.1 Abstract

Aging coastal defences around the UK are challenging managers to redesign schemes to be resilient to extreme events and climate change, be cost-effective, and have minimal or beneficial environmental impact. To enable effective design, reduced uncertainty in the assessment of flood risk due to natural variability within the coastal forcing is required to focus on conditions that pose highest threat. The typical UK standard of protection for coastal defences is to withstand a 0.5% annual probability event, historically also known as a 1 in 200 year return period event. However, joint wave-water level probability curves provide a range of conditions that meet this criterion. We examine the Dungeness and Romney Marsh coastal zone, a region of high value in terms of habitat and energy assets, to quantify the uncertainty in flood depth and extent generated by a 0.5% probability event, and to explore which combination of wave and water levels generates the greatest threat.

4.2 Introduction

Coastal managers need to consider many different aspects when planning new coastal defence schemes to maintain resilience to coastal flooding in locations with aging defence structures. New structures need to be resilient to extreme events and the impacts of climate change over the defences' design life, typically 75-100 years (Buijs et al., 2007). However, new coastal defences also need to be cost-effective and implemented in a timely manner to reduce the economic impact from present and future extreme events. This means an understanding of both the probability of extreme events occurring and the probability of a defence being exceeded is required (Buijs et al., 2007). To enable effective adaptation, better understanding of the uncertainty around the probability of a flooding event due to natural variability is required to enable implementation of cost-effective design (Wadey et al., 2013).

Sources of coastal flooding are varied and range from sources that contribute to the still extreme water level such as astronomical tides and storm surges (A. McMillan et al., 2011) to wave run up driven by significant wave height and peak period of any waves that are present during an extreme still water level.

A storm surge occurs when high winds and low atmospheric pressure during a storm act on the sea surface to cause a temporary increase in water level (Wells, 1997). If this occurs in conjunction with a high tide, particularly a spring tide, an extreme still water level (EWL) event arises. EWLs will have an increased impact in the future due to rising mean sea level (McInnes et al., 2003). With higher mean sea level, the probability of an EWL event will

increase (Prime et al., 2015). From here on, this study refers to this extreme still water level as an EWL.

Wind blowing across the sea surface will produce waves either locally as wind waves or from a storm offshore as swell waves. If they impact on the coastline at the same time as the EWL, waves will increase the observed water level over the EWL alone due to wave run up which further increases the impact of the extreme event (Longuet-Higgins, 1970) (Chini and Stansby, 2012).

This paper demonstrates the uncertainty in the flood hazard due to natural variability within the combined forcing of extreme events. The UK design standard for sea defences varies depending on what the defences are protecting, for example, nuclear power stations are designed to be resilient to a 1 in 10,000 year event, but a typical event that coastal defences are designed to withstand is a 1 in 200 year event, or a 0.5% annual probability of occurrence (Wyse, 2015). This design standard can be applied using one variable such as EWL, which has been calculated at a national scale for 16 return periods of extreme water levels at 2 km intervals along the UK coastline (A. McMillan et al., 2011). A more comprehensive standard is one that uses both EWL and significant wave height and calculates the probability of a given EWL and significant wave height occurring together. This can then be used to understand further contributions to coastal flooding such as wave run up. Combining two variables in this way is known as multivariate probability analysis, or joint probability analysis (Coles and Tawn, 1990). In the context of water level and wave height, joint probability methods were until the 1980's rare, this was mainly due to the lack of long term wave data. In addition to the lack of suitable data, there were also no suitable statistical tools

to analyse the joint occurrence of water level and wave height. Therefore, the standard process at this point was to consider the wave and water levels separately (Hames and Reeve, 2007). As it became clearer that there was a need for better understanding of joint probability, research was undertaken by HR Wallingford and Lancaster University to try and overcome these barriers (P. J. Hawkes and Svensson, 2006). One of the outputs from this research was specialist joint probability analysis software JOIN-SEA, which is used by industry as well as academic researchers and also for the research in this paper (Hawkes and Gouldby, 1998).

Using the joint probability of water level and wave height is more representative of an extreme event than combining waves and EWL of a given return period calculated in isolation. Classifying the wave heights and extreme water elevations that occur at the same time as well as their probability of occurrence provides a better understanding of how resilient the current sea defences are to extreme events (Wadey et al., 2015). Different combinations of wave height and extreme water elevations can have the same probability of occurrence. The varying impacts from these different combinations of a given return period has not been examined before.

For this study we selected the annual probability of 0.5% or in return period (RP) terms 1 in 200 years, representative of a typical UK standard of defence. This is consistent with the UK Environment Agency flood mapping service that shows areas benefiting from flood defences at this annual probability of occurrence (Wyse, 2015). The objective of this study is to show that there is uncertainty in the inundation extent and flood depths for conditions that are all similarly classified as a 0.5% probability event at a given location. This will inform coastal

managers of the most hazardous combinations of events that attain this probability of occurrence for the purpose of designing new build or maintenance schemes to withstand a specific standard of protection.

4.3 Study Site

The study site selected to research this issue was Dungeness and Romney Marsh (Figure 4.2), a region of the UK that has a high value both in terms of protected habitat and important energy infrastructure. It is also an internationally important location for geomorphology, plant and invertebrate communities as well as birdlife (JNCC, 2015; Long et al., 2007). It is part of a designated Site of Scientific Special Interest (SSSI), which covers Dungeness, Romney Marsh and Rye Bay (Natural England, 2006). The closest tide gauge at Dover shows that storm surges can reach up to 1.6 m (British Oceanographic Data Centre, 2015). The closest wave buoy shows that the most common directions for wave approach is from the southwest and the northeast, with the southwest being associated with the larger waves up to 5 m high and peak periods of up to 18 seconds (Mason et al., 2009). For the area under study the typical direction for coastal wave impact is from the southwest due to the orientation of the peninsula.

Dungeness has both 'natural' defences in the form of a maintained gravel barrier, and engineered structures. Better understanding of the uncertainty of the flood hazard to the region is critical in managing human intervention within the nature reserve and in maintaining resilience for the nearby operational power station which is currently licenced to operate beyond 2018 (EDF, 2012). As it is a licensed nuclear site there will be a nuclear

installation here undergoing decommissioning up to and beyond 2100. There is also a decommissioned nuclear power station that is currently projected to be cleared and no longer a nuclear site in 2097 (Magnox, 2014).

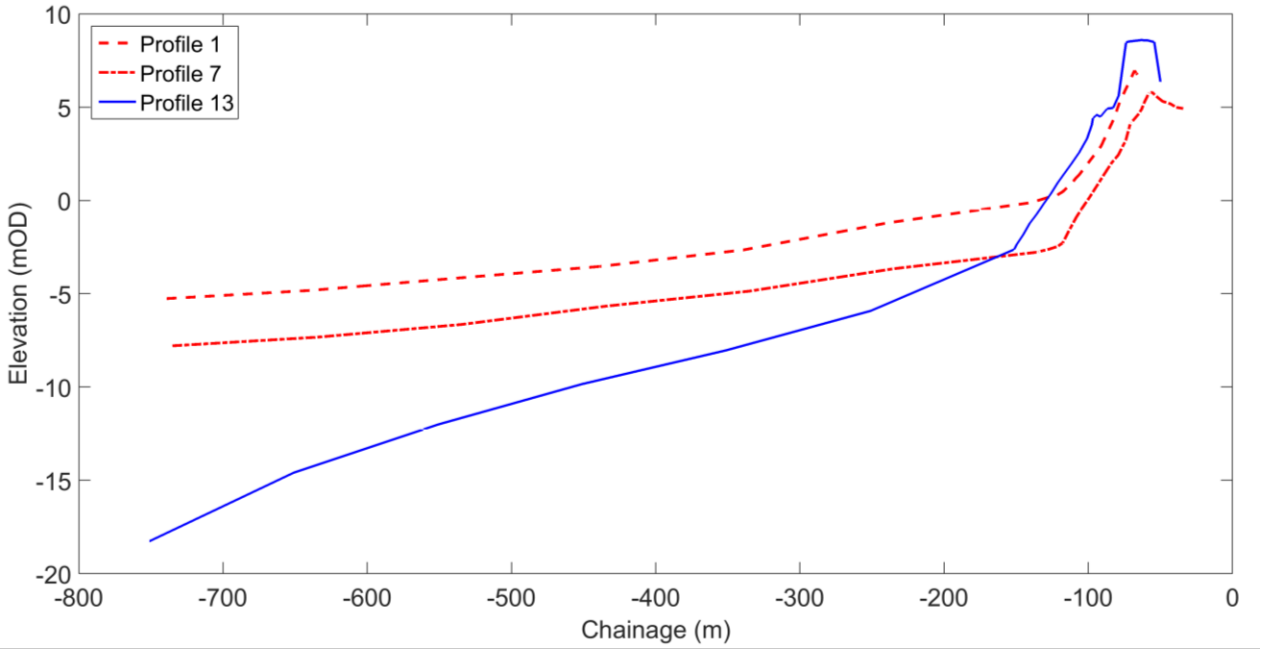

Figure 4.1: Example 1D beach profiles showing variability in shoreline, the red line (profile 5) is an example of the natural defences to the west and the blue line (profile 13) is an example of the engineered defences in front of the power stations.

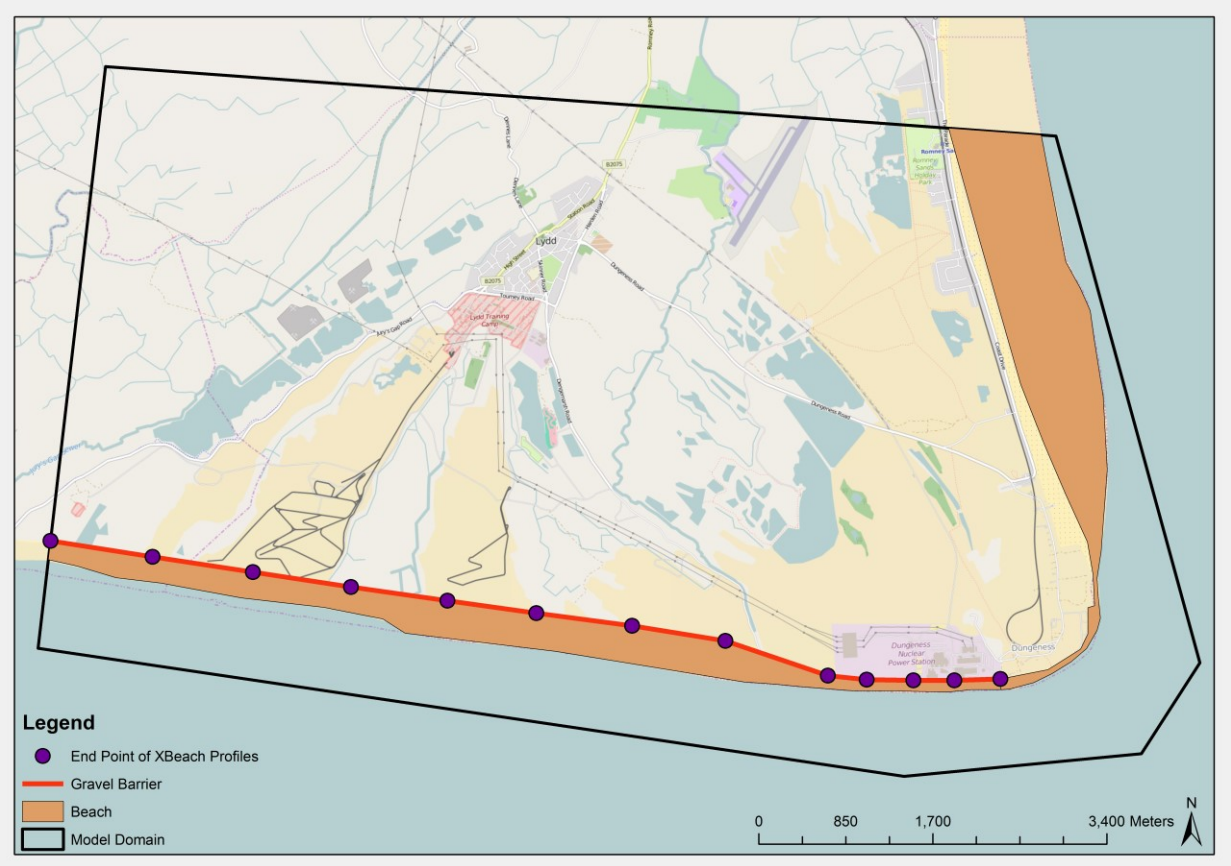

Figure 4.2: Studied section of the coastline at Dungeness and Romney Marsh; the black line represents the model boundary. The purple dots denote the beach profiles used within the storm impact model. The orange area denotes the location of the beach and the red line shows the gravel barrier acting as a sea defence.

The defences along the southern shore of the Dungeness foreland comprise gravel beaches with a secondary defence behind that consists of an earth embankment known locally as the "Green Wall". At the western end the Green Wall is immediately behind the beach and at the eastern end it is several hundred metres behind the beach. The latest shoreline management plans show that the current defence policy for these coastal defences is "Hold the Line". In front of the energy infrastructure there is a large gravel barrier that has been augmented to provide a standard of protection to a 1 in 10,000-year event.

Using the tidal predicting software POLTIPS, the maximum predicted tidal range at Dungeness is 8.6 m OD (Ordnance Datum). The mean high water spring tide was calculated to be 3.54 m OD, with a highest predicted tide of 4.48 m OD (National Oceanography Centre, 2014). From the EA return period data, the 1 in 200 year or 0.5% probability EWL has an average elevation of 4.8 m OD. This is the average EWL based on the data points that are every 2 km along the UK coastline in the model domain (A. McMillan et al., 2011). A similar EA study has calculated the return period of swell wave heights around the UK coastline (A McMillan et al., 2011). For swell waves originating from the southwest heights of 3.43 m were calculated to be the 1 in 200 year return period value for the study area. Both values have been calculated independently and so cannot be assumed to be a joint 0.5% probability event. The joint probability analysis in section 4.4.1 shows that combining these values would result in an event with a probability of occurrence much lower than 0.5%.

4.4 Methodology

This study investigates 30 different combinations of water elevation and wave height that have the same annual probability of occurrence, allowing the assessment of uncertainty in the 0.5% extreme event under present-day sea level. The approach combines a storm impact model with a flood inundation model. The storm impact model is able to take wave climate parameters and, when combined with a time-varying EWL curve, output the overwashing discharge at the defence crest of a 1D beach profile. Two examples of these 1D beach profiles are shown in Figure 4.1. This then feeds into the flood inundation model as a boundary condition, for the duration overwashing occurs, thus simulating the inundation extent and volume for that wave height and extreme water level combination.

The outputs from the inundation model show the uncertainty around a 0.5% event and how the inundation and overwashing rates can vary depending on the input wave and EWL combinations. Figure 4.2 shows the domain considered in the flood inundation model; it covers both nuclear sites on Dungeness foreland at the eastern end of this section of the coastline (Dungeness Point), and runs west through Denge Marsh, past Holmstone to Jury's Gap. The town of Lydd is also within the flood domain. The orange dots show the locations of the 1D beach profiles that are used as boundary conditions for the flood model (Figure 4.2). Profiles 5 and 13 in Figure 4.1 highlight the variability in the beach profile along the studied coastline.

4.4.1 Joint probability of extreme water level and wave height

To calculate joint probability a dataset of wave height and period along with a corresponding water elevation is needed. The UK has a WaveNet system of nearshore buoys that have been deployed since 2002 and are maintained by the Centre for Environment, Fisheries and Aquaculture Science (CEFAS) for the Environment Agency (EA) and Department of Environment Food and Rural Affairs (Defra). The closest buoy to the study site is located off the coastline at Hastings, which will collect data from 26th November 2002 to 1st April 2018 (CEFAS, 2015).

The tide gauge at Dover was used to provide the observed water elevation data. It is part of the UK tide gauge network, the data from the 43 gauges that are part of this network is looked after and quality controlled by the British Oceanographic Data Centre (BODC).

The closest significant wave height value to the peak of the observed water level at each high water was extracted from the wave buoy dataset. This input was then used in a joint probability program, JOIN-SEA (Hawkes et al., 2002; Hawkes and Gouldby, 1998), which has been extensively used and is well validated (Hawkes and Svensson, 2003); The approach JOIN-SEA uses is based on proposals by Coles and Tawn (1990). This is where a bivariate or a mixture of two bivariate probability distributions is fitted to the largest values or upper tail of the wave height and water level dataset. The output from JOIN-SEA is in the form of joint probability curves, shown for the area under study in Figure 4.3. An important caveat in this analysis is that the input datasets for the joint probability analysis are limited by the length of the wave buoy dataset. This has resulted in a lack of extreme data points, therefore reducing the confidence of the analysis. With longer datasets either from the continued collection of data via the wave buoy or from a hindcast wave and surge model this confidence could be improved for future studies. It should also be noted that the still water level 1 in 200 year return period of 4.8 m OD from the EA analysis is not directly comparable to the comparable return period from the joint probability derived water levels. This is because the EA analysis does not use any wave data within its analysis.

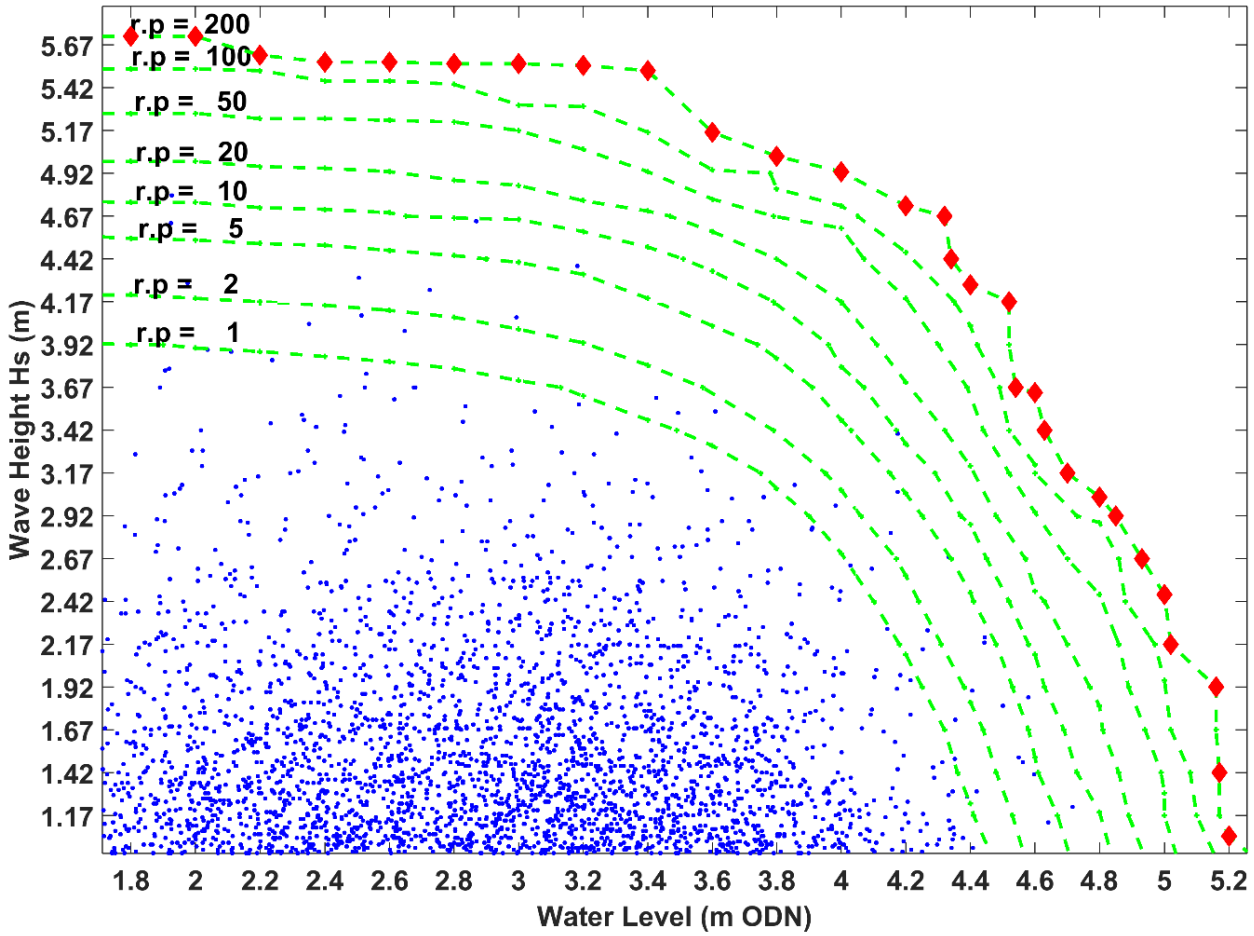

Figure 4.3: Joint probability of the observed wave height and water level for Dungeness, green lines denote the return periods of probability of occurrence, ranging from 1 in 1 year up to 1 in 200 years. The blue dots are wave height and water observations. Red diamonds show the 30 selected combinations of wave height and EWL that will be modelled.

The return period curve (Figure 4.3) shows that there is a range of water levels and wave heights that could potentially occur with a probability of 0.5%. With increasing EWL, a lower wave height is required to achieve the 0.5% probability level. Table 4.1 lists the combinations (shown in Figure 4.3 as red diamonds) that are modelled to show the uncertainty in flood inundation for this return level.

Table 4.1: List of wave height and water elevations with the incremental change in each parameter representing the 30 selected 0.5% event probability events.

Scenario Number	Water Elevation (m)	Change in Water Elevation (m)	Significant Wave Height (m)	Change in Wave Height (m)	Peak Wave Period (s)	Change in Period (s)
1	1.8	N/A	5.72	N/A	10	N/A
2	2	0.2	5.72	0	10	0
3	2.2	0.2	5.61	-0.11	10	0
4	2.4	0.2	5.57	-0.04	10	0
5	2.6	0.2	5.57	0	10	0
6	2.8	0.2	5.56	-0.01	10	0
7	3	0.2	5.56	0	10	0
8	3.2	0.2	5.55	-0.01	10	0
9	3.4	0.2	5.52	-0.03	9.1	-0.9
10	3.6	0.2	5.16	-0.36	8.3	-0.8
11	3.8	0.2	5.02	-0.14	10	1.7
12	4	0.2	4.93	-0.09	10	0
13	4.2	0.2	4.73	-0.2	9.1	-0.9
14	4.32	0.12	4.67	-0.06	10	0.9
15	4.34	0.02	4.42	-0.25	10	0
16	4.4	0.06	4.27	-0.15	10.5	0.5
17	4.52	0.12	4.17	-0.1	9.1	-1.4
18	4.54	0.02	3.67	-0.5	10	0.9
19	4.6	0.06	3.64	-0.03	10	0
20	4.63	0.03	3.42	-0.22	10.5	0.5
21	4.7	0.07	3.17	-0.25	10.5	0
22	4.8	0.1	3.03	-0.14	10	-0.5
23	4.85	0.05	2.92	-0.11	10	0
24	4.93	0.08	2.67	-0.25	10.5	0.5
25	5	0.07	2.46	-0.21	10.5	0
26	5.02	0.02	2.17	-0.29	10	-0.5
27	5.16	0.14	1.92	-0.25	10	0
28	5.17	0.01	1.42	-0.5	10	0
29	5.2	0.03	1.05	-0.37	13.3	3.3
30	5.28	0.08	0.92	-0.13	16.7	3.4

The peak wave periods were selected using the observed wave climate by plotting the significant wave height against peak wave period. The data has two clear linear relations (not shown) between the wave height and peak period, representing locally generated and

swell wave conditions. Longer period waves are associated with larger wave run-ups and wave overwashing of defences (Palmer et al., 2014). Therefore, to maximise impact, the longest period wave for each wave height was selected, creating wave events which were considered to represent the swell wave period rather than the local wind waves that were also present in the data set. Due to the need to maximise the number of data inputs within the limited data record the full dataset was used. As the highest waves originate from the southwest, which directly impact on the coastline under study. This means that the wave heights generated by the joint probability study are less likely to be overestimated than if the coastline was sheltered from the southwest.

4.4.2 Synthetic storm tide

Calculating the EWL as described in Section 4.4.1 is the first stage in creating the synthetic storm tide; A time varying water level curve that represents the tide, and the overlying storm surge that peaks at the calculated EWL is required, this is known as a storm tide curve. To produce a suitable curve, the dataset provided by (A. McMillan et al., 2011) provides synthetic scaled storm surge curves for each tide gauge location around the UK. Using the extreme water elevations calculated in Section 4.4.1 combined with the closest synthetic storm surge curve for Dungeness and a locally predicted spring tide, a time-varying water elevation curve that is representative of the study area peaking at the desired level for each scenario was produced. The curve was used as one of the input parameters for the storm impact model. The peak of the surge was assumed to occur at the same time as the peak of the tide, which follows the methodology of (A. McMillan et al., 2011). This approach will overestimate the hazard of the extreme water level as it is more likely to be the case that the

surge does not occur at the peak of the tide. However, given that this study is focussed on the uncertainty in the combination of events the approach of aligning the tide and surge peaks is considered to be appropriate.

In addition, the synthetic scaled storm surge curve is a potential source of uncertainty given that the one used has been tailored to Dover whereas the study site is approximately 30km to the west. However, it is the one suggested for the region by (A. McMillan et al., 2011).

4.4.3 Storm impact model

XBeach-G is the storm impact model that was used to simulate the overwashing of defences for a section of coastline at Dungeness (Figure 4.2). XBeach-G is a model for simulating storm impacts on gravel barrier beaches (McCall et al., 2014). It currently consists of a 1D model that is able to simulate the discharge over a defence crest. As the defences at Dungeness are primarily composed of a gravel barrier, this makes XBeach-G highly suitable for this work (McCall et al., 2015, 2014). For different study sites different models would be required, for example XBeach, which XBeach-G is developed from, would be suitable for sandy beaches (Bolle et al., 2011).

To represent alongshore coastal variability, 13 transects along the modelled section of coastline (Figure 4.2) are located at approximately 1 km intervals. The inputs used to force the model are the synthetic storm tide curve produced in Section 4.3.2 and the joint probability wave height and period calculated in Section 4.4.1. The storm impact model derives a JONSWAP wave spectrum based on the wave height and period values derived in Section 4.4.1. Wave direction was not taken into account during the XBeach-G simulations.

The final requirement that XBeach-G requires is the beach defence profile, examples of these are shown in figure 4.1. At Dungeness there are regular beach profiles at 50 m intervals along the section studied. Selected beach profiles were used to produce the input profiles with offshore bathymetry determining the sub-tidal gradient of the profile. In the case of Dungeness this profile becomes steeper and deeper the further east along the coastline. The bathymetry extends 1 km offshore which allows the use of offshore waves and surge curves. Each of the 13 profiles was run for each of the 30 0.5% probability scenarios, resulting in 390 XBeach-G simulations, each producing the overwash discharge at a defined point for the current defences for each of the 30 scenarios.

XBeach-G is able to calculate the morphology of the beach profile over the course of the simulation; a value of 0.025 m was used for the D50 of the gravel sediment (Dornbusch, 2005). Morphological change was enabled for the simulations in this study as it is important to allow the defence profile to change during the simulation as additional protection from an increase in the crest height due to wave action would be beneficial.

XBeach-G simulates many different output variables, such as water level and wave run-up, only one was used for this study was discharge in m^2s^{-1} per metre of the defence crest. The discharge outputs for the 13 profiles provided a spatially variable overwashing discharge of the defences suitable to use as a boundary condition for the inundation model at the crest level of the defences.

4.4.4 Flood inundation model

The flood inundation model used is the freely available LISFLOOD-FP; this is a two dimensional finite difference hydrodynamic model based on the storage cell approach. LISFLOOD-FP has been successful in coastal applications, and offers a good fit between observed and predicted inundation extents (Skinner et al., 2015). This model was first formulated by (Bates and De Roo, 2000) and is capable of being computationally efficient while running on high resolution LiDAR model domains (Bates et al., 2010). The LiDAR data for the domain covering the Dungeness and Romney Marsh area were provided at a horizontal resolution of 2 m by the Environment Agency Geomatics department. The key requirements for LISFLOOD-FP to ensure a good model simulation is an accurate terrain model (provided by the EA LiDAR), boundary forcing (provided by XBeach-G, as described in Section 4.3.3) and a friction parameter that determines how quickly water will flow from model cell to cell. Variable friction values for different cells can be used to denote low friction areas such as urban areas and high friction areas such as salt marshes. The domain under study at Dungeness and Romney Marsh has limited urbanisation and there are no forests or salt marshes requiring high friction areas, hence a single value typical of the main gravel terrain was used. Sensitivity analysis was performed with an example inundation scenario (Number 14 in Table 4.1) being run with high (0.1 Manning's n typical value for a forest) and a low (0.018 Manning's n typical urban value) values of friction. Outputs from this analysis were then compared with that produced using a 0.04 value of Manning's n used for all scenarios, which represents gravel areas. The percentage difference in extent between each of the three different friction value simulations was found to be of the order of +/- 0.04%.

Therefore, the domain is considered to be insensitive to the friction parameter and 0.04 is suitable to use as the only single global parameter for friction. The LiDAR was resampled to 5 m horizontal resolution to improve computational efficiency while maintaining a high resolution to accurately capture the inundation extent. This 5 m resolution is also a high enough to capture the defence crests within the model domain.

The model outputs, at 5 m horizontal resolution, the flood water depths at the maximum simulated inundation extent, and the maximum hazard map during the duration of the simulation. These consist of grids that match the input DEM although with either flood water depth and hazard value in the place of land elevation.

The hazard is calculated for each grid cell at each time-step using the following equation based on Ramsbottom et al. [2003]:

$$Hazard = (Water\ Depth * (Water\ Velocity + 1.5\ ))$$

Equation 1 shows that the hazard value is based on the water depth and velocity with the addition of a constant of 1.5. This constant has been added to compensate for the fact that flood water depths with low or zero velocities are still hazardous, but very low flood water depths are not regardless of the water velocity. Table 2 shows what different hazard value thresholds mean in relation to danger to people.

Table 4.2: The different values and thresholds of the hazard value and what that means for the general public, emergency services and vulnerable people (elderly and children).

Hazard Value	Category
Hazard Value >2.0	Danger for all (including emergency services
1.25< Hazard Value ≤2.0	Danger for most (general public)
0.75 < Hazard Value ≤ 1.25	Danger for some (elderly and children)
Hazard Value ≤ 0.75	Very low danger

4.5 Results

4.5.1 Output from Inundation Model Simulations

The results from the work detailed in Section 3 are shown below; the results include water depth and hazard 5th, 50th and 95th percentile values for all 30 scenarios (Figures 4.4A and 4.4B). The inundation area and volume are also calculated for all scenarios (Figure 4.4C). The mean discharge over the simulation across all 13 profiles has also been calculated and is shown in Figure 4.4D.

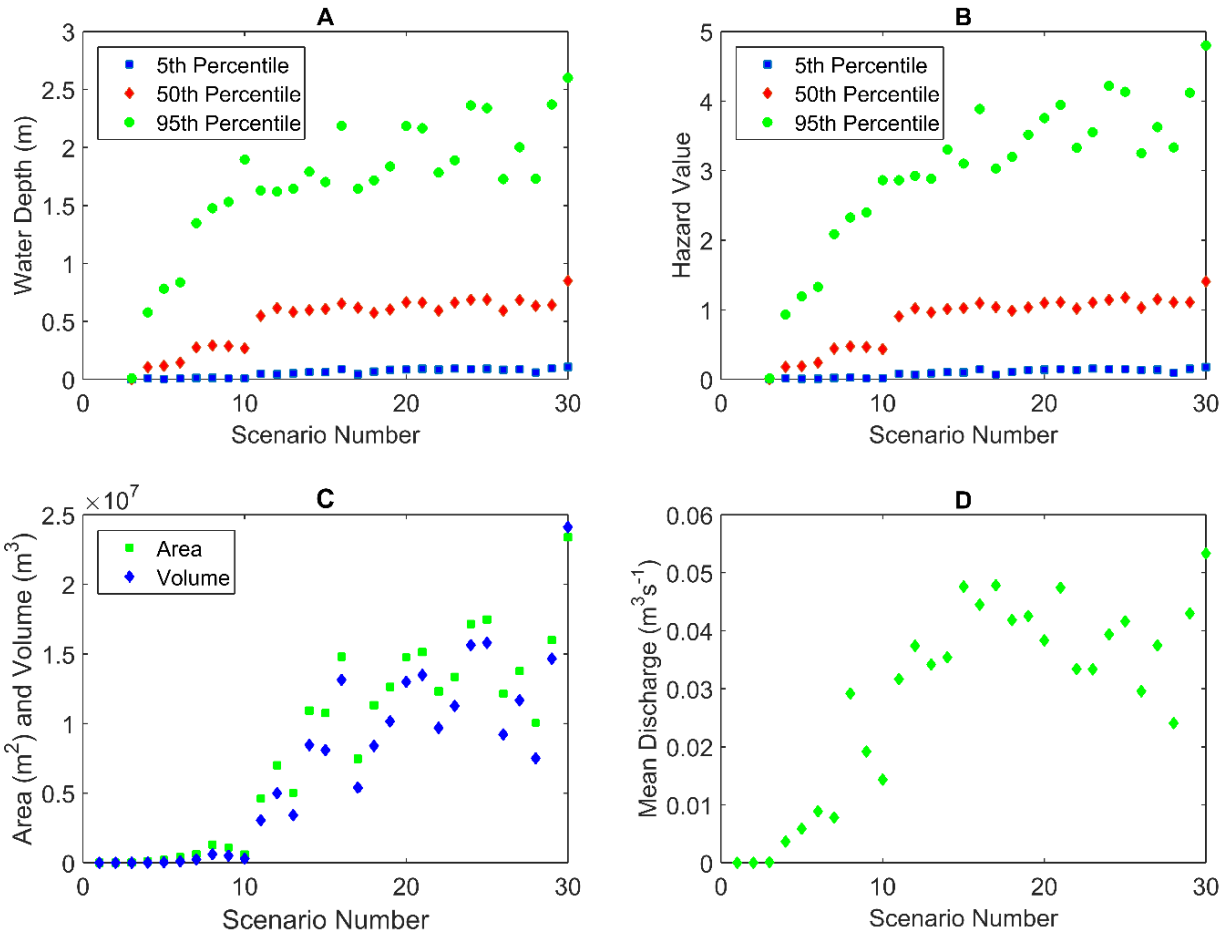

Figure 4.4: All subfigures show different results for each of the 30 0.5% annual probability extreme events. Table 1 details the different combinations that make up these events but increasing scenario number equates to increasing EWL and decreasing wave height. Subfigures are as follows: A water depths, B hazard value, C area and volume and finally D mean discharge over defences

The general trend across Figures 4.4A to 4.4D is increasing hazard value, water depth, area, volume and mean discharge with increasing scenario number, which corresponds to increasing EWL elevation and decreasing wave height. Figure 4.5 shows an example of the flood extent outlines from the 30 scenarios, the ones shown are Scenario 3, 8, 10, 16, 17 and 30 (Table 1), the minimum and maximum extent (3,30), and two tipping points in the inundation extent, a large increase (10,11) and a large decrease (16, 17). The general trend is of increasing extent and volume but there is variability in the maximum inundation extent

of the simulation results over increasing EWL and decreasing significant wave height. This variability is the result of the wave period used for each scenario, the period was selected by identifying the maximum period for that wave height in the wave buoy dataset as the maximum impact event for that wave height was desired.

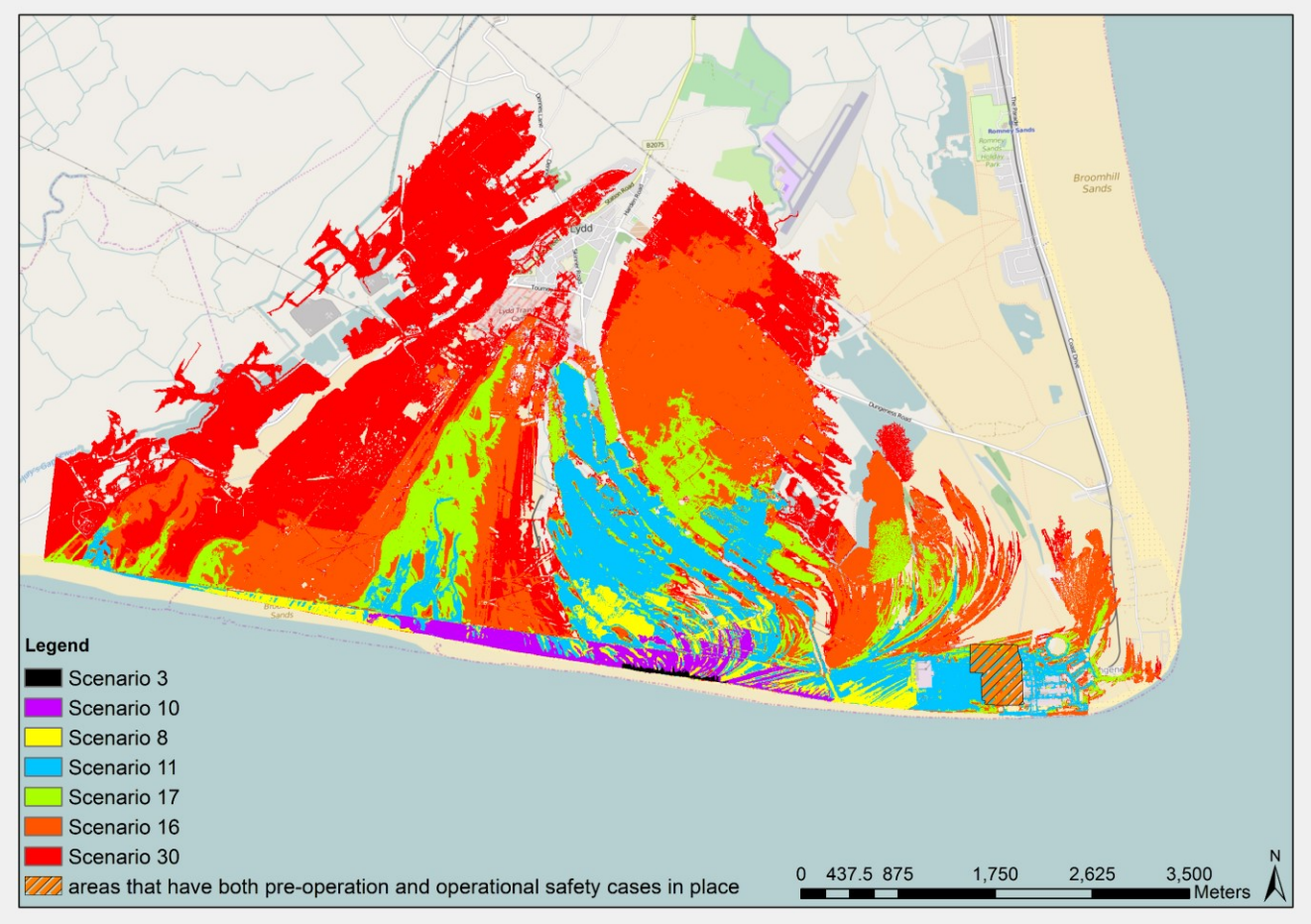

Figure 4.5: Maximum flood extent outlines for Scenarios 3, 8, 10, 11, 16, 17 and 30. The hatched area is covered by existing pre-operational and operational safety cases for the nuclear energy assets. Scenarios are listed in order of extent from minimum to maximum.

4.5.2 Variation in inundation area and volume

Figure 4.5 shows a significant variation in inundation extent between the maximum (red area) and minimum extent (black area). It also shows spatial variation along the coastline. This is related to variability in the beach/defence profile as well as the overwashing discharge rates for different combinations of wave height and extreme water elevation that have the same annual probability of occurrence. It also related to the wave period used for each scenario, the wave period selected varies due to a lack of data for large wave heights and a switch from wind to swell waves at lower wave heights.

Areas with lower crest level or that evolve to have a lower crest level cause overwash fans (Bradbury and Powell, 1992). Occurrences of these fans become more widespread and increase in size with increasing extreme water level. As morphology has been enabled for the simulations in XBeach-G this allows the potential for the crest level to lower. Ideally a second set of simulations would have been undertaken with the morphology turned off to see the impact of this, but the computational cost in doing so meant it was not completed for this study.

Figures 4.4A to 4.4C in section 4.4 show a distinctive trend of increasing area, volume, water depths and hazard values for increasing scenario number. The progression from scenario 1 to 30 moves to higher EWLs, lower wave heights and typically longer period waves. The first two scenarios show no overwashing of the defences, then in scenario 3 a slight increase in EWL allows the largest waves (although slightly lower than in scenarios 1 and 2) to overwash the defences. In Figure 4.4C there is a distinctive threshold or 'tipping point' in

scenario 11 where the area and volume of the maximum inundation extent increases rapidly. Figure 4.4D showing the mean discharge over the defence frontage also shows the same threshold.

The values for inundation area and volume after scenario 10 show greater scatter while still showing a positive trend or increase. The first 8 scenarios also show an increase in inundation area and volume (albeit much less than the increases after scenario 10). Reductions in both area and volume for scenario 9 and 10 are observed before the tipping point at scenario 11 due to the flood waters overwashing the secondary defences producing a large increase in area and volume for the scenarios after.

Figure 4.4C shows that after scenario 10 there is an increasing trend in area and extent of inundation with a significant amount of variability. This greater variability is due to the wave period of the relevant scenario. Table 4.1 shows the changes in wave period for each scenario, it can be seen that reduced increases in area and volume in Figure 4.4C are associated with lower wave periods. Examples of this are between scenarios 16 (orange) and 17 (green) in Figure 4.5, which represent a decrease in peak period of 1.4 seconds; this can also be seen in the areas and volumes of scenarios 21 and 22 and also 25 and 26 in Figure 4.4C where decreases in period of 0.5 seconds leads to an associated decrease in area and volume. However, longer wave periods cause greater increases in flood area and volume. This is most apparent between scenarios 10 and 11 but is also present for the volumes and areas of scenario 29 and 30, which are noticeably higher than the trend from scenario 10 onwards, which would suggest there may be another threshold with larger associated flood extents if there were higher wave periods scenarios associated with the 0.5% annual

probability wave height levels. The increases in wave period of 3.3 and 3.4 seconds, respectively, combined with the small increases of water elevation, 0.03 m and 0.08 m respectively, and large decreases in wave height, 0.37 m and 0.13 m respectively, shows that wave period has a large effect on the overwashing discharge over the defence crest for these two sets of scenarios (10 to 11 and 29 to 30) and thus on the inundation extent.

4.5.3 Variation in flood water depths and hazard value

Figure 4.4A and 4.4B show similar trends since the hazard value (Figure 4.4B) is proportional to the water depth. The tipping point after scenario 10, present in Figure 4.4C, is also apparent in these figures, although it is most evident in the 50^{th} percentile data series. Again, more scatter is noticed after scenario 10 within all the data series. The decreasing trend (8-10) in the extent (Figure 4.4C) is also weakly evident in the depths and hazard values (Figure 4.4A and 4.4B) for the 50^{th} and 5^{th} percentile values. Beyond scenario 10, unlike Figure 4.4C, the rate of increase in depth and hazard plateaus. Since the hazard value trends correlate to depth, here we only discuss the change in trend to the depth, which in turn influences the hazard.

Using Figure 4.5 to locate areas exposed to inundation we analyse Figures 4.4A and 4.4C to determine the changing trends in flood extent and depth. From scenarios 1 to 6 there is little change in flood extent, low water levels limit the ability of waves to overwash. The first two scenarios show no overwashing in the domain (Figure 4.4A). With flooding first occurring in scenario 3, the point where flooding occurs in scenario 3 is approximately 3 km west of the energy infrastructure towards the middle of the coastline in the model domain. This

demonstrates that the gravel barrier provides a lower level of protection than the augmented gravel barriers in place defending the critical infrastructure, which remain resilient. Flooding over the defences in later scenarios increases east and west from this point as more overwash fans develop, allowing floodwater into the floodplain that is initially contained by the Green Wall, but it in later scenarios it exceeds these defences as well.

Figure 4.5 shows the extent for scenario 10 (purple) and scenario 11 (blue); the latter extent is much larger than the former outline. Up to this point the inundation has been largely contained by secondary defences, the Green Wall. Scenario 8 (yellow) is the maximum depth and extent up to this point. These secondary defences restrict growth in the extent of flooding and enable the coastal water depth to increase until these defences are also exceeded in scenario 11, causing a state change in the inundation extent and depth trends. The extent and volume can then rapidly increase in the unconstrained state, while the depth remains shallow in the spreading water. This explains the why the 95th percentile water depth, representative of the outline of the area of constrained water, for scenario 8 to 10 increases peaking at scenario 10, despite the reduction in area and volume due to shorter wave periods limiting the number of overwash fans. Scenario 11 breaches these secondary defences which results in a much greater extent and volume but a reduction in the percentile flood water depths, which is most clearly reflected in the 95th percentile water depth value representing a large proportion of the outer area of the flooded region. Lower percentiles represent the shallow unconstrained depths towards the outer edge of inundation. The divergence in the percentile depth lines after scenario 10 suggests there is a large shallow outer margin to the spreading flood water, and that the coastal areas remain deep due to the constraining Green Wall. This is also mirrored in Figure 4.4C where the inundation area and

volume increase noticeably creating a tipping point where the impact of the event is greatly increased.

Once scenario 11 is reached the increase in flood depth is again quite constant, while the area and volume increases. This suggests the increase in overwashing causes the flood water to spread with a consistent depth over the domain. There is a noticeable dip in the inundation area and volume for scenario 17, again this is associated with waves of lowest period. For the larger extents, variability will also occur as new pathways become accessible to the flood water, enabling it to advance inland.

4.6 Discussion

4.6.1 Previous research

There has been a large amount of research into the behaviour of gravel barriers and beaches during extreme events. Physical modelling of gravel barriers has been used to investigate the morphological response of the barrier to wave and EWL conditions (Matias et al., 2014). Numerical models have also been developed to simulate the response of gravel barriers and beaches to storms. Recent research has found that the model used in this study provides a good predication of wave run up and initial overtopping (McCall et al., 2014). Another study has also found that it can be applied to predict storm impacts on pure gravel beaches and barriers with reasonable confidence for a range of forcing conditions (McCall et al., 2015). However, this work has only focused on the beach or barrier, and does not attempt to quantify the impact of storms on the areas at risk of inundation behind the defences.

Research in coastal inundation still commonly only considers EWL. While wave run up and over washing are present in some studies it tends to be in complicated coupled modelling studies which require a lot of resources to undertake (Stansby et al., 2013). Other coastal inundation research that focuses on the impact of sea-level rise also tends to neglect wave run up and overwashing impacts (Lewis et al., 2011; Wadey et al., 2015, 2013). Using joint probability analysis in estimating the joint probability of an EWL and significant wave height is not common in academic literature although examples do exist (Wadey et al., 2015). However, it is more widely used in commercial flood risk studies, making the results and conclusions drawn from this study useful and applicable to decision makers when redesigning or upgrading coastal defences or shoreline management policy.

4.6.2 Effect of wave period on inundation extent variability

It is well known that wave period has a significant effect on wave run up and overwash (Stockdon et al., 2006). However, since the swell wave period for the continually decreasing wave height remains at a similar value (10 s) to the largest wind waves it is suggested that the main factor changing the flood extent and depth is the EWL, and that 3.8 m total water level is the trigger level for waves of ~ 5 m to overwash the defences. The more variable wave period after scenario 11 is thought to be the cause of the greater scatter in results as the longer period waves generate greater overwash discharge. This tipping point saturates the coastal flood zones, causing water to flow inland once the maximum flood retention depth, due to the secondary defences, is reached at the coast. This trigger point also causes a wider area of overwashing both to the east and west and shows that increases in extreme

water level combined with increase in peak wave period drive the biggest increases in overwashing of coastal defences.

As wave period has a significant impact on flood inundation extent, scenario 30 - which has the maximum inundation extent and volume - was repeated with a smaller wave period, typical of a locally driven wind wave. This was found to be 2.8 seconds rather than 16.7 seconds of a swell wave with the same height. The re-simulation resulted in no overwashing. Since swell waves coincident with high water levels cause the highest flood hazard and the rate of increase in the hazard seems related to the increase in extreme water level it is suggested that trends in sea-level rise will translate directly into trends in hazard rating.

Changes in wave climate will also influence the uncertainty and probability of occurrence of events. This study has found the tipping point in wave water level combinations representative of the 0.5% probability event (between 3.6 and 3.8 m EWL and 5.16 and 5.02m significant wave height). Events to the right in Figure 4.3 require a lower water level to cause a tipping point, the events correspond to a lower return period and so have a greater flood risk associated with them.

4.6.3 Limitations of research

Limitations of this research are the short wave record, which is only 12 years long, reducing the confidence in the joint probability analysis to generate occurrence curves of 0.5% probability. Correction for sea-level rise in the EWL values has not been considered in this short dataset for joint probability analysis. For this near-decadal record the change in mean sea level is of the order 2.6 cm (rising at approximately 2.18 mm/yr. at Dover, Woodworth

(Woodworth et al., 2009). For longer term analysis beyond a decade it is suggested sea-level rise should be considered within the EWL analysis to allow better comparison of historic events over the time (Wadey et al., 2014). Wave direction that would clearly moderate wave-beach interaction and thus influence run up and beach profile response, was not considered in the analysis and the wave-water level data was obtained from available observations. To obtain the conditions directly offshore at the same location would require either modelling or additional observations.

Deciding where to extract the discharge from the beach profile is also difficult as the profile will change over the simulation due to the morphology being calculated in the storm impact simulations as the system is an evolving one. In this study the defence crest in the profile at the end of the simulation was used to define the point where the discharge was extracted from the storm impact output.

4.7 Conclusions

The scenario with the largest flood extent is number 30, this consisted of an extreme water level of 5.28 m OD and 0.92 m significant wave height, the swell period associated with that wave height was 16.7 s: this was also the scenario with largest wave period. Scenario 1 had the largest significant wave height at 5.72 m but with an extreme water level of 1.8m this combination had the least inundation with no flooding observed.

The analysis has shown that increasing extreme water levels drives increasing flood inundation of the floodplain; large waves with the corresponding water elevation to produce a 0.5% probability event do not cause significant flooding due to the shallow inter-tidal

gradient of the beach dissipating the wave energy before it can overwash the defences. Wave conditions have been shown to have a large effect on the scatter in inundation depth distribution, area and volume. Higher wave periods drive higher overwashing rates and thus flood inundation extents for the same annual probability value, and create the upper level in the scatter.

It was also found that swell waves (i.e. long wave period waves) were the ones responsible for the increased inundation. This was tested by re-simulating the event that posed greatest hazard with a wind wave period of 2.8 s, which resulted in no flood inundation.

This study has shown that relying on a single return period standard of protection is too simplistic as the many different combinations of wave height and extreme water elevation have significant differences in overwashing rates and inundation extents. Applying the methods in this paper to other locations would help with the decision making in refurbishing or building of new defences while also reducing the uncertainty in what the defences need to be resilient to. This will ensure the defences are not over or under engineered to cope with a 0.5% annual probability extreme event, thus giving coastal managers and stakeholders more confidence of the sea defences' resilience to this level of protection.

For this location, high water levels and low, long (swell) waves give rise to the greatest flood hazard. Combining the available 0.5% probability swell wave with 0.5% probability water level could underestimate the flood risk as wind waves would influence the wave return period analysis. Small positive increments in water level result in a larger increase in hazard when compared with the resulting increase in hazard from the same increment in wave

conditions. Showing that increases in water elevation is the main source of increased flood risk in locations where the variability in total elevation is small and waves are large.

4.8 Acknowledgements

We would like to acknowledge the ARCC "Adaptation and Resilience of Coastal Energy Supply" (ARCoES) project (EPSRC EP/I035390/1) and the ERIIP "Sandscaping for Mitigating Coastal Flood and Erosion Risk to Energy Infrastructure on Gravel Shorelines: a case study approach" project (NERC NE/M008061/1) in partnership with the Crown Estate. Finally, we gratefully acknowledge the contributions of Tom Dauben, a local EA representative, for highlighting potential study locations.

5 Quantifying the Impact of Saltmarsh Erosion on Coastal Resilience

5.1 Abstract

Saltmarshes can enhance the resilience of a coastline by attenuating waves, particularly during extreme events where they reduce the impact of wave action on the section of coastline behind the marsh. The benefit a saltmarsh provides in terms of resilience to a 1 in 200 year or 0.5% annual probability extreme event has been investigated to progress research into saltmarsh wave attenuation studies. This research quantifies the impact of eroding saltmarshes, trapped between fixed shorelines and rising mean sea level, on the benefits that the saltmarsh provides in terms of coastal resilience. By using a storm impact model to simulate the wave run-up that arises during an extreme event, we investigate the current resilience of Dengie marsh, Essex located in the southeast of the United Kingdom (UK). For coastlines protecting urban areas a common resilience standard is to withstand a 0.5% annual probability extreme event. Using a storm impact model able to simulate the presence of a saltmarsh during an extreme event, the saltmarshes' resilience was assessed using a R2% parameter - this variable is the elevation that 2% of waves will reach or exceed over a ten-minute interval. Multiple erosion scenarios were then simulated with the saltmarsh partially and fully eroded. The R2% parameter was used to examine the impact of erosion on the resilience properties of the saltmarsh compared with the present-day. This research used many different initial marsh profile shapes, making this a representative study which can indicate the potential impacts of erosion on the coastal resilience properties of saltmarshes in general. The results show that there is a critical saltmarsh width of 810 m

where the linear increase in R2% in response to reducing width, plateaus at a constant value. A second critical width at around 270 m can be observed where the R2% starts to increase again, but at a rate three times of that previously for widths of 810 m and greater. This indicates that the saltmarsh is able to maintain coastal resilience even while being eroded between these two threshold widths, until 270 m where the resilience reduces significantly. The height of the saltmarsh frontage was also found to be important, where decreasing height resulted in an increase in R2%. However, the relationship is not as significant as width. Beach slope had a trend of increasing slope resulting in increased wave run-up, but was very inconsistent across the range of gradients simulated and was not a significant factor in the change in resilience during the erosion of saltmarshes. Therefore, while all parameters are important in controlling the resilience properties of the saltmarsh, width is the most important contribution, followed by height, and lastly beach slope.

5.2 Introduction

5.2.1 Shoreline Management and Climate Change

The world is changing - shorelines are under pressure from rising mean sea levels and increasing populations living at the coast. The amount that sea levels will rise by is uncertain, with latest global projections suggesting an increase of 1.8 m being possible by 2100 - albeit at the 95th percentile (Jevrejeva et al., 2014). Shoreline management will aim to mitigate these impacts but there are also other potential impacts in the form of increased wave height, storminess and tidal range. However, the projected changes in these parameters are much less certain than the projections made for sea-level rise (Lowe et al., 2009). On a regional scale, land subsidence will also have an impact by amplifying the impact of sea-level rise

(SLR). In this changing climate, managing the coast over time will become more difficult as the increased impacts of climate and environmental change will be felt. Coastal communities will face an increased risk of flooding as a result of these changes. In the UK, the coastline is currently informed and guided by shoreline management policies where different sections of the coast have different management options applied (Cooper and Pontee, 2006), i.e. "hold the line", "no active intervention" and "managed realignment". Hold the line is common in urban areas or critical infrastructure, such as energy infrastructure, that tend to have hard defences protecting them. These defences draw a line in the sand beyond which no further erosion of the land is acceptable. While this can protect terrestrial areas and infrastructure, it has an adverse impact on the natural environment where intertidal habitats are trapped between rising sea level and the hold the line policy, resulting in "coastal squeeze" (French, 2001). This process can also be ultimately detrimental to hard defences as when any "soft" defences that front them (including beaches, mudflats or saltmarshes) are eroded away, the hard defences will feel the full impact of extreme events and day to day wave and tidal action, resulting in a higher cost in maintaining them and a potentially shorter lifetime. Areas with a policy of no active intervention rely on any natural defences or existing defences that will no longer be maintained or replaced. Managed realignment relies on working with the natural environment and allowing some "slip" in the defences where it can erode, recover etc. rather than trying to fix the defence in place. Managed realignment can also consist of actively removing or breaching defences, returning previously reclaimed lowlands to inter and supratidal habitats. This approach complements soft defences, such as beaches and saltmarshes, and is usually used to allow the creation of new intertidal habitat, replacing that lost by the presence of hold the line policies elsewhere in the region.

Saltmarshes currently act as a natural buffer zone, providing protection from extreme events by attenuating wave and tidal flow (Möller et al., 2014b). However, the effectiveness of the saltmarsh in attenuating waves during extreme events is poorly understood. Physical modelling has quantified the reduction in wave height over a saltmarsh during extreme events (Möller et al., 2014b). Numerical modelling of saltmarshes has also been undertaken, revealing that they are vulnerable to erosion during normal wave conditions (Fagherazzi, 2014). This is due to the waves impacting on the saltmarsh scarp peak when the water level is just above the saltmarsh surface, which is common over a tidal cycle. However, during extreme events numerical modelling has also supported that waves during a storm surge can be attenuated by the underlying vegetation. It has also noted that empirical studies of wave dissipation over transplanted saltmarsh are limited to wave flumes that are too small to quantify the effects of extreme events. Saltmarshes are able to resist the impact of extreme events and recover well but are at risk from normal weather conditions (Fagherazzi, 2014).

Recent research into the response of saltmarsh boundaries to wave action during extreme and normal weather conditions has determined a linear relationship. As wave energy increases, the saltmarsh response remains linear and there is no critical threshold that leads to increased erosion (Leonardi et al., 2016). This study also found that extreme events only contribute around 1% of the erosion of the saltmarsh, while moderate storms produce the bulk of the observed erosion.

Changes in wave climate, increasing mean sea level and infrastructure construction, such as embankments, are currently believed to be the main contributions to saltmarsh erosion. This will result in an impact on any benefits that the saltmarsh provides in wave attenuation and

resilience to extreme events (van der Wal and Pye, 2004). There is also the concern that new saltmarshes will not develop on any managed realignment sections of coastline due to biological effects (Wolters et al., 2005).

As well as waves, saltmarshes are able to attenuate the impact of a storm surge within an estuary, where lower wetland elevations result in more attenuation of a spring tide but higher elevations provide more attenuation for storm surges. The larger the surface area the better the attenuation up to a threshold size where larger area does not contribute to greater attenuation of the storm tide (Smolders et al., 2015).

This study assesses the coastal resilience provided by saltmarshes, i.e. mitigation of wave and storm impacts, and how this resilience is impacted as the saltmarsh erodes. The inclusion of saltmarshes in quantitative flood risk assessments has been hampered by the lack of empirical evidence and quantitative understanding of their ability to act as wave dissipaters during extreme events, although recent research indicates this is changing (Fagherazzi, 2014; Leonardi et al., 2016; Möller et al., 2014a). It is important to understand how much resilience or wave attenuation a saltmarsh can provide during an extreme event and at what point that the marsh's resilience properties are significantly affected by erosion processes, i.e. is there a critical width or height that, once passed, significantly impairs the saltmarsh's ability to attenuate waves? The relationship between saltmarsh width and height against wave attenuation is therefore important to quantify.

Defences are designed to be resilient to a specified extreme event. This design standard is generally the 1 in 200 years or a 0.5% annual extreme event (Wyse, 2015). For coastal areas these extreme events can be classified by the annual probability of a given water level and

wave height occurring. What waves are present during an extreme water level event is important as wave action will contribute towards the impact of the extreme event and cause overwashing of defences at a lower threshold then when considering extreme water levels alone (Prime et al., 2016). Extreme water levels are caused by storm surges, a storm surge occurs when high winds and low atmospheric pressure act on the sea surface to cause a temporary increase in water level (Wells, 1997). If this occurs in conjunction with a high tide, particularly a spring tide, an extreme still water level (EWL) event arises. EWLs will have an increased impact and increased probability of occurrence in the future due to rising mean sea level (McInnes et al., 2003). In areas where wave action is less important, i.e. sheltered estuaries, rivers etc., then a return period based on water level only or possibly with the addition of river flow would be more appropriate. Projecting the probability of a combination of two dependent variables is known as joint probability analysis (P. J. Hawkes and Svensson, 2006).

5.2.2 Study site

The Blackwater estuary in southeast, UK is situated between Maldon and West Mersea in Essex (Figure 5.1 and 5.2). It is a high value area with around five and half thousand hectares designated as a Site of Special Scientific Interest (SSSI) (Natural England, 1993). It is also the location of a Special Protection Area (SPA) (JNCC, 2001). It is estimated that 10% of the saltmarshes have been eroded and lost to the sea between 1964 and 1985 (Harmsworth and Long, 1986). Northey Island in the estuary is home to the first experiments in the UK for managed realignment. Here, saltmarsh has been created by setting back sea walls and

reducing coastal squeeze. The site was found to be developing satisfactorily to the managed realignment works (Harmsworth and Long, 1986).

Figure 5.1: Image shows study area location in context of UK. Black box denotes regional area.

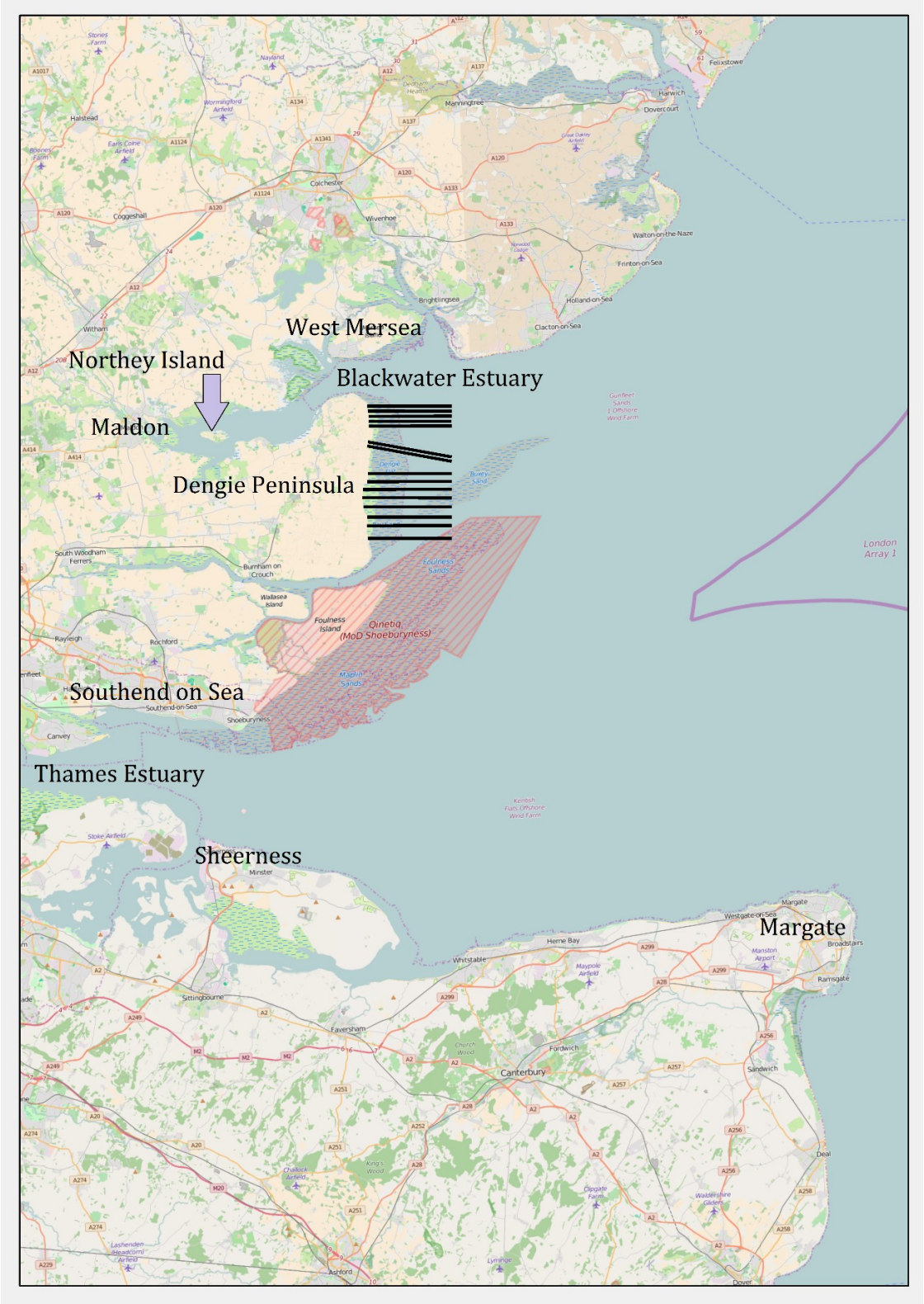

Figure 5.2 Image shows regional area surrounding the Blackwater estuary. The black lines highlight the position of the 15 1D cross-shore profiles used in the study.

The Blackwater estuary is also home to important energy infrastructure in the shape of Bradwell nuclear power station and associated transmission capacity. Bradwell started generating in 1962, and operations ceased in 2002. The power station is currently in preparation for its 'care and maintenance' phase where it has been defueled and buildings not exposed to radiation have been removed, e.g. turbine hall etc. Final site clearance is projected to occur by 2095. Bradwell is also important as it is has been identified as a potential site for a new build nuclear power station, meaning that as well as the current site being present up to 2100, if a new station is built there will be a nuclear site present well past 2100. As a consequence, these sites are required to be resilient to changing climate over an extended timescale.

The specific section of coastline under study is on Dengie peninsula as shown in Figure 5.2 and 5.3. The coastline of the Dengie peninsula comprises saltmarshes with varying widths, heights and profiles. Dengie marshes is in a macro-tidal area, with tidal ranges up to 5.82 m and a mean high water springs of 2.52 m. The local wave climate has two directions that the majority of the waves originate from, particularly the extreme waves. The largest waves are over 5 m and originate from between 195 and 235 degrees (CEFAS, 2015; National Oceanography Centre, 2014). Given the orientation of the coastline under study these large waves do not directly impact upon the study area. However, the other dominant direction, i.e. from 35 to 70 degrees, also has waves that are nearly as extreme, with values between 4 and 5 m. This is a direction that will directly impact on the coastline and is the one used for the model runs. This direction is also the primary direction for waves under 2 m.

As this section of coastline is exposed to the North Sea, understanding the impact of extreme events and what resilience the saltmarsh provides against these extreme events is a crucial element of future resource planning, particularly as it erodes and mean sea level increases. It is important to be able to ensure the correct management policy is applied to ensure the habitats remain and the area is resilient for critical energy infrastructure up to 2100 and beyond.

This study has undertaken joint probability analysis to determine the 0.5% annual probability event combination of significant wave height and extreme water level that has the greatest wave run-up. This combination has been used as the boundary forcing to drive a storm simulation across 15 1D profiles that are representative of the saltmarsh in the region (Figure 5.3). The results from the storm impact model will allow us to assess the relationship between saltmarsh width and the coastal resilience provided by these saltmarshes.

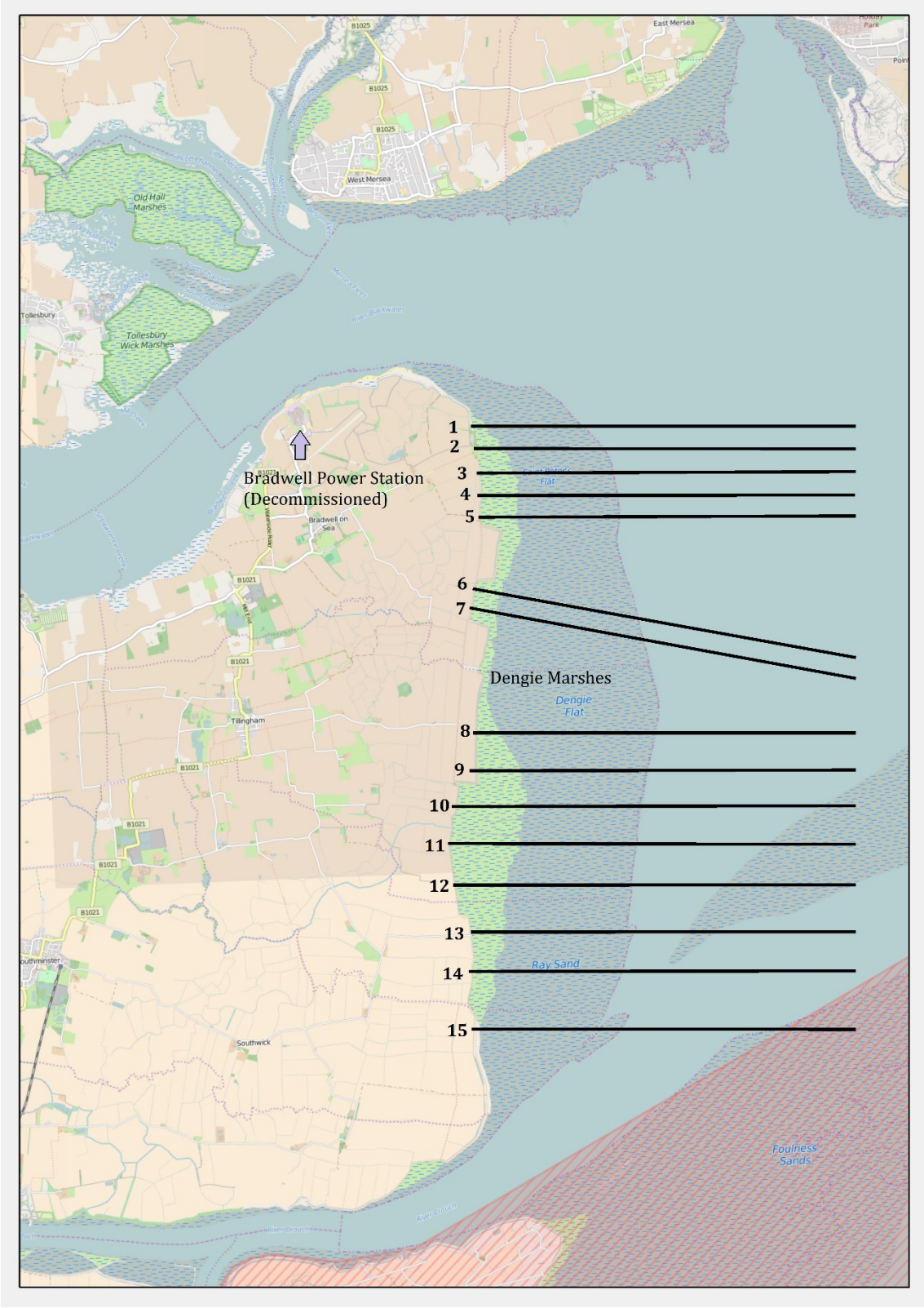

Figure 5.3: Close-up of Dengie Marshes showing the location of 15 cross-shore profiles that capture the variability of the saltmarsh and offshore bathymetry.

Dengie marsh is characterized by many different plants, although two common varieties are *Spartina. anglica* and *Puccinellia. maritima. S. anglica* is a perennial grass typically occurring in the pioneer zone and low saltmarsh (Adam, 1993). Throughout the last century it has spread from its original site (southern coast of the UK) to saltmarshes all over Europe both through natural processes and deliberate transplantation. The main reason for this was the perceived stabilization benefits it provided (Rupprecht et al., 2015). *P. maritima* is a perennial grass which has been identified as a typical habitat in the low to mid saltmarsh. This is a common grass of European saltmarshes and is tolerant to trampling, biomass loss and water-logging. Both of these species are present at Dengie, with *S. anglica* dominating the lower marsh and *P. maritima* making up the mid to upper marsh. It was assumed that the threshold between the lower and upper saltmarsh was located at 2.4 m ODN (Rupprecht et al., 2015).

5.3 Method

The methodology used in this study consists of the following stages, first performing a joint probability analysis of significant wave height and extreme water level for the study area. The next step consists of determining the biggest impacting 0.5% annual joint probability event for significant wave height and extreme water level from the range of combinations possible on the 0.5% annual probability contour (Figure 5.4). For this study impact is defined by the magnitude of wave run-up during the extreme event. The higher the run-up the larger the impact and thus a reduction in resilience of the defences against extreme events. Once the biggest impact combination has identified, these are then used as boundary conditions for each of the 15 cross-shore profiles at different sections of the saltmarsh (Figure 5.3). The

simulations are then re-run with the same extreme event conditions, but with modified cross-shore profiles that result from 50%, 75% and 100% erosion of the saltmarsh width for each given profile. For a few selected profiles, simulations were also run with 25% of the saltmarsh being eroded away. The output metric used to compare results is the R2% value for wave run-up; this is the water elevation that 2% of waves reach or exceed during the simulation.

5.3.1 Joint Probability analysis and input data

An extreme event can be made up of different sources that contribute to its impact. For coastal extreme events the most prominent contributions are extreme water level and significant wave height (H_S). Both of these sources can be assessed to have an annual probability of occurrence singularly or together. To calculate the joint probability, i.e. their probability of occurring together, wave height at the peak of the observed tide is required. This can be provided by a nearby wave buoy (if present) and tide gauge, as undertaken by Prime et al. (2016). However, this usually has the disadvantage of being a short dataset and is not necessarily in close proximity to, or representative of, the waves within the study area. To mitigate this a 30-year wave hindcast model dataset was used, which has the advantage of being over three times longer than the closest wave buoy and can also provide wave and surge output that is within the study area, and thus provides more appropriate wave and water level parameters to use within the analysis. The model data were validated by also extracting data from the model at the site of the nearest wave buoy and comparing with the wave buoy data set. Comparing the hindcast model with the wave buoy found a bias of -0.001 m with a Root Mean Squared Error of 0.4 m.

The 30-year hindcast can now be used as input to the joint probability analysis. The H_s during each observed high water was used in a joint probability program, JOIN-SEA (Hawkes and Gouldby, 1998), which has been extensively used and is well validated (P. J. Hawkes and Svensson, 2006). The approach JOIN-SEA uses is based on proposals by Coles and Tawn (1990). This is where a bivariate or a mixture of two bivariate probability distributions is fitted to the largest values or upper tail of the wave height and water level dataset.

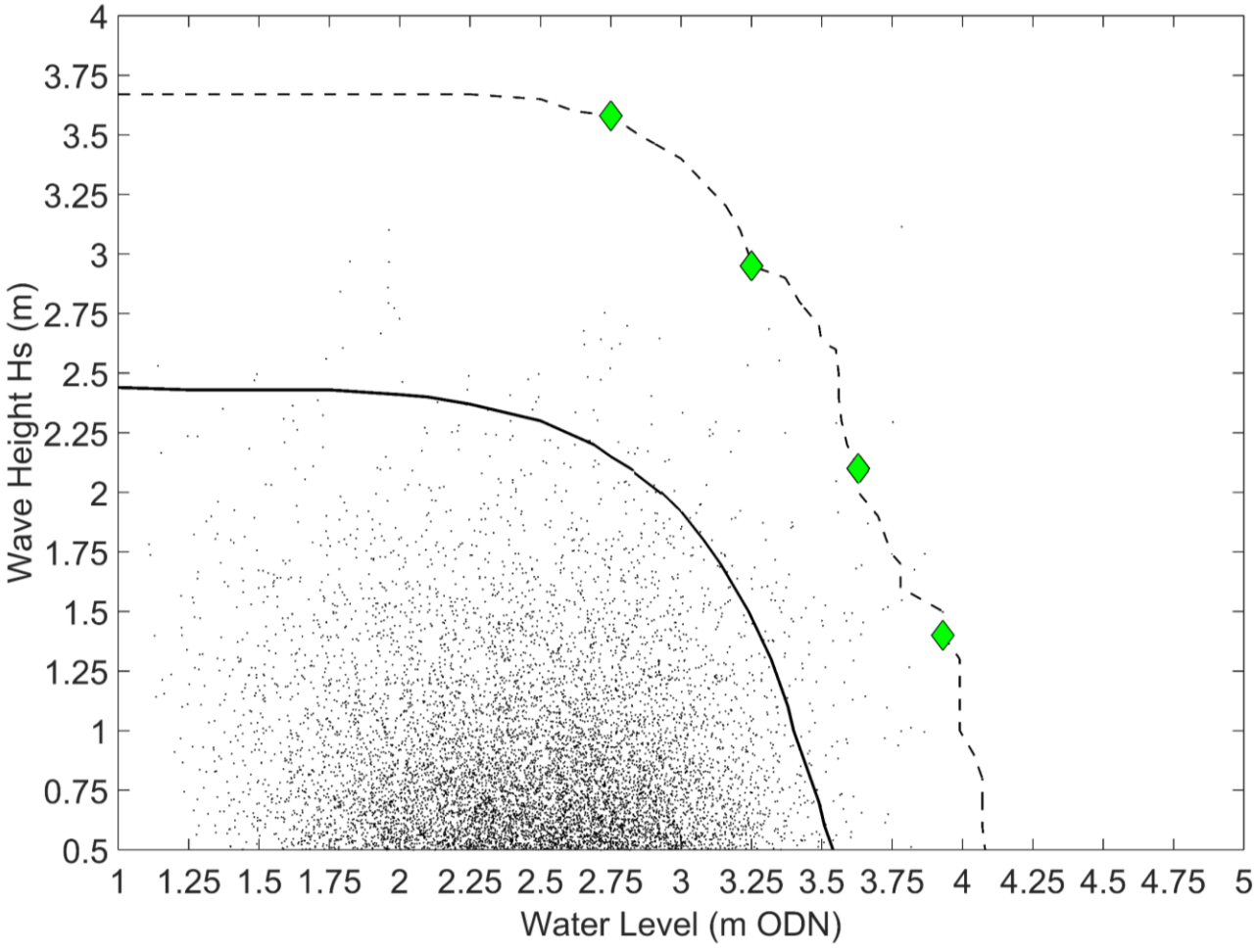

Figure 5.4: Joint Probability plot for Dengie Marshes. Dots show the wave height at the peak of the observed tide, solid line shows the 1 in 1 year combination contour, dashed line highlights the 1 in 200 year (0.5% joint probability event) contour. Green diamonds highlight which different combinations were simulated on the 0.5% probability event contour.

The outputs from JOIN-SEA are presented as joint probability curves (Figure 5.4). The return period curve (Figure 5.4) shows the range of H_s and WL that could potentially occur with a probability of 0.5%. With increasing WL, a lower H_s is required to track the 0.5% probability level. Prime et al. (2016) demonstrated that different combinations of wave height and water level that have the same probability occurrence can have widely varying overwashing rates and inundation extent. This means consideration of the varying combinations of water level and wave height that have same probability. The 4 combinations shown as diamonds on the dashed 0.5% probability contour in Figure 5.4 were used as input to cross-shore profile 9 from the study area. These points are at equal intervals along the probability contour, between the section of the contour where both parameters are changing. I.e. where the contour is no longer horizontal and before it becomes vertical. These different combinations are used as input conditions to the storm impact model to assess which combination has the greatest wave run-up and thus the biggest impact on the resilience of the coastline in the study area.

5.3.2 1D extreme event simulations

The storm impact model used in this study is XBeach (Roelvink et al., 2010). XBeach is an open source numerical model which was originally developed to simulate hydrodynamic and morphodynamic processes and impacts on sandy coasts, with a domain size of kilometers and on the timescale of storms. Since then, the model has been applied to other types of coasts and purposes. The model includes the hydrodynamic processes of short wave transformation (refraction, shoaling and breaking), long wave (infra-gravity wave) transformation (generation, propagation and dissipation), wave-induced set-up and

unsteady currents, as well as overwash and inundation. The morphodynamic processes include bedload and suspended sediment transport, dune face avalanching, bed update and breaching. The wave attenuation effect of vegetation present in a saltmarsh can also be simulated within the model (see below). XBeach has been validated with a series of analytical, laboratory and field test cases using a standard set of parameter settings (Roelvink et al., 2010).

As the sea bed is predominately sand in the study area, XBeach is appropriate to use for these simulations. XBeach can be run as a 2DH or 1DH model. To save on computational cost, this study selected 1D profiles at 15 points along the coastline. Figure 5.3 shows the location of these profiles in the study area. The locations selected are a good representation of the variability in the saltmarsh along this section of the coastline.

5.3.3 Storm impact model inputs

Each cross-shore profile was created by combining LiDAR elevation data provided by the Channel Coast Observatory (Channel Coast Observatory, 2016). These are usually timed so that they survey at low tide, meaning that large parts of the beach and intertidal areas are part of the survey. This is in contrast with the Environment Agency surveys which focus on terrestrial surveying and are inconsistent in their coverage of beaches and intertidal areas. However, they have a much higher coverage of the UK. The offshore part of the profiles was completed using a gridded bathymetry data provided by EDINA digimap services (University of Edinburgh, 2016). The bathymetry has a horizontal resolution of approximately 30 m, whereas the LiDAR has a horizontal resolution of 1 m. Figure 5.5 shows an example of one of these profiles, it does not show the offshore bathymetry just the LiDAR elevation values that

cover the sea defences and saltmarsh. From an initial profile, the salt-marsh width was reduced by half, three quarters and completely removed. This was achieved by removing the relevant section of saltmarsh between the sea defence and seaward face of the saltmarsh. The remaining profile is then set back so it aligns with the sea defence. It is assumed that the beach slope remains the same to fill the gap between the original position of the saltmarsh seaward edge and its new position. Figure 5.5 shows this process with the present-day saltmarsh being present on the left image and 50% eroded being shown on the right. The assumption that the beach slope continues as a replacement for lost marsh is a key assumption. If the marsh cliff height is maintained and the foreshore lowered then this could have an impact on the results and it is recommended that further studies investigate this.

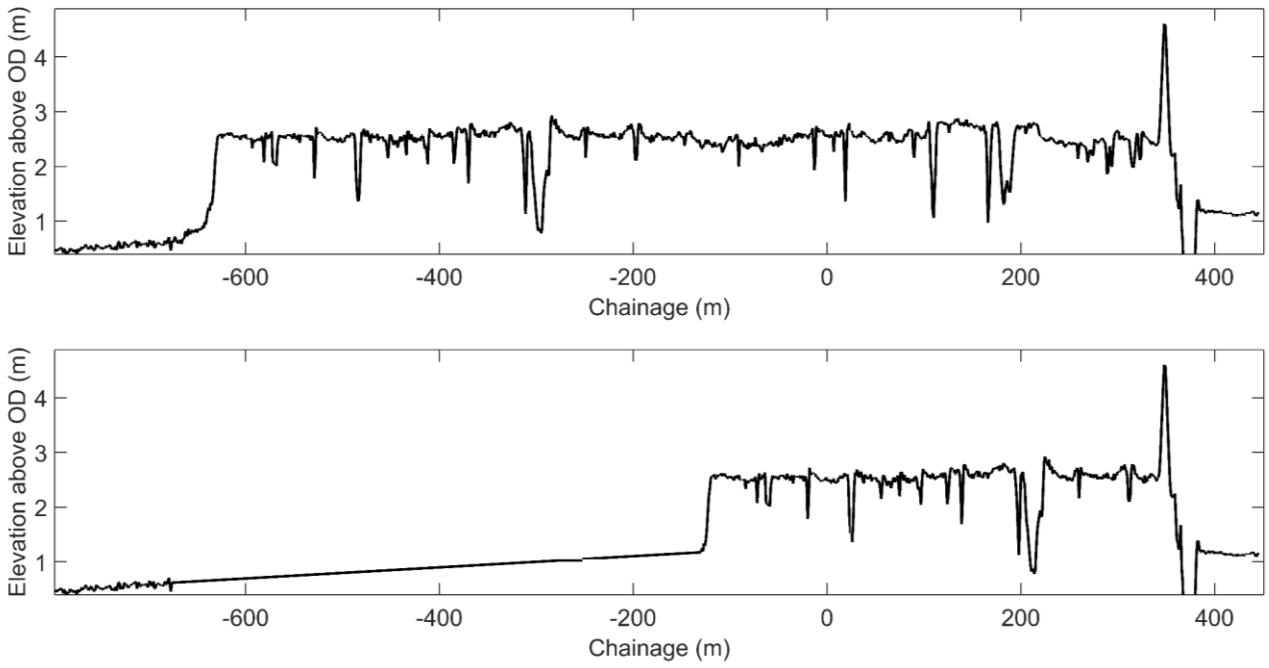

Figure 5.5: Example of saltmarsh cross-shore profile, (offshore bathymetry not shown). Top graph shows present-day saltmarsh, and the bottom graph shows 50% eroded saltmarsh with beach slope continued to replace eroded saltmarsh.

The joint probability analysis provides the input wave height and extreme water level conditions, but other wave parameters such as direction and peak period are required. The representative storm surge boundary conditions were created by using the methodology of (A. McMillan et al., 2011). This uses a synthetic storm tide curve; one has been created for each tide gauge around the UK. Combining this curve with a spring tide for the study area and applying the extreme water level calculated by the joint probability analysis to the synthetic curve results in a time-varying water level that is a good representation of a storm tide. This was fed into the storm impact model along with the cross-shore profile and wave parameters. The additional wave parameters were taken from the subset of wave data that corresponds to the peak of the observed tide. Xbeach takes the wave parameters and produces a JONSWAP spectrum that is applied at the nearshore end of the beach profile. The JONSWAP spectrum was derived after analysing data from the Joint North Sea Wave Observation Project (JONSWAP) where it assumed that if the wind blew steadily for a long time over a large area, the waves would come into equilibrium with the wind (Pierson and Moskowitz, 1964). However it was found that the wave spectrum is never fully developed and peak enhancement factor was added to improve the fit to the measurements of the project (Hasselmann et al., 1973). Vegetation is added into the model by defining the physical aspects of the different plants within the saltmarsh, friction coefficient, stem diameter and density etc. The type of plant present is then defined for every section of the 1D cross-shore profile. For this study two different plant types were used, one to represent the lower saltmarsh and the other to represent the upper saltmarsh. These plants were *P. maritima* and *S. anglica*.

5.3.4 Storm impact model outputs

XBeach is able to simulate and output many different parameters, such as discharge, bed change across the profile and water level. The output that is of interest is the wave run-up gauge; this was set up to output the run-up of the waves during the 0.5% annual joint probability extreme event. The output time step for run-up was set at 0.5 seconds, with all other parameters being set at 10 seconds. The reason for the high-frequency output time-step for run-up is to be able to capture the high variability in the parameter during the simulation. For this study, the R2% is generated by calculating the 98th percentile value for every 600 s section of the 0.5 s time series. The maximum of these calculated values is taken to be the R2% value. Figure 5.6 shows an example output from the model with diamonds showing the 98th percentile value for each 600 s section.

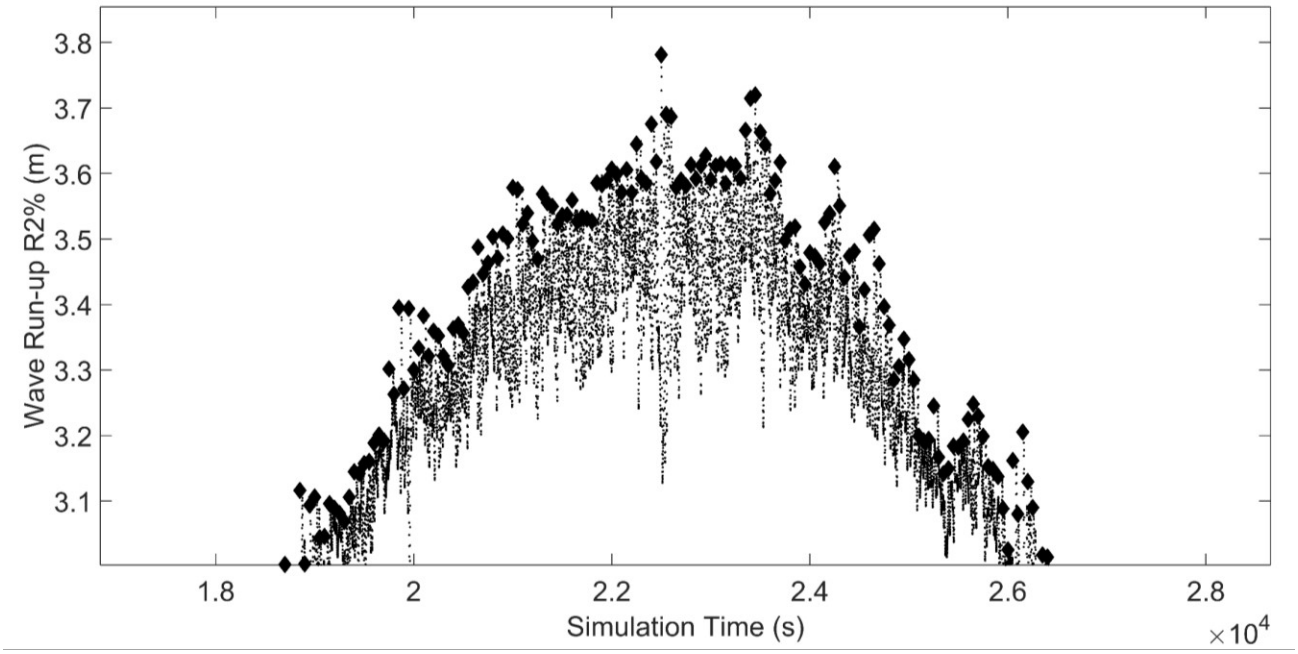

Figure 5.6: Example run-up output from simulation. Only the peak of the extreme event is shown with black dots denoting the 0.5 s run-up output and black diamonds showing the R2% values for each 600 s bin over the simulation.

5.3.5 Selecting 0.5% annual probability combination for simulations

The previous sections have shown how the joint probability is derived and how the storm impact model is set up, and also defined the output variable that is being studied. The four combinations highlighted in Figure 5.4 have been set up for one example profile, in this case profile 9. Each combination was simulated and the R2% metric was calculated as described in section 5.2.4. The simulations were repeated 5 times to give a mean R2% value for each 0.5% annual joint probability combination. Table 5.1 shows the results of these simulations. It can be seen that combination number 4 resulted in the biggest mean R2% value and this is the combination of extreme water level and significant wave height that will be used as the input conditions for the 15 profiles covering the saltmarsh in the study area and for all erosion scenarios (0%, 25%, 50%, 75% and 100% eroded). This research found that the combination with the highest extreme water level had the greatest impact on resilience. This is consistent with Prime et al. (2016) where, using wave and water level combinations of the same joint probability, the impact on resilience is greatest by combinations that consist of the biggest extreme water level rather than combinations with a large significant wave contribution.

Table 5.1: Mean R2% outputs for each 0.5% annual probability combination of wave height and extreme water level simulated across profile 9.

0.5% Probability Combination	Significant Wave Height (m)	Extreme Water Level (m)	Peak Period (s)	Mean R2% (m)
1	3.63	2.75	7.2	3.16
2	2.95	3.25	6.3	3.18
3	2.10	3.63	6.5	3.62
4	**1.42**	**3.9**	**6.2**	**3.99**

The peak period values used within these simulations were selected from the 30-year hindcast data, using the subset of data that corresponds to the wave conditions at the peak of the observed tide. The largest peak period associated with the relevant significant wave height was used. The wave direction that matched all of the different significant wave heights used and would also impact on the coastline was used in all simulations. From the hindcast model dataset it was found that a direction of 40 degrees would meet both of these criteria.

5.4 Results

Each of the 15 profiles for each of the erosion scenarios was run 5 times to capture any variability in wave run-up at the peak of the storm tide. Table 5.2 shows the resulting mean R2% results for each of the 15 profiles over each erosion scenario. Profiles 1 and 15 are not shown as they did not have any saltmarsh to erode in the initial profile. Some profiles did not have the 25% eroded scenario simulated; this was due to 25% eroded widths being similar to other erosion scenarios on other profiles. It can be seen that at 0% erosion the R2% values across all profiles are broadly similar and within 0.20 m of each other. Over the erosion scenarios the value of R2% across all profiles moves further apart, with a difference of 0.33 m when 50% of the saltmarsh has eroded, increasing to a difference of 0.62 m for a fully eroded saltmarsh. This indicates that while the current saltmarsh along the coastline has a similar resilience to extreme events, the resilience properties change as the saltmarsh is eroded - with some sections of coastline having less resilience to extreme events than others in terms of erosion extent.

Table 5.2: Mean R2% values for each profile and erosion scenario simulated. NS signifies that this scenario was not simulated.

Profile	Percentage of Saltmarsh Eroded				
	0%	25%	50%	75%	100%
2	4.04	NS	4.05	4.10	4.12
3	3.81	NS	4.10	4.27	4.63
4	4.03	NS	4.05	4.11	4.35
5	3.85	NS	3.85	4.04	4.32
6	3.97	NS	4.02	4.02	4.11
7	3.99	NS	4.04	4.07	4.01
8	4.09	NS	4.18	4.33	4.53
9	3.99	4.04	4.06	4.17	4.49
10	3.88	4.02	4.04	4.14	4.50
11	3.89	4.01	4.05	4.17	4.52
12	4.04	4.06	4.07	4.26	4.62
13	3.99	NS	4.02	4.05	4.06
14	3.99	NS	4.00	3.99	4.01

For each profile, the saltmarsh width from the sea wall to the seaward edge and height of this edge above the intertidal beach (hereafter 'saltmarsh height') has been calculated. The R2% for each erosion scenario and for each profile has been plotted against its corresponding width and height (Figures 5.7 and 5.8). In Figure 5.7 the max and min R2% values across the 5 sets of simulations runs has also been plotted. It can be seen that there is little variation at high saltmarsh widths but this increases the more the saltmarsh is eroded. From a saltmarsh width of 810 m the R2% values effectively plateau with decreasing saltmarsh width until approximately 270 m where the trend in R2% starts to increase with eroding saltmarsh. A general trend of 0.11 m increase in R2% for every decrease of 100 m of saltmarsh can be seen. The trend from 270 m downwards is almost three times greater than the trend between 1080 and 810 m. The variability in R2% across the 15 profiles as the saltmarsh width erodes increases with decreasing width: between 1080 and 810 m the difference between the maximum and minimum values of R2% is 0.19 m, the plateau section

between 810 m and 270 m has a variability of 0.13 m, increasing to 0.36 m between 270 m and 100 m, before reaching a maximum range of 0.68 m with the saltmarsh fully eroded. These variability calculations ignore the outliers, with values of R2% less than 3.9 m present between 100 m and 700 m, but these outliers are included in the trend calculation. Overall, the behaviour of R2% across the simulated profiles as the saltmarsh erodes is one of increasing R2% and increasing variability of R2%.

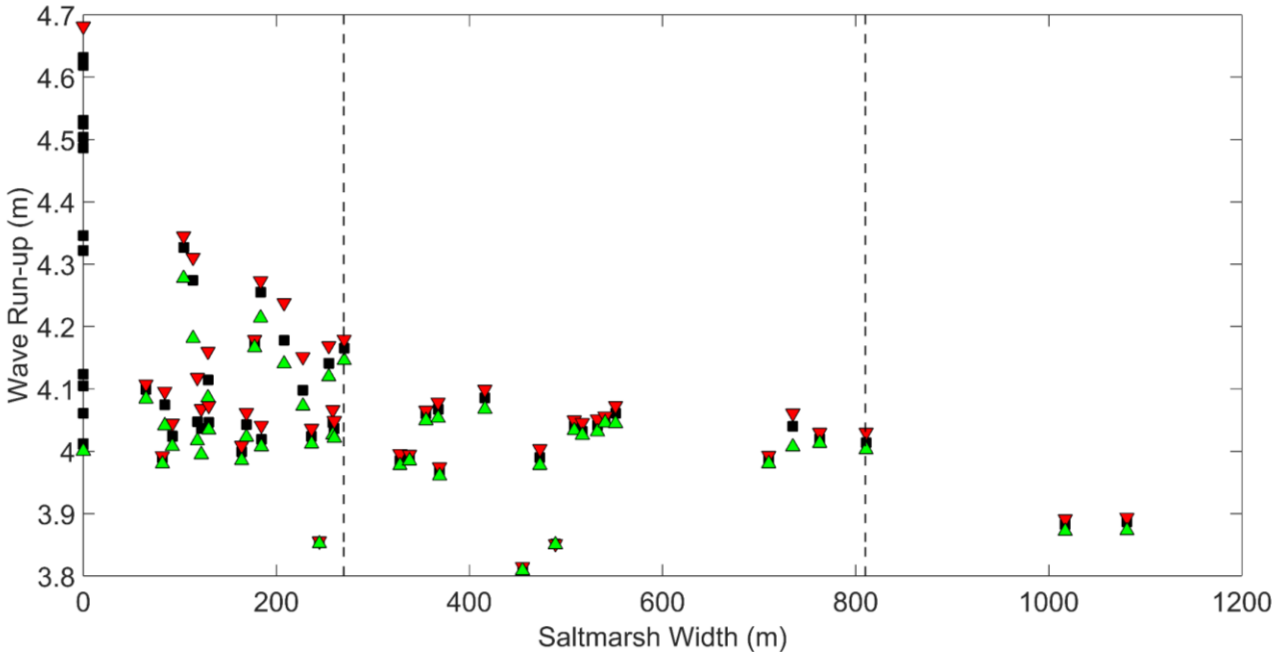

Figure 5.7: Mean (black square), maximum (red arrow) and minimum (green arrow) R2% across all 13 profiles and erosion scenarios for the saltmarsh width of each profile erosion scenario.

Figure 5.8 shows the relationship between R2% and 'saltmarsh height'. This reduces as the saltmarsh erodes as it is assumed that the beach slope remains constant based on inference from other profiles. The general trend shows that R2% increases at a rate of 0.16 m for every 1 m of decreasing saltmarsh height. The variability in R2% across the profiles also increases as a function of reducing saltmarsh width. At a saltmarsh height of 2.5 m, the variation in

possible R2% values is 0.17 m. Figure 5.8 also shows that saltmarshes with a height greater than 2 m have a limit to R2% of 4.1 m - once the saltmarsh has reduced in height below this threshold large increases in R2% are evident.

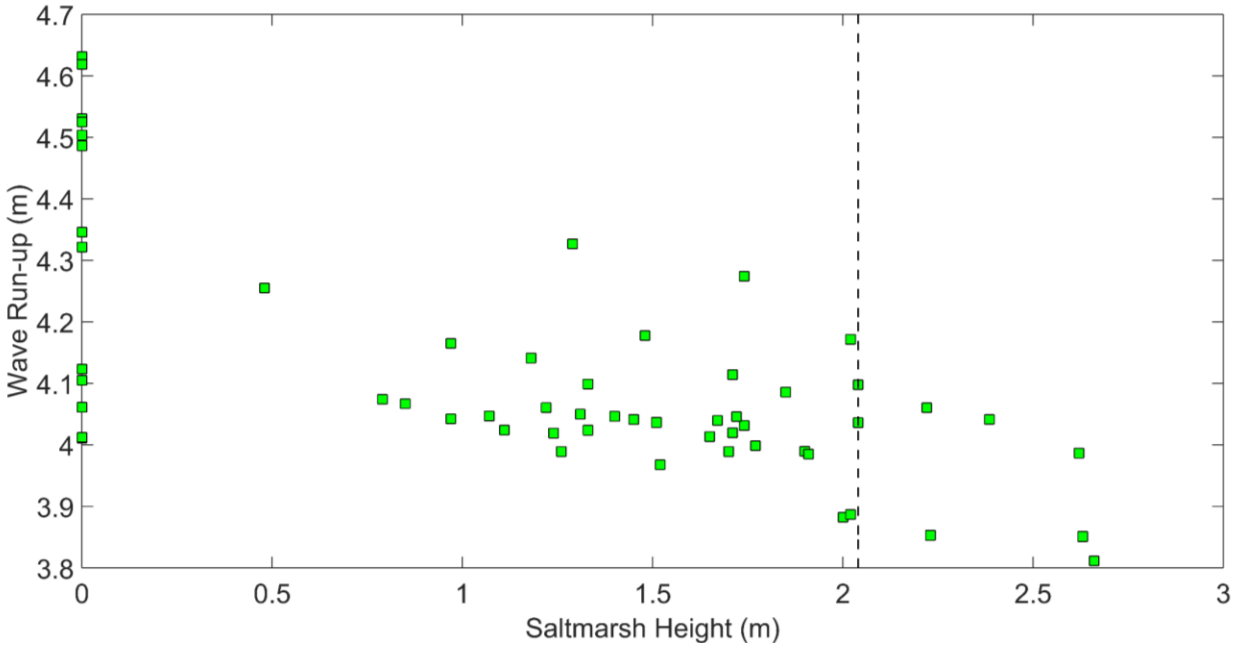

Figure 5.8: R2% wave run-up against the height of the seaward saltmarsh edge (saltmarsh height) above the beach for all 13 profiles and erosion scenarios. Dotted vertical line shows ~2 m threshold for R2% limited to 4.1 m.

Figure 5.9 shows the relationship of R2% against the intertidal beach slope that is seaward of the saltmarsh in each cross-shore profile. The slope varies along the shore due to the presence of sand banks and shipping lanes. It can be seen that the gradient of the intertidal beach has an impact on the R2% where steeper slopes result in higher R2% values. This applies for each erosion scenario where eroded saltmarsh and steeper slope results in higher R2% values. However, there is no obvious trend present for beach slope gradient and R2%, at least for the range of slopes simulated. This is in contrast to empirical formulae to calculate

R2% that rely on the beach slope, but they do not take into account wave attenuation from the presence of a saltmarsh.

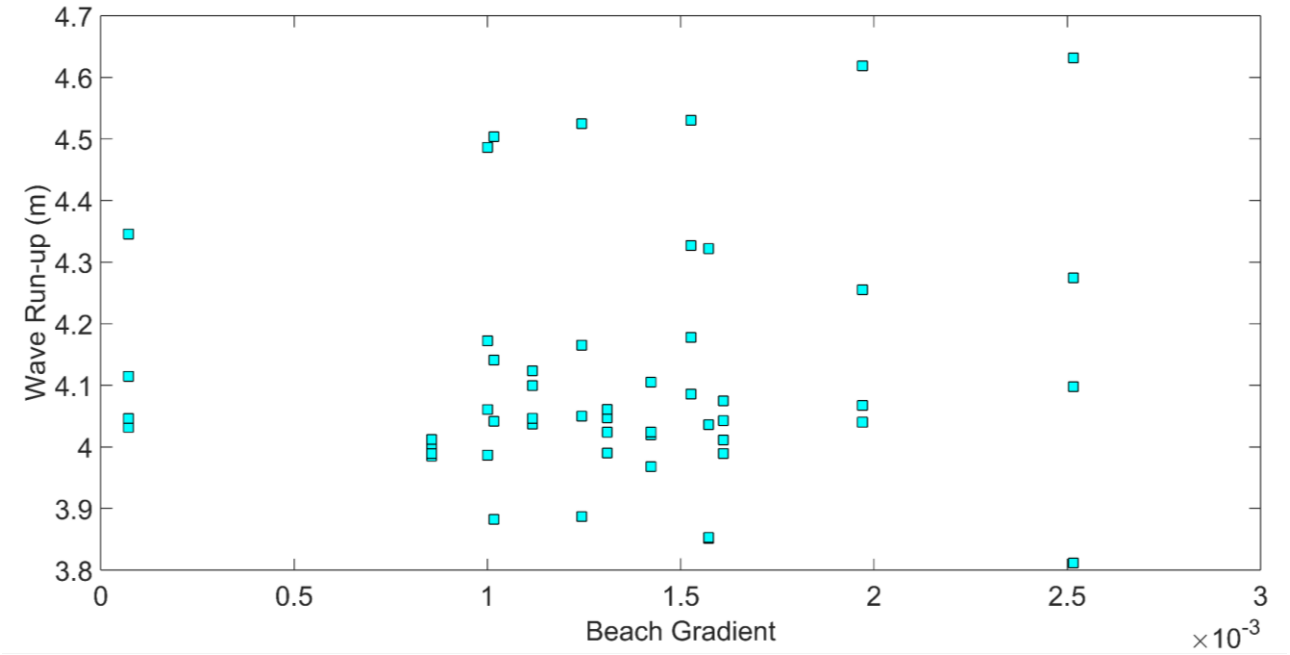

Figure 5.9: Wave run-up as R2% against intertidal beach gradient for each profile and erosion scenario.

Figure 5.10 shows the relative percentage change in R2% from the initial profile against the percentage of saltmarsh eroded. As expected, the more the saltmarsh is eroded the greater the positive percentage change in R2% from the starting point of each profile. The variation in percentage change also increases from a relatively small variation of 0 to 3.5% at 25% erosion, increasing through 50% and 75% erosion to finally resulting in a range of values from 0.7% to just above 20% for a fully eroded saltmarsh.

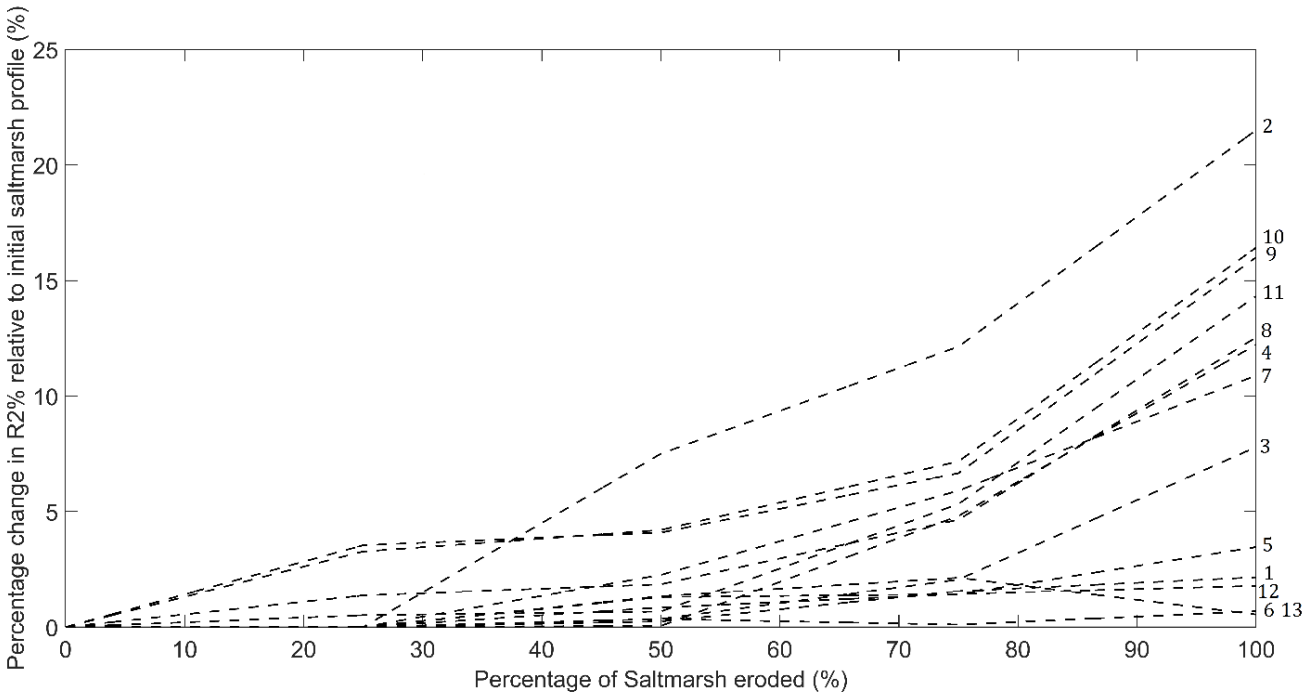

Figure 5.10: Percentage change of R2% relative to initial saltmarsh profile against the percentage of saltmarsh eroded. Numbers to right of graph relate to the relevant profile number that each dashed line represents.

5.5 Discussion

Saltmarshes are dynamic environments that respond to changes in the climate, sea-level, storm magnitude-frequency, wind/wave climate, tidal regime and sediment supply (van der Wal and Pye, 2004). Saltmarshes are under particular pressure from increasing mean sea-level and hold the line policies that result in them being eroded. Studies covering Dengie marshes and the Blackwater estuary have found that they have lost up to 10% of their area over a 21-year period (Harmsworth and Long, 1986). In the 1970's the rapid erosion that was occurring has been attributed to various causes, both natural and anthropogenic. A positive finding was that vertical sedimentation rates have been able to keep up with increasing mean sea-levels over the last century (van der Wal and Pye, 2004). However, the

increasing rate of SLR will increase the pressure on the sedimentation rate of the saltmarsh, which will require an increased rate of vertical sedimentation to maintain the saltmarsh height. Research has shown that erosion and accretion are processes that affect different parts of the saltmarsh at different rates. While accretion rates may be sufficient to raise the saltmarsh height at a rate that keeps pace with sea-level rise. However, at the same time lateral erosion of the seaward edge of the marsh can lead to a reduction in the area of the saltmarsh. This means that the height of the saltmarsh is maintained but not the area (Wolters et al., 2005). The results of this study have shown maintaining the height of the saltmarsh is beneficial to maintaining resilience to wave run-up. However, the reduction of the width of the saltmarsh will have a large impact on the resilience properties as it is the dominant factor for saltmarshes under 2 m in height, above this threshold the saltmarsh height is also a large factor in controlling the R2% value.

It was thought that the plants of a saltmarsh help to reduce erosion from lateral waves by binding soil at the seaward marsh edges. However, physical modelling and controlled field experiments have shown from this is that vegetation does not mitigate erosion at the edge of the saltmarsh (Feagin et al., 2009). It was found that the soil type is the dominant controlling factor in the lateral erosion rate (Feagin et al., 2009). So vegetation may not directly reduce erosion but may do so by influencing the soil parameters (Feagin et al., 2009). The conclusion from this that saltmarshes are more suited to gradual changes such as sea-level rise or changes in tidal range, than wave attenuation during extreme events. While the vegetation may not be the controlling factor for saltmarsh erosion, it is very important in attenuating waves and reducing run-up.

It has been estimated that wave heights can be reduced by as much as 50% over the first 10-20 m of vegetated saltmarsh surface (Möller et al., 1999). Previous studies have identified that saltmarshes particularly in the study area, have had large episodes of erosion, are under pressure from changes in climate and are able to help to protect coastlines by attenuating waves (Harmsworth and Long, 1986; Möller, 2006; van der Wal and Pye, 2004; Wolters et al., 2005). However, so far there has been little research into the resilience of the saltmarsh during extreme events.

A physical modelling study has been carried out where a section of saltmarsh was transplanted into a flume tank in which the presence of saltmarsh caused wave attenuation even at high water levels and wave heights (Möller et al., 2014b). Duplicate experiments were also performed without vegetation and it was estimated that 60% of the observed wave reduction was due to the saltmarsh being present. It was also noted that even when vegetation had been flattened and damaged, the saltmarsh was still able to resist erosion of its substrate. This meant the saltmarsh was able to maintain its resilience during an extreme event while also recovering quickly. In this study the wave height was reduced by 10 and 20% within the first 40 m of saltmarsh (Möller et al., 2014b).

The findings of a review analysing the literature focused on wave attenuation and shoreline stabilisation processes found that the vegetation of the saltmarsh has a positive effect on both of these processes (Shepard et al., 2011). The characteristics of the saltmarsh that were positively correlated to both shoreline stabilization and wave attenuation were vegetation density, biomass production and saltmarsh size (Shepard et al., 2011). This agrees with the results of this study where the wider and taller the saltmarsh, the better the resilience to

extreme events. Further work in varying the density of the vegetation could be undertaken to assess how much of an impact this has on the marshes ability to withstand an extreme event.

This study has built on the work undertaken by previous research by studying the impact of extreme events on the resilience of the saltmarsh as its width reduces (Feagin et al., 2009; Meijer, 2005; Möller, 2006; Möller et al., 2014b; Wamsley et al., 2010). The results show that decreasing saltmarsh width and edge height with a steepening beach slope result in a larger R2% value and therefore a reduction in the resilience of the coastline, i.e. reduced wave attenuation. This trend is what would be expected from the wave attenuation action of a saltmarsh, i.e. the wider and higher (relative to the fronting intertidal beach) the saltmarsh is, the more the waves are attenuated. This study has identified the presence of critical widths or thresholds in saltmarsh width that impact on the rate of increase of R2%. A threshold at 810 m indicated a change from a linearly increasing R2% based on an eroding saltmarsh with a plateau where the R2% stays stable despite decreasing saltmarsh width. Another critical width occurs at 270 m with a linear increase in R2% three times greater than before the first critical width at 810 m. The results imply that a coastal manager, at least for this coastline, would not need to act to mitigate the perceived decreasing resilience of saltmarsh if it is between these two critical widths as saltmarsh erosion does not substantially decrease the coastline's resilience to flooding during extreme events.

This research has only simulated two types of plant within the model, one that is common on the lower saltmarsh and the other on the upper marsh. This means there is uncertainty regarding the wave attenuation properties of the saltmarsh, as in reality there are more

varieties of plant with differing physical properties. This uncertainty can be explored by simulating different plants to understand how large this uncertainty is, and with field surveys. These would allow the correct representation of plants in the model. At this point it should be noted that the vegetation function added to XBeach is a recent addition and it has not been calibrated as rigorously as other aspects that XBeach is also able to simulate, such as beach morphology. This is expected to improve in time as field studies are carried out allowing calibration to take place. This was also a concern about numerical models raised by Fagherazzi (2014).

5.6 Conclusions

For the two plant types considered, decreasing saltmarsh width results in a critical threshold width at 810 m where R2% stops increasing at a rate and plateaus before reaching a second threshold width at 270 m where R2% increases linearly again, but at rate three times quicker than the one for wider saltmarshes. Different plant types are likely to make a difference to the R2% values depending the difference in the parameters such as the number of plants per m^2. Future work could explore this uncertainty to see what impact different plants would have. Thus a saltmarsh is able to maintain its resilience present at the first critical threshold in spite of being eroded, until the lower critical width is reached.

Saltmarsh edge height modelling shows a threshold value at 2 m. Saltmarshes below this height exhibit a significant increase in the value in R2% and a corresponding decrease in resilience (i.e. reduced wave attenuation), making coastlines with saltmarshes edge heights below this threshold more vulnerable to extreme events. A saltmarsh eroding to widths

below 270 m and heights less than 2 m will provide less coastal resilience than a saltmarsh that is wider or its edge higher. Thus, shoreline management should seek to maintain saltmarshes at least wider and taller than this if resilience of the coastline during extreme events is a priority. Saltmarsh width has the largest and clearest impact on wave attenuation, followed by height and then intertidal beach slope which, while giving an inconsistent response, does tend to result in higher R2% values for steeper slopes.

This research has only been applied to one study area and it would be beneficial to test other locations to see if the saltmarsh response to extreme events is universal or varies with greater saltmarsh width and height. Other variables such as, different vegetation or changes to wave climate or sediment supply could also have an impact that would benefit from futher study.

5.7 Acknowledgments

We would like to acknowledge the ESPRC-funded ARCC “Adaptation and Resilience of Coastal Energy Supply” (ARCoES) project (EPSRC EP/I035390/1).

6 Morphological Control on the Resilience of Gravel Barrier-Beach Coastlines

6.1 Abstract

In Northern Europe, vulnerable sections of coastlines are commonly protected by gravel beaches; these landforms are effective at being resilient to extreme events, primarily comprising an extreme water level and significant wave height. This study investigates the impact of different gravel beach morphologies in maintaining resilience to storms. A storm impact model simulates a joint 0.5% annual probability event of combined wave height and extreme water level for 15 1DH profiles in the study area (Sizewell, eastern UK). Different scenarios of beach morphology and geomorphic response are simulated where the beach barrier and nearshore bar in the 1DH profiles are modified by changing the height, width and slope to examine changes to the resilience of the coastline. It was found that the nearshore bar had no impact on resilience due to the extreme water level of the event considered being sufficiently high above the feature that it was not able to attenuate the waves during the peak of the storm tide. For other combinations of extreme water level and wave height this may not be the case. It was found that the seaward slope of the gravel barrier at the top of the beach was the dominant factor in determining wave run-up and therefore storm resilience. Wave run-up increased at a rate of 8.5 times the increase in slope. Two thresholds were identified for both barrier height and width. Barrier widths over 125 m were much more resilient to the extreme event than those below. Similarly, barrier heights below 5 m had a clear increasing trend in wave run-up for increasing crest height. Crest heights below 4.3 m resulted in overwashing and flooding, making this a critical height for

flood resilience to the 0.5% annual probability extreme event. A large variability in wave run-up for barrier crests over 5 m show that this is not a dominant factor in determining the shoreline resilience. This research has identified the dominant factors in determining the resilience of present-day gravel barriers as being the beach slope, followed by barrier height and width above and below a threshold of 5 and 125 m, respectively. This research demonstrates an effective approach to assess the current barrier beach resilience and identify suitable ways to adapt to a changing climate.

6.2 Introduction

6.2.1 Resilience of Vulnerable Coastlines

Coastlines are under pressure, trapped between rising mean sea level and a world that is reluctant to retreat from the coast (Stevens et al., 2015). Some sections of the coast rely on hard defences, such as sea walls and breakwaters. This is particularly common when protecting urban areas and critical infrastructure. However, hard structures are not the only way to make the coastline more resilient. Resilience can also be provided by 'soft' defences (Anderson and Smith, 2014). These can take the form of saltmarshes, mudflats and beaches. Resilience can be defined as the ability of a defence structure such as hard defences to withstand an extreme event, or the ability of a soft defence to recover the damage incurred during an extreme event. While the benefits from 'soft' defences may not be as clear as with hard defences, soft measures can help to reduce the impact of extreme events (Möller et al., 2014b; Smolders et al., 2015). An example of this is the attenuation of wave height as it crosses over a saltmarsh during an extreme event, thus reducing the impact of the event on the shoreline (Möller et al., 2014b). Beaches, particularly ones with a sand or gravel barrier

at their upper limit, are able to withstand or recover from extreme events (Masselink and van Heteren, 2014). Understanding how the resilience of the coast will change if there are morphological changes to the beach and natural barrier coasts is important. While some changes may provide improved resilience, other morphological changes may have a negative impact on resilience to extreme events.

In the UK, different management plans are applied to the coastline. These consist of different policy options that are applied to sections of the coast across different epochs. The first short-term epoch is until 2025, the second medium-term from 2025 and 2055 and the final long-term epoch is 2055 to 2105 (Environment Agency, 2009b). The "hold the line" management option is where the shoreline is fixed in place, usually by hard defences, and that resources will continue to be deployed to maintain this defence line. There is also "no active intervention" where the shoreline is left alone, whether it is characterized by hard or soft defences. This option can apply to previously defended places, so these defences will no longer be maintained and "held" in place, or as soft defences they would be left to naturally evolve and potentially retreat. Finally, there is "managed realignment" where the coastline is actively reshaped to take account of changing pressures such as increased mean sea level (Environment Agency, 2009b). This is a common policy to apply in medium- or long-term epochs of shoreline management plans to compensate for lost intertidal habitat and soft defences that have eroded, often due to "hold the line" policies elsewhere in the region (Halcrow Group Ltd., 2010).

The designed level of protection for urban areas is commonly to withstand a 1 in 200 years or 0.5% annual probability extreme event (Wyse, 2015). This standard of protection can vary

depending on the type of land that the given shoreline is protecting, e.g. lower valuable arable land is likely to have lower standard of protection than higher value urban areas. Critical infrastructure, such as nuclear power stations, will have much higher standard of protection - nuclear power stations are required is to withstand a 1 in 10,000 year extreme event (EDF, 2012). This much higher standard is justified in relation to the resultant costs and impacts of the station being inundated.

Extreme events that occur and impact on the coast are typically driven by extreme water levels caused by storm surges. These occur when high winds and low atmospheric pressure during a storm raise the water level above the predicted tide at the coast (Wells, 1997). If the surge occurs in conjunction with a high tide, particularly a spring tide, then an extreme water level (EWL) can result. The impact of the extreme event is also influenced by any waves that impact on the coast during the extreme event. Wave run-up is where the observed water level is raised by wave action, if this occurs during an extreme water level, it will have a greater impact on the hard or soft defences protecting the coast than the observed water level alone. This process can be ameliorated by the presence of soft defences (Möller, 2006). Waves are attenuated and break further from the coastline, helping to improve its ability to attenuate the impact of extreme events. Knowing the likelihood of a given wave height occurring with a given extreme water level is important in assessing the ability of the coastline to withstand an annual probability extreme event (P. J. Hawkes and Svensson, 2006).

Maintaining the current standard of protection that a coastline currently affords will become more difficult in the future (McGranahan et al., 2007), particularly as “soft” defences will

typically be eroding and under pressure from increased mean sea levels, projected changes in storminess and "hold the line" shoreline management policies (Shepard et al., 2011). These pressures are likely to cause morphological change to the soft defences and other features on the beach, such as natural bars. These changes could include higher, lower, wider and narrower barriers and bars, potentially modifying the protection they offer to the coastline.

This study has taken a high value section of coastline in the east of the UK, which incorporates important critical infrastructure and wildlife reserves. The research investigates the impact of different morphological response scenarios to the natural barrier beach and other features, such as a nearshore sand bar, on the observed wave run-up that occurs during an extreme event. This understanding will assist coastal managers in identifying which morphological changes would require intervention to ensure the ability to withstand or recover from extreme events is maintained along the coast.

6.2.2 Study Site

The study site is an area of high value located in eastern UK (Figures 6.1 and 6.2), with a relatively sandy lower beach with coarse gravel barrier above (Environment Agency, 2010; Pye and Blott, 2006). This low-lying area landward of the barrier, Minsmere reserve, is particularly vulnerable to rising mean sea level. To the south of the reserve, are two nuclear power stations, one decommissioned and operational, with potentially a new nuclear build being built nearby in the near future. This means the area is important environmentally and as well as strategically in terms of future energy security.

For the study site, the predominant origin direction of waves is between 020 and 070 degrees. Small numbers of waves higher than 5 m originate from this direction but the vast majority are under 3 m (ECMWF, 2016). Mean High Water Springs (MHWS) for the study site is 1.55 m OD with a possible tidal range of 2.76 m, making the coast meso-tidal. Storm surges of up to 1.5 m above the predicted tide have been observed (British Oceanographic Data Centre, 2015; NOC, 2015).

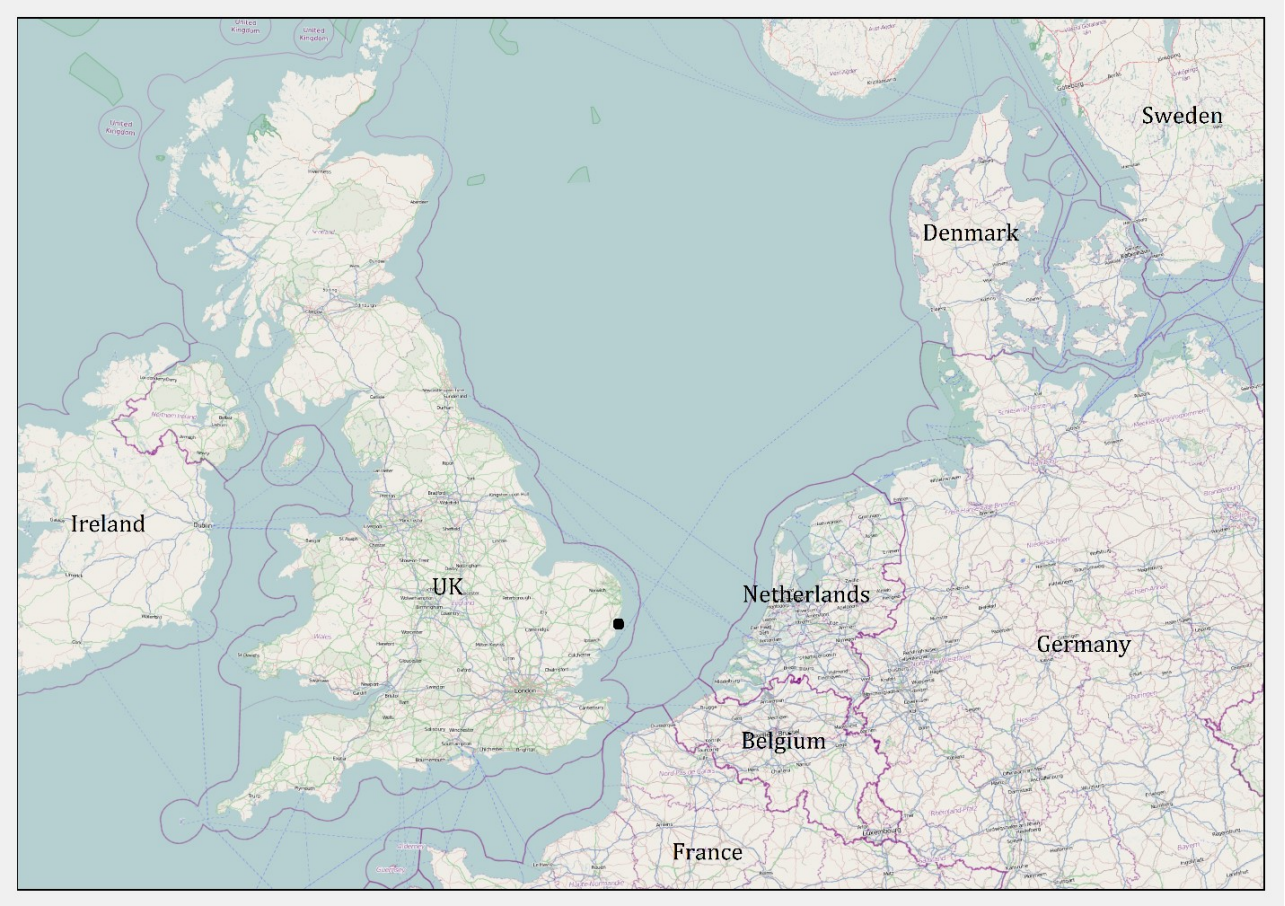

Figure 6.1: Image shows study site location with reference to the UK and North Europe, the black mark shows the location of the study site on the southeast coast of the UK.

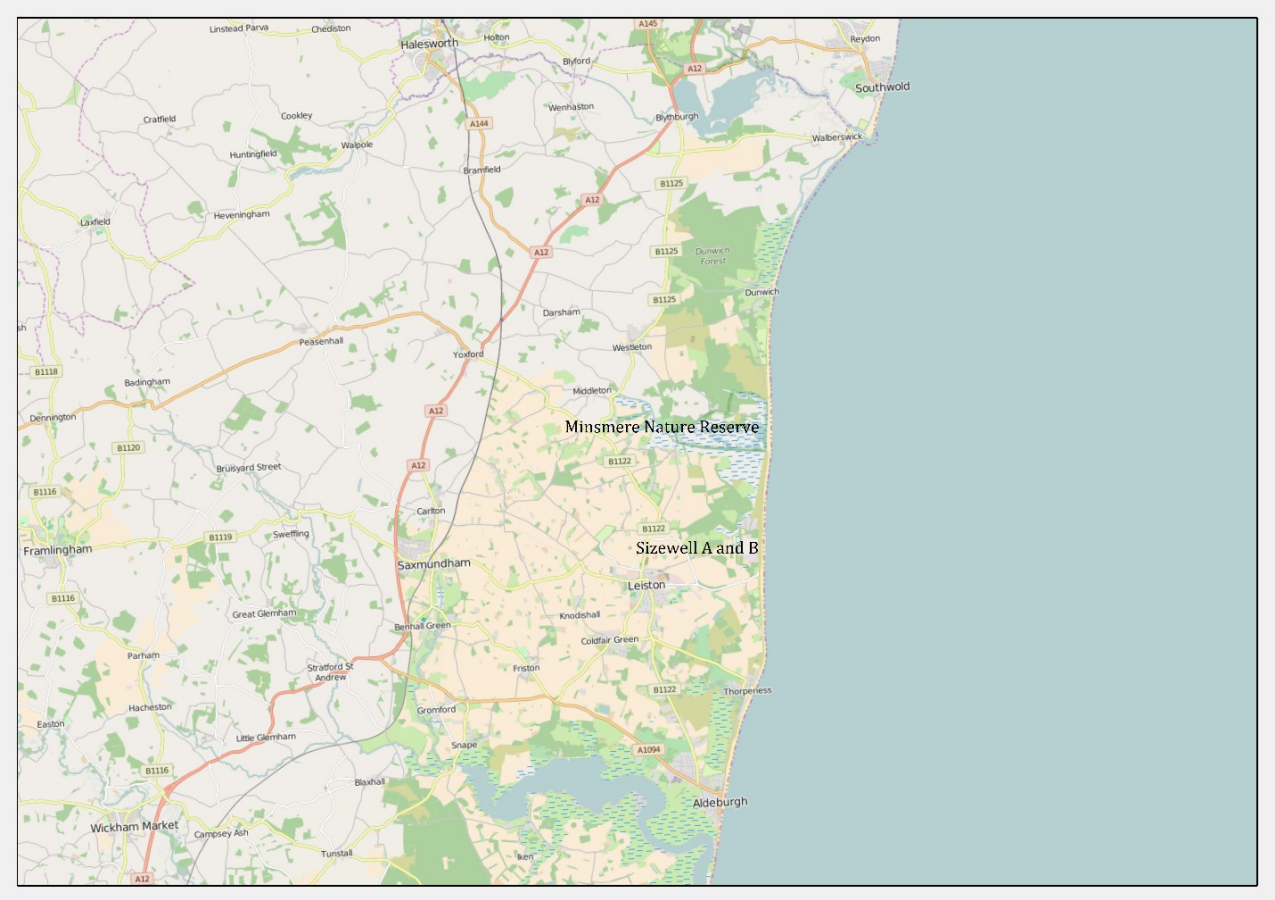

Figure 6.2: Image shows the regional location of the study site.

6.2.2.1 Wave and tidal climate at study site

6.2.2.2 Beach and offshore areas

The beach within the study site comprising an relatively sandy lower beach with a coarse gravel upper and barrier (Environment Agency, 2010; Pye and Blott, 2006). A distinct gravel barrier at the top of the beach helps to protect the vulnerable land behind. Large parts of the Minsmere nature reserve are at 0.6 m OD elevation, making them vulnerable to storm surges and sea-level rise (Pye and Blott, 2006). A larger bank is present in front of the nuclear power stations, making it much more resilient to extreme events than the nature reserve. The power station site itself is also protected from extreme flooding as it is located on higher

ground and designed according to operational safety requirements. There is a nearshore bar present in the study area just inside the intertidal area with a much larger bank offshore (Pye and Blott, 2006). There has been debate about how much wave attenuation this offshore bank offers, with studies using wave buoys moored close to shore finding that its presence made negligible difference over a four year period (Fortnum and Hardcastle, 1979). Another study used wave buoy data from either side of the bank, finding that large waves break on the offshore side of bank, reducing the impact on the coast and providing some protection (Tucker et al., 1983). Computer modelling has found that the bank reduces the height of the waves by 0.5 m but has negligible impact on wave heights impacting on the shoreline itself (Halcrow, 2000).

6.2.2.3 Minsmere Nature Reserve

Minsmere nature reserve is owned and operated by the Royal Society for the Protection of Birds (RSPB). It is part of the county of Suffolk and lies on the North Sea coast, around 10 km south of Southwold and 11 km north of Aldeburgh. There are many environmental designations in the area, such as SSSI, SAC, SPA and RAMSAR. Minsmere is also part of the Suffolk Coast and Heaths Area of Outstanding Natural Beauty. The site is around 10 km^2 and consists of reed beds, lowland heaths, wet grasslands and shingle vegetation. The reserve is an important feeding, nesting and roosting site for a wide variety of birdlife. It is also an important site for other wildlife such as adders, otters, water voles and red deer. Minsmere is also used as a demonstration site of successful reed bed management and is considered to be one of the best bird watching sites in the UK. Figure 6.3 shows a close up of the study area with both Minsmere and both Sizewell power stations highlighted.

Figure 6.3: Close up of study site showing locations of Minsmere nature reserve and both Sizewell power station sites. The black lines indicate the locations of the 15 1DH profiles used as input to the storm impact model.

6.2.2.4 Sizewell Nuclear Power Station

There are two nuclear power stations at Sizewell, located just to the south of Minsmere Reserve. Sizewell A is in the process of being decommissioned and Sizewell B is an operational station running the UK's only pressurized water reactor. Sizewell A ceased generation in 2006, having generated a lifetime output of 110 TWh (Magnox, 2016). It is currently in care and management preparations having been fully defueled in 2014. Final site clearance is projected between 2102 and 2110. Sizewell B is a single reactor built and

commissioned between 1987 and 1995 and is currently licensed to operate to 2035. A 20-year extension is currently being considered.

Sizewell A is licensed as a nuclear site until at least 2100, and Sizewell B is licensed to at least 30 years after that. With the addition of a new nuclear build being considered, critical infrastructure could well be present on this coastline well beyond 2100 and potentially up to 2180. Given that these sites will have a fixed boundary, with a "hold the line" management policy, it is important to understand the potential future changes in the soft coastline as a result of increasing mean sea-level and or wave climate.

6.3 Method

The methodology applied to the study site used a storm impact model to simulate a 1 in 200-year extreme event or 0.5% annual probability event. This is a common level of extreme event that coastlines are designated to be able to withstand (Wyse, 2015). The storm impact model requires boundary conditions that are representative of the extreme event. Additionally, a 1DH cross-shore profile that represents the offshore bathymetry, beach slope and barrier beach is also required. The boundary conditions for the extreme event are projected using joint probability analysis which provides a range of combinations of significant wave height and extreme water level that correspond to a 0.5% annual joint probability. The combination that has the greatest wave run-up on the coastline is the one that will be used in this study. A synthetic surge curve that is representative of the study area is then used to provide a time-varying water level that corresponds to one tide cycle that peaks at the desired extreme water level (A. McMillan et al., 2011). The storm impact model

is able to produce many output variables, to assess the resilience of the coastline. For this study the R2% parameter is used, this is the elevation that only 2% of waves will exceed, and can be used to assess the storm resilience of the coastline.

6.3.1 Storm Impact Model

The storm impact model used in this study is XBeach-G. This is a branch of the XBeach storm impact model, which is an open source numerical model which originally was developed to simulate hydrodynamic and morphodynamic processes and impacts on sandy coasts with a domain size of kilometres and on the timescale of storms. Since its origins, the model has been applied to other types of coasts and purposes (Roelvink et al., 2010). XBeach-G differs from XBeach in that is has been developed to simulate storm impacts on gravel beaches.

XBeach-G uses the one-layer, depth-averaged, non-hydrostatic extension to the XBeach model, which is similar to the SWASH model (Zijlema et al., 2011) to solve wave-by-wave flow and surface elevation variations due to short waves in intermediate and shallow water depths. This is particularly important for application on gravel beaches where, due to steep slopes, swash motion is mainly at incident wave frequencies. Further, infra-gravity wave motion, which dominates the inner surf and swash zone on sandy beaches during storms, is of secondary importance (Deltares, 2014). To correctly account for upper swash infiltration losses and exfiltration effects on lower swash hydrodynamics on gravel beaches, XBeach-G computes groundwater dynamics and the exchange between groundwater and surface water using the XBeach groundwater model (Deltares, 2014). Again, interaction between swash flows and the beach groundwater table are considered particularly important on gravel beaches due to the relatively large hydraulic conductivity of the sediment, while on sandy

beaches this process is of significantly less importance (Austin and Masselink, 2006). Finally, gravel sediment transport processes have been included in XBeach-G to simulate the morphodynamics of gravel beaches during storms (Deltares, 2014).

XBeach-G can only be run as a 1DH model, unlike XBeach which can also run in 2DH mode. This study produced 15 1DH profiles at equal intervals along the coastline within the study area. Figure 6.3 shows the location of these profiles. Given that there is some sand in the study area, the morphological change function in XBeach-G has been disabled as so far it has only been developed for use with pure gravel beaches (Masselink et al., 2015).

XBeach-G is able to simulate and output many different parameters, such as discharge, bed change across the profile and water level. The output variable of interest in this study is wave run-up, which was set-up to output the run-up of the waves during the 0.5% annual probability extreme event. The output time-step for wave run-up was set at 0.5 seconds with all other parameters being set at 10 seconds. The reason for the high output time-step for run-up is to allow capture of the high variability in wave run-up during the simulation. For this study the output value of interest is the R2% metric which is defined as the level at which only 2% of waves will reach or exceed. For this study, the R2% is generated by calculating the 98^{th} percentile value for every 100 second interval of the 0.5 second time series. The maximum of these calculated values is taken to be the R2% value.

6.3.2 Suitability of the Storm Impact Model

The storm impact output from XBeach-G has been compared with measurements at four field sites and one wave flume experiment. The model showed a good prediction of wave

transformation, run-up and initial overtopping (McCall et al., 2014). More recently, research comparing XBeach-G to 10 separate storm events showed that XBeach-G can be applied to predict storm impacts on gravel beaches with reasonable to high confidence for a range of hydrodynamic forcing conditions (McCall et al., 2015). XBeach-G has been designed for use on pure gravel beaches and has not been tested on mixed and composite sand–gravel beaches. Although XBeach-G should be able to compute wave transformation and wave run-up correctly on sand–gravel beaches given correct schematizations for groundwater processes, the model does not contain sediment transport processes for (sandy) suspended sediment transport. This means it is not suitable for simulating morphological change on the mixed sand-gravel beach and has been disabled for this research, but could be enabled in the future if further development of the model occurs (Masselink et al., 2015).

The storm impact model has also been used previously to investigate the resilience of gravel barrier beaches to storms. The research showed that the incident wave flux and wave run-up levels are relative to the barrier crest height, crest width and sediment grain size which are the main factors in conditioning the response of gravel barriers to storms (McCall et al., 2015). The research also demonstrated that groundwater processes are particularly important for coarse gravel barriers under high hydrodynamic loads (McCall et al., 2015). This prior research all means that XBeach-G is a suitable choice for this study and will produce meaningful results.

6.3.3 Joint Probability Analysis

Contributions towards the severity of an extreme event can originate from different sources. For coastal extreme events the most prominent contributions are extreme water level (WL)

and significant wave height (H_s). Both of these contributions can be assessed as an annual probability of occurrence either as separate sources or together. Assessing the probability of WL and H_s occurring at the same time is not as straightforward as combining their individual probabilities. This is because they are not isolated phenomena and are interdependent with each other (P. J. Hawkes and Svensson, 2006). The process that assesses this interdependence and derives their joint probability is known as joint probability analysis.

Joint probability requires the longest dataset that can be found of the two variables that are being assessed for joint probability. In this study this is significant wave height and water level. There are various sources of data, such as wave buoys and tidal gauges. These provide significant wave height and the water level along with other variable such as peak period and wave direction. However, there are issues with these sources of data, they tend to be short and with poor spatial coverage. To overcome this issue, a 30-year hindcast wave model was used that is able to provide wave data and water levels within the study area for the last 30 years (ECMWF, 2016). This is much longer than the nearest wave buoy and tide gauge while also having the advantage of being within the study area. An initial step is to validate the hindcast model data. This was achieved by comparing output from the hindcast model that coincided with location of the nearest wave buoy. Comparing the two datasets resulted in a bias of -0.01m with a Root Mean Squared Error of 0.56 m.

The process of calculating joint probability is a well-known and widely used process and it has been extensively validated (P. J. Hawkes and Svensson, 2006). This research used a joint probability program called JOIN-SEA(Hawkes and Gouldby, 1998). The process that follows consists of fitting a bivariate probability distribution to the upper tail of both of the variables,

which are based on proposals by Coles and Tawn (1990). Figure 6.4 shows the output of the analysis where contours that follow the combinations of wave height and water level that meet the calculated annual probability of occurrence. In this study the joint annual probability of 0.5% is represented as a dotted line with a 100% annual probability shown as a solid line for reference (Figure 6.4). It can be seen for of the study area that with increasing water levels, an increasing lower significant wave height is required to follow the joint probability curve.

Prime et al. (2016) demonstrated that different combinations of significant wave height and extreme water level that have the same joint probability of occurrence can have widely varying overwashing rates and inundation extent. This means consideration of the varying combinations of water level and wave height that have same probability is important. The 6 combinations shown as squares on the dashed 0.5% probability contour in Figure 6.4 were used as input to cross-shore profile number 4 from the study area (Figure 6.3). The 6 combinations selected represent the main changes in water level and wave height that occur from one end of the 0.5% annual probability contour to the other. These different combinations would be used as boundary conditions to the storm impact model to assess which combination has the biggest impact on the coastline resilience in the study area. The peak period values that would be suitable for of the different 0.5% combinations were selected by finding the maximum peak period value associated with the wave height in the 30-year hindcast model data. This provided plausible waves to use within the extreme event simulations.

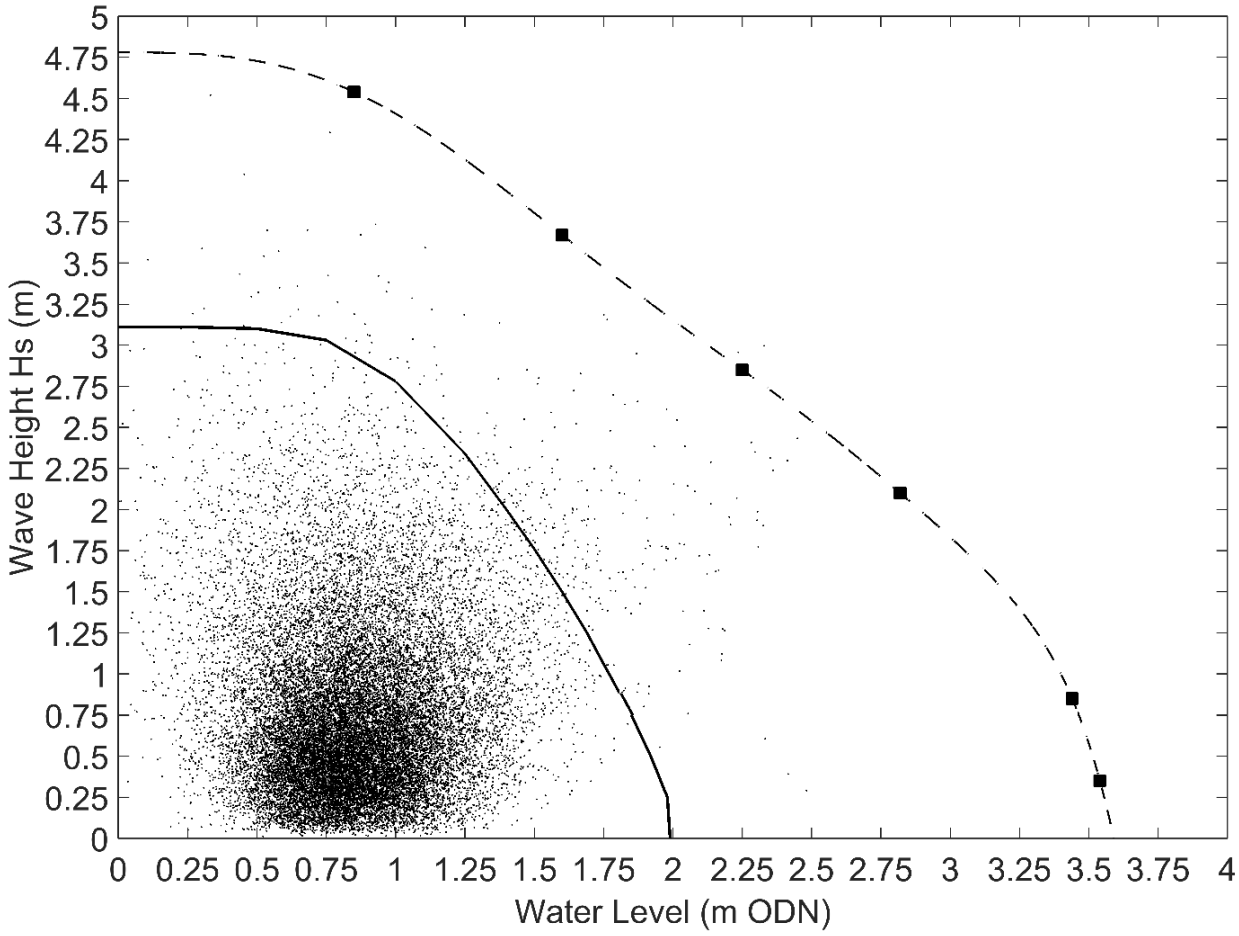

Figure 6.4: Joint probability plot for Sizewell, showing the peak of the observed tide against the significant wave height at that point. The solid line represents a 1 in 1 year or 100% annual probability event. The dashed line shows the 0.5% annual probability contour with the squares highlighting the different combinations simulated.

Table 6.1 shows the max R2% output value for each of these combinations and the parameters that were used as boundary conditions for the 0.5% annual probability extreme event.

It can be seen that the event with the highest R2% value is combination number 5 (highlighted in bold). This had the R2% value of 4.56 m. Other combinations were not too far behind, with 3, 4 and 6 having a R2% values within 0.2 m. Only combinations 1 and 2 were much lower, demonstrating that for resilience to a 0.5% annual probability event large

waves are not a threat to resilience. This is due to the corresponding lower extreme water level required to maintain the 0.5% annual probability standard results in them breaking further offshore, thereby reducing wave run-up.

Table 6.1: Output of joint probability combinations, the input conditions for each combination and the output value of R2% is displayed.

0.5% Combination	Extreme Water Level (m)	Significant Wave Height (m)	Peak Period (s)	R2% (m)
1	0.85	4.54	9.2	3.00
2	1.6	3.67	9.1	3.66
3	2.25	2.85	10.8	4.34
4	2.82	2.1	9.8	4.43
5	**3.44**	**0.85**	**9.6**	**4.56**
6	3.54	0.35	14.6	4.32

6.3.4 Synthetic Storm Tide Curves

This study has followed the methodology outlined in (A. McMillan et al., 2011) where return periods for the annual probability of a still water level have been calculated every 2 km along the UK coastline. While these data are not required for the joint probability analysis, the methodology also outlines a process where it converts the single extreme water level that comes out of the joint probability analysis into a suitable time-varying water level that is representative of a joint 0.5% annual probability storm tide.

(A. McMillan et al., 2011) provides a representative surge curve for every tide gauge around the UK. This curve represents a typical storm surge curve for that region and consists of values between 0 and 1, where 0 is no surge and 1 is the peak of the surge. This curve then needs to be combined with a spring high tide curve from the tide gauge, where the peak of the tide is aligned with the peak of the surge. To combine the curves, the difference between the desired extreme water level and the height of the predicted tide is multiplied by the

representative surge curve. At the peak this equals 1, and when added to the spring tide, means the water level will reach the extreme water level. This is repeated for every time step where there is a value for the representative surge curve between 1 and 0. Figure 6.5 illustrates this process, resulting in a synthetic storm tide curve that can be used as a time-varying water level boundary condition in the storm impact model.

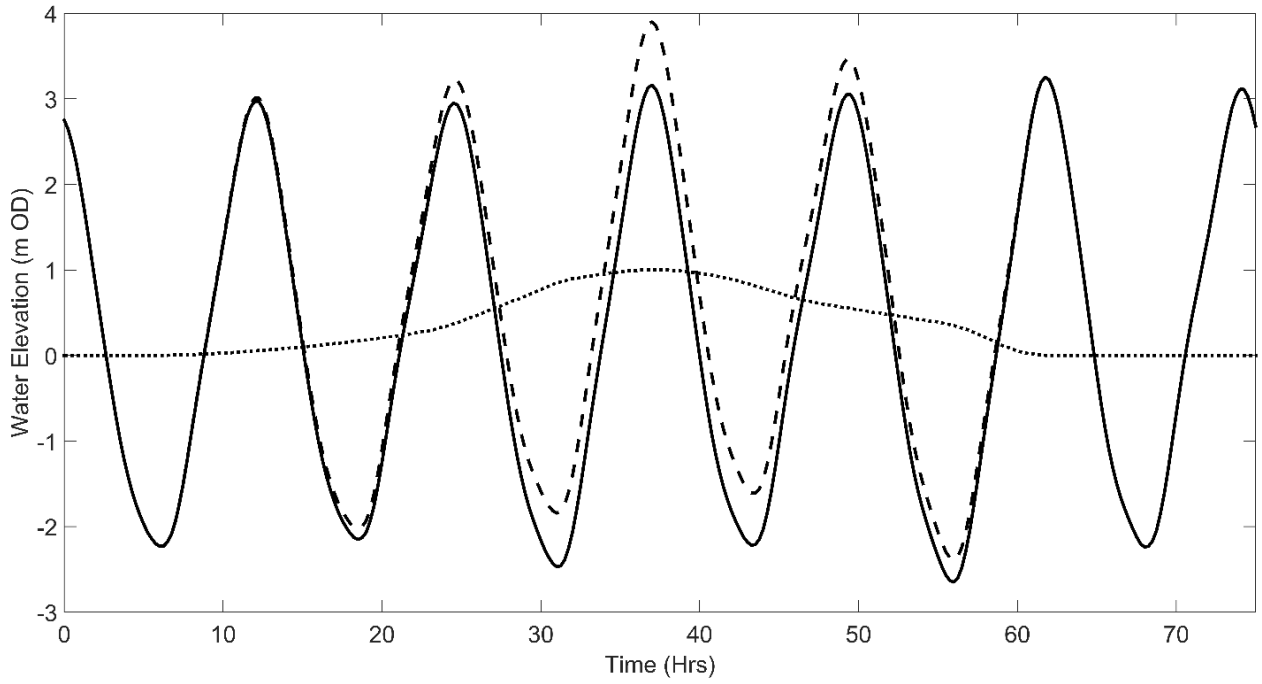

Figure 6.5: Graph showing process of producing synthetic storm tide. Solid line is the underlying mean high water springs tide, dashed line is the synthetic storm tide and the dotted line with values from zero to a peak of one is the representative surge curve.

6.3.5 Cross-shore profiles: selection, simplification and modification

One of the requirements of running the storm impact model is a 1DH cross-shore profile of the coastline. A number of profiles were simulated, the spatial locations of which can be seen in Figure 6.3. The 15 cross-shore profiles were assembled from a range of data sources, to produce the most accurate profile possible from the available data. The crest and slope of the

barrier beach and upper beach profile was produced using the latest beach survey data available from the Channel Coast Observatory. This was combined with LiDAR data for the intertidal area. Finally, one arc second offshore bathymetry was provided by EDINA digimap services. An example of a combined profile is shown in Figure 6.6 (Channel Coast Observatory, 2016; University of Edinburgh, 2016).

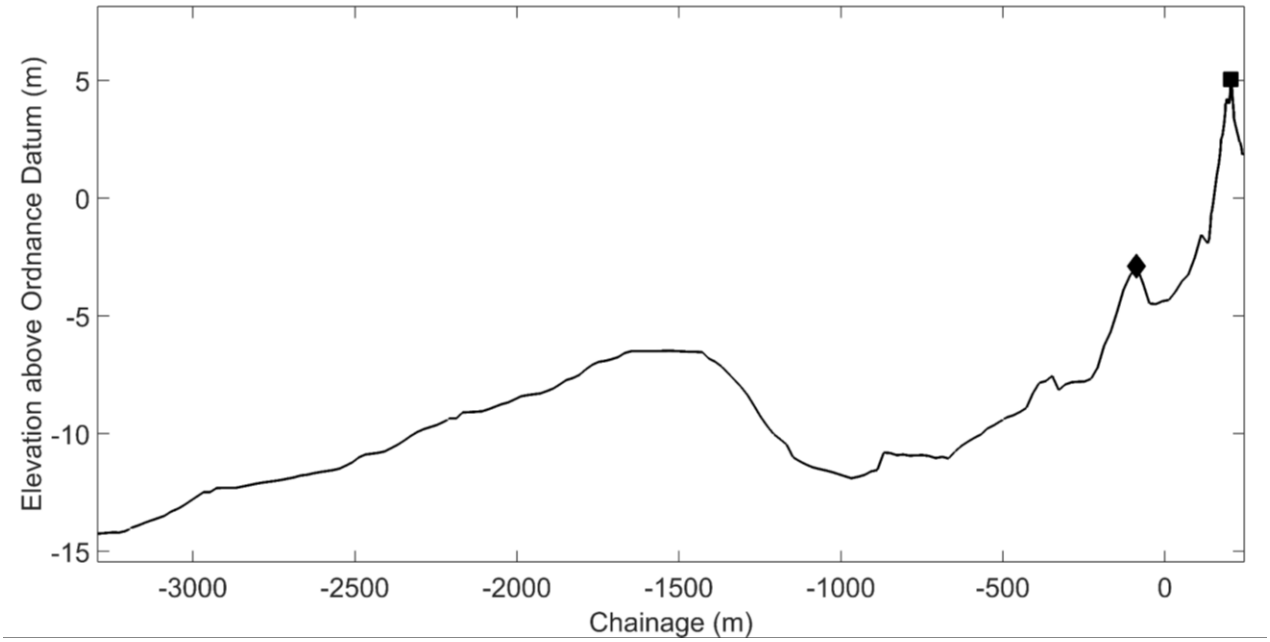

Figure 6.6: Example profile from study area showing combined, survey, LiDAR and bathymetry datasets. The diamond shows the location of the nearshore bar and the square denotes the barrier beach.

To simulate morphological changes, two main features were modified within the profile. Figure 6.6 shows the location of the nearshore bar and barrier beach as a diamond and a square, respectively, on an example profile. Being able to change the height and width of these features and simulating the same extreme event will show which changes are beneficial to improving shoreline resilience and which are negative or neutral. To do this the profiles were simplified to a simple triangle shape that was used to represent the nearshore

bar and barrier beach. Figure 6.7 shows an example of this, only the upper 700 m of the profile is shown to make it easier to discern the differences in the real and simplified profiles. Figure 6.7 also shows the three points marked by A, B and C that make up the triangle used to define the start, crest and end of simplified features that replace the real nearshore bar and barrier beach.

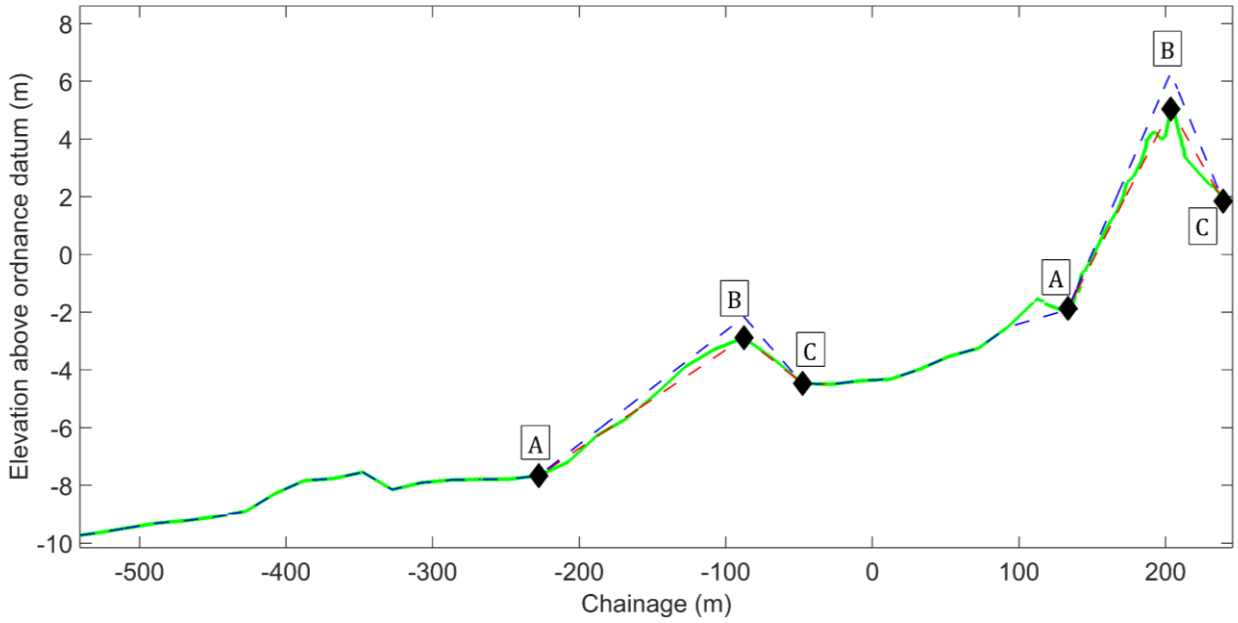

Figure 6.7: Example simplified profile (solid line) with real profile it is based on (dotted line). Dashed black line shows profile with increased height of both the barrier beach and nearshore bar. The letters A, B, C denote the points of the triangle, where the seaward point (A), crest (B) and shoreward point are moved to simulate different morphology scenarios.

To see if the simplified profiles were still representative of the real profiles, the storm impact model was run using the same boundary conditions for the 15 "real" profiles and then repeated for the 15 "simplified" profiles. The R2% values for each profile for both real and simplified are plotted against each other in Figure 6.8 to show how well the simplified profiles represent the real ones. The coefficient of determination value (R_2) for the linear

regression in Figure 6.8 (solid line) has a value of 0.8, showing that the simplified profiles are a suitable representation of the real ones. The p value was calculated as 2.3×10^{-5}, as this is much less than 0.05 it allows the rejection of the null hypothesis. Meaning that there is a significant relationship between the storm impact model output based on the "real" and "simplified" profiles. Figure 6.8 also shows a dashed line that is 1:1 or a perfect representation. It can be seen that the simplified profiles slightly under-predict high run-up values and over-predict low run-up values.

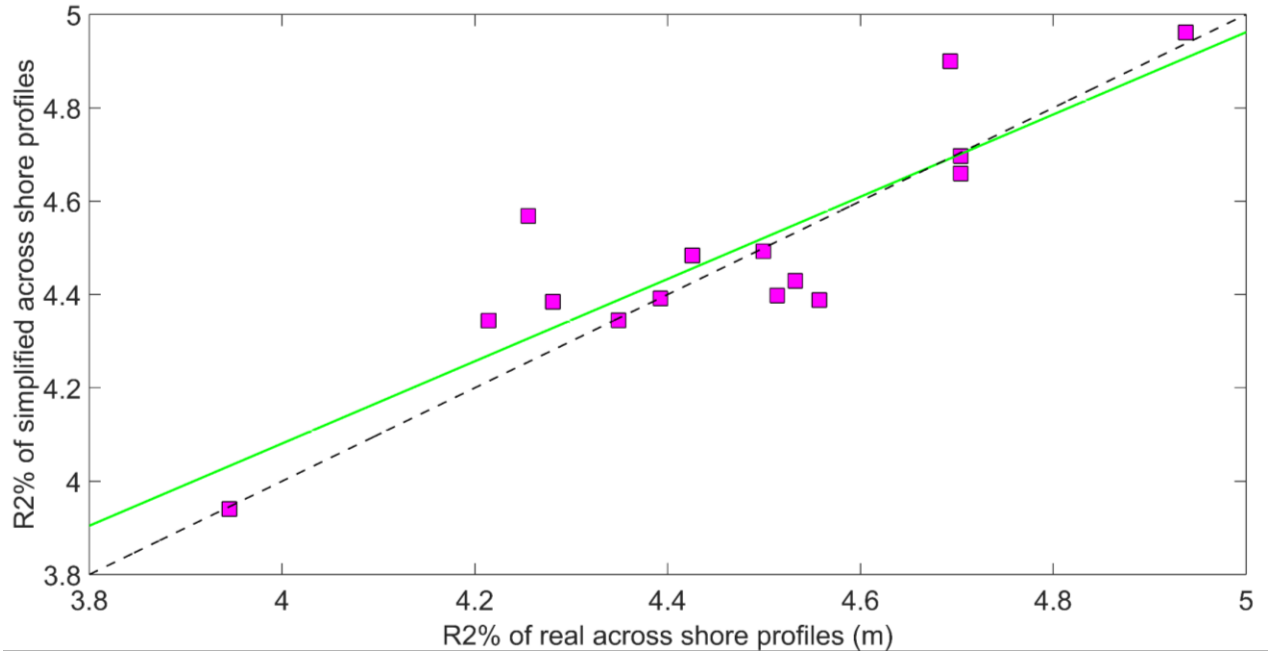

Figure 6.8: R2% values for each of the 15 profiles for the present-day profiles against the R2% values for the same extreme event but with simplified profiles. The solid line shows the linear regression for these values, it has an R_2 value of 0.8 and a P value of 2.3×10^{-5} The dashed line shows a line with an R_2 value of 1.

These simplified profiles can then be modified for different morphology scenarios by changing the position of the three points of the triangle (A, B and C in Figure 6.7). For increasing or decreasing height, B is moved up and down, for narrower or wider defences A

and C of the triangle are moved closer together or further apart. Examples of a profile modified for a different morphology scenario are shown in Figure 6.7 as a dashed line, and represents a scenario where both the nearshore bar and barrier beach are increased in height.

6.3.6 Morphology Scenarios

The previous section showed how the profiles were modified to be able to simulate different morphology scenarios. Table 6.2 shows the different scenarios that were applied, the first one being the simplified profiles, allowing a comparison of the impact on the resilience of the coastline for each of the morphology scenarios. Each scenario involved changes to both the barrier and the nearshore bar. Either raising or lowering the crest of each feature or widening or narrowing the features.

Table 6.2: Table showing morphology changes applied to barrier beach and nearshore bar for each morphology scenario.

Morphology Scenario	Barrier Beach	Nearshore Bar
1	Baseline	Baseline
2	Higher	Higher
3	Lower	Lower
4	Higher	Lower
5	Lower	Higher
6	Wider	Wider
7	Narrower	Narrower
8	Wider	Narrower
9	Narrower	Wider
10	Lower	Wider
11	Wider	Lower
12	Higher	Narrower
13	Narrower	Higher

Each of the 15 profiles were modified to reflect the different scenarios by changing the relevant height or width by 25%. The height is defined as the vertical distance between A and B (Figure 6.7). The width is defined as the horizontal distance between A and C (Figure 6.7).

6.4 Results

Each of the 15 beach profiles has been used within the storm impact model for each of the 13 morphological scenarios, this results in 195 different sets of simulation results. The mean R2% value across all 15 profiles for each morphology scenario has been calculated and plotted against the morphology scenario number, as shown in Figure 6.9.

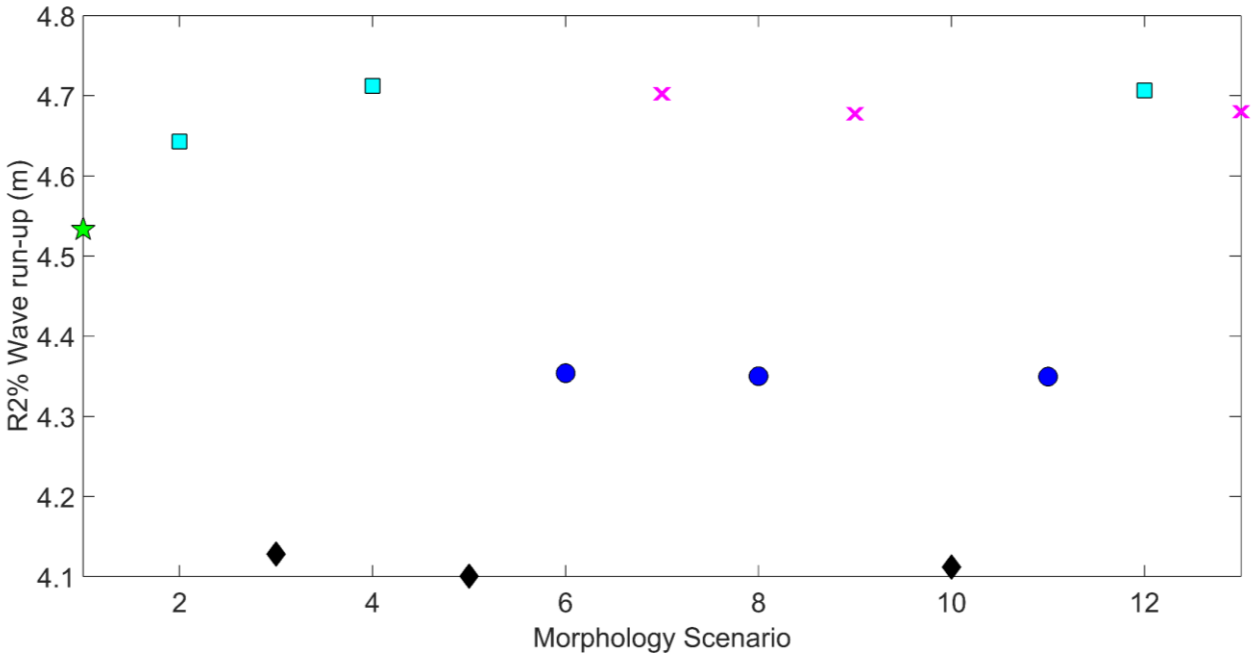

Figure 6.9: Morphology Scenario against mean R2% value for that scenario. Diamonds indicate scenarios with decreased barrier beach height, circles denote scenarios with a wider barrier, squares show scenarios with higher barrier crests and crosses correspond to narrower barriers. The baseline scenario is denoted by a star.

The different symbols on Figure 6.9 relate to the morphological scenarios that correspond to changes in the barrier beach. E.g. diamonds relate to scenarios 3, 5 and 10 all of which involve a lowering of the barrier beach crest. There are three of every symbol, which relate to the changes in the nearshore barrier. Given that there is little variation between each of the same symbols shows that the nearshore bar has little impact on the R2% value across all profiles during the simulated extreme event. The star in Figure 6.9 corresponds to the baseline morphology scenario - a simplified version of the present cross-shore profiles. Comparing it with the higher and narrower barrier scenarios shows little change in the R2% value and therefore resilience of the coastline. Wider barrier scenarios result in a lower R2% than the baseline, indicating that this has increased the resilience of the barrier beach to the extreme event. A wider barrier therefore has the potential to attenuate wave height and reduce their impact. The R2% values for scenarios 3, 5 and 10 are even lower. This is misleading as while it looks like the resilience has increased under these morphology scenarios, it is actually much less as in these scenarios waves have over-washed the defences with resultant flooding. The lower R2% values arise from the fact that the wave run-up is limited by the low defence crest and over-washes rather than contributes to further run-up. This means the coastline is no longer resilient to a 0.5% annual joint probability event under these morphology scenarios.

There are three variables that can be measured from the cross-shore profile that could potentially impact on the R2% run-up value. These are the height of the 'barrier triangle', the width of the barrier triangle and the slope of the seaward face of the barrier triangle (based on the seaward edge) (see Figure 6.7). Figures 6.10, 6.11 and 6.12 show the values of R2% for each profile and for each of the morphology scenarios against each of these variables.

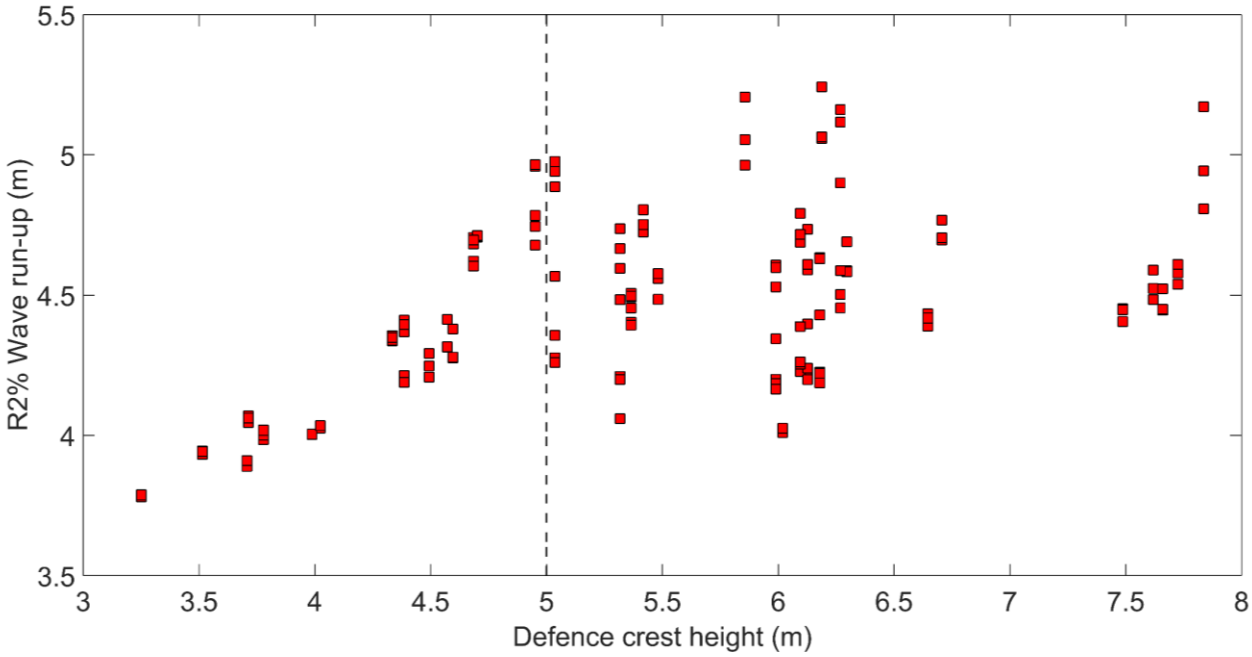

Figure 6.10: The R2% of each profile against barrier crest height for each of the morphology scenarios simulated

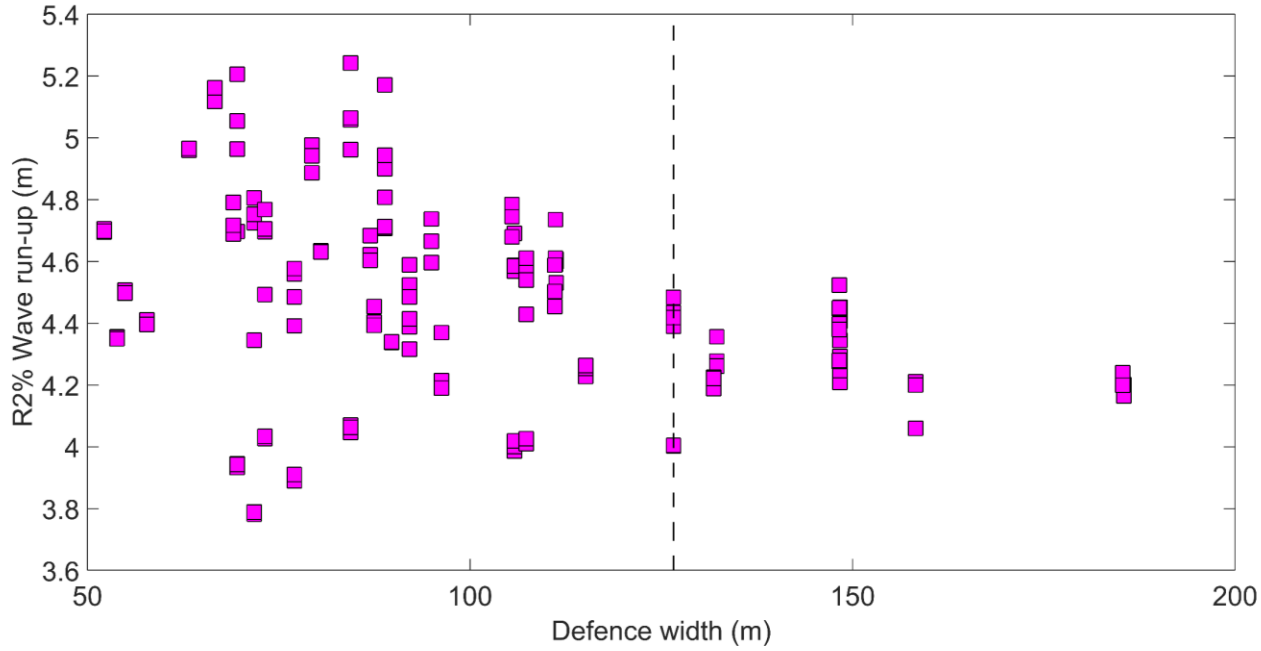

Figure 6.11: The R2% of each profile against barrier width for each of the morphology scenarios simulated.

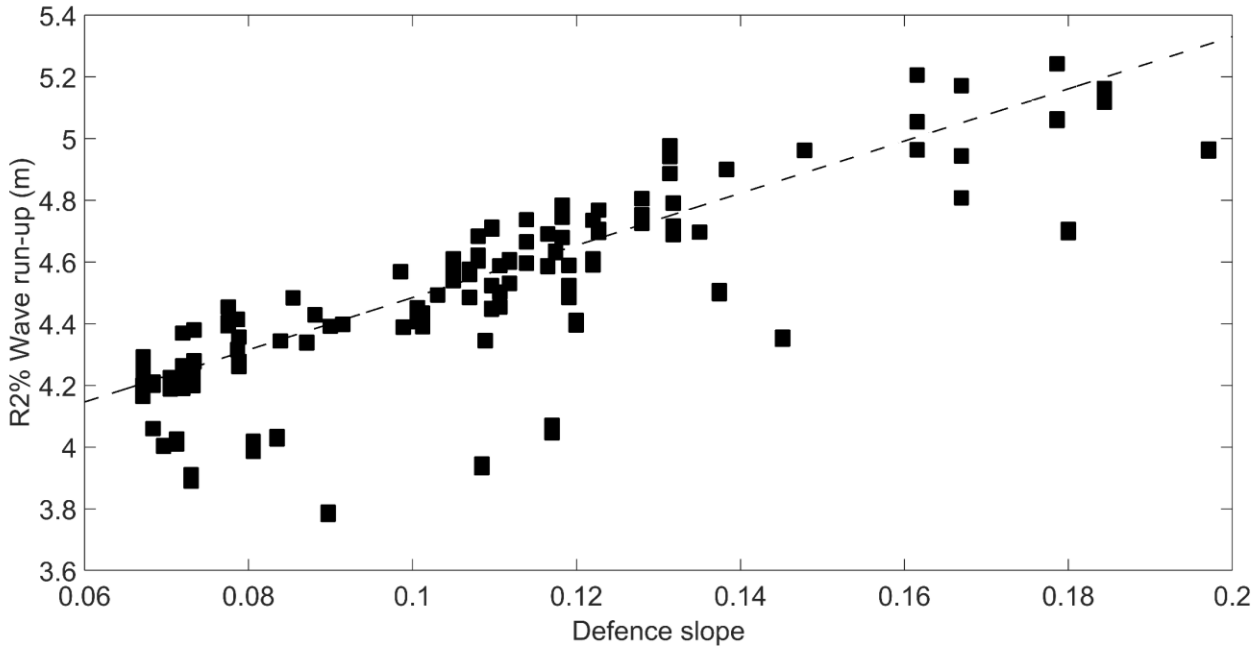

Figure 6.12: The R2% of each profile against barrier slope for each of the morphology scenarios simulated.

Figure 6.12 shows the barrier slope variable correlated with R2% where increasing slope results in a higher R2% value which reduces the ability of the coastline to withstand the simulated extreme event. For any given barrier the lower the gradient the more R2% is reduced. Figure 6.10 has a threshold highlighted by a dotted line at 5 m crest height, this threshold indicates a point where there is a large increase in the variability in R2%. Above 5 m, crest height is not a dominant factor in reducing R2% with no obvious relationship between R2% and barrier height. Below this threshold there is a linear relationship with barrier height and R2%. However, the R2% values below 4.3 m crest height are the result of waves overwashing the barrier, this means the barrier is not resilient to the extreme event below this threshold. Barrier width, as shown in Figure 6.11, has a large variability in R2% of up to 1.4 m between widths of 50 and 100 m. For barriers wider than this there is a decrease in the range of R2% to 0.8 m. Widths greater than 125 m (threshold marked with a

vertical dotted line on Figure 6.11) have a much smaller range in R2% (0.3 m) with no large or small values of R2%. This shows that no over-washing is occurring and that the waves are being attenuated by the increased barrier width, resulting in no high or excessively low (indicating over-washing) values of R2%. The threshold at 125 m shows that barrier beaches wider than this are likely to much more resilient to wave run-up than ones narrower as R2% values up to 0.7 m higher for the same extreme event are possible.

6.5 Discussion

6.5.1 Wave Run-up

Figure 6.9 in the results section shows that the 13 morphology scenarios can be sorted into three different categories. The first is for scenarios that do not result in a significantly different R2% value from the original baseline scenario. This category covers morphology scenarios such as increased barrier beach height and a narrowing width. The second category is where the R2% value is reduced, resulting in greater resilience to events as a result of wider barrier beaches. Finally, the last category is made up of lower barrier height scenarios where waves during the extreme event are able to over-wash the defences.

The three variables that have been measured across all cross-shore profiles are the height, width and seaward slope of the 'barrier triangles' that have been used to replace the 'real' features in the simplified profiles. These variables have all been plotted against R2%. There is a clear relationship with the seaward slope of the barrier, where the R2% increases at a rate 8.5 times the rate of increasing slope. There is no such linear relationship with the other variables although it is clear that the barrier width and height are also important factors in

the resilience of the coastline. To obtain a shallow slope gradient that will correspond to a lower R2% value, would also mean wider barrier beaches assuming the height of the barrier crest stays the same. This relationship is confirmed in Figure 6.11 where above a threshold at 125 m an increase in the barrier width results in a reduction in the magnitude of R2% values. For these simulations, the morphology of the beach and barrier are fixed in place, necessary to allow comparison between different barrier widths and heights but in practise the shape of the barrier would react to the prevailing wave conditions.

6.5.2 Nearshore Bar and impact of Sea-level Rise

While the nearshore bar was also modified within the morphology scenarios, it was found that changing its width and height had very little impact on the resilience of the coastline. This is likely due to the fact that the combination of extreme water level and significant wave height used to represent the 0.5% annual joint probability event consisted of a higher extreme water level and a correspondingly low significant wave height. The result of using this combination would mean that at the peak of the storm tide the water level would be well above the nearshore bar. For breaking waves the limiting amplitude to depth ratio is one of the most frequently re-investigated topics in water waves with at least nine estimates published (Meyer, 2013). The average of the values is 0.82, with 0.83 being the modal and most recent number the max and min values are 1.03 and 0.73 respectively (Meyer, 2013). As the waves in the simulations have a significant height of 0.85 m then a water depth of between 0.88 m and 0.62 m is required above the nearshore bar before waves would start to break. Given that the elevation of the bar is around -2 m and the extreme water level is 3.44 m then it's clear that the nearshore bar will have little impact on waves during this

extreme event. Although different combinations of wave height and water level, particularly ones with higher significant wave heights and lower extreme water levels could be impacted by the nearshore bar in the form of wave attenuation, therefore reducing the wave impact on the barrier or by potentially breaking on the bar itself. This is due to lower extreme water elevations above the bar and higher waves being affected by bottom friction sooner. Future studies could identify this impact and determine what joint extreme events if any benefit from the presence of the nearshore bar.

This is why the combinations of water level and wave height at 0.5% annual joint probability with taller waves and a corresponding lower extreme water level did not have high R2% values as they would have been attenuated by the nearshore bar and broken further offshore on the beach. In the future, increasing mean sea level will shift the 0.5% annual joint probability contour higher up the extreme water level scale (X axis Figure 6.4). At increased mean sea level this could potentially impact directly on the defences rather than breaking on the foreshore, leading to a dramatic reduction in the resilience of the coast. With sea-level rise this does open the possibility that the increase in R2% for 0.5% annual joint probability combinations 1 and 2 (Table 6.1) may be greater than just the increase in sea-level as the waves will not be attenuated as much by the nearshore bar and will travel much further inshore before breaking.

6.6 Conclusions

The research has shown that the slope of the barrier beach is a dominant factor in controlling the R2% value experienced during an extreme event. Increases in barrier height and

narrowing of the barrier were found to not noticeably change the average wave run-up values. Across all profiles, wider barriers were found to decrease the R2% by around 0.2 m and therefore increase the resilience of the coastline to the extreme event. A threshold at 125 m for barrier width was found where the wave run-up was reduced by around 0.8 m compared with the run-up values for widths narrower than this threshold. Barrier heights below 5 m demonstrated a steadily increasing run-up value for increasing height. Above a threshold of 5 m, the height of the barrier is not a factor in the control of the wave run-up as there is a large amount of variability in R2% values. Crest heights below 4.3 m result in over-washing demonstrating that this is a critical threshold for resilience to the extreme event being simulated.

This work has shown that the barrier slope variable is the best indicator in assessing the resilience of a vulnerable gravel beach coastline while undergoing morphological change. While barrier height and width are important factors, i.e. if it is above (for height) or below (for width) a certain threshold, these variables are not dominant factors in determining the resilience of the coastline to a changing environment. The seaward slope of the barrier is the most important factor in changing the R2% value and thus a shallower slope will create greater resilience while a steeper one will reduce the extent of the wave run-up.

6.7 Acknowledgements

We would like to acknowledge the ESPRC-funded ARCC “Adaptation and Resilience of Coastal Energy Supply” (ARCoES) project (EPSRC EP/I035390/1) for the funding to undertake this research. We would like to thank Jean-Raymond Bidlot from the European

Centre for Medium-Range Weather Forecasts for the provision of the 30-year wave ECWAM cycle 41R1 model hindcast dataset. In addition, our thanks go to CEFAS for providing the full dataset for the Sizewell wave buoy.

7 Conclusions and Implications

Each of the five previous chapters is a standalone research project. However, each relates to the other as a coherent body of research that contributes to the planning of future coastal adaptation. Chapter 2 demonstrates a method that simulates a range of plausible extreme events that are made up of a combination of different flood sources: storm surge, sea-level rise, high river flow and wave overtopping. The chapter also detailed a method where the physical impact of inundation is converted into an economic cost. The simulations showed that the flood sources do not combine in a linear way and that relying on one source of flooding to estimate the impact of an extreme event can underestimate the economic impact of said event by up to 7.7 times, and the physical extent by up 3 times. This also highlights the non-linearity in increasing flood inundation extent and resulting economic cost. Mapping the economic cost will help investigations into the cost:benefit analysis of adaptation to these extreme events. Different ways of disseminating the inundation information have been explored, particularly for local stakeholders such as residents to see the impact of the extreme event, by showing the inundation in brick courses and displaying colours such as green, yellow and red indicating the impact of the flooding on the local area. Chapter 3 builds on the research from chapter 2, where the economic impact of potential future sea-level rise on coastal energy infrastructure is assessed to determine if, and if so when, it is beneficial to invest in flood defences to protect that infrastructure. Combining physical flood modelling with economic analysis is achieved by using a depth damage curve. For a given classification, e.g. energy substation the cost in clean up and repair is expressed as a function of water depth. This is applied across a model domain giving a map of the economic cost of flooding.

The research found a tipping point in 2030 in the number of infrastructure assets in NW England where the damage cost due to extreme events increased the benefit that would result from building defences. In essence, investment achieves sufficient potential averted damage cost to make it cost-effective to invest in defences. This methodology is able to assess options for intervention across a large region at local spatial scales. The demonstration of the methodology allows an optimal allocation of when and where investment resources should be deployed or deferred to ensure the energy infrastructure remains protected against future climate change.

Chapter four quantified the uncertainty in flood risk assessments where a different combinations of water level and significant wave height have the same annual probability of occurrence, i.e. the 0.5% annual joint probability. It was found that combinations with the highest extreme water levels had the largest flood extent. Therefore, increasing extreme water levels drive an increasing inundation of the floodplain. The larger waves that do occur have a corresponding lower water elevation to produce the same annual joint probability do not have same impact on flooding due to the lower water level, resulting in the waves breaking further offshore and dissipating the wave energy before it can overwash and flood. The use of the longest peak period associated with the relevant significant wave height, consistent with swell waves is important as re-simulating events with wind wave conditions rather than swell, resulted in no flood inundation. This research has shown that ensuring a coastline is resilient to a given annual joint probability extreme event is difficult. Where many different combinations may equally apply resulting in a wide range of overwashing rates and inundation extents. Using this method will allow the testing the range of extreme

events that meet the criteria and give coastal managers and stakeholders more confidence that the defences are resilient to the standard of protection specified.

The fifth chapter examined how the resilience of a saltmarsh, i.e. its ability to reduce wave run-up, changes as it erodes. Two critical saltmarsh widths were discovered, one at 810 m and the other at 270 m. The first critical width is a threshold where the linearly increasing wave run-up with decreasing saltmarsh width changes to a constant wave run-up value despite decreasing width. The second critical width denotes another threshold where the constant wave run-up value changes to a linearly increasing one, but at a rate three times quicker than before the before first threshold width. The research shows that a saltmarsh is able to maintain the resilience it provides at the first critical threshold until the narrower threshold width is reached. As well as width, the height of the saltmarsh edge is also important, with heights below 2 m having much less resilience or greater wave run-up values. The findings from the study showed that maintaining a saltmarsh wider than 270 m and taller than 2 m will have the greatest impact on wave attenuation. These width and height thresholds have been established as critical points but only for the studied location. Further work with different saltmarshes in different locations with different vegetation and exposure will help to build the evidence that these widths are universal.

The sixth chapter investigated how the morphology of a barrier beach could contribute or hinder the resilience it could provide during an extreme event. A very clear linear relationship was found between the slope of the gravel barrier and the wave run-up experienced. This clear relationship means that the slope of the barrier is the dominant factor in controlling wave run-up. Increasing the height of the barrier and narrowing the

barrier did not impact on the wave run-up in either a negative or positive way. Across the whole studied section of coastline, it was found that wider barrier beaches decrease the wave run-up experienced during an extreme event by around 0.2 m, thus increasing the resilience of the coastline. A threshold at 125 m width was found where wave run-up was reduced by 0.8 m compared with widths narrower than 125 m. Above a barrier height of 5 m it was found that there was no control on the wave run-up, where a linear relationship was present below this height. A critical height at 4.3 m was found where barrier heights below this were no longer resilient to the extreme event being simulated. The main finding was that barrier slope variable is the best indicator in assessing the resilience of a gravel barrier located at the top of a beach.

The implications of this research are that explorative modelling within an economic framework provides useful inputs for a decision-support tool (DST). The DST should display the inundation extent resulting from a combination of different flood sources such as storm surges, river flows and waves as shown in chapter 2. It should also display a range of extreme events based on annual probability and a range of SLR and show the projected investment date for critical assets as undertaken in chapter 3. The DST allows a much easier way to disseminate the results of the research and show areas of interest. The research undertaken in chapters 5 and 6 could also be extended to show the inundation resulting from saltmarsh erosion and future shoreline changes within the DST. The Adaptation and Resilience of Coastal Energy Supply project or ARCoES has developed a DST that has incorporated some of this work particularly the inundation extents and cost of flooding from chapters 2 and 3 (Knight et al., 2015). Using numerical models to assess future vulnerability and resilience while also building an economic modelling framework has contributed an important

evidence base for planning future coastal adaptation. The results of this research have been incorporated in the DST developed within the ARCoES project and have been demonstrated at various locations such as stakeholder meetings with National Grid and Magnox. It has also been demonstrated at specifically organised ARCoES conferences and at other national conferences with positive feedback received for the tool and how it could be used by stakeholders and managers.

Future directions to advance the work in this research project would be to combine the erosion and morphology change research with a flood inundation model to project the combined impact of erosion and coastal morphology on flood risk. In addition, sea-level rise will change the joint probability of extreme water level and significant wave height by increasing the extreme water level contribution for a given annual probability. With future climate change, changes in storminess and tidal range are also possible. This could affect the wave height increasing the significant wave height contribution for a given annual probability combination. Projecting the impact these changes would have on the joint probability of extreme events is important because this could then be used to assess any flood risk change under different future sea-level rise scenarios.

8 Bibliography

Abadie, L.M., Chamorro, J.M., 2014. Valuation of Wind Energy Projects: A Real Options Approach. Energies 7, 3218–3255.

ABI, 2014. Association of British Insurers Press Release 2014 Flood in Numbers.

Adam, P., 1993. Saltmarsh ecology. Cambridge University Press.

Anderson, M.E., Smith, J.M., 2014. Wave attenuation by flexible, idealized salt marsh vegetation. Coast. Eng. 83, 82–92.

Austin, M.J., Masselink, G., 2006. Swash–groundwater interaction on a steep gravel beach. Cont. Shelf Res. 26, 2503–2519.

Bartos, M.D., Chester, M. V., 2015. Impacts of climate change on electric power supply in the Western United States. Nat. Clim. Chang. 5, 748–752.

Bates, P.., De Roo, A.P.., 2000. A simple raster-based model for flood inundation simulation. J. Hydrol. 236, 54–77.

Bates, P.D., Dawson, R.J., Hall, J.W., Horritt, M.S., Nicholls, R.J., Wicks, J., Mohamed Ahmed Ali Mohamed Hassan, 2005. Simplified two-dimensional numerical modelling of coastal flooding and example applications. Coast. Eng. 52, 793–810.

Bates, P.D., Horritt, M.S., Fewtrell, T.J., 2010. A simple inertial formulation of the shallow water equations for efficient two-dimensional flood inundation modelling. J. Hydrol.

387, 33–45.

Baxter, P.J., 2005. The east coast Big Flood, 31 January-1 February 1953: a summary of the human disaster. Philos. Trans. A. Math. Phys. Eng. Sci. 363, 1293–312.

Black, F., Scholes, M.S., 1973. The Pricing of Options and Corporate Liabilities. J. Polit. Econ. 81, 637–54.

Bolle, A., Mercelis, P., Roelvink, D., Haerens, P., Trouw, K., 2011. Application and validation of XBeach for three different field sites. Coast. Eng. Proc. 1, 40.

Bosello, F., De Cian, E., 2014. Climate change, sea level rise, and coastal disasters. A review of modeling practices. Energy Econ. 46, 593–605.

Bowker, P., 2007. Flood resistance and resilience solutions: an R&D scoping study. DEFRA Report, London.

Bowker, P., Escarameia, M., Tagg, A., Britain, G., Britain, G., Britain, G., 2007. Improving the flood performance of new buildings: Flood resilient construction. RIBA.

Boyle, P.P., 1977. Options: A Monte Carlo approach. J. financ. econ. 4, 323–338.

Bradbury, A.P., Powell, K.A., 1992. The Short Term Profile Response of Shingle Spits to Storm Wave Action. Coast. Eng. Proc.

British Oceanographic Data Centre, 2015. Download processed UK Tide Gauge Network data from BODC [WWW Document]. Br. Oceanogr. Data Cent. URL https://www.bodc.ac.uk/data/online_delivery/ntslf/

Brown, S., Hanson, S., Nicholls, R.J., 2013. Implications of sea-level rise and extreme events around Europe: a review of coastal energy infrastructure. Clim. Change 122, 81–95.

Buijs, F., Britain, G., Britain, G., 2007. Performance and reliability of flood and coastal defences. DEFRA.

Burke, R.W., Stolzenbach, K.D., 1983. Free surface flow through salt marsh grass. Massachusetts Institute of Technology.

Caminha-Noronha, J.C., Marangon-Lima, J.W., Leite-Ferreira, T.G., Unsihuay, C., Zambroni de Souza, A.C., 2006. Optimal Strategies for Investment in Generation of Electric Energy through Real Options.

CEFAS, 2015. Cefas - WaveNet interactive map [WWW Document]. URL https://www.cefas.co.uk/cefas-data-hub/wavenet/

CEFAS Wavenet, 2014. Blackpool Wave Data [WWW Document]. URL https://www.cefas.co.uk/cefas-data-hub/wavenet/

Channel Coast Observatory, 2016. Channel Coast Observatory - Map Viewer and Data Catalogue [WWW Document]. URL http://www.channelcoast.org/data_management/online_data_catalogue/ (accessed 6.7.16).

Chini, N., Stansby, P., Leake, J., Wolf, J., Roberts-Jones, J., Lowe, J., 2010. The impact of sea level rise and climate change on inshore wave climate: A case study for East Anglia (UK). Coast. Eng. 57, 973–984.

Chini, N., Stansby, P.K., 2012. Extreme values of coastal wave overtopping accounting for climate change and sea level rise. Coast. Eng. 65, 27–37.

Coles, S.G., Tawn, J.A., 1990. Statistics of Coastal Flood Prevention. Philos. Trans. R. Soc. A Math. Phys. Eng. Sci. 332, 457–476.

Cooper, N.J., Pontee, N.I., 2006. Appraisal and evolution of the littoral "sediment cell" concept in applied coastal management: Experiences from England and Wales. Ocean Coast. Manag. 49, 498–510.

Cox, J.C., Ross, S.A., Rubinstein, M., 1979. Option pricing: A simplified approach. J. financ. econ. 7, 229–263.

Cradden, L.C., Harrison, G.P., 2013. Adapting overhead lines to climate change: Are dynamic ratings the answer? Energy Policy 63, 197–206.

Dawson, R.J., Hall, J.W., Bates, P.D., Nicholls, R.J., 2005. Quantified Analysis of the Probability of Flooding in the Thames Estuary under Imaginable Worst-case Sea Level Rise Scenarios. Int. J. Water Resour. Dev. 21, 577–591.

DEFRA, 2012. The UK Climate Change Risk Assessment 2012 Evidence Report.

Deltares, 2014. Coastal Research with Plymouth University, XBeach-G [WWW Document]. URL https://oss.deltares.nl/web/xbeach/xbeach-og

Dornbusch, U., 2005. Beaches at Risk: Beach material properties.

Duffield, S., Macgregor, N., 2012. Natural England's climate change risk assessment and

adaptation plan.

ECMWF, 2016. ECMWF - European Centre for Medium-Range Weather Forecast 30 Year Wave Hindcast [WWW Document]. URL http://www.ecmwf.int/

EDF, 2012. EU Stress Test Dungeness B [WWW Document]. URL https://www.edfenergy.com/sites/default/files/jer-srt-stt-pub-fin-001_dnb_stress_test_v1.1.pdf (accessed 1.18.16).

Edina Digimap, 2013. Miniscale Map of the UK [WWW Document]. URL http://digimap.edina.ac.uk

Energy Network Association, 2007. Vegetation Management Near Electricity Equipment-Principles of Good Practice [WWW Document]. URL http://www.energynetworks.org/assets/files/electricity/engineering/engineering documents/ENA_ETR_136_Issue_1_080109.pdf (accessed 5.13.16).

Energy Network Association, 2009. Resilience to Flooding of Grid and Primary Substations.

Environment Agency, 2009a. Peaks Over Threshold CSV Data Files.

Environment Agency, 2009b. Shoreline management plans (SMPs) - GOV.UK [WWW Document]. URL https://www.gov.uk/government/publications/shoreline-management-plans-smps/shoreline-management-plans-smps (accessed 4.29.16).

Environment Agency, 2010. Suffolk SMP2 Sub-cell 3c.

Environment Agency, 2013. Northwest UK Coast Defence Data.

Environment Agency, 2016. Risk of Flooding from Rivers and Sea [WWW Document]. URL http://watermaps.environment-agency.gov.uk

Environment Agency Geomatics, 2014. LiDAR dataset [WWW Document]. URL http://www.geostore.com/environment-agency/survey.html#/survey

Environment Agency Northwest Office, 2013. River Wyre Hydrograph.

Fagherazzi, S., 2014. Coastal processes: Storm-proofing with marshes. Nat. Geosci. 7, 701–702.

Farrell, A.N., 2012. An Economic Evaluation of Wave Energy Conversion Devices.

Feagin, R.A., Lozada-Bernard, S.M., Ravens, T.M., Moller, I., Yeager, K.M., Baird, A.H., 2009. Does vegetation prevent wave erosion of salt marsh edges? Proc. Natl. Acad. Sci. 106, 10109–10113.

Fortnum, B.C.H., Hardcastle, P.J., 1979. Waves recorded at Aldeburgh, Dunwich and Southwold on the east coast of England. Data for June 1975-May 1977 at positions between 52, 9N and 52, 20N, and between 1, 37E and 1, 42E. Summary analysis and interpretation report.

French, P.W., 2001. Coastal defences: processes, problems and solutions. Psychology Press.

Galarneau, T.J., Davis, C.A., Shapiro, M.A., 2013. Intensification of Hurricane Sandy (2012) through Extratropical Warm Core Seclusion. Mon. Weather Rev. 141, 4296–4321.

Gallien, T.W., Sanders, B.F., Flick, R.E., 2014. Urban coastal flood prediction: Integrating

wave overtopping, flood defenses and drainage. Coast. Eng. 91, 18–28.

Gerritsen, H., 2005. What happened in 1953? The Big Flood in the Netherlands in retrospect. Philos. Trans. R. Soc. A Math. Phys. Eng. Sci. 363, 1271–1291.

Gilles, D., Moore, M., 2010. Review of Hydraulic Flood Modeling Software used in Belgium, The Netherlands, and The United Kingdom.

Government Accountability Office, 2014. Climate Change: Energy Infrastructure Risks and Adaptation Efforts [WWW Document]. URL http://www.gao.gov/products/GAO-14-74 (accessed 4.21.16).

Green, Carl, 2014. Rossall Sea Defences Wyre Council.

Haigh, I., Nicholls, R., Wells, N., 2010. Assessing changes in extreme sea levels: Application to the English Channel, 1900–2006. Cont. Shelf Res. 30, 1042–1055.

Halcrow, 2000. Lowestoft to Thorpeness Coastal Process/Strategy Study. Part 2. Swindon, UK: Strategy Assessment Report, November 2000.

Halcrow Group Ltd, 2010. North West & North Wales Coastal Group North West England and North Wales Shoreline Management Plan SMP2.

Hall, J.W., Sayers, P.B., Walkden, M.J., Panzeri, M., 2006. Impacts of climate change on coastal flood risk in England and Wales: 2030–2100. Philos. Trans. R. Soc. A Math. Phys. Eng. Sci. 364, 1027–1049.

Hames, D., Reeve, D., 2007. The joint probability of waves and high sea levels in coastal

defence. Proc. Flood Risk Assess. II Conf. Inst. Math. Its Appl. Southend Sea 97–106.

Handmer, J., Honda, Y., Kundzewicz, Z., Arnell, N., Benito, G., Hatfield, J., Mohamed, I., Peduzzi, P., Wu, S., Sherstyukov, B., Takahashi, K., Yan, Z., 2012. Changes in impacts of climate extremes: Human systems and ecosystems 231–290.

Harmsworth, G.C., Long, S.P., 1986. An assessment of saltmarsh erosion in Essex, England, with reference to the Dengie Peninsula. Biol. Conserv. 35, 377–387.

Hasselmann, K., Barnett, T.P., Bouws, E., Carlson, H., Cartwright, D.E., Enke, K., Ewing, J.A., Gienapp, H., Hasselmann, D.E., Kruseman, P., Meerburg, A., Müller, P., Olbers, D.J., Richter, K., Sell, W., Walden, H., 1973. Measurements of wind-wave growth and swell decay during the Joint North Sea Wave Project (JONSWAP). Hydraul. Eng. Reports.

Hawkes, P., Svensson, C., 2003. Joint Probability: Dependence Mapping and Best Practice.

Hawkes, P.J., Gouldby, B.P., 1998. The joint probability of waves and water levels: JOIN-SEA Version 1.0 - User manual.

Hawkes, P.J., Gouldby, B.P., Tawn, J.A., Owen, M.W., 2002. The joint probability of waves and water levels in coastal engineering design. J. Hydraul. Res. 40, 241–251.

Hawkes, P.J., Svensson, C., 2006. Joint Probability: Dependence Mapping and Best Practice. HR Wallingford.

Hawkes, P.J., Svensson, C., 2006. Use of Joint Probability Methods in Flood Management: A guide to best practice :: Repository Hydraulic Engineering Reports [WWW Document].

HM Government, 2013. The National Adaptation Programme Making the country resilient to a changing climate.

Hoozemans, F.M.J., Marchand, M., Pennekamp, H.A., 1993. A global vulnerability analysis: vulnerability assessment for population, coastal wetlands and rice production on a global scale.

Jevrejeva, S., Grinsted, A., Moore, J.C., 2014. Upper limit for sea level projections by 2100. Environ. Res. Lett. 9, 104008.

Jevrejeva, S., Moore, J.C., Grinsted, A., 2012. Sea level projections to AD2500 with a new generation of climate change scenarios. Glob. Planet. Change 80, 14–20.

JNCC, 2001. Minsmere Walberwick Special Protection Area [WWW Document]. URL http://jncc.defra.gov.uk/page-2009

JNCC, 2015. Joint Nature Conservation Commitee: Dungeness - Special Area of Conservation [WWW Document]. Dungeness - Spec. Area Conserv. URL http://jncc.defra.gov.uk/protectedsites/sacselection/sac.asp?EUCode=UK0013059

Jonkman, S.N., Kelman, I., 2005. Deaths during the 1953 North Sea storm surge. In: Proceedings of the Solutions to Coastal Disasters Conference, American Society for Civil Engineers (ASCE), Charleston, South Carolina. pp. 8–11.

Kates, R.W., Colten, C.E., Laska, S., Leatherman, S.P., 2006. Reconstruction of New Orleans after Hurricane Katrina: A research perspective. Proc. Natl. Acad. Sci. 103, 14653–14660.

Kiriyama, E., Suzuki, A., 2004. Use of Real Options in Nuclear Power Plant Valuation in the Presence of Uncertainty with CO 2 Emission Credit. J. Nucl. Sci. Technol. 41, 756–764.

Kjærland, F., 2007. A real option analysis of investments in hydropower—The case of Norway. Energy Policy 35, 5901–5908.

Knight, P.J., Prime, T., Brown, J.M., Morrissey, K., Plater, A.J., 2015. Application of flood risk modelling in a web-based geospatial decision support tool for coastal adaptation to climate change. Nat. Hazards Earth Syst. Sci. 15, 1457–1471.

Lapidez, J.P., Tablazon, J., Dasallas, L., Gonzalo, L.A., Cabacaba, K.M., Ramos, M.M.A., Suarez, J.K., Santiago, J., Lagmay, A.M.F., Malano, V., 2015. Identification of storm surge vulnerable areas in the Philippines through the simulation of Typhoon Haiyan-induced storm surge levels over historical storm tracks. Nat. Hazards Earth Syst. Sci. 15, 1473–1481.

Le, T.V.H., Nguyen, H.N., Tran, T.C., Haruyama, S., 2007. The combined impact on the flooding in Vietnam's Mekong River delta of local man-made structures, sea level rise, and dams upstream in the river catchment. Estuar. Coast. Shelf Sci. 71, 110–116.

Leake, J., Wolf, J., Lowe, J., Hall, J., Nicholls, R., 2009. Response of marine climate to future climate change: application to coastal regions.

Leonardi, N., Ganju, N.K., Fagherazzi, S., 2016. A linear relationship between wave power and erosion determines salt-marsh resilience to violent storms and hurricanes. Proc. Natl. Acad. Sci. 113, 64–68.

Lewis, M., Horsburgh, K., Bates, P., Smith, R., 2011. Quantifying the Uncertainty in Future Coastal Flood Risk Estimates for the U.K. J. Coast. Res. 276, 870–881.

Long, A.J., Waller, M.P., Plater, A.J., 2007. Dungeness and the Romney Marsh: barrier dynamics and marshland evolution. Oxbow Books.

Longuet-Higgins, M.S., 1970. Longshore currents generated by obliquely incident sea waves: 1. J. Geophys. Res. 75, 6778–6789.

Lowe, J.A., Gregory, J.M., Flather, R.A., 2001. Changes in the occurrence of storm surges around the United Kingdom under a future climate scenario using a dynamic storm surge model driven by the Hadley Centre climate models. Clim. Dyn. 18, 179–188.

Lowe, J., Howard, T., Pardaens, A., Tinker, J., Holt, J.T., Wakelin, S.L., Milne, G., Leake, J., Wolf, J., Horsburgh, K.J., Reeder, T., Jenkins, G., Ridley, J., Dye, S., Bradley, S., 2009. UK Climate Projections Science Report: Marine and Coastal Projections.

Magnox, 2014. Dungeness Site Strategic Environmental Assessment Site Specific Baseline [WWW Document]. URL https://magnoxsites.com/wp-content/uploads/2014/10/Dungeness-SEA-FINAL.pdf

Magnox, 2016. Sizewell Site Strategic Environmental Assessment Site Specific Baseline [WWW Document]. URL https://magnoxsites.com/wp-content/uploads/2014/11/Sizewell-A-SEA-FINAL.pdf

Majd, S., Pindyck, R.S., 1987. Time to build, option value, and investment decisions. J. financ. econ. 18, 7–27.

Maskell, J., Horsburgh, K., Lewis, M., Bates, P., 2013. Investigating River-Surge Interaction in Idealised Estuaries. J. Coast. Res. 30, 248–259.

Mason, T., Bradbury, A., Poate, T., Newman, R., 2009. Nearshore Wave Climate of the English Channel - Evidence for Bi-modal Seas. In: Coastal Engineering 2008. World Scientific Publishing Company, pp. 605–616.

Masselink, G., McCall, R., Poate, T., Geer, P. van, 2015. Modelling storm response on gravel beaches using XBeach-G. Proc. Inst. Civ. Eng. - Marit. Eng.

Masselink, G., van Heteren, S., 2014. Response of wave-dominated and mixed-energy barriers to storms. Mar. Geol. 352, 321–347.

Matias, A., Blenkinsopp, C.E., Masselink, G., 2014. Detailed investigation of overwash on a gravel barrier. Mar. Geol. 350, 27–38.

Matthews, T., Murphy, C., Wilby, R.L., Harrigan, S., 2014. Stormiest winter on record for Ireland and UK. Nat. Clim. Chang. 4, 738–740.

McCabe, M.V., Stansby, P.K., Apsley, D.D., 2013. Random wave runup and overtopping a steep sea wall: Shallow-water and Boussinesq modelling with generalised breaking and wall impact algorithms validated against laboratory and field measurements. Coast. Eng. 74, 33–49.

MCCALL, R., MASSELINK, G., POATE, T., ROELVINK, D., 2015. Modelling gravel barrier resilience during storms with XBeach-G: The role of infiltration. In: The Proceedings of the Coastal Sediments 2015. WORLD SCIENTIFIC.

McCall, R.T., Masselink, G., Poate, T.G., Roelvink, J.A., Almeida, L.P., 2015. Modelling the morphodynamics of gravel beaches during storms with XBeach-G. Coast. Eng. 103, 52–66.

McCall, R.T., Masselink, G., Poate, T.G., Roelvink, J.A., Almeida, L.P., Davidson, M., Russell, P.E., 2014. Modelling storm hydrodynamics on gravel beaches with XBeach-G. Coast. Eng. 91, 231–250.

McGranahan, G., Balk, D., Anderson, B., 2007. The rising tide: assessing the risks of climate change and human settlements in low elevation coastal zones. Environ. Urban. 19, 17–37.

McInnes, K.L., Walsh, K.J.E., Hubbert, G.D., Beer, T., 2003. Impact of Sea-level Rise and Storm Surges on a Coastal Community. Nat. Hazards 30, 187–207.

McMillan, A., Batstone, C., Worth, D., Tawn, J., Horsburgh, K.J., Lawless, M., 2011. Coastal flood boundary conditions for UK mainland and islands. Project SC060064/TR2: Design sea levels.

McMillan, A., Worth, D., Johnson, A., Keming, H., 2011. Coastal flood boundary condiitons for UK mainland and islands. Project SC060064/TR5 Practical guidance swell waves.

Meijer, M.C., 2005. Wave attenuation over salt marsh vegetation.

Menéndez, M., Woodworth, P.L., 2010. Changes in extreme high water levels based on a quasi-global tide-gauge data set. J. Geophys. Res. 115, C10011.

Meyer, R.E., 2013. Waves on Beaches and Resulting Sediment Transport: Proceedings of an Advanced Seminar, Conducted by the Mathematics Research Center, the University of Wisconsin, and the Coastal Engineering Research Center, US Army, at Madison, October 11–13, 1971. Elsevier.

Möller, I., 2006. Quantifying saltmarsh vegetation and its effect on wave height dissipation: Results from a UK East coast saltmarsh. Estuar. Coast. Shelf Sci. 69, 337–351.

Möller, I., Kudella, M., Rupprecht, F., Spencer, T., Paul, M., van Wesenbeeck, B.K., Wolters, G., Jensen, K., Bouma, T.J., Miranda-Lange, M., Schimmels, S., 2014a. Wave attenuation over coastal salt marshes under storm surge conditions. Nat. Geosci. 7, 727–731.

Möller, I., Kudella, M., Rupprecht, F., Spencer, T., Paul, M., van Wesenbeeck, B.K., Wolters, G., Jensen, K., Bouma, T.J., Miranda-Lange, M., Schimmels, S., 2014b. Wave attenuation over coastal salt marshes under storm surge conditions. Nat. Geosci. 7, 727–731.

Möller, I., Spencer, T., French, J.R., Leggett, D.J., Dixon, M., 1999. Wave Transformation Over Salt Marshes: A Field and Numerical Modelling Study from North Norfolk, England. Estuar. Coast. Shelf Sci. 49, 411–426.

National Grid, 2010. Climate Change Adaptation Report [WWW Document]. URL http://webarchive.nationalarchives.gov.uk/20130123162956/http://archive.defra.gov.uk/environment/climate/documents/adapt-reports/01benchmark/bench-national-grid-cca-report.pdf (accessed 5.6.16).

National Oceanography Centre, 2014. POLTIPS-3 - POLTIPS | National Oceanography

Centre | from coast to deep ocean [WWW Document]. URL http://noc.ac.uk/using-science/products-services/software/poltips3-tidal-prediction-software

Natural England, 1993. Minsmere-Walberswick Heaths and Marshes SSSI [WWW Document]. URL https://designatedsites.naturalengland.org.uk/SiteDetail.aspx?SiteCode=S1000721&SiteName=mins&countyCode=&responsiblePerson=

Natural England, 2006. Dungeness, Romney Marsh and Rye Bay SSSI Site [WWW Document]. Nat. Engl. Des. SSSI Sites. URL https://designatedsites.naturalengland.org.uk/SiteList.aspx?siteName=dungeness&countyCode=&responsiblePerson=

Nicholls, R.J., 2004. Coastal flooding and wetland loss in the 21st century: changes under the SRES climate and socio-economic scenarios. Glob. Environ. Chang. 14, 69–86.

Nicholls, R.J., de la Vega-Leinert, A.C., 2008. Implications of Sea-Level Rise for Europe's Coasts: An Introduction. J. Coast. Res. 242, 285–287.

Nicholls, R.J., Hoozemans, F.M.J., Marchand, M., 1999. Increasing flood risk and wetland losses due to global sea-level rise: regional and global analyses. Glob. Environ. Chang. 9, S69–S87.

Nicholls, R.J., Marinova, N., Lowe, J.A., Brown, S., Vellinga, P., Gusmão, D. de, Hinkel, J., Tol, R.S.J., 2011. Sea-level rise and its possible impacts given a "beyond 4°C world" in the twenty-first century. Philos. Trans. R. Soc. A Math. Phys. Eng. Sci. 369, 161–181.

NOC, 2015. POLTIPS-3 - POLTIPS | National Oceanography Centre | from coast to deep ocean [WWW Document]. URL http://noc.ac.uk/using-science/products/software/poltips/poltips-3 (accessed 1.18.16).

Ordnance Survey, 2013. Ordnance Survey Topography data. EDINA Digimap Ordnance Survey Service,.

OS, 2007. Land Cover Dataset 2007. EDINA Digimap.

Palmer, T., Nicholls, R.J., Wells, N.C., Saulter, A., Mason, T., 2014. Identification of "energetic" swell waves in a tidal strait. Cont. Shelf Res. 88, 203–215.

Penning-Rowsell, E., Priest, S., Parker, D., Morris, J., Tunstall, S., Viavattene, C., Chatterton, J., Owen, D., 2014. Flood and Coastal Erosion Risk Management: A Manual for Economic Appraisal. Routledge.

Phung, D., 1980. Cost comparison of energy projects: Discounted cash flow and revenue requirement methods. Energy 5, 1053–1072.

Pierson, W.J., Moskowitz, L., 1964. A proposed spectral form for fully developed wind seas based on the similarity theory of S. A. Kitaigorodskii. J. Geophys. Res. 69, 5181–5190.

Pietruszczak, S., Niu, X., 1992. A mathematical description of macroscopic behaviour of brick masonry. Int. J. Solids Struct. 29, 531–546.

Prime, T., Brown, J.M., Plater, A.J., 2015. Physical and economic impacts of sea-level rise and low probability flooding events on coastal communities. PLoS One 10, e0117030.

Prime, T., Brown, J.M., Plater, A.J., 2016. Flood inundation uncertainty: The case of a 0.5% annual probability flood event. Environ. Sci. Policy 59, 1–9.

Pringles, R., Olsina, F., Garcés, F., 2015. Real option valuation of power transmission investments by stochastic simulation. Energy Econ. 47, 215–226.

Purvis, M.J., Bates, P.D., Hayes, C.M., 2008. A probabilistic methodology to estimate future coastal flood risk due to sea level rise. Coast. Eng. 55, 1062–1073.

Pye, K., Blott, S.J., 2006. Coastal Processes and Morphological Change in the Dunwich-Sizewell Area, Suffolk, UK. J. Coast. Res. 453–473.

Quinn, N., Bates, P.D., Siddall, M., 2013. The contribution to future flood risk in the Severn Estuary from extreme sea level rise due to ice sheet mass loss. J. Geophys. Res. Ocean. 118, 5887–5898.

Reichl, J., Schmidthaler, M., Schneider, F., 2013. The value of supply security: The costs of power outages to Austrian households, firms and the public sector. Energy Econ. 36, 256–261.

Roelvink, D., Reniers, A., Van Dongeren, A., Van Thiel de Vries, J., Lescinski, J., McCall, R., 2010. XBeach model description and manual. Unesco-IHE Inst. Water Educ. Deltares Delft Univ. Tecnhology. Rep. June 21, 2010.

Rupprecht, F., Möller, I., Evans, B., Spencer, T., Jensen, K., 2015. Biophysical properties of salt marsh canopies — Quantifying plant stem flexibility and above ground biomass. Coast. Eng. 100, 48–57.

Shepard, C.C., Crain, C.M., Beck, M.W., 2011. The Protective Role of Coastal Marshes: A Systematic Review and Meta-analysis. PLoS One 6, e27374.

Skinner, C.J., Coulthard, T.J., Parsons, D.R., Ramirez, J.A., Mullen, L., Manson, S., 2015. Simulating tidal and storm surge hydraulics with a simple 2D inertia based model, in the Humber Estuary, U.K. Estuar. Coast. Shelf Sci. 155, 126–136.

Small, C., Nicholls, R.J., 2003. A global analysis of human settlement in coastal zones. J. Coast. Res.

Smith, R.A.E., Bates, P.D., Hayes, C., 2011. Evaluation of a coastal flood inundation model using hard and soft data. Environ. Model. Softw. 30, 35–46.

Smolders, S., Plancke, Y., Ides, S., Meire, P., Temmerman, S., 2015. Role of intertidal wetlands for tidal and storm tide attenuation along a confined estuary: a model study. Nat. Hazards Earth Syst. Sci. 15, 1659–1675.

Stansby, P., Chini, N., Apsley, D., Borthwick, A., Bricheno, L., Horrillo-Caraballo, J., McCabe, M., Reeve, D., Rogers, B.D., Saulter, A., Scott, A., Wilson, C., Wolf, J., Yan, K., 2013. An integrated model system for coastal flood prediction with a case history for Walcott, UK, on 9 November 2007. J. Flood Risk Manag. 6, 229–252.

Steers, J.A., Stoddart, D.R., Bayliss-Smith, T.P., Spencer, T., Durbidge, P.M., 1979. The Storm Surge of 11 January 1978 on the East Coast of England. Geogr. J. 145, 192.

Stevens, A.J., Clarke, D., Nicholls, R.J., Wadey, M.P., 2015. Estimating the long-term historic evolution of exposure to flooding of coastal populations. Nat. Hazards Earth Syst. Sci.

15, 1215–1229.

Stockdon, H.F., Holman, R.A., Howd, P.A., Sallenger, A.H., 2006. Empirical parameterization of setup, swash, and runup. Coast. Eng. 53, 573–588.

Stocker, T.F., Qin, D., Plattner, G.-K., Tignor, M., Allen, S.K., Boschung, J., Nauels, A., Xia, Y., Bex, V., Midgley, P.M., 2013. Climate change 2013: The physical science basis. Intergov. Panel Clim. Chang. Work. Gr. I Contrib. to IPCC Fifth Assess. Rep. (AR5)(Cambridge Univ Press. New York).

SurgeWatch, 2016. A Database of UK Coastal Flood Events [WWW Document]. URL https://www.surgewatch.org (accessed 10.28.16).

Tucker, M.J., Carr, A.P., Pitt, E.G., 1983. The effect of an offshore bank in attenuating waves. Coast. Eng. 7, 133–144.

University of Edinburgh, 2016. Digimap - access to maps and geospatial data [WWW Document]. URL http://digimap.edina.ac.uk/ (accessed 6.7.16).

van der Wal, D., Pye, K., 2004. Patterns, rates and possible causes of saltmarsh erosion in the Greater Thames area (UK). Geomorphology 61, 373–391.

van Vliet, M.T.H., Yearsley, J.R., Ludwig, F., Vögele, S., Lettenmaier, D.P., Kabat, P., 2012. Vulnerability of US and European electricity supply to climate change. Nat. Clim. Chang. 2, 676–681.

Wade, S., Wallingford, H.U.H.R., 2008. Supplementary note on flood hazards and thresholds

1–5.

Wadey, M.P., Brown, J.M., Haigh, I.D., Dolphin, T., Wisse, P., 2015. Assessment and comparison of extreme sea levels and waves during the 2013/14 storm season in two UK coastal regions. Nat. Hazards Earth Syst. Sci. 15, 2209–2225.

Wadey, M.P., Haigh, I.D., Brown, J.M., 2014. A century of sea level data and the UK's 2013/14 storm surges: an assessment of extremes and clustering using the Newlyn tide gauge record. Ocean Sci. 10, 1031–1045.

Wadey, M.P., Nicholls, R.J., Haigh, I., 2013. Understanding a coastal flood event: the 10th March 2008 storm surge event in the Solent, UK. Nat. Hazards.

Wadey, M.P., Nicholls, R.J., Hutton, C., 2012. Coastal Flooding in the Solent: An Integrated Analysis of Defences and Inundation. Water 4, 430–459.

Wahl, T., Jensen, J., Frank, T., Haigh, I.D., 2011. Improved estimates of mean sea level changes in the German Bight over the last 166 years. Ocean Dyn. 61, 701–715.

Wamsley, T. V., Cialone, M.A., Smith, J.M., Atkinson, J.H., Rosati, J.D., 2010. The potential of wetlands in reducing storm surge. Ocean Eng. 37, 59–68.

Wells, N., 1997. The atmosphere and ocean: a physical introduction. Wiley, Chichester; New York.

Wolf, J., Flather, R.A., 2005. Modelling waves and surges during the 1953 storm. Philos. Trans. R. Soc. A Math. Phys. Eng. Sci. 363, 1359–1375.

Wolters, M., Bakker, J.P., Bertness, M.D., Jefferies, R.L., Moller, I., 2005. Saltmarsh erosion and restoration in south-east England: squeezing the evidence requires realignment. J. Appl. Ecol. 42, 844–851.

Woodward, M., Gouldby, B., Kapelan, Z., Khu, S.-T., Townend, I., 2011. Real Options in flood risk management decision making. J. Flood Risk Manag. 4, 339–349.

Woodworth, P. l., Teferle, F. n., Bingley, R. m., Shennan, I., Williams, S. d. p., 2009. Trends in UK mean sea level revisited. Geophys. J. Int. 176, 19–30.

Wyse, I.A./ G.A./ P., 2015. Flood Map - your questions answered.

Zijlema, M., Stelling, G., Smit, P., 2011. SWASH: An operational public domain code for simulating wave fields and rapidly varied flows in coastal waters. Coast. Eng. 58, 992–1012.

Zong, Y., Tooley, M.J., 2003. A Historical Record of Coastal Floods in Britain: Frequencies and Associated Storm Tracks. Nat. Hazards 29, 13–36.

9 Appendix

9.1 Sources of Data

A wide variety of data was used within this thesis, the full range used is listed here:

- LiDAR
- Bathymetry
- Beach survey
- Sea-Level return period
- Waves
- Tide gauge
- Predicted tide
- Depth damage curves
- Spatial locations of coastal community assets
- Regional relative sea-level rise projections

9.1.1 LiDAR

The LiDAR used in this research was obtained from two sources the Environment Agency Geomatics website and the Channel Coast Observatory. Both LiDAR datasets fulfilled different roles, the EA data has a high coverage at 2 m horizontal resolution, with a lower coverage at 1 m. It also is regularly updated with new surveys. However, the downside of EA coverage is that it does not focus on intertidal areas (i.e. by surveying at low spring tides) the result being that survey data may or may not have good data for these areas.

Conversely the Channel Coast Observatory undertakes surveys with the coast in mind so intertidal areas have good quality data but the coverage across the UK is poor with not many surveys being undertaken. Originally the EA LiDAR was only available free for noncommercial purposes, but has since been made available for commercial purposes.

EA Geomatics LiDAR is available here:

http://www.geostore.com/environment-agency/survey.html#/survey

Channel Coast Observatory LiDAR is available here:

http://www.channelcoast.org/data_management/online_data_catalogue/metadata/search/index2.php

9.1.2 Bathymetry

The bathymetry was sourced from the EDINA Digimap resource provided by Edinburgh University where it hosts various spatial datasets such as Ordnance Survey maps and HydroSpatial One bathymetry charts provided by SeaZone mapped to International Hydrographic Organization standards. The bathymetry used was the 1 arc second gridded dataset which required transforming to British National Grid and Ordnance Datum to be compatible with the LiDAR datasets. Unfortunately, EDINA Digimap is only available to certain academic institutions, which luckily University of Liverpool is one of them.

EDINA Digimap is available here: http://digimap.edina.ac.uk/

9.1.3 Beach Survey

The beach survey data was sourced from the Channel Coast Observatory, this has a wide range of data in addition to LiDAR, one of these being survey elevation data taken at regular intervals along coastlines at many locations around the UK. This data is useful in ensuring the latest defence crest height and beach profile is used within the research. This data is updated more regularly than LiDAR surveys and can change on short timescales, particularly if an extreme event has occurred.

Channel Coast Observatory beach surveys are available here:

http://www.channelcoast.org/data_management/online_data_catalogue/metadata/search/index2.php

9.1.4 Sea-level return periods

McMillian et al., 2011 has produced a dataset of still water levels every 2 km around the UK coastline for 16 return periods ranging from 1 in 1 year to 1 in 10,000 year. McMillian et al., 2011 also produced a methodology that would produce a synthetic storm surge curve based on the surge information for the nearest tide gauge. This was used to produce boundary conditions for the flood inundation model.

The sea-level data is available from the Environment Agency at:

enquiries@environment-agency.gov.uk

9.1.5 Waves

There are various sources of wave data that have been used within the research project. There is wave buoy data and model wave data. The Centre for Environment, Fisheries and Aquaculture (CEFAS) has numerous wave buoys around the coastline of the UK as part of a project called Wavenet. There are a wide range of lengths to the wave buoy datasets, ranging from over 10 years to 6 months. The data for most of these buoys is freely available to download, from the CEFAS website.

As well as wave data collected by buoy, a 30 year hindcast model was used to provide wave data. This had the advantage of being a longer dataset over the wave buoys which are commonly only a few years long. This wave model is

The wave buoy data is available from the CEFAS website at:

http://wavenet.cefas.co.uk/Map

The wave model hindcast can be requested from: The European Centre for Medium-Range Weather Forecasts (ECMWF) at:

http://www.ecmwf.int/en/research/modelling-and-prediction/marine

9.1.6 Tide Gauge

The tide gauge data provided data that would be used in tandem with wave data for joint probability analysis. The data was acquired from the British Oceanographic Data Centre

(BODC) this has lots of oceanographic data available for download. In this case, the UK tide gauge network, where the full data set for the relevant tide gauge was downloaded.

BODC UK tide gauge network download here:

https://www.bodc.ac.uk/data/online_delivery/ntslf/

9.1.7 Predicted Tide

The predicted tide is used as the underlying curve in producing the synthetic storm tide curve. To produce the curves a piece of software called POLTIPS3 was used. This is able to produce the predicted tide at many points around the UK. The software is available from Marine Data Products at the National Oceanography Centre, Liverpool.

Request POLTIPS3 here:

dataproducts@noc.ac.uk

9.1.8 Depth Damage Curves

The curves converting water depth into a monetary cost were provided by Penning-Roswell et al 2014. This is the Flood and Coastal Erosion Risk Management handbook where the curves relating to residential housing, industrial buildings, roads and various types of arable land were used to assess the financial impact of flooding.

Middlesex University produces this resource and it can be purchased here:

http://www.mdx.ac.uk/our-research/centres/flood-hazard/flood-hazard-research-centre-publications

9.1.9 Spatial locations of coastal community assets

The locations of coastal community assets, such as residential housing and industrial buildings were provided by the Ordnance Survey Mastermap, this high resolution dataset shows the spatial locations of all assets that could be impacted by flooding. This was provided by EDINA digimap hosted by Edinburgh University. This resource is only freely available to certain academic institutions, but can also be sourced from Ordnance Survey directly.

OS Mastermap can be downloaded from EDINA here:

http://digimap.edina.ac.uk/

9.1.10 Regional relative sea-level rise projections

Relative Regional sea-level rise projections were provided by the United Kingdom Climate Projections 2009 which has comprehensive datasets for many different variables, the relative sea-level rise for different regions around the UK up to 2100 in annual intervals. This data is freely available.

The UKCP09 datasets are available here:

http://ukclimateprojections-ui.metoffice.gov.uk/ui/admin/login.php

9.2 Numerical Models

This body of work used numerous numerical models, the complete list is as follows:

- LISFLOOD-FP
- SWAB
- XBeach
- XBeach-G
- JOIN-SEA

9.2.1 LISFLOOD-FP

LISFLOOD-FP is a 2DH hydrodynamic model developed by the University of Bristol, it is capable to simulating flood plain inundation. It can be requested here:

http://www.bristol.ac.uk/geography/research/hydrology/models/lisflood/downloads/

9.2.2 Shallow WAter Boussinesq (SWAB)

A semi-implicit shallow-water and Boussinesq model has been developed to account for random wave breaking, impact and overtopping of steep sea walls including recurves. Developed by the Manchester University it is available to use as an online model here:

http://modelling.mace.manchester.ac.uk/user/login/?next=/

9.2.3 XBeach

XBeach is a two-dimensional model for wave propagation, long waves and mean flow, sediment transport and morphological changes of the nearshore area, beaches, dunes and backbarrier during storms. It is a public-domain model that has been developed with major funding from the US Army Corps of Engineers, Rijkswaterstaat and the EU, supported by a consortium of UNESCO-IHE, Deltares (formerly WL|Delft Hydraulics), Delft University of Technology and the University of Miami. It can be downloaded here: https://oss.deltares.nl/web/xbeach/home

9.2.4 XBeach-G

XBeach-G is a branch of the main XBeach development that is being developed to simulate storm impacts on gravel beaches. The development of XBeach-G is taking place as a joint collaboration between Plymouth University and Deltares, as part of the EPSRC-funded NUPSIG-project. It can be downloaded here:

https://oss.deltares.nl/web/xbeach/xbeach-og

9.2.5 JOIN-SEA

With respect to coastal engineering, joint probability refers to two or more partially related environmental variables occurring simultaneously to produce a response of interest. Damage to sea defences and flooding are often associated with times of high waves and high water levels. It is therefore necessary to consider the joint probability of these variables when assessing design conditions for coastal structures. New, practical and rigorous

methods for the analysis of large waves and high water levels have been developed jointly by HR Wallingford and Lancaster University. The new methods consist of a series of computer programs; this report is intended as a guide for the day to day running of the programs. Information about JOIN-SEA can be downloaded from here: http://eprints.hrwallingford.co.uk/701/